IMPROVEMENTS IN DESIGN AND FITNESS EVALUATION OF ABOVE GROUND STEEL STORAGE TANKS

by

© Sridhar Sathyanarayanan

A Thesis submitted to the

School of Graduate Studies

in partial fulfillment of the requirement for the degree of

Doctor of Philosophy in Engineering

Faculty of Engineering and Applied Science

Memorial University of Newfoundland

May, 2014

St. John's **Newfoundland and Labrador**

ABSTRACT

Above ground steel storage tanks are widely used to store liquids in a variety of industries. The design and fitness for service procedures for such tanks are a concern for international standards and need to be continually improved upon to ensure better safety and serviceability. Several important aspects about tank design and assessment are studied in this thesis.

The bottom plate material near the shell to bottom joint in the tank is generally in plastic range. It is a critical failure point in many modes of tank failure. The effect of increasing the bottom plate projection length at this joint for tanks with rigid ring wall foundations is studied both theoretically and numerically. A theoretical beam model is validated using finite element analysis (FEA) and extended to determine the length of bottom plate projection needed for maximum effect. The formation of plastic hinges in the bottom plate on the inside and outside of this joint is discussed in detail using FEA.

Tanks operating at elevated temperatures (200°F to 500°F) need to consider additional stresses due to thermal expansions and restraints from the tank shell and bottom plate interactions. The frictional forces from the foundation cause significant stresses at the tank bottom. The design guidelines by API 650 standard address this issue using a factor named ‘C’ that defines the ratio of actual expansion against free expansion of the tank bottom. At present, an empirical range of ‘C’ values (0.25 – 1.0) is allowed without clear guidelines for selecting a suitable value. This thesis evaluates the current procedure and suggests an alternate method by incorporating the friction coefficient

directly in the stress equations, instead of the C-factor. The fill/draw down cycle of the stored liquid could lead to low cycle fatigue near shell to bottom joint. The peak alternating stress (strain) at this location determines the fatigue life of the tank. The widely used API 650 procedure employs beam on elastic foundation theory to determine the fatigue life for all tanks. The thesis shows that this is incorrect for tanks on concrete ring wall. The appropriateness of using this theory is studied and an alternative beam model is proposed. It is verified using FEA.

Damage due to corrosion in the form of local thin area (LTA) is a widespread problem in storage tanks. Fitness for service (FFS) methods are quantitative engineering evaluations used to demonstrate the structural integrity of an in-service tank containing damage like LTA and make run, repair or replace decisions. The m_α-tangent method is a simplified limit load procedure that can be used for such FFS evaluations. This thesis uses a modified reference volume for m_α-tangent method applied to tanks and reports initial results for FFS evaluations. The study also finds that for large cylinders like tanks with very high R/t ratio, the circumferential decay lengths will be smaller than those previously reported ($2.5\sqrt{Rt}$ rather than $6.3\sqrt{Rt}$).

ACKNOWLEDGEMENTS

I would like to express my sincere gratitude to my supervisor, Dr. Seshu M. R. Adluri for his intellectual guidance, support and valuable discussions during the course of my Doctoral program. I also wish to express my gratitude to Dr. R. Seshadri for all his supervision, generous support and patience.

I would also like to thank Dr. A. S. J. Swamidas and Dr. Katna Munaswamy for all their help and support.

The financial support provided by the School of Graduate Studies and the Faculty of Engineering and Applied Science, Memorial University is gratefully acknowledged. I also thank Dr. Leonard Lye, Associate Dean of Graduate Studies, Ms. Moya Crocker and Ms. Mahoney Colleen at the Office of Associate Dean, for all the administrative support during the course of my program. I also wish to thank the computing services at the engineering faculty for their continuous assistance throughout my program.

I would like to thank all my friends for their support and encouragement. I also wish to thank my friend Dr. Geeta Iyer for her motivation and support during difficult times. I owe my deepest thanks to my wife, Hemalatha, for her unconditional love, constant encouragement, sacrifice and understanding during all these years. I also express my heartfelt gratitude to my beloved parents and sister for their love, support and encouragement at all times.

Lastly, I profoundly thank the almighty for giving me the strength and perseverance to pursue and complete this program successfully.

TABLE OF CONTENTS

LIST OF TABLES

LIST OF FIGURES

LIST OF APPENDICES

LIST OF SYMBOLS AND ABBREVIATIONS

Symbols

a	Projection of bottom plate outside the tank wall
b	Length of bottom plate inside the tank wall
C	Reduction factor to account for the partial expansion of tank bottom due to temperature change
D	Diameter of tank
D_s	Flexural Rigidity of tank wall
E	Young's Modulus
G	Specific gravity of liquid
G_m	Shear modulus
EI_P	Flexural rigidity of bottom plate/unit width
H	Tank filling height
K	Foundation modulus
K_a	Width of annular plate
K_c	Stress concentration factor at shell to bottom joint
L	Total uplift length of the bottom plate
L_{msd}	Shortest distance between the edge of corrosion area and any closest structural discontinuity
M	Folia's factor
M_T	Moment due to thermal loading at bottom joint

M_b Moment due to pressure loading at bottom joint

M_x Long moment at a distance ‘x’ from tank bottom

M_{bp} Inelastic moment in the bottom plate

M_o Moment at the bottom of the shell

M_P Plastic moment capacity of the bottom/annular plate

m^0 Upper-bound limit load multiplier

m_L Lower-bound limit load multiplier

m_α^T m_α-tangent multiplier

N Number of load cycles estimated for the design life capacity of tank

N_x Membrane Force Per unit length in the meridional direction

N_θ Circumferential (hoop) Force per unit length in tank wall

P Load

P_f Failure load (pressure) of damaged component

P_{fo} Failure load (pressure) of undamaged component

q_o Uniform internal pressure

q Uniformly distributed load (Pressure)

Q_o Shear force at bottom of tank wall

Q_{xs} Shear force in the tank wall at distance ‘x’ from bottom

Q_T Shear force due to thermal loading at bottom joint

R Nominal (mean) radius of tank wall at bottom

r Radial distance from the centre of the tank

S Alternating stress range in the bottom plate near shell to bottom joint ($S_b/2$)

s	Length of flaw in height direction (= 2b)
S_b	Pseudo elastic bending stress (strain range) in the bottom plate near shell to bottom joint
S_x	Stress in bottom plate in the radial direction
S_Y	Specified minimum yield strength at the design temperature
S_Y	Yield Strength
S_f	Flow stress
$\overline{s}_{ij}^{0}$	Statically admissible deviatoric stress for impending plastic flow
T	Shell self weight
t	Nominal thickness of the tank wall
t_s	Thickness of the tank bottom shell course
t_a	Annular plate thickness (is equal to t_b if not given exclusively)
t_b	Thickness of bottom plate
t_p	Bottom plate thickness (assuming uniform thickness and friction coefficient for the entire tank; same as t_b unless specifically noted)
t_{mm}	Minimum measured remaining wall thickness
t_c	Corroded thickness of the tank wall
t_{min}	Minimum required wall thickness
u	Radial displacement of any point in bottom plate
u_x	Displacement in the x_s direction of shell
U_D	Distortional energy density
U_o	Strain energy density

w	Hydrostatic pressure at tank bottom
x	Distance from the tank shell towards center of the tank
x_s	Distance from the tank bottom along the height of tank
X_c	Decay length in the circumferential direction
X_l	Decay length in the longitudinal direction
y	Deformation/Deformation in annular plate
y_s	Radial deformation of tank shell
Z	Pressure acting normal to shell surface
α	Coefficient of thermal expansion
β	Shell parameter $\sqrt[4]{3(1-\nu^2)/R^2t_s^2}$
ε	Strain
ε_a	Applied strain
ε_p	Plastic strain
ε_y	Yield strain
$\varepsilon_{1,2,3}$	Principal strains
ΔT	Change in temperature (°C)
ΔT_L	Limiting temperature (°C)
δ	Final radial displacement of tank wall bottom
φ^0	Point function
γ	Unit weight of stored liquid
μ	Coefficient of friction

μ_L Limiting Coefficient of friction

μ^0 Flow parameter

ν Poisson's ratio (0.3 for carbon steel)

σ Stress/Normal stress

$\sigma_{1,2,3}$ Principal stress

σ_e von Mises equivalent stress

σ_y Yield strength of the material

τ Shear stress

τ_{max} Maximum shear stress

Ψ Moment ratio (M_{fx}/M_o)

θ_s Slope of the shell at the bottom

2a Width of LTA

2b Height of LTA

Abbreviations

2-D Two dimensional

3-D Three dimensional

APDL ANSYS parametric design language

API American petroleum institute

ASME American society of mechanical Engineers

BKIN Bilinear kinematic hardening

CTP Critical thickness profile

COV Coefficient of variation

DOF	Degree of freedom
EPFEA	Elastic-Plastic finite element analysis
FCA	Future corrosion allowance
FEA	Finite element analysis
FFS	Fitness for service
LEFEA	Linear elastic finite element analysis
LF	Load factor
LTA	Locally thinned area
LTAH	LTA height
LTAW	LTA width
MAWP	Maximum allowable working pressure
$MAWP_r$	Reduced maximum allowable working pressure
MFH	Maximum fill height
MPC	Multi point constraint
PTR	Point thickness reading
RSF	Remaining strength factor
RSF_a	Allowable remaining strength factor

CHAPTER 1

INTRODUCTION

1.0 BACKGROUND

Storage tanks are part of many industries. Tanks are used for storing petroleum products or any fluids/gases at ambient/elevated/low temperatures. Tanks could be either above ground or below ground. Above ground storage tanks (AST) are constructed just above the ground or at a higher elevation using structural supports. In an industrial setup, both above and below ground tanks are widely used to store water, petroleum or other chemical fluids. Generally tanks above ground have much higher capacity than below ground tanks. The above ground steel tanks can either be vertical or horizontal. Most large ASTs are generally vertical cylindrical vessels which are built with flat bottoms that rest directly on prepared subgrades or concrete ring wall with suitable infill. Ambient temperature tanks store and operate the infill liquid at atmospheric temperature whereas elevated temperature tanks have arrangements to heat the liquid while in storage. In petroleum industries, tanks are extensively used to hold liquids like asphalt, residuum, high pour point hydrocarbons, etc., at higher temperature than the ambient. In the U.S alone it is estimated that over 700 million gallons of petroleum is consumed daily. The number of ASTs in the US is in the range of 950,000 to 1,100,000. In Canada there could be another 100,000. Among these, shop built ASTs account for approximately 85% and the remaining 15% are field erected. For ease of definition, shop-built ASTs are

generally considered to be available in capacities less than 1000 barrels (42,000 gallons) and less than 15 feet in diameter [Digrado and Thorp, 2004]. Tanks of larger capacity are fabricated at site. Design life and failure of such storage tanks has a major impact on the process cycle and the environment. The design and fitness-for-service procedures are a concern for many international standards and are continually improved upon to ensure better safety and serviceability. This thesis focuses on the design and fitness for service issues of above ground cylindrical (vertical) steel tanks used in petroleum and other industries.

The analysis and design of such tanks in North America is generally based on American Petroleum Institute standard API 650 [2012]. This standard is also used or referenced to extensively in other countries and is sometimes seen as “de facto” international standard. It governs the design, erection and testing requirements of above ground storage tanks operating at ambient atmospheric pressure or slightly higher pressures. The wall of such a tank can have a single thickness throughout its height or several shell courses with varying thicknesses. The design principle is based on small deflection theory of thin walled cylindrical shells. The wall is predominantly designed for the hoop stresses due to the tank liquid, with some considerations for discontinuity stresses at joints. The bottom of the tank is a thin plate generally considered to be a membrane without any structural requirements. However this thin plate is subjected to very high bending near the shell joint due to shell rotation and can cause failure. Although API 650 has been in use for a long time, just like any other design standard, it needs periodic evaluation to examine or re-examine its provisions. The present thesis is

aimed at this objective. Some of the current technical issues in tanks are briefly discussed below.

The bottom plate of the tank extends to a small length outside the shell wall. This projection length is generally prescribed for welding requirements. It influences the stresses in the tank wall/ bottom plate. Hence a detailed study is needed for selecting this projection length and examining relevant issues. At present there are no detailed studies on this issue. In many situations, tanks are used at operating temperatures ranging from ambient to 500° F (260° C). Such 'elevated temperature tanks' have significant thermal stresses especially near the shell to bottom discontinuity. The magnitude of thermal stress occurring in the tank wall and the bottom plate is influenced by the amount of radial restraint, which in turn depends upon factors like liquid pressure, friction between the bottom plate and the foundation and differential settlement, if any. It is reported that this zone undergoes low cycle fatigue [Karcher, 1978a, b] and hence needs to be analyzed in detail for such situations. API 650 only provides minimum guidelines for elevated temperature tanks and hence the designer needs to do a rigorous analysis if the conditions are critical.

Like any other process equipment, damage due to erosion/corrosion is a common problem in the tanks. Localized corrosion damages and thermal hot spots are typical of damage that occurs in ageing pressure vessels, piping or storage tanks. In the case of above ground storage tanks, an average size tank may cost around one-half million dollars to construct/replace and substantial portion would go for repair and rehabilitation, if required [Andreani, et al., 1995]. In addition to the cost, issues concerning logistics, the

effect on the process cycle due to out of service tanks, safety permits, etc., cause huge losses in resources and time that cannot be exactly accounted for. Hence, periodic inspection of the tanks for structural health and safety is part of the engineer's duties. The engineer or tank operator is expected to periodically monitor the structural health and integrity, asses the degradation and take decisions regarding repairs/replacement. Fitness for service assessments are the primary tools adopted to carry out this task. They are quantitative and qualitative engineering evaluations performed to determine the structural integrity of an in-service component containing damage and estimate the remaining life of degraded components and to make run/repair/replace decisions. They can be applied to storage tanks, pressure vessels, boilers, piping systems and pipelines, etc. American Petroleum Institute (API) standards API 579 & 653 provide a general procedure for assessing fitness for service in tanks. Based on the problem, different levels of fitness for service need to be employed to ensure the safety and serviceability of tank. Practitioners usually proceed sequentially from Level 1 to Level 3 analysis (unless otherwise directed by the assessment techniques). Level 1 is the most conservative, but is easiest to use. The engineer proceeds to the next level, if the current assessment level does not provide an acceptable result or a clear course of action cannot be determined.

1.1 NEED FOR RESEARCH

As mentioned above, the shell to bottom joint in tanks is an important location where the discontinuity stresses are very high and tanks have historically failed at this location [Cornell and Baker, 2002]. In large tanks, the bottom plate near this joint is usually thickened for a small width (Fig.1.1), whereas in small tanks the same thickness

is provided throughout. The thickened portion of bottom plate is termed as "annular plate".

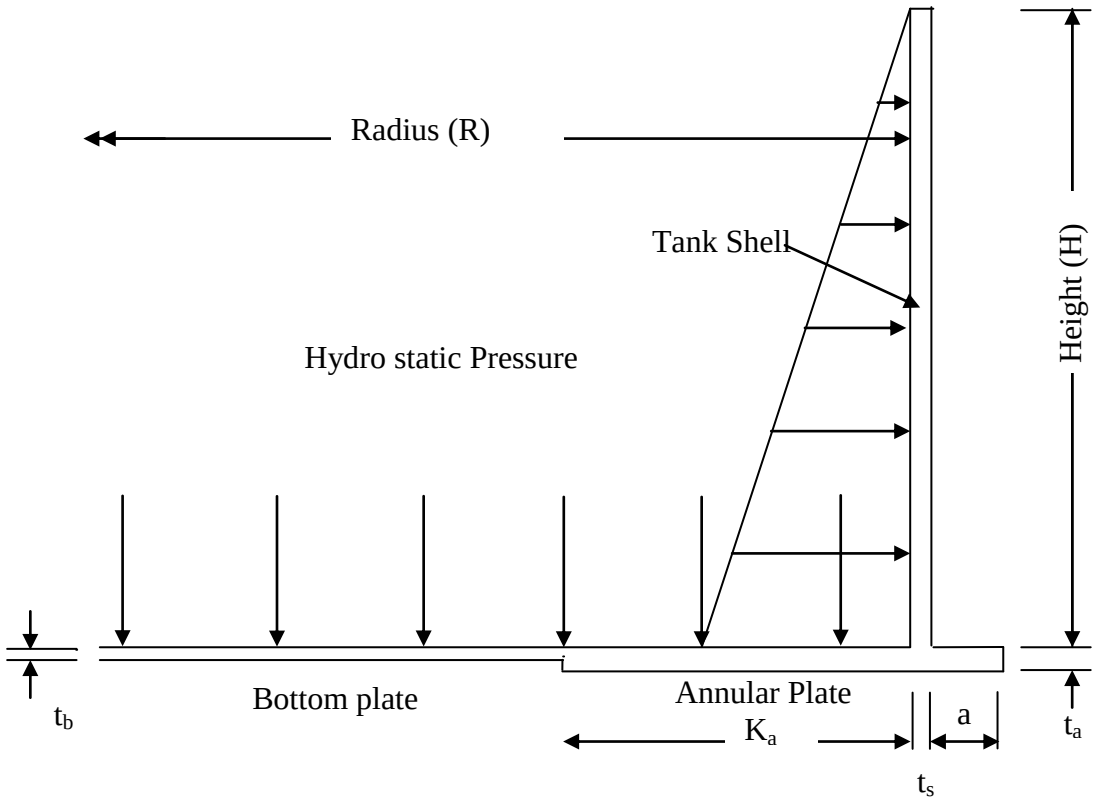

Fig. 1.1 Tank with Annular Plate

The designer needs to determine the width of the annular plate from the inner surface of the shell towards the tank centre (K_a), the thickness of the plate (t_a) and the projection length of the plate outside the shell (a).

Wu and Liu [2000], report that codes and standards in many countries do not have equations to design the annular plate. Denham, et al., [1968 a, b] proposed a model for

finding the elastic stresses near the shell to bottom joint. This model, based on beam and shell theory, was developed for a fixed annular plate projection length (3") and the theoretical results were compared with strain gage measurements. In case of shell, the measured stresses confirmed the validity of the theoretical approach. For annular plate, the field results indicated that it could reach yield close to the shell, and hence a low cycle fatigue situation could be expected near this joint. The study indicated that the projection could influences the stresses, but the effect of changing the projection length and its upper limit on the stresses was not studied.

In case of elevated temperature tanks, the thermal stresses induced due to partial expansion of the tank was studied by Karcher [1978a]. The restraint causing partial expansion at the bottom was addressed using an expansion factor called 'C'. However, there are no clear guidelines to choose a particular value for this factor for a given situation. Hence the influence of 'C' on tank stresses and fatigue life has to be clearly understood and explicit guidelines are needed to choose a value for this factor. It can be shown that 'C' is directly related to coefficient of friction between tank bottom and the foundation. At present this is not explored in any systematic manner. Another significant issue in the current practice is the use of beam-on-elastic foundation theory with tanks resting on concrete ring walls. The design community has largely ignored this discrepancy. This needs closer examination.

As mentioned earlier, locally thinned areas (LTA) due to corrosion is a common occurrence in pressure vessels and tanks. Application of simplified limit load methods in fitness for service (FFS) evaluation of LTA is still in the initial stages and can be

explored further to improve the accuracy of the results. Moreover in the current practice, the FFS procedures are mainly calibrated for pipes and merely used for tanks without much verification. It would be good to develop procedures specifically for large tanks and their special type of geometry and loading. This is especially so since the R/t ratios of tank could well exceed 1000 whereas most pipes fall in the range of 20~100.

1.2 OBJECTIVES OF RESEARCH

The following objectives have been selected for the current research:

1. Study the influence of annular plate on the internal moment at the shell to bottom joint of tanks and determine the upper design limit of the annular plate projection length outside tank wall.
2. Study the influence of friction forces below the tank bottom and propose a more rational procedure to determine the value of the expansion factor.
3. Improve the existing procedure for fatigue design of tanks on concrete ring wall foundation vis-à-vis the use of beam-on-elastic foundation theory.
4. Explore the use of simplified fitness for service methods for tanks with LTA using the m_α-tangent multiplier.

1.3 SCOPE OF THE STUDY

This study applies to tanks in non-refrigerated service with internal pressures approximating atmospheric pressure. The analyzes of the tanks are carried out for hydrostatic test condition, i.e., the infill liquid is assumed to be water for finding relevant stresses. However the treatment is also valid for any other liquid. For elevated

temperature tanks the temperature range is considered between 200°F (93°C) and 500°F (260°C). The foundation of the tank is assumed to have concrete ring wall with well compacted infill. In the finite element analysis, the tank is modeled using elastic-plastic ductile material which is able to absorb significant deformation beyond the elastic limit without the danger of fracture. Strain hardening is assumed to be small.

For the study of locally thinned areas, the flaw area is considered with the remaining thickness ratio (defined as the ratio of the corroded wall thickness to the nominal thickness) not less than 0.5. The discontinuity of corrosion damage is assumed to be tapered down smoothly and corrosion damage is considered as blunt patch (non-crack like flaw). For ease of analysis, the shape of the flaw is assumed to be rectangular with different aspect ratios. The location of the flaw is assumed to be remote from other major structural discontinuities, such as nozzles, or geometry changes. The tanks studied in the current work are assumed to be designed and constructed in accordance with a recognized code or standard such as API 650.

1.4 STRUCTURE OF THE THESIS

This thesis is organized in eight Chapters. The first Chapter introduces the background to the problem, the need for research, objectives and scope of the study.

The second Chapter presents a general review of literature. It briefly reviews the basic theories associated with tank analysis and design. The tanks are designed similar to any mechanical component or pressure vessel, and hence a short summary of different failure theories of material is provided. Even though the tank bottom is not designed for

structural loads, the zone near the shell should safely carry the localized bending stresses and be checked for fatigue due to cyclic loading. The local bending at the shell to bottom joint, causes yielding and shakedown in the bottom plate. The formulas used for this evaluation are obtained considering the bottom plate as a beam-on-elastic foundation and hence the basics of beam-on-elastic foundation are included. The tank wall is a thin shell structure and all the design and analysis is carried out using shell theory and therefore basic shell theory is reviewed. The concept of fitness for service and its application to AST is introduced. Finally the survey of previously reported research works relevant to the scope of the current research is included.

In Chapter 3 finite element modeling details of the present study including geometry, constraints, material models and samples of typical mesh are provided. Details about the friction model used for interaction between bottom plate and foundation are explained. The problems encountered during modeling and the solution techniques adopted are discussed briefly.

Chapter 4 introduces the basic tank design procedures and describes the behavior of shell to bottom joint, the purpose of annular plate and its design basis. The mechanism of formation of plastic hinges near the shell to bottom joint is explained. The influence of the annular plate projection length on tank stresses is studied. The procedure to determine the length of the annular plate projection (required to minimize the stresses in the shell) is provided and the theoretical results are compared with the finite element Model results.

Chapter 5 discusses the friction interaction between bottom plate and foundation. The procedure by Karcher that uses a factor called 'C' to account for the partial expansion of the tank is explained. A more rational alternative procedure using friction coefficient instead of C factor is proposed. Theoretical results are validated using finite element analysis.

Chapter 6 presents the procedure for fatigue evaluation of shell to bottom joint in tanks. It discusses about the suitability of using beam-on-elastic foundation theory for determining the peak stress values in tanks on concrete ring walls. The current procedure is modified by replacing the beam-on-elastic foundation theory with beam theory to reflect the bottom plate uplift near this zone. The results of the modified procedure are compared with the existing procedure and finite element analysis.

Chapter 7 discusses a modified reference volume scheme for determination of remaining strength factor (RSF) in tanks using the m_α-tangent method. The RSF determined using modified reference volume is compared with the API procedure and the elastic-plastic FEA results. The circumferential decay length for large tanks with high R/t ratio is studied using FEA and a suitable value is recommended.

Chapter 8 summarizes the current work and gives conclusions and recommendations for future work.

CHAPTER 2

LITERATURE REVIEW

This Chapter reviews briefly the basic theories associated with tank analysis and design. Since tanks are basically thin cylindrical shells, the basic shell theory is presented here. A brief summary of failure theories, basics of beam-on-elastic foundation theory and concepts of shakedown analysis are presented. Pertinent concepts about fitness for service procedures and their application to storage tanks are introduced. The concept of limit analysis, limit load multipliers and the estimation of remaining strength factor of damaged tanks using limit analysis are also explained. A survey of previously reported research works relevant to the scope of current research is included.

2.0 THEORIES OF FAILURE

Structural members subjected to loads may fail to perform their intended function in various ways. Depending on the loading, geometry and material properties they may fail because of excessive deformation, material yielding, fracture, instability, etc. Yielding of the material is an important mode of failure in many components. For unidirectional stress field, the yield strength obtained from a standard uniaxial test can be the criterion. But for multi-axial state of stress, the yielding is governed by some quantity representing the state of strain, stress, components of strain energy, etc. Hence, the yield criterion is usually expressed in mathematical form by means of a yield function $f(\sigma_{ij,}$

$\sigma_{y,}$), where σ_{ij} is the state of stress and σ_y is the uniaxial yield strength. $f(\sigma_{ij,}\ \sigma_y) = 0$ implies that yield boundary has been reached and $f(\sigma_{ij,}\ \sigma_y) < 0$ indicates that the stress state is elastic. The yield function is developed such that the components of multi-axial stress can be combined in to a single quantity and termed as effective stress $\sigma_{e.}$ The effective stress is then compared with the yield strength σ_y (obtained from uniaxial test), in some appropriate form, to determine if yield has occurred. The following are some of the yield criteria that are often used in engineering practice. The following is a simple summary of the material found in solid mechanics text books.

2.0.1 Maximum Shear Stress Criterion

The maximum shear-stress criterion, also known as the Tresca criterion, states that yielding begins when the maximum shear stress at a point in the structure equals the maximum shear stress at yield in uniaxial tension (or compression). The maximum shear stress (τ_{max}) is given by half of the difference between maximum and minimum principal stress components.

$$\sigma_e = \tau_{max} = (\sigma_1 - \sigma_3)/2 \tag{2.1}$$

$$f = (\tau_{max} - \sigma_y/2) \tag{2.2}$$

In ductile metals, the crystals have slip planes along which the resistance to shear force is the weakest. Hence yield criterion based on shear stress is more appropriate for ductile metals. The Tresca criterion generally gives conservative results for metals. Because it is simple to use, many engineers and codes (e.g., ASME B&PV) prefer it for

metal structures. The yield surface for this criterion is a regular hexagon in 2D principal stress space as shown in Fig. 2.1(a).

2.0.2 Distortional Energy Density Criterion

This criterion, also referred as von Mises criterion or octahedral shear stress criterion states that yielding begins when the distortional strain energy density at a point in the structure equals the distortional strain energy density at yield in uniaxial tension (or compression). This criterion assumes that the energy associated with volume change has negligible effect on yielding and the energy associated with distortion alone is responsible for the yielding of material. The distortional energy density U_D is expressed as

$$U_D = \frac{1}{12G_m}\left[(\sigma_1-\sigma_2)^2+(\sigma_2-\sigma_3)^2+(\sigma_3-\sigma_1)^2\right] \tag{2.3}$$

where, G_m is the shear modulus. Using this, the effective (von Mises stress) is given by

$$\sigma_e = \sqrt{\frac{1}{2}\left[(\sigma_1-\sigma_2)^2+(\sigma_2-\sigma_3)^2+(\sigma_3-\sigma_1)^2\right]} \tag{2.4}$$

The yield function then becomes

$$f = \sigma_e^2 - \sigma_y^2 \tag{2.5}$$

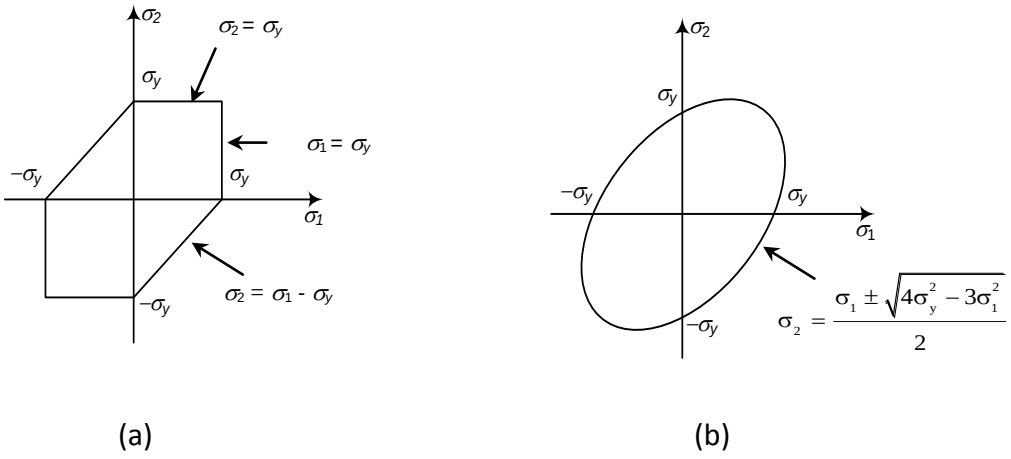

Fig. 2.1 Yield Criteria in σ1 - σ2 plane: (a) Tresca Criterion, (b) von-Mises Criterion

The von Mises or Tresca criteria are more suitable for ductile metals and predict the initiation of yielding quite well and are the most popular and hence are presented here. However the von Mises criterion is slightly more accurate than Tresca criterion and has a smooth profile unlike the Tresca function. Since the von Mises yield function is continuously differentiable, it is preferred in computational plasticity studies in which plastic flow and strain hardening are considered. Similarly there are many other theories of failure suitable for different types of materials. The current work uses von Mises exclusively.

2.1 SHELL THEORY

In the present research, Above Ground Storage Tanks (AST) of cylindrical shape are studied. The theory of cylindrical shells is used in the analysis and design of AST. Hence a brief summary of this theory is presented here. Detailed analysis of this theory is presented by many authors e.g., Timoshenko and Woinowsky-Kreiger [1959].

.

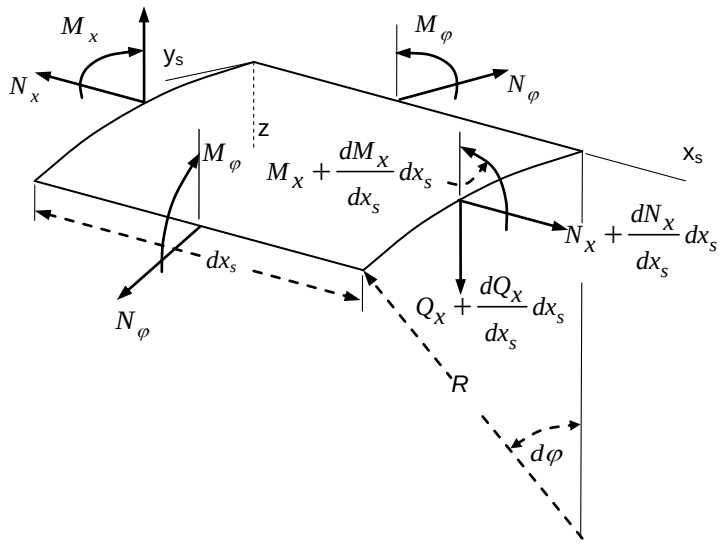

Fig. 2.2 Forces and Moments Acting on a Cylindrical Shell Element

Consider the equilibrium of an element of the shell as shown in Fig. 2.2. The term $N_{x\varphi}$ indicates membrane force in the plane perpendicular to 'x_s' axis and in the direction of φ. Because of axi-symmetry, the membrane shearing forces $N_{x\varphi}$ & $N_{\varphi x}$ vanish and hence the hoop force N_φ is constant along the circumference. Similarly, because of symmetry the twisting moments $M_{x\varphi}$ & $M_{\varphi x}$ vanish and M_φ remains constant along the circumference. Assuming that the external forces consist only of pressure (Z) normal to the surface, the following equilibrium equations are obtained

$$\frac{dN_x}{dx_s} R\ dx_s\ d\varphi = 0 \tag{2.6}$$

$$\frac{dQ_x}{dx_s} R\ dx_s\ d\varphi + N_\varphi\ dx_s\ d\varphi + Z\ R\ dx_s\ d\varphi = 0 \tag{2.7}$$

$$\frac{dM_x}{dx_s} R\, dx_s\, d\varphi - Q_x\, R\, dx_s\, d\varphi = 0 \tag{2.8}$$

Eq. 2.6 indicates that force N_x is constant. It can be taken as zero if the self-weight and stress due to forces applied axially on the cylinder is neglected. If they are significant, they can be superimposed on top of other stresses appropriately. Equations 2.7 and 2.8 give, respectively,

$$\frac{dQ_x}{dx_s} + \frac{1}{R} N_\varphi = -Z \tag{2.9}$$

$$\frac{dM_x}{dx_s} - Q_x = 0 \tag{2.10}$$

Since the problem is axisymmetric, the displacement along the circumferential direction is zero. Hence, only the displacements u_x and y_s in the x_s and y directions, respectively, exist.

Using Hooke's law,

$$N_x = \frac{Et_s}{1-\nu^2}(\varepsilon_x + \nu\varepsilon_y) = \frac{Et_s}{1-\nu^2}\left(\frac{du_x}{dx_s} - \nu\frac{y_s}{R}\right) = 0 \tag{2.11}$$

$$N_\varphi = \frac{Et_s}{1-\nu^2}(\varepsilon_\varphi + \nu\varepsilon_x) = \frac{Et_s}{1-\nu^2}\left(-\frac{y_s}{R} + \nu\frac{du_x}{dx_s}\right) \tag{2.12}$$

where t_s is the thickness of the shell. From Eq. 2.11 and 2.12,

$$N_\varphi = -\frac{Et_s y_s}{R} \tag{2.13}$$

Since there is no change in curvature in the circumferential direction, the curvature in the x_s-direction is equal to $\frac{-d^2y_s}{dx_s^2}$. Hence

$$M_x = -D\frac{d^2y_s}{dx_s^2},\ M_\varphi = \nu M_x,\ \text{where, } D_s = \frac{Et_s^3}{12(1-\nu^2)} \tag{2.14}$$

Using Eqns. (2.8) and (2.9) and eliminating Q_x,

$$\frac{d^2}{dx_s^2}\left(D_s\frac{d^2y_s}{dx_s^2}\right) + \frac{Et_s}{R^2}y_s = Z \tag{2.15}$$

If D_s doesn't vary along x_s,

$$\frac{d^4y_s}{dx_s^4} + 4\beta^4 y_s = \frac{Z}{D_s},\quad \text{where, } \beta^4 = \frac{3(1-\nu^2)}{R^2t_s^2} \tag{2.16}$$

This equation is similar to that of a beam-on-elastic foundation, as explained in the next section. The general solution of Eq. 2.16 is given by

$$y_s = e^{\beta x_s}(C_1\cos\beta x_s + C_2\sin\beta x_s) + e^{-\beta x}(C_3\cos\beta x_s + C_4\sin\beta x_s) + f(x_s) \tag{2.17}$$

where, $f(x_s)$ is the particular solution and C_1 to C_4 are constants of integration. These constants have to be determined from the boundary conditions of the shell. For cylindrical tanks with uniform wall thickness, the pressure acting normal to the shell surface is the hydrostatic load $Z = -\gamma(H - x_s)$, where, γ is the specific weight of the liquid and H is the height of the liquid. Eq. 2.16 can be written as

$$\frac{d^4y_s}{dx_s^4} + 4\beta^4 y_s = \frac{-\gamma(H-x_s)}{D_s} \tag{2.18}$$

The particular solution for the above equation will be $y_s = -\frac{\gamma(H - x_s)}{4\beta^4 D_s} = -\frac{\gamma(H - x_s)R^2}{Et_s}$.

This expression represents the radial expansion of the cylindrical shell with free edge under the action of hoop stresses. The constants C_1 and C_2 are zero if the shell is long. Hence Eq. 2.17 can be written as

$$y_s = e^{-\beta x_s}(C_3 \cos\beta x_s + C_4 \sin\beta x_s) - \frac{\gamma(H - x_s)R^2}{Et_s} \qquad (2.19)$$

The constants C_3 and C_4 can be obtained from the boundary condition at the bottom of the tank.

2.2 BEAM-ON-ELASTIC FOUNDATION

Beam-on-elastic foundation theory is used to analyze structures that can be idealized as a beam of relatively low stiffness placed on a flexible foundation and loads are applied on the beam. This theory finds applications in a variety of practical engineering problems like a rail road placed on soil subgrade, floor systems with beams (as used in ships), buildings, bridges and components made of thin shells of revolution like tank walls, boilers, etc. In ASTs, this theory is also used to determine the minimum length of the annular plate [Karcher, 1978b], the fatigue life of the shell to bottom joint of tanks, etc.

The theory is based on the assumption that the reaction forces of the foundation are proportional at every point to the deflection of the beam at that point. This assumption was first introduced by Winkler in 1867. The vertical deformation characteristics of the foundation are defined by means of identical, independent, closely spaced, discrete and

linearly elastic springs. The constant of proportionality of these springs is known as the modulus of sub grade reaction (K). The Winkler model, which has been originally developed for the analysis of railroad tracks, is very simple and does not accurately represent the characteristics of many practical foundations. One of the most important deficiencies of the Winkler model is that a displacement discontinuity appears between the loaded and the unloaded part of the foundation surface. In reality, the soil surface does not show any discontinuity as shown in Fig. 2.3(b).

(a) Winkler Foundation (b) Practical Soil Foundations

Fig. 2.3 Deflections of Elastic Foundations under Uniform Pressure

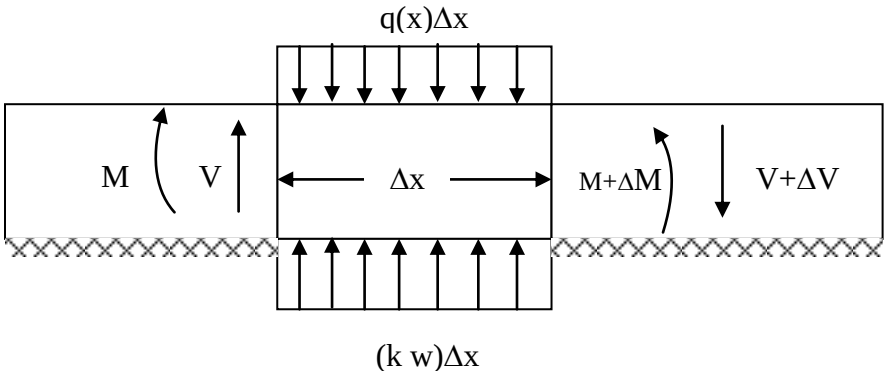

Fig. 2.4 Beam-on-Elastic Foundation

Various models have been proposed by researchers [Wang, 2005] to overcome this deficiency in Winkler's model by introducing the interactions between the individual springs using interconnecting elements like beams or plates. In the model proposed by Hetényi [1947], interaction between the independent spring elements is accomplished by incorporating an elastic beam (2-D) or an elastic plate (3-D), that can deform only in bending.

Considering the equilibrium of an infinitesimal element of the beam-on-elastic foundation as shown in Fig. 2.4, the vertical equilibrium leads to

$$\frac{dV}{dx} = Ky - q(x) \tag{2.20}$$

Similarly, moment equilibrium leads to

$$\frac{dM}{dx} = V \tag{2.21}$$

From the small deflection beam theory, the moment curvature relationship is

$$M = -EI\frac{d^2y}{dx^2} \tag{2.22}$$

Hence

$$\frac{d^4y}{dx^4} + 4\beta^4 y = \frac{q}{EI} \text{ where } \beta = \sqrt[4]{\frac{K}{4EI}} \tag{2.23}$$

The general solution of the equation is given by

$$y = e^{\beta x}(C_1 \cos\beta x + C_2 \sin\beta x) + e^{-\beta x}(C_3 \cos\beta x + C_4 \sin\beta x) + w(q) \tag{2.24}$$

where, y(q) is the particular solution associated with the applied load q(x), and disappears when q = 0. It can be seen that both the beam-on-elastic foundation theory and the shell theory gives the same governing equation. The beam on elastic foundation theory will be used later for discussing annular plate behavior of tanks.

2.3 SHAKEDOWN ANALYSIS

In studies on tanks, researchers [Karcher, 1981a, Long, 2004] have assumed that shakedown occurs at the shell to bottom plate joint. A brief review of shakedown in general is given here.

Shakedown is a phenomenon, that can occur in structures/components (of ductile material) when they are subjected to repetitive loads. Apart from the regular modes of failure that are expected in static loading conditions, failure due to fatigue, alternate plasticity or ratcheting can occur due to such repetitive loads. When the cyclic loads cause stresses beyond the yield strength, some sort of re-adjustment of stress distributions can happen through limited plastic flow which results in residual stresses that will minimize the plastic fatigue strains in subsequent cycles [Calladine, 2000]. Hence the study of shakedown performance of the structure is needed for design considerations.

For example, if a load ‘q’ causes the structure to begin yielding, and if the load is further increased to 1.25q and brought down to zero load to complete the first load cycle, then the residual stresses set up in the structure will enable the structure to respond to the second load cycle by purely elastic action completely up to the load of 1.25q. The stress distributions tend to adjust themselves under cyclic loading, to an elastic state whenever

possible, since for a given amount of external work performed by the applied loading, the internal strain energy will be a minimum when the stress distribution is linearly elastic. Hence the structure 'shakes down' to elastic behavior.

The shakedown limit, i.e., the load up to which the structure will shakedown to elastic behavior depends upon the material, the structure geometry and the loading pattern. Similar limits exist for alternate plasticity and ratcheting. Generally in pressure components, the plasticity/shakedown occurs near the discontinuities because of the secondary stress effects. Since the secondary stresses are self-equilibrating stresses, the shakedown limit can be found using elastic analysis. During the initial loading of the structure, if the stresses computed on elastic basis are everywhere less than twice yield stress, then it can be ensured that the structure will shake down [Burgreen, 1975].

2.4 LOW CYCLE FATIGUE

Fatigue is a progressive and localized structural damage that occurs when a material is subjected to cyclic loading. The nominal stress values that cause such damage need not necessarily be equal to the yield/ultimate strength of the material. Fatigue is classified as High cycle (HCF) and Low cycle fatigue (LCF). Failure in HCF is caused by lower amplitude of stress level and higher number of load cycles ($>10^4$) whereas in LCF, it is higher amplitude of stress level (generally higher than yield strength) and lower number of load cycles ($<10^4$). For the LCF case, when the plastic deformation occurs, the accounting of the loading in terms of stress is less useful and hence the strain in the

material offers a simpler and more accurate description. Low-cycle fatigue is usually characterized by the Manson-Coffin relation as given below [Wiki, 2013]:

$$\frac{\Delta\varepsilon_p}{2} = \varepsilon_f^{'} \left(2N_f\right)^{\eta} \tag{2.25}$$

where, $\Delta\varepsilon_p$ /2 is the plastic strain amplitude; ε_f' is an empirical constant known as the fatigue ductility coefficient, the failure strain for a single reversal; $2N_f$ is the number of reversals to failure (N_f cycles), η is an empirical constant known as the fatigue ductility exponent, commonly ranging from -0.5 to -0.7 for metals.

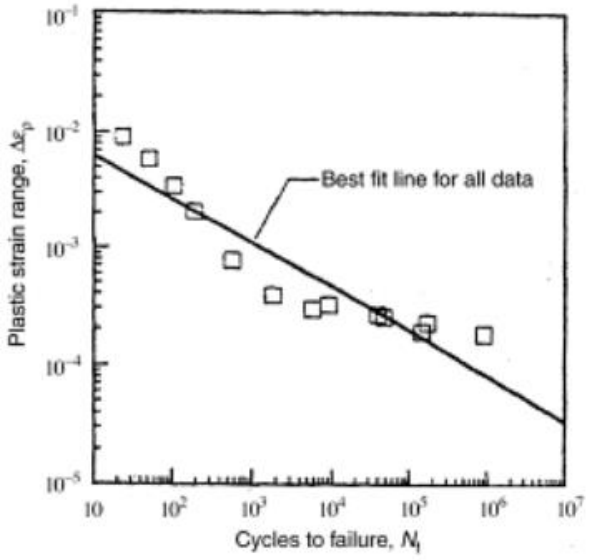

Fig. 2.5 Manson-Coffin Strain – Life relation for AISI 304 Stainless Steel [Manson & Halford, 2006]

The above relationship was obtained by Manson and Coffin independently in the 1950s from the results of experiments which suggested that a logarithmically linear relation between plastic range and fatigue life exists as shown in Fig. 2.5. Since determination of plastic strain alone was difficult for practical engineering problems, the

plastic strain was later replaced by the total strain appropriately [Manson & Halford, 2006]. This work gave the fundamental insight that fatigue life as a function of plastic strain reversal and formed the basis of all the future work in fatigue. Langer [1962] proposed the following expression relating the total alternating strain and the fatigue life.

$\varepsilon_a = A1(N)^{-n1} + A2$ (2.26)

where, $\Delta\varepsilon_a$ is the applied strain amplitude, N is the fatigue life and

A1, A2,n1 are coefficients of the model. The Equation 2.26 can also be expressed in terms of stress amplitude S_a as

$$S_a = \frac{E}{4\sqrt{N}} In\left(\frac{100}{100-A}\right) + B \quad (2.27)$$

where E is the elastic modulus, A and B are constants related to reduction in area in a tensile test and endurance limit of the material at 10^7 cycles. The strain amplitude is converted to stress amplitude using material modulus i.e. $Sa = E\ \varepsilon_a$.

The ASME fatigue design curves were obtained by strain controlled experiments based on Langer's expression. The design curves have been developed as the best fit curves to the experimental data [Chopra, K., and Shack, W. J., 2003].

2.5 TANK RESEARCH

A number of researchers have worked on various aspects of tank design and analysis. The current section discusses the works that are relevant to the proposed research.

Zick and McGrath [1968] carried out detailed theoretical studies to understand the stresses in the shell wall of cylindrical storage tanks and proposed the variable design

point method of shell design which was adopted by the API. In their study, they also considered the effect of bottom plate on shell stresses and concluded that both the restraining/resisting moment (offered by the bottom plate) and radial growth at the joint reduce the circumferential stresses in the shell near the bottom, but to a small degree. This implies that the higher the restraining moment, the (slightly) lower the stresses in the shell. Regarding the plastic hinges in the bottom plate, Zick and McGrath [1968] say *"where the resisting moment of the tank bottom is to be evaluated, a reasonable approach would be to use the full yielding moment in the bottom plate on one side for an earth grade foundation and to use two moments (one on each side) for a ring wall foundation."*

In their analysis, for the bottom boundary condition of the shell, they assumed a restraining moment equal to one yielding moment (M_P) of a bottom plate thickness (supposedly standard thickness, although the details were not specified) without any radial growth. This assumption will be conservative since occurrence of the second hinge will further reduce the stresses in the shell for the most part, which will be explained later in this report.

Denham, et al. [1968a, b], proposed a method to determine the restraining moment at the shell to bottom joint and the stresses in shell and bottom plate, when the stresses are elastic. The method is based on beam and shell theory and the derivation is based on the concept of establishing slope compatibility for the shell and bottom plate at the shell to bottom joint. The authors compared their theoretical data with actual strain measurements from an instrumented tank and stated that measured shell stresses

confirmed the validity of theoretical approach. In the annular plates, the theoretical calculations indicated that the stresses would reach yield close to the shell and this was also confirmed from the field data. But for locations away from the shell to bottom joint, the field data showed considerable variation. The theoretical model was not verified with numerical models like FEA.

Karcher (1978a, 1981a) proposed a method to find the stresses in the shell and the bottom plate for elevated temperature tanks. The method is based on the elastic shell theory for the tank wall and beam-on-elastic foundation theory for the bottom plate. It assumes that complete plastic hinges are formed in the bottom plate near the shell to bottom joint and that the shell stresses are elastic. This is justified since the tanks are constructed such that bottom plate is very thin compared to shell wall and, it is assumed that during loading the bottom plate completely yields and forms plastic hinge before the shell wall yields. The equations as given by Timoshenko [1959] for cylindrical tanks with clamped end conditions were suitably modified to have the plastic moment at bottom as the boundary condition instead of the clamped condition. The plastic hinge condition was adopted from the work by Zick and McGrath [1968]. A single plastic hinge is assumed for earthen foundation, whereas two hinges are assumed to form in case of concrete ring wall foundation. The recommendations by Karcher are included in API 650 [2012], Appendix M "Requirements of Tanks Operating at Elevated Temperatures" for evaluating the design cyclic life of tanks.

Jones and Seshadri [1989] studied the validity of Karcher's equations using linear finite element method and found them to be satisfactory in predicting the stresses in shell.

They concluded that Karcher's analysis based on a single plastic hinge is conservative for deflection and fatigue life estimates. The authors opined that, to properly assess the formation of plastic hinges in the annular-plate, a pseudo-elastic analysis be carried out by modeling the subgrade. The authors have used a pseudo elastic tank wall model to compare the stresses with Karcher's theory, i.e., plastic moments are applied at the tank bottom as shown in Fig.2.6 Though this will give a good understanding of the wall stresses for a given bottom moment, it may not reflect the exact way in which the hinges, if any, are formed in bottom plate and loads are distributed in the actual tank.

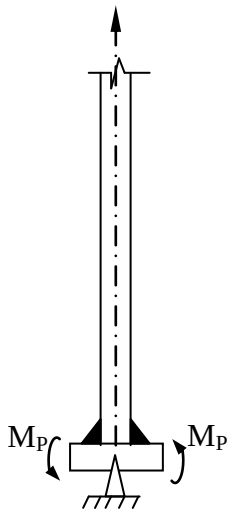

Fig. 2.6 Pseudo Elastic Tank Model

Wu [1996 and 2000] proposed a method similar to Denham's method but had taken into account the effect of elastic foundation beneath the bottom plate near the joint. The inside part of the annular plate towards the tank centre was considered as a semi-infinite plate flexibly supported by the foundation. The reaction force of the subgrade was assumed to be linear with the annular plate vertical displacement. He also compared the

theoretical results with field data. The author also commented that, based on the proposed method and Denham's model, the wider the width of the bottom plate that projects beyond the outer surface of the shell, the smaller is the maximum stress in the annular plate. However, guidelines to find the maximum projection length were not given. The other important aspect mentioned by the study was that in practice the shell is assumed to coincide with the centre line of the ring wall and hence the load from the shell acts on the centre line of the wall, but in actually the load gets applied at the peripheral point of the annular plate causing eccentricity in load application. This was also confirmed from field data on the soil pressure beneath the ring wall. The study did not report any numerical analysis to compare with the field data and the proposed theory.

Kim, et al., [2009] studied failure of oil storage tank due to crack in the fillet weldment between the reactor shell and annular plates. Failure studies such as fractography, tensile test, hardness test, corrosion test and chemical analysis were performed. They conclude that although cracks were initiated by corrosion, failure was generated by propagation of crack caused by stress concentration. It was recommended that the local stresses be reduced by improved weld toe geometry and reinforcement be used to reduce the stress concentration.

Chen, et al., [2007] proposed a simplified long-short shell method to determine the stresses in multiple layer shell wall. The classical short shell method as proposed by Timoshenko and others is cumbersome when the number of layers are more, while the long shell method is simple but the results are erroneous near the joints. Hence the authors have proposed a model in such a way that, the first shell is regarded as a short

shell while the others are long cylindrical shells. The authors support the results by comparing the field measured strain data from a 150,000 m^3 oil tank during its hydro static test.

2.6 FITNESS FOR SERVICE

In the case of above ground storage tanks, a typical tank may cost in the millions of dollars to construct/replace and a substantial portion of that would be needed for repair and rehabilitation [Andreani, et al., 1995]. In addition to the cost, issues concerning logistics, environmental impact, effect on the process cycle due to out of service tanks, safety permits, etc., cause huge losses in resources and time that cannot be exactly accounted for. If the tank fails by flooding, explosion, etc., it creates a severe impact on the environment and the surrounding community. It sets in a series of crisis like situations at multiple levels adversely affecting the lives of the population [Comfort, et al., 1989]. Hence, periodic inspection of the tanks for structural health and safety is a part of the engineering duties. The engineer is expected to periodically monitor the structural health and integrity, asses the degradation and take decisions regarding repairs/replacement. Fitness for service assessments are the primary methods to do the task. They are quantitative and qualitative engineering evaluations performed to demonstrate the structural integrity of an in-service component containing damage, determine the remaining life of degraded components and make run/repair/replace decisions.

Common reasons for assessing the fitness for service of equipment include the discovery of a flaw such as a locally thin area or crack or corrosion, settlements, failure to

meet current design standards, and plans for operating under more severe conditions than originally expected. Fitness for service assessment applies analytical methods to evaluate flaws, damage, and material aging. The analytical methods are based on stress analysis, but they also require information on equipment operations, nondestructive examination (NDE), and material properties. Stress analysis can be performed using standard handbook or design code formulas or by means of finite element analysis (FEA), which is increasingly becoming more common. The main results of the assessment are (1) a decision to run, alter, repair, monitor, or replace the equipment and (2) guidance on inspection interval for the equipment. Engineers and tank users can take decisions based on engineering inputs, whether to carry out repairs immediately or at a later time or go for immediate replacement. Fitness for service assessment requires both knowledge of past operating conditions and a forecast of future operating conditions. American Petroleum Institute (API) codes of practice API 579-1/ASME FFS-1/653 provide a detailed procedure for assessing fitness for service in tanks.

2.6.1 Levels of FFS Assessment

Three Levels of assessment are provided in API 579-1/ASME FFS-1 [2009] standard. In general, each assessment level provides a balance between conservatism, the amount of information required for the evaluation, the skill of the personnel performing the assessment, and the complexity of analysis being performed. Level 1 is the most conservative, but is easiest to use. Practitioners usually proceed sequentially from a Level 1 to a Level 3 analysis (unless otherwise directed by the assessment techniques) if

the current assessment level does not provide a clear result, or a course of action cannot be determined.

Level 1 Assessment

The assessment procedures included in this level are intended to provide conservative screening criteria that can be utilized with a minimum amount of inspection or component information. A Level 1 assessment may be performed either by plant inspectors or engineering personnel. The only load considered is internal pressure, and a single thickness with one or two surface area dimensions are used to characterize the local metal loss. Level 1 assessments are limited to components covered by a recognized code or standard which have a design equation that specifically relates pressure (or liquid fill height for tanks) to a required wall thickness. Hence it is not applicable for complex loading or damage conditions.

Level 2 Assessment

The assessment procedures included in this level are intended to provide a more detailed evaluation that produces results that are more precise than those from a Level 1 assessment. In a Level 2 assessment, inspection information similar to that required for a Level 1 assessment is needed; however, more detailed calculations are used in the evaluation.. More general loading is considered (e.g., net-section bending moments on a cylindrical shell), and rules are provided for the evaluation of local metal loss at a nozzle connection. Level 2 assessments would typically be conducted by plant engineers, or engineering specialists experienced and knowledgeable in performing FFS assessments.

The Level 2 assessment rules provide a better estimate of the structural integrity of a component when significant variations in the thickness profile occur within the region of metal loss. Hence a component that fails to be fit for service from Level 1 assessment can pass from a detailed Level 2. However, the Level 2 procedures still have some limitations regarding the component type, location of damage, loading and damage type that can be assessed.

Level 3 Assessment

The assessment procedures included in this level are intended to provide the most detailed evaluation which produces results that are more precise than those from a Level 2 assessment. In a Level 3 assessment, the most detailed inspection and component information is typically required, and the recommended analysis is based on numerical techniques such as the finite element method or physical testing when appropriate. Level 3 assessment rules are intended to evaluate components with complex geometries, regions of localized metal loss and/or components with details where only limited design rules are provided in the original construction code or standard. A Level 3 assessment is primarily intended for use by engineering specialists experienced and knowledgeable in performing FFS assessments. Since advanced numerical procedures are used for stress analysis, the limitations of level 1 or level 2 procedures are surpassed in this level.

2.6.2 FFS Procedures for Local Thin Areas

Damages due to corrosion/erosion in the form of blunt metal loss are a widespread problem in pressure vessels. Elaborate research had been carried out to

address the FFS issues due to locally thinned areas. These LTA damages can be global (over the entire area) or local (at certain locations). These damages are progressive and may or may not adversely affect the safety of the equipment at a particular instant. Hence FFS assessments are periodically carried out to evaluate the damages and ensure the required safety and serviceability of the equipment. The fitness for service procedures for wall thinning or metal loss is generally divided in to three categories:

1. General Metal Loss (GML)
2. Local Metal Loss (also referred to as local thin area or LTA)
3. Pitting

The objective of performing FFS assessment is to check for rupture, bulging and leakage. The procedures ensure that the corroded (or eroded) component has sufficient strength to resist applied loads and is sufficiently thick to prevent pinhole leaks. The rupture prevention is based on the concept of metal reinforcement, i.e., the weak thin metal area is reinforced by surrounding sound metal provided the thin metal area is not too large and leak prevention is ensured by keeping the remaining wall thickness above a minimum threshold.

The principal failure mode for a pressure vessel (including tanks) with LTA subject to constant internal pressure is plastic collapse [WRC 465, 2001]. Plastic collapse may be evaluated using elastic stress analysis, limit load analysis, plastic collapse analysis or using the concept of remaining strength factor. The remaining strength factor method has been adopted in API 579-1/ASME FFS-1 standard. It has proven to be

effective in several applications [WRC 505, 2005]. The method using limit analysis and remaining strength factor are reviewed below.

2.6.2.1 Limit Load Analysis

Limit analysis is a design philosophy used for designing mechanical components and engineering structures. The method is based on maintaining equilibrium of the structure at all stages of loading and thereby determining the safe load called the limit load just prior to plastic failure (unconstrained plastic flow) of the structure/component. It is the load, that triggers overall structural instability or plastic collapse, corresponding to a point in the load-displacement curve at which the rate of external work of applied load does not balance the rate of plastic dissipation [WRC 505]. Limit analysis offers a more realistic and economical design than the methods based purely on elastic analysis.

The limit load can be determined using analytical methods, detailed numerical procedures or simplified methods. The analytical procedures use the bounding theorems of limit analysis, while the numerical procedures employ the widely used finite element analysis (or similar methods) to determine the limit load. The analytical procedure will not be feasible for complicated structures and is restricted to simple geometry and loading. Hence, nonlinear FEA is a widely adopted and recognised procedure for detailed limit analysis. However, performing nonlinear FEA involves huge computing resources, time and expertise. Simplified methods derived from the basic limit theorems and variational plasticity concepts might be able to predict limit load using the much simpler

linear FEA. Limit analysis using simplified procedures can also be used in the fitness for service procedures for pressure vessels and tanks [Seshadri, 2004 & 2005].

2.6.2.2 The m_α- Tangent Method

Among numerous simplified procedures for estimation of limit load, this thesis adopted the m_α-tangent method developed by Seshadri and co-workers [e.g., Seshadri and Hossain, 2008]. The procedure is briefly reviewed here. Detailed explanation is provided in Chapter 7. The method is based on variational principles in plasticity and makes use of a statically admissible stress field based on linear elastic analysis. Limit load multiplier is a factor that scales the applied load proportionately to obtain the limit load. The m_α-tangent multiplier is a limit load multiplier that depends on the upper bound multiplier m^o and the lower bound multiplier m_L and can be expressed as

$$m_\alpha^T = \frac{m^0}{1+0.2929\,(\zeta - 1)} \tag{2.28}$$

$$\text{where } \zeta = \frac{m^0}{m_L}$$

The m^o depends on the 'reference volume' of the structure whereas the m_L is based on the magnitude of maximum stress in the structure. The reference volume is the part of the entire volume that actually participates in the plastic failure of the structure or component. Recently, Ahmad and Seshadri [2010] demonstrated the use of this simplified limit analysis procedure in FFS methods for damages in above ground tanks. The detailed review of the procedure is given in Chapter 7.

2.6.2.3 Remaining Strength Factor Method

The use of remaining strength factor (RSF) for the assessment of LTA in pressure vessels and tanks was proposed by Sims, et al., [1992]. The RSF factor is defined as:

$$\text{RSF} = \frac{\text{Collapse Load of Damaged Component}}{\text{Collapse Load of Undamaged Component}}$$

In API standards, the RSF is used to define the acceptability of a damaged component for continued service. The acceptability criteria can be quantitatively established in terms of plastic collapse load using RSF in combination with closed form solutions, limit analysis or elastic-plastic analysis depending on the complexity of the assessment. The RSF can be used to estimate the failure pressure at the plastic collapse or the reduced (or rerated) working pressure called the Maximum Allowable Working Pressure (MAWP) of damaged components. The failure pressure of the damaged component (P_f) is given by:

$$P_f = P_{fo}\,(RSF) \tag{2.29}$$

where, P_{fo} is the failure pressure of the undamaged component. Similarly, the reduced Maximum Allowable Working Pressure ($MAWP_r$) can be calculated as follows:

$$MAWP_r = MAWP\left(\frac{RSF}{RSF_a}\right) \quad \text{for} \quad RSF < RSF_a \tag{2.30}$$

$$MAWP_r = MAWP \quad \text{for} \quad RSF \geq RSF_a \tag{2.31}$$

where RSF_a is the allowable Remaining Strength Factor. It is a function of the allowable stress and the design criteria used in the original construction code. The API recommends

an RSF_a value of 0.9 for equipment in process services. If conservative design procedure with lower allowable stresses were used in the vessel construction, then a lower RSF_a value can be used.

2.6.3 API 579-1/ASME FFS-1 Metal Loss Assessment Procedure

Before any standardized procedures were introduced, regions of metal loss were assessed using thickness averaging techniques. In these methods, since the flaw depth is generally irregular and varies over the entire area, it is averaged over the flaw length (or width) and a uniform depth is assumed for that length of LTA. Assessment techniques were developed by Texas Eastern Transmission Corporation and AGA Pipeline research committee in the late 1960s and later incorporated in the ASME codes as B31.G method. Though the averaging technique is not accurate for complex damage profiles, it gives the most conservative results of all the proposed methods [Janelle, 2005]. This method forms the foundation for most of the local thin area assessments that are currently in use.

API Standard "Fitness for Service - API 579-1/ASME FFS-1, 2012" is a compendium of consensus methods for reliable assessment of the structural integrity of equipment containing identified flaws or damage. It provides standardised and technically sound consensus approaches. It is written as a Recommended Practice rather than as a mandatory standard or code and is to be used in conjunction with the refining and petrochemical industry's existing codes for pressure vessels, piping and aboveground storage tanks (API 510, API 570 and API653).

API 579-1/ASME FFS-1 uses modified thickness averaging rules as well as specific problem based procedures. This assessment method has two main classifications namely the Local Metal Loss and Global Metal Loss. The procedure has three levels of assessment as mentioned in Section 2.5.1

2.6.3.1 Data Requirements for Characterizing Metal Loss

Several non-destructive techniques are available to inspect the extent of the metal loss/leakage in tanks and pressure vessels. The choice depends upon the material, type of flaw, access to surface, availability, cost, etc. Some of the inspection techniques used in the process industry are visual examination, magnetic particle testing, radiographic testing, ultrasonic testing, acoustic emission testing and thermography.

Fitness for service assessments for wall thinning cannot be performed from thickness measurement at a single sample point. Usually ultrasonic thickness readings are measured in a grid with a minimum spacing equal to twice the nominal wall thickness of the vessel [Antaki, 2005]. The region of metal loss can be characterised by two thickness measurement techniques, namely point thickness reading (PTR) and critical thickness profile (CTP). PTR is random sampling of thickness measurement that can be used only if the variation in thickness readings is statistically small. The variation in the thickness reading is expressed using Coefficient of Variation (COV), which is defined as the standard deviation of a sample divided by the mean of the sample. If the COV of the thickness reading population minus the Future Corrosion Allowance (FCA) is less than 10%, then the metal loss can be considered as uniform over the area and hence the

average thickness value calculated directly from the population can be used for FFS calculations. If COV is not less than 10%, then critical thickness profiles are required to determine the average thickness value [API 579-1/ASME FFS-1, 2012].

The CTP is established using thickness reading from a measurement grid (Fig.2.7) with suitable interval to allow for accurate characterisation of the metal loss. In Fig.2.7., gridlines M1-M5 and C1-C7 represent the meriodional and circumferential inspection planes respectively. For most of the pressure vessels and pipe lines, the CTP should be established in both the meridional (longitudinal) and circumferential directions. But for atmospheric tanks, only the CTP along the meriodinal direction is required by the standard and hence the meriodional inspection planes are sufficient. The circumferential inspection planes are not required because the stress in the direction normal to the hoop is considered negligible and does not govern the design thickness calculation [API 579, 2012, pp.4-26]. After obtaining the thickness readings of individual locations in the grid, the CTP in the meriodional direction is established by projecting the minimum thickness point at each interval along the M1-M5 inspection planes on to a common plane. The detailed procedure to establish the CTP is given in API 579-1/ASME FFS-1 Cl.4.3.3.3. In Fig.2.7(b), t_c represents uniform wall thickness (after general metal loss resulting from corrosion, erosion, or both) away from the local metal loss, to be used in FFS assessment procedures and t_{mm} represents minimum measured wall thickness in the LTA.

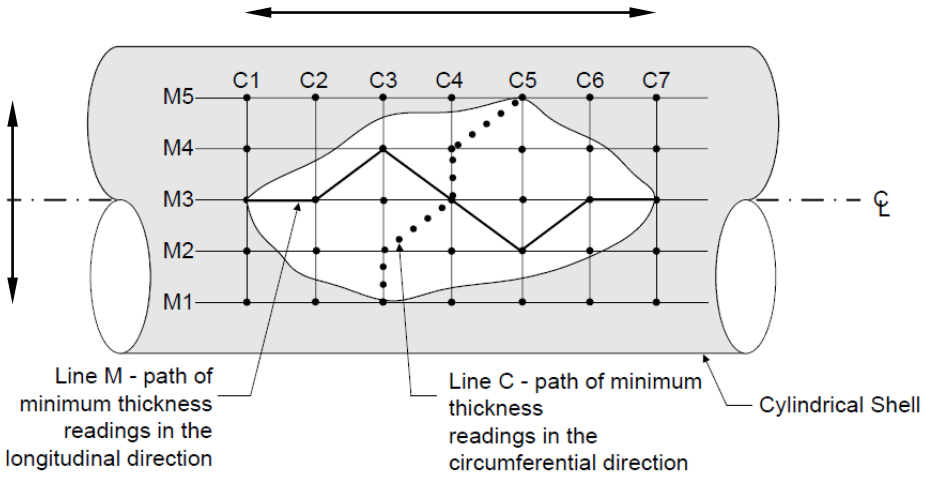

(a) Inspection Planes and the Critical Thickness Profile

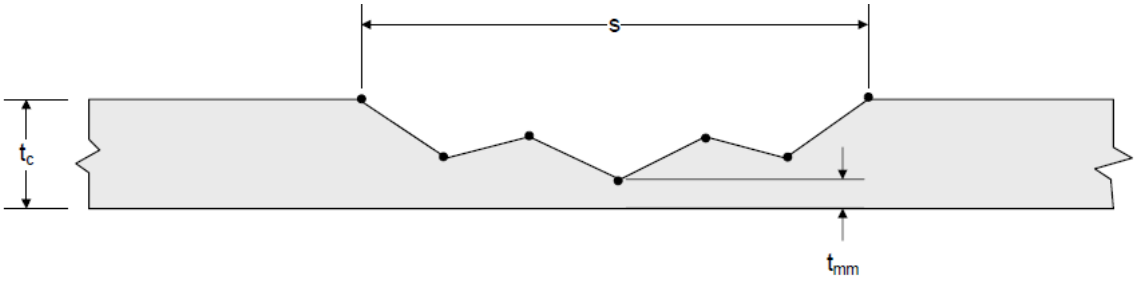

(b) Critical Thickness Profile (CTP) - Longitudinal Plane (Projection of Line M)

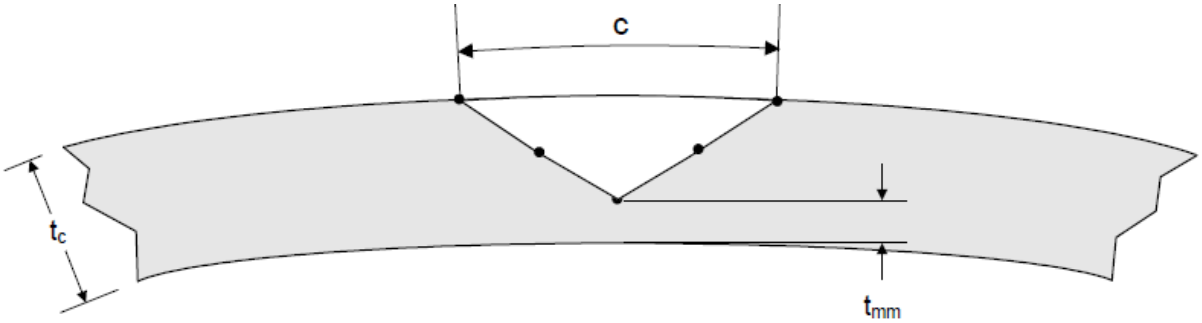

(c) Critical Thickness Profile (CTP) - Circumferential Plane (Projection of Line C)

Fig. 2.7 Critical Thickness Profile [API 579-1/ASME FFS-1, 2010]

After establishing the CTP, FFS procedures are used for three different levels of assessment. A detailed description of the LTA assessment is given in Chapter 7.

2.6.4 FFS Research for Locally Thinned Areas

Determination of fitness for service condition of damaged equipment is not yet an exact science [Janelle, 2005]. Researchers have continuously improved the safety and reliability of the FFS procedures using full scale burst tests, finite element analysis and statistical methods. The following is a brief list of research by various authors.

Folias, [1969, 1999] formulated detailed analytical expression to correlate stress field in flat and curved plates with finite crack. He extended the study and proposed analytical expressions to determine the state of stress near the crack tip in a spherical/cylindrical shell. Modified versions of the expression proposed by him are now widely used as “Folias factor” or “Folias bulging factor” in many fitness for service procedures involving LTA or crack like flaw. His theory is probably the most influential of the many available ideas.

Kiefner, et al.,[1973, 1989, 1990] has published a series of papers on LTA assessment in pipes. His work forms the basis of many FFS procedures that are in practice. He has reported experimental data from a large number of burst tests on pipes with LTA. He has made important contribution to the development of the widely used ASME B31.G, RSTRENG FFS criterion.

Kanninen, et al., [1991 and 1994] developed a theoretical model based on elastic shell theory to address the LTA assessment in pipes. The objective of the work is to

provide a theoretical basis to include combined loading cases which are not usually addressed by the empirical procedures used in practice. The authors expect that this approach provides the flexibility to reduce excess conservatism that is known to exist in B31.G guidelines.

Sims, et al., [1992] proposed the use of RSF factor for LTA in pressure vessels and tanks. The authors developed an empirical equation to conservatively estimate the remaining strength of spherical and cylindrical shells with LTAs by curve fitting the results obtained from elastic-plastic FEA. Additional criteria for acceptance of LTA were also presented. The results were compared with ASME B31G method prevalent at that time.

Stephens, et al., [1997] presented an overview, comparison and evaluation of acceptability criteria for LTA in cylindrical pressure vessels and pipes. Eleven different models were compared and evaluated against experimental database from the literature. The authors comment that although all the models have adequate safety, there is variability in predicting the failure and hence additional work is recommended to reduce the conservatism. The study also suggests which criteria are most desirable based upon adequate levels of safely and minimum levels of variability.

Chen, et al., [2000] proposed an empirical formula for obtaining the load carrying capacity of pressure vessels with two part-through defects. The article discusses the effects of the distance between the two defects on the load carrying capacity of pressure vessels. The authors conclude that their numerical results confirm the applicability of the simplified numerical method.

Janelle, et al., [2005, 2007] presented an extensive review on the technical basis of FFS procedures for global and local metal loss. Most of the existing procedures were compiled and statistically compared with burst test data to arrive at the most accurate method. A new method is proposed and guidelines were provided for standardizing the margin on calculated MAWP against failure pressure. The authors have recommended best practices to be included in API 579-1/ASME FFS-1 standard. The study is reported as welding research council bulletin [WRC 505].

Konusu [2009] proposed an assessment procedure for multiple volumetric flaws (locally thin areas). He comments that in the current practice as prescribed in ASME BPVC, BS 7910, API 579 and similar standards, multiple flaws are characterized as a single larger flaw enveloping the individual smaller flaws, which may provide unrealistic assessment in some cases. Hence a new assessment procedure is proposed in this article, which is based on the interaction between differently sized flaws.

Mukaimachi [2009] proposed a simplified evaluation procedure for locally thinned areas under plastic condition in cylinders. It is based on the IBARAKI FFS procedure where the internal pressure and external bending moment are considered simultaneously in the cylinder using the pressure and moment interaction diagram to predict the plastic collapse. But, since this method has limitation with respect to flaw depth, it cannot be applied to deep flaws. This paper proposes a solution to include deep flaws. The author validated his work by comparing it with nonlinear FEA results.

Seshadri [2004] used shell equations to obtain decay length in circumferential direction and proposed a Level 2 FFS assessment for hot spots based on elastic analysis

and the m_α – method. The localized effect of discontinuities on the cylindrical shell is discussed and the concept of reference volume is introduced as the "kinematically active" portion that participates in plastic action. The reference volume is defined by using a characteristic length called "decay length" for local load effects on the cylinder. In order to verify the evaluation assessment, inelastic finite element analyzes were carried out on the basis that the maximum strain is limited to 1%.

Indermohan and Seshadri [2004] proposed a Level 2 FFS methodology for evaluating corrosion in cylindrical shells. Thin cylindrical shells with radius to thickness ratio of about 50 subject to internal corrosion of various sizes were studied. The remaining thickness ratios were taken as 0.9, 0.8, and 0.6. The results were compared with inelastic finite element analysis results. It was concluded that the RSF obtained were conservative and compared to nonlinear FEA results. The work was later extended by Ramkumar and Seshadri [2005] to a thicker cylindrical shell with radius to thickness ratio of around 30 with either internal or external corrosion.

Tantichattanont, et al., [2006a, 2006b, 2007a, 2007b, and 2009] presented three methods of Level 2 FFS assessment for thermal hot spots and corrosion damages in cylindrical/spherical pressure components. They were based on variational principles in plasticity, the m_α method, reference volume and the concept of decay lengths in shells. The study proposes decay lengths for cylindrical shells subject to local forces, in terms of shell geometric properties. The decay length in circumferential direction was different from the earlier studies. The extent of "local" damage in cylindrical shells and interactions of damage effects in longitudinal and circumferential directions of the shells

were investigated based on these decay lengths. The stretching and bulging effects due to damage were studied.

Seshadri and Hossain [2008] developed the m_α-tangent method, an extension of the m_α-method, to predict the limit load for a general class of mechanical components and structures. Based on the m_α-tangent method they have also presented a Level 2 FFS procedure (as per API 579-1/ASME FFS-1) to evaluate thermal hot spot and corrosion damage in pressure vessels and piping systems [Hossain, 2009]. The authors report that the proposed procedure provides reasonably accurate estimate of the remaining strength of ageing pressure components. It was compared to the results obtained Level 3 inelastic FEM based FFS procedures.

Ahmad and Seshadri [2010] proposed a level 2 FFS procedure for structural integrity assessment of storage tank with LTAs in tank wall. The authors proposed two methods based on m_α-tangent multiplier to determine the RSF, the first one was an analytical method involving limit load multipliers and the second one was based on elastic finite element analysis. The study is an initial step in the use of m_α type methods for tanks. Even though the article claims the applicability of the method; the results were comparatively limited to small LTAs in smaller tanks. Also the entire volume was taken as the reference volume for the method using LEFEA. It is further discussed in Chapter 7.

Peng, et al., [2011] studied about multiple wall thinning defects in pipes. The interaction of multiple LTAs under different geometric arrangements, loading conditions

and depth ratios were studied. An index based on the limit load from twice elastic slope procedure was presented to define the interaction effects quantitatively.

American Petroleum Institute's Standard - API 650 is the premier standard for tank design in North America. The standard establishes minimum requirements for material, design, fabrication, erection, and testing for vertical, cylindrical, aboveground, closed and open-top, welded storage tanks in various sizes and capacities for internal pressures approximating atmospheric pressure. This standard applies only to tanks whose entire bottom is uniformly supported and to tanks in non-refrigerated service that have a maximum design temperature of 93℃ (200° F) or less. Separate guidelines are given as an Appendix if the tank has to be designed for higher temperature of pressure. This standard provides procedures for design of tank shell (wall), annular plate, bottom plate, roof, nozzles, stiffeners, wind girders etc., Most of the work in the current thesis is geared towards evaluation of design procedures of this standard with a view to provide additional insights and improve the guidelines.

The European Standard EN 14015-2004 is the construction standard equivalent to API 650 with a similar scope. The applicability of this standard with respect to internal pressure and metal temperature is specified as 20 to 500 mbar and -40 to +300℃. This standard restricts the maximum design strength of tank material to be 260 MPa. Unlike API, this standard does not have any explicit equations or guidelines regarding design of elevated temperature tanks.

API Standard "Tank Inspection, Repair, Alteration and Reconstruction - API 653" [2009], is a post construction standard that provides minimum requirements for

maintaining the integrity of tanks after they have been placed in service and addresses inspection, repair, alteration, relocation, and reconstruction issues. This standard covers steel storage tanks built in accordance to API 650 (or its predecessor API 12C). It recognizes fitness-for-service assessment concepts for evaluating in-service degradation of tanks in a limited way. But API 579-1/ASME FFS-1, Fitness-For-Service standard [2012], provides detailed assessment procedures or acceptance criteria for specific types of degradation referenced in API 653 standard. When API 653 standard does not provide specific evaluation procedures or acceptance criteria for a particular type of degradation, API 579-1/ASME FFS-1 may be used to supplement or augment the FFS requirements in API 653.

The British standard BS 7910 "Guide to methods for assessing the acceptability of flaws in metallic structures" is equivalent to API 579-1/ASME FFS-1 addressing similar issues. For assessment of single LTA flaws, the BS 7910 provides general guidelines to assess remaining strength factor (similar to Residual Strength factor of API) based on the work by Batte, et al., [1997] and Fu and Kirkwood [1995]. The remaining strength factor is determined based on the strength of the remaining ligament in the LTA portion to prevent plastic collapse due to bulging. Since the guidelines provided are not exhaustive, it refers to the work by Sims, et al., [1992] for further details. It should be noted that Sims was responsible for developing the RSF acceptability criterion adopted in API 579 as well.

The literature review about FFS procedures given in this section gives the global picture of the research carried out in developing the general procedure for determination

of RSF in corroded pressure vessels. The objective of this thesis work is to improve the FFS procedure using m_α-tangent multiplier method. This approach is different from most of the earlier research works in this area. The use of m_α-tangent multiplier for FFS evaluations was proposed by Seshadri and coworkers. An attempt was made recently by Ahmad et al [2010] to use this technique for LTAs in tanks. Hence only the publications using this approach are critically reviewed here and others are presented to give an overall idea about the development of general FFS methods.

2.7 SUMMARY

The basic theories of mechanics pertaining to the area of this research work are briefly presented. The current thesis aims to re-evaluate and improve specific design aspects researched mainly by Karcher, Denham, Zick & McGrath, Seshadri, and Tantichattanont. Publications by these authors are critically reviewed. Even though, Zick and McGrath [1968] did a seminal work in tank design, their research is focussed on shell stresses and has limited results regarding bottom plate behaviour. Denham [1968] studied the bottom plate stresses without the influence of temperature or friction. His work had a fixed projection length of bottom plate beyond the tank wall. He did not consider the effect of changing this projection length. There could be beneficial aspects for such a study. Karcher [1978a, 1981a] was the first person to consider elevated temperature tanks systematically. He accounted for the restrained expansion using a reduction factor without clear guidelines for predicting its value. However friction forces were not directly considered by Karcher. This needs to be re-

evaluated to determine if friction can be included directly and if so, whether it will be easier than the current approach for estimating the expansion factor.

The fitness for service of pressure vessels and pipelines is a well-researched area for past several decades. The salient articles in the development of this area are briefly reviewed. Most of the assessment procedures till now are empirical in nature and hence there is a continuous attempt to improve the accuracy of these models. The widely used FFS standard API 579-1/ASME FFS-1 still has several limitations in its methods regarding the applicability to the type of component, damage, location, and loading conditions. Using LEFEA and simplified limit load procedures for Level 2 FFS procedures is a recent development in this area. The interest in this thesis work is to study the improvements in using m_{α}-tangent multiplier method with LEFEA for FFS assessments of tanks with blunt corroded patches.

CHAPTER 3

FINITE ELEMENT MODELING

This Chapter describes the Finite Element Model used to analyze the tank. A brief description of the material model, type of the elements used and their properties is provided. A summary of the contact algorithms used for modeling the friction interaction between the tank bottom plate and foundation is presented. Assumptions used in modeling and the solution control parameters for nonlinear analyzes are specified. The convergence issues faced and the solution procedure adopted are also described.

3.0 BASIC ASSUMPTIONS

For the studies described in this thesis, the finite element modeling was carried out using ANSYS software (ANSYS version 12, SASIP Inc., 2011). ANSYS is a multipurpose, commercially available finite element analysis software with inbuilt pre/post processors. The tank is modeled as an axisymmetric structure (Fig. 3.2) for cases when the overall behavior of the tank is studied, like the shell to bottom joint behavior or friction interaction at tank bottom. Tanks with quarter/half symmetry or no symmetry are modeled as 3D components when localized behavior is studied for LTAs. The foundation is generally assumed to be a concrete ring wall with suitable infill. The interface between the tank bottom and the foundation is modeled using contact elements to understand the influence of friction forces. The contact model has the capability to stick, separate, and

slide over the contact surfaces depending upon the forces developed. The friction coefficient between the tank bottom and the subgrade depends upon the characteristics of the sand used, level of compaction, presence of moisture and other factors. Friction coefficient values ranging from 0.3 – 1.0 are used in this thesis to check for worst case scenarios depending upon the type of analysis. In general, a coefficient of 0.3 is used unless mentioned otherwise. It is to be noted that the aim of this thesis is not to establish a proper friction coefficient value at the tank bottom. More importantly the findings from this research work are independent of the actual value of friction coefficient. The friction coefficient of 0.3 is only used as an example value to evaluate and compare the results from mathematical procedures with the numerical models.

The tank material is assumed to be A841M grade steel with Young's modulus of 200,000 MPa and Poisson's ratio of 0.3. The yield strength is 345 MPa with a product design stress of 194 MPa for operating pressure. For hydrostatic test, the value is 208MPa. For the nonlinear analysis, the constitutive relationship is taken as bilinear kinematic hardening (BKIN). This option as used in ANSYS assumes that the total stress range is equal to twice the yield stress, so that the Bauschinger effect is included. BKIN may be used for materials that obey von Mises yield criterion. The material behavior is described by a bilinear stress - strain curve starting at the origin and with positive stress and strain values. The initial slope of the curve is taken as the elastic modulus of the material. At the specified yield stress, the curve continues along the second slope defined by a tangent modulus. Elastic-perfectly plastic material model (Fig.3.1) is used for most of the analyzes except for cases where the material model is changed with a post yield

plastic modulus of 1000 MPa. SI units are used throughout the thesis. The stress and deformation data shown in ANSYS plots have units of MPa and mm.

For tanks with locally thinned area for FFS studies, plastic failure of the tank is assumed to have occurred when equilibrium (primary) plastic strain is 1%. In addition, 5% peak plastic strain condition is imposed as recommended by API. The peak stress is the highest stress produced locally in a region due to stress concentration caused by any structural discontinuity or some form of thermal stresses. The associated strain in that region is the peak strain. This approach is conservative and is consistent with the work reported by earlier researchers on FFS assessment of thermal hot spots and corrosion damage [Seshadri, 2004; Tantichattanont et al., 2008].

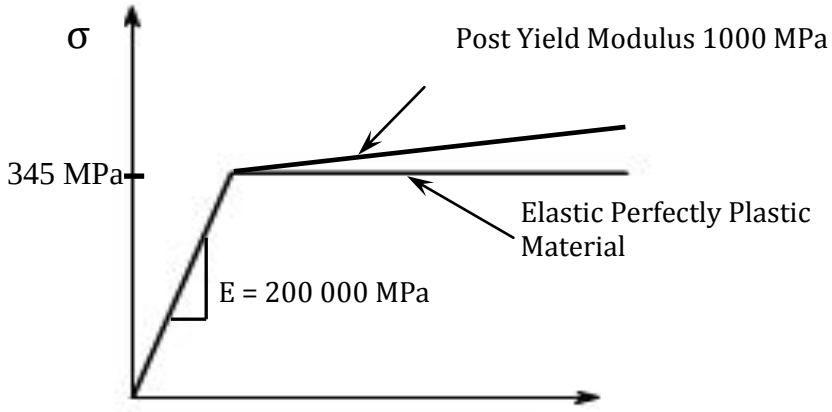

Fig. 3.1 Elastic - Plastic Material Model for Steel

3.1 MODELING USING PLANE AXISYMMETRIC ELEMENTS

Quadrilateral elements with four corner nodes with 2x2 integration points (PLANE 182) were used for the tank wall and bottom plate with axisymmetric option.

The bottom plate is modeled using flexible contact elements (Fig. 3.2), wherever applicable, concrete foundation is assumed to be rigid. The blue and red lines indicate the target and contact modules of the interacting friction model. There is no physical gap between the elements and the surfaces of bottom plate and the top of the foundation.

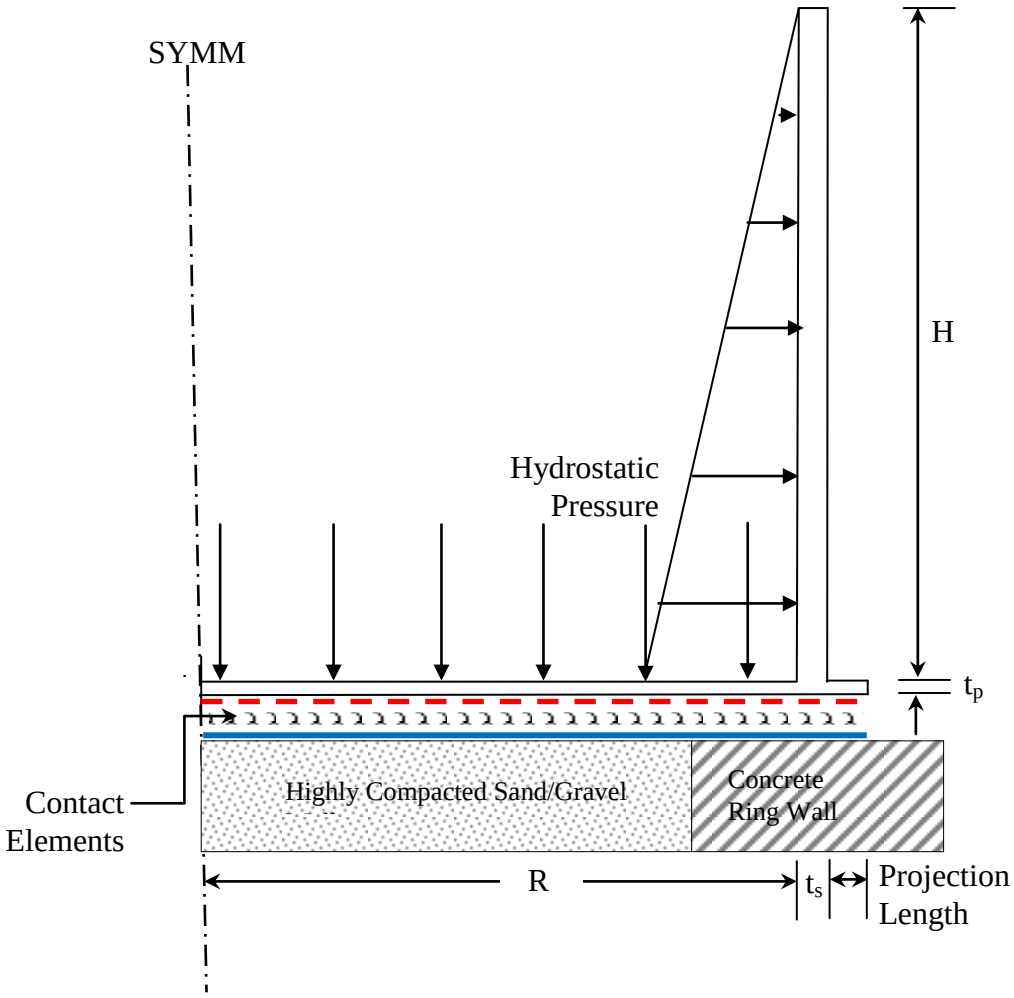

Fig. 3.2 Axisymmetric Tank Model (Not to Scale)

On performing the analysis with these assumptions, it was found that the solution does not converge easily. For the examples studied, the solution was found to converge without much difficulty if thicker bottom plates (say, 8 mm and above) were used (where

localized bending strain was reduced). For thinner plates (e.g., 6 mm), using four-node plane elements subjected to very high bending near the shell-to-bottom joint could result in shear/volumetric locking Volumetric locking is an overly stiff behavior that is due to incompressibility of plastic material. This occurs when plastic deformation is dominant. Shear locking causes the elements to be too stiff in bending (also known as parasitic shear), especially in thin members, or in elements with large aspect ratios. Shear strains (the change in the element angle at a node) for pure bending loads should be zero. Because a lower-order element can only have straight edges, the element angle at each node cannot be maintained when the nodes deform, inducing an artificial strain. Increasing the mesh density significantly and using higher order elements would reduce the problem. In order to compare the efficiency, some plane element models were solved with different conditions and element types. However such trials could not be used for the bulk of analyzes, since they took far too long to be completed.

Because the bottom plate tends to be very thin, to avoid shear locking a higher order 8 noded quadrilateral element (PLANE 183) with Mixed U-P option was used (Fig.3.3). The solution with this element converged well although it still took long to complete the analysis. The Mixed U-P (also called Hybrid, or Hermann) formulation solves the problem of incompressible material behavior by solving the hydrostatic stress (volumetric) as an additional degree of freedom. The stiffness matrix is broken up into displacement and pressure terms, and instead of solving just for the displacements, ANSYS also solves for pressure degrees of freedom for each element. Because the hydrostatic pressure in the element is a separate DOF, it is no longer dependent on

Poisson's ratio. The element has quadratic displacement behavior and is defined by 8 nodes having two degrees of freedom at each node: translations in the nodal x and y directions for axisymmetric models. Using these elements and fine tuning the friction model parameters, convergence was achieved even with 6 mm thick bottom plate.

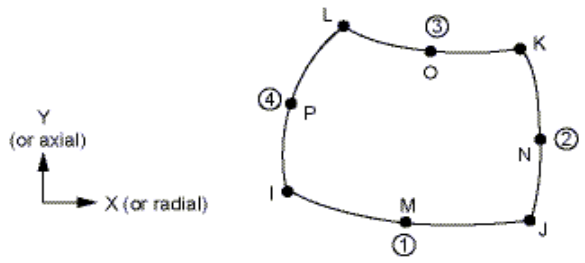

Fig. 3.3 Element Geometry for 8-Node Plane Element (PLANE 183)

The element may be used as a general plane element (plane stress, plane strain and generalized plane strain) or as an axisymmetric element. This element has plasticity, hyper elasticity, creep, stress stiffening, large deflection, and large strain capabilities.

3.2 MODELING USING SHELL ELEMENTS

Because of the inordinate amount of run time and other modeling issues associated with plane elements, modeling options using shell elements were considered for repeat analyzes (whereas detailed analyzes with plane 183 elements were reserved for typical cases and special problems). For the present problem with all types of nonlinearity and very high bending strain in a small portion, the element SHELL 209 was found suitable. It can be used for analyzing thin to moderately thick axisymmetric shell structures. It is a 3-node element with 3 DOFs at each node: translations in the X, Y direction (radial and axial direction), and a rotation about the Z-axis. A fourth

translational degree of freedom in Z direction can be included to model uniform torsion. When membrane option is used, the rotational degree of freedom is excluded. This element is well suited for linear, large rotation, and/or large strain nonlinear applications. Fig. 3.4 shows the geometry, node locations (I, J, K), and element coordinate system for this element. For material property labels, the local x-direction corresponds to the meridional direction of the shell element. The local y-direction is the circumferential direction. The local z-direction corresponds to the through-the-thickness direction.

As a first step, the tank wall was assumed with fixed boundary condition and modeled with shell elements. The results were verified using a similar model with PLANE 183 elements and found to be matching. Later, the tank wall was modeled using a hinged joint with a moment equal to the plastic moment of the bottom plate. This exercise was done to verify the validity of Karcher's model [Karcher, 1978a, 1981a] without changing any of the assumptions involved. The results from these analyzes are discussed in Chapter4.

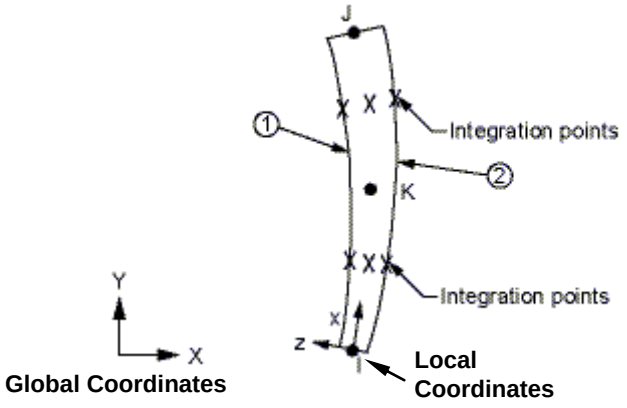

Fig. 3.4 Geometry of Axisymmetric Shell Element (SHELL 209)

The tank bottom was modeled using the contact elements between the bottom plate and the foundation. Figure 3.5 shows the deflection profile of a tank modeled using shell elements and subjected to both temperature change and hydro static load.

When elastic-perfectly plastic material models were used for the material, there were convergence issues due to localised yielding near the shell to bottom joint which was overcome by increasing the mesh size and number of layers in the element. In general the analysis was carried out using up to 7 integration points across each layer. Multiple layers were used along the thickness when needed. A macro was developed in ANSYS to incorporate decay lengths in the post processing analyzes and extract stress values from different layers of the shell element, if needed.

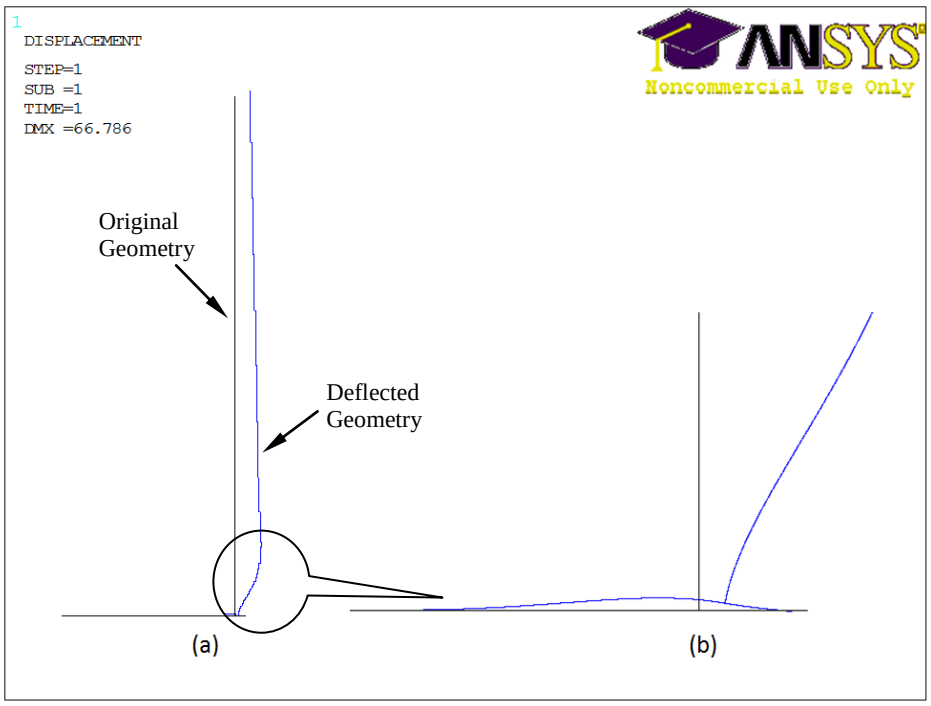

Fig. 3.5 Deformation Profile of a Tank Modeled Using Shell Elements

For fitness for service studies, quarter or half symmetric models were used with SHELL 281 element (Fig.3.6). It was suitable for analyzing thin to moderately-thick shell structures. The element has eight nodes with six degrees of freedom at each node: translations in the X, Y, and Z axes, and rotations about the X, Y, and Z-axes.

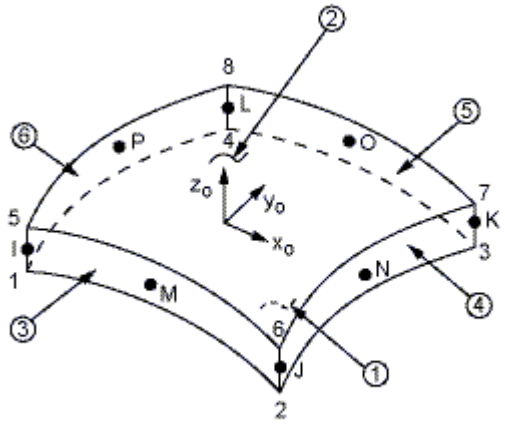

Fig. 3.6 Eight-Node Shell Element (SHELL 281)

Even though the PLANE elements took more computational time, the main advantage of using them (rather than SHELL elements) is that the model clearly shows the yielding behavior, formation of plastic hinges and stress/strain profile across the plate thickness. The results for stresses are straigthforward to interpret. Shell elements need much less computation effort and have less convergence problems compared to plane elements. However, shell models need a fair bit of post processing in order to interpret the results.

3.3 CONTACT ELEMENTS

Contact problems are highly nonlinear and require significant computer resources. They present two significant difficulties. Firstly, in general the regions of contact are not known until the problem is analyzed. Depending on the loads, material, boundary conditions and other factors, surfaces can come into and go out of contact with each other in a largely unpredictable manner. Secondly, most contact problems need to account for friction. There are several friction laws and models to choose from and all are nonlinear. Frictional response sometimes becomes chaotic, making solution convergence difficult. In addition to these two difficulties, many contact problems must also address multi-field effects, such as the conductance of heat, etc. [Ansys Contact Technology Guide, 2009]

Contact elements can be grouped into four general categories based on increasing levels of sophistication or complexity: Point-to-point gap elements, Point-to-line (or slide-line) contact elements, Point-to-surface contact elements, Surface-to-surface contact elements. For the present work, surface to surface element CONTA172 is used as the contact source element and TARGE169 is used as the contact target element.

TARGE169 (Fig. 3.7) is an element used to represent various 2-D "target" surfaces for the associated contact elements. The contact elements themselves overlay the underlying solid/shell elements describing the boundary of a deformable body and are potentially in contact with the target surface. This target surface is discretized by a set of target segment elements (TARGE169) and is paired with its associated contact surface

via a shared real constant set. Any translational or rotational displacement constraint can be imposed on the target segment element, if required.

CONTA172 (Fig. 3.8) is used to represent contact and sliding between 2-D target surfaces (TARGE169) and a deformable surface. The element is applicable to 2-D structural and coupled field contact analyzes. This element is located on the surfaces of 2-D solid elements or shell elements with mid side nodes that can be used with a specific set of elements that includes PLANE183 and SHELL 209, both of which are used for modeling the tank wall and base plate. The contact element has the same geometric characteristics as the solid/shell element face with which it is connected. Contact occurs when the element surface penetrates one of the target segment elements (TARGE169) on a specified target surface. Coulomb and shear stress friction is allowed. This element also allows separation of bonded contact to simulate interface delamination.

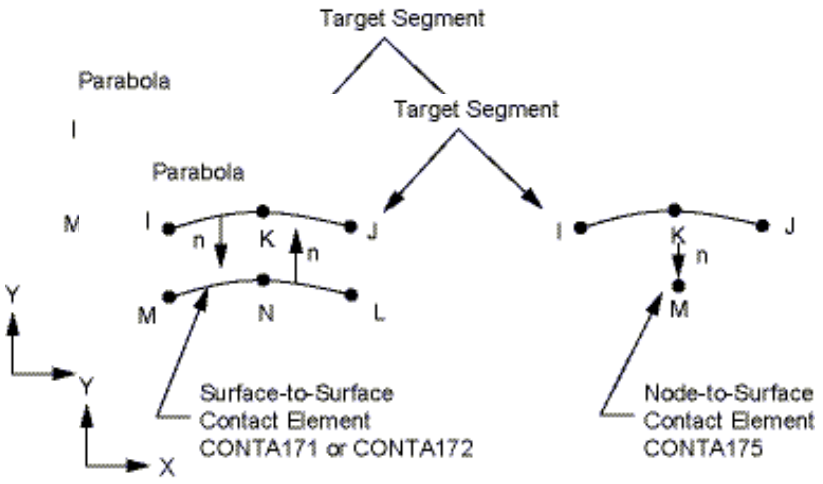

Fig. 3.7 Target Element Geometry [ANSYS Reference Manual, 2009]

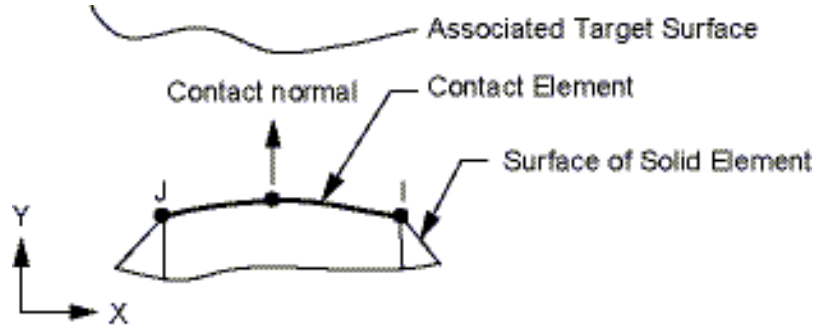

Fig. 3.8 Contact Element Geometry [ANSYS Reference Manual, 2009]

Figure 3.7 show that the normals ‘n’ of the contact and target surface should meet each other for the contact to happen. Hence the numbering of nodes and positioning of the normal should be appropriate for the contact to occur. The nodes must be ordered such that the target must lie to the right side of the contact element when moving from the first contact element node to the second contact element node. The 2-D contact surface elements are associated with the 2-D target segment elements (TARGE169) via a shared real constant set. ANSYS looks for contact only between surfaces with the same real constant set. For either rigid-flexible or flexible-flexible contact, one of the deformable surfaces must be represented by a contact surface. This element supports various 2-D stress states, including plane stress, plane strain, and axisymmetric conditions. The stress state is automatically detected according to the state of the underlying element.

3.3.1 Contact Algorithm

For surface-to-surface contact elements, ANSYS offers several different contact algorithms: Penalty method, Augmented lagrangian, Lagrange multiplier on contact

normal and penalty on tangent, Pure Lagrange multiplier on contact normal and tangent, Internal multipoint constraint. The details about these models can be found in any ANSYS reference manual. [ANSYS reference manual, 2009]

Initially many trial runs were performed with different types of contact algorithms and it was found that the augmented Lagrangian type is suitable. By default ANSYS uses the material property of the underlying elements to calculate appropriate contact stiffness and these values need to be tuned for proper convergence. Many guidelines and theoretical descriptions are provided by ANSYS and other sources for properly selecting the contact algorithms and contact parameters, reviewing all the literature is beyond the scope of current report. In the augmented Lagrangian method which is used here, the factors for the normal and tangential stiffness are required to be specified. The amount of penetration between the contact and target surfaces depends upon the normal stiffness, while the amount of sliding depends upon the tangential stiffness. Higher stiffness values decrease the amount of penetration or slip, but can lead to ill-conditioning of global stiffness matrix and hence cause convergence difficulties. Lower stiffness value can lead to greater amount of penetration and slip and hence the results may be erroneous. Even though ANSYS uses default values, some experimentation is necessary to determine an optimum stiffness and tolerance factors. In general, a low contact stiffness value is used in the beginning and the analysis is carried out with the fraction of the total load. Based on the resulting contact penetration/slip and the number of equilibrium equations, the normal/tangential stiffness is adjusted till penetration/slip is less the tolerance levels. Using this procedure, the appropriate stiffness and tolerance values for the tank were

determined after several trials. The Penetration Tolerance Factor (FTOLN) is kept at -0.02 and the Normal Penetration Stiffness Factor (FKN) value is kept at 1 for most cases and as 10 for a few situations. Table 3.1 gives the gist of element types used in this study and their associated characteristics.

Table 3.1 Element Types used in Finite Element Method

FE Model	Element type	Element Name	Analysis type	Objective of analysis
2D - Axisymmetric model	Shell	SHELL 209	Nonlinear Analysis with friction interaction at tank bottom	To study effect of friction, projection length and fatigue
2D - Axisymmetric model	Plane	PLANE 182/PLANE 183	Nonlinear Analysis with friction interaction at tank bottom	To study plastic hinge formations
3D- Half or quarter symmetry problem	Shell	SHELL 209	Nonlinear Analysis without friction interaction -i.e bottom fixed boundary condition	To study LTAs

These solution control values are extremely important in determining if an analysis will succeed or fail. If there are too few sub steps, the contact nodes may be driven through the target elements before ANSYS "realizes" it has happened. In this case the solution will resemble that of an analysis that didn't have contact elements defined at all. Therefore it is important to choose a relatively large number of sub steps initially to ensure the model is defined properly. The time step size must be small enough to capture the proper contact zone. The smooth transfer of contact forces is disrupted if the time step size is too large. Once everything is working, the number of sub-steps can be reduced to optimize the computational time. Also, if the maximum number of sub steps or iterations

is left too low, ANSYS may stop the analysis before it has a chance to converge to a solution.

3.4 ISSUES IN FEM MODELING

In the present work, modeling the problem includes material, geometric and contact nonlinearity. As modeled, it may take 3 to 4 days (in a dual core 2.4Ghz processor) with for a single detailed nonlinear analysis run. After several trials, many of the solution parameters were finalised. It was observed that the plane element model may need more than 1500 sub-steps for convergence to happen. Also, the storage space required for a single analysis was more than 30 Giga Bytes. Refining the meshes near the discontinuity increased the size of the problem. With the same condition of geometry and loading, for cyclic load conditions, it took almost a week to complete a single run. In case of tanks with both water and temperature load applied in a cyclic manner, it takes longer to complete the analysis. It should be noted that, separate thermal analysis is not necessary for the thermal stress case since the rise in temperature is uniform across the wall thickness and full depth of liquid. The assumption of uniform temperature rise is appropriate and it is explained in Chapter 6.

Since the tank wall, for the most part is predominantly a membrane structure governed only by hoop forces, the size of the mesh can be increased as the height increases from bottom. Similarly in the bottom plate, the portion away from the shell to bottom joint is not subjected to bending and hence doesn't need a refined mesh. It is not necessary to model the entire width of bottom plate from the centre to periphery; a major

portion of the bottom plate except for the small length near the shell is subjected to uniform pressure and is fully supported by the foundation. Hence there is very low stress in this region. This portion can be curtailed in the model which will considerably reduce the size of the problem. Studies were performed using models with full width and curtailed width of bottom plate and it was found that there was no significant difference in using this assumption, for the hydraulic load alone. However, in case of tank with thermal loading, the full length of the radius has to be modeled since the thermal expansion ($R\alpha\Delta T$) is the product of radius.

The other important issue observed was modeling the tip/periphery of the bottom plate using plane elements. As mentioned earlier, when the tank (with the standard 50 mm bottom plate projection) is loaded, the portion of the bottom plate below the shell lifts up, and the outer edge of the tank is supported by the foundation only at a single point. The concentrated application of reaction force locally at this point, results in very high strains and distorts the element shape (Fig. 3.9). The FE analysis sometimes fails to converge because of this reason. The alternatives used are (i) increasing the mesh density (ii) increasing the projection length and (iii) increasing the strength of the material near the tip. Increasing the mesh density helps to an extent, but the same problem arises at a higher load. Increasing the strength (Young's modulus) locally is not very effective, while increasing the projection length proved to be very effective (Fig.3.10). Apart from the above issues, modeling contact behavior as explained in the previous section is a laborious task that needs fine tuning several parameters.

The shell to bottom joint as shown in Fig. 3.10 is not modeled with weld details. The residual stress and the change in material property after welding are not included in the analysis. The residual stress effects are self-equilibrating and hence can only alter the load at which yielding starts, but not the final load at which the plastic hinges are fully formed. Ignoring the weld size increases the lever arm for moments slightly. This is conservative. Also, ignoring the slight increase in material strength due to the weld is likely to be conservative. On the other hand, welding would have an increase in stress concentration effect. This is addressed separately by API 650 in the fatigue evaluation equation (see Chapter 6).

3.4.1 Mesh Convergence Study

In order to reduce the size of the problem, different mesh sizes are adopted at appropriate locations. Seven different areas are used as shown in Fig. 3.11 which included areas for smoother transition of mesh size from fine to coarse or vice versa. Figure 3.12 shows typical areas where different mesh densities are adopted. The stress distribution plots at the shell to bottom joint for the hydrostatic load are shown in Fig.3.13 and 3.14. Limit load analysis is carried out by proportionately increasing the loading till material failure stops further increase.

For tanks with locally thinned areas, the LTA and the surrounding area is finely meshed while the element size is increased in the remaining area since hoop is the predominant force away from the LTA (Fig. 3.15). The von Mises stress contours of a typical tank with LTA are shown in Fig. 3.16. The von Mises stress at the time of failure (1% plastic strain) of LTA is shown in Fig. 3.17. If quarter model of a tank is used to

study the LTA, it must be ensured that the decay length [$6.3\sqrt{(RT)}$] should be less than one fourth of the circumferential length as explained in Chapter 7.

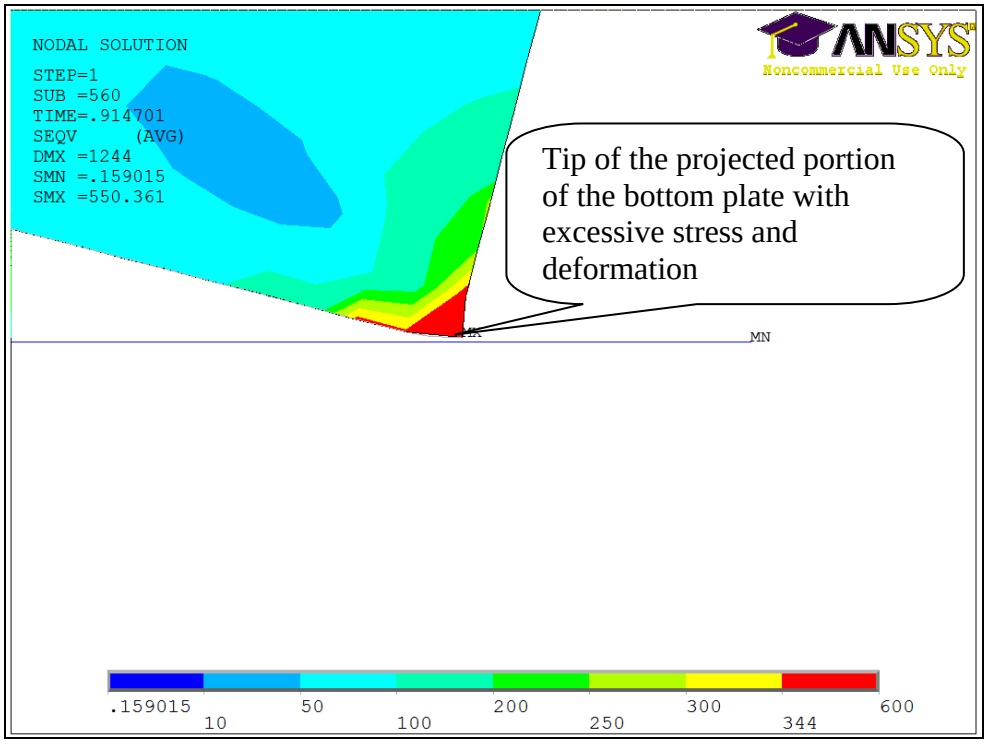

Fig. 3.9 Localized Deformation at the Bottom Corner of Bottom Plate

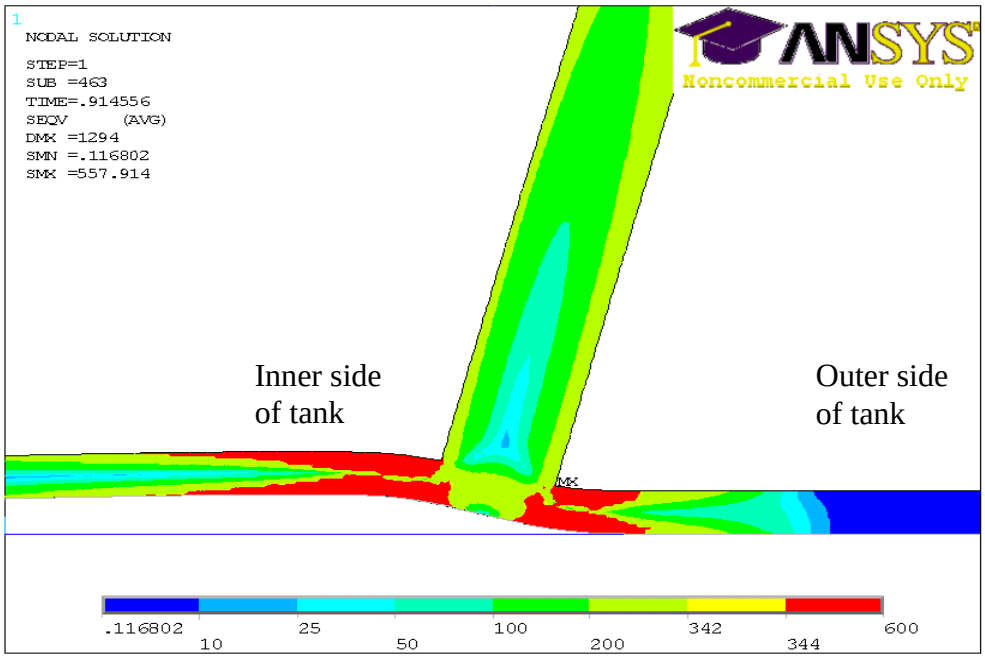

Fig. 3.10 Deformation in the Bottom Plate (with Extra Projection)

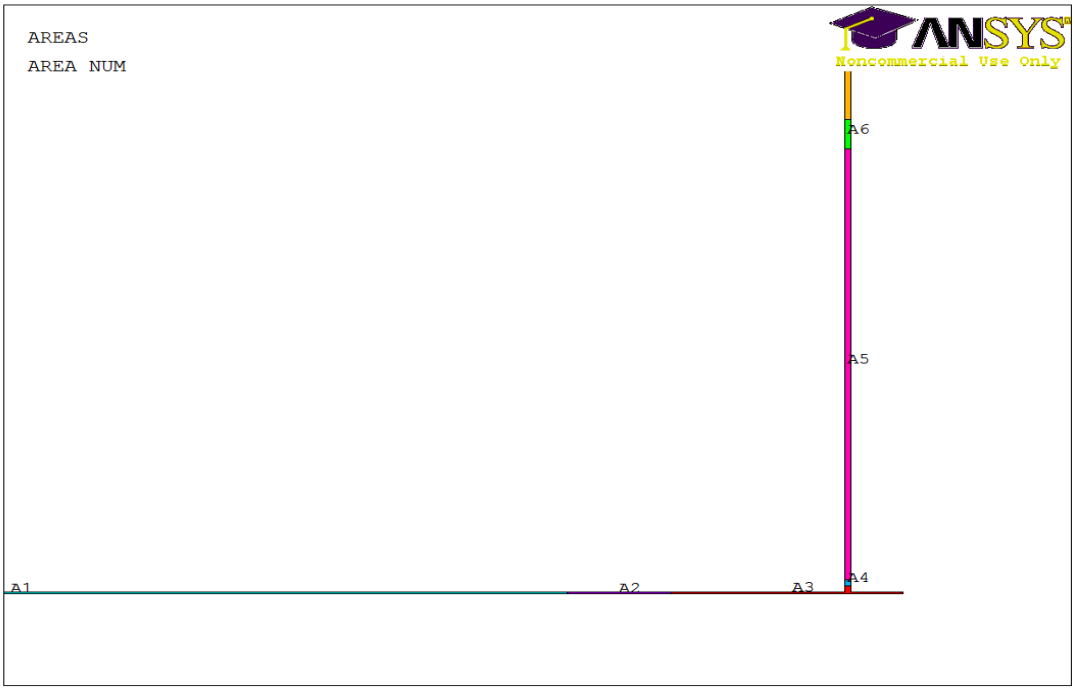

Fig. 3.11 Zones Specifying Different Mesh Densities

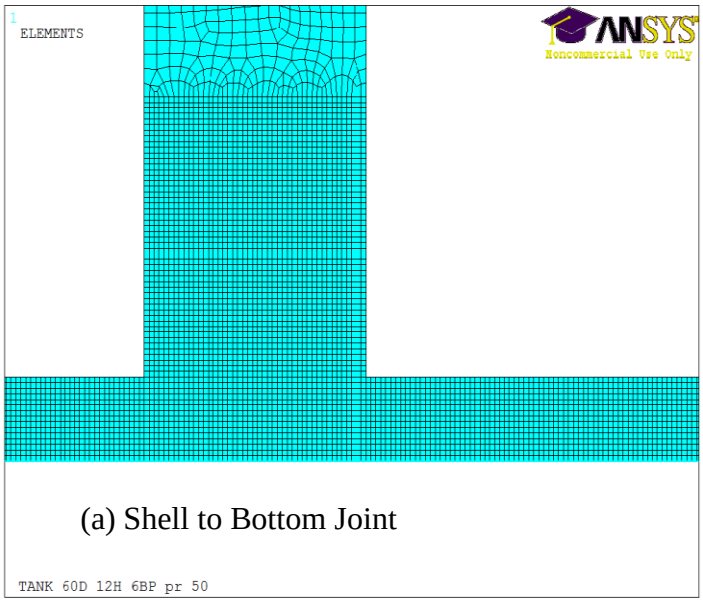

(a) Shell to Bottom Joint

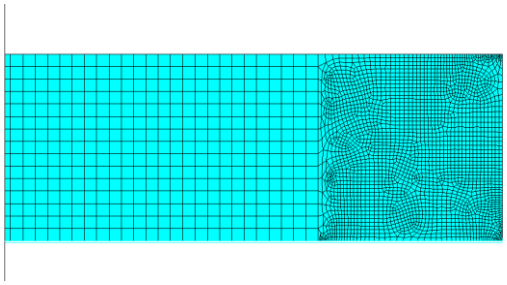

(b) Tip of Bottom Plate Projection

Fig. 3.12 Typical Mesh at Shell to Bottom Joint

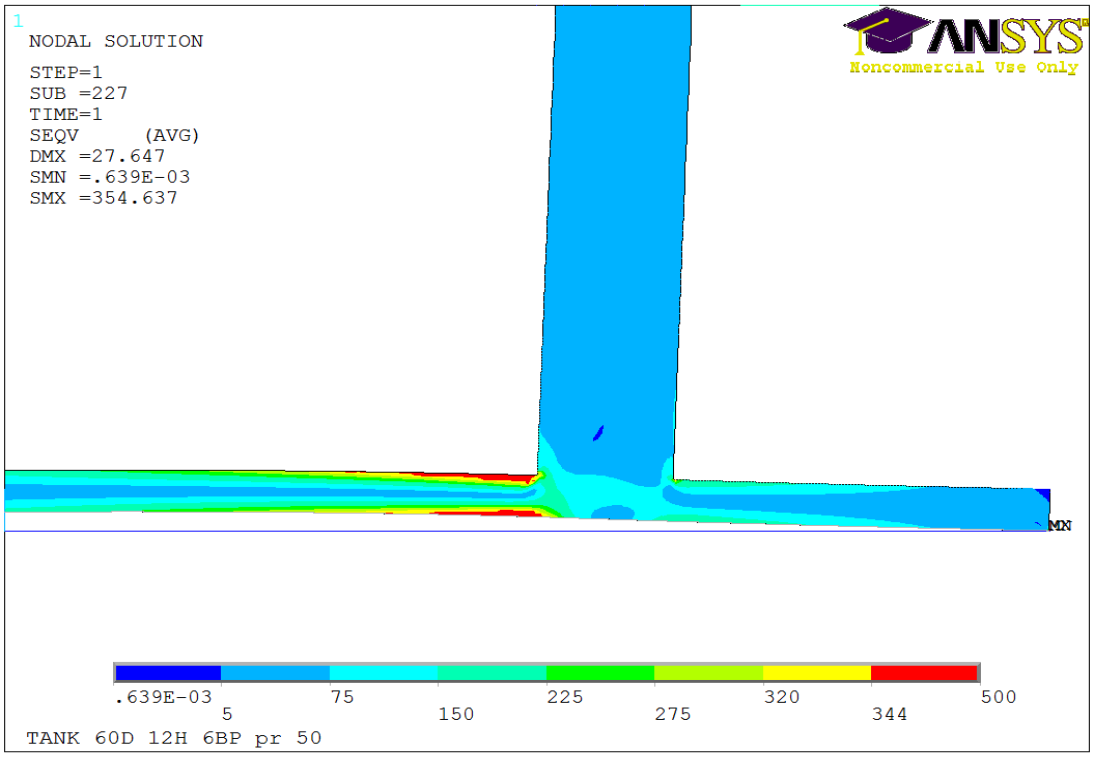

Fig. 3.13 Stress Distribution for Partial Plasticity

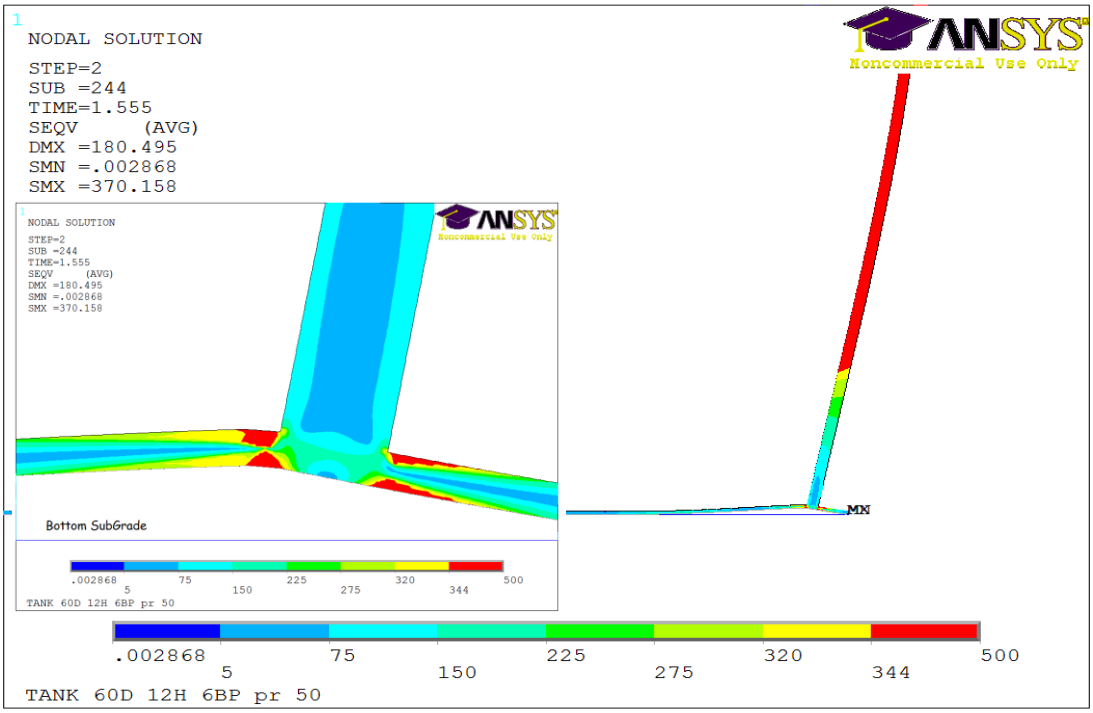

Fig. 3.14 von Mises Stress Distribution at Limit Load

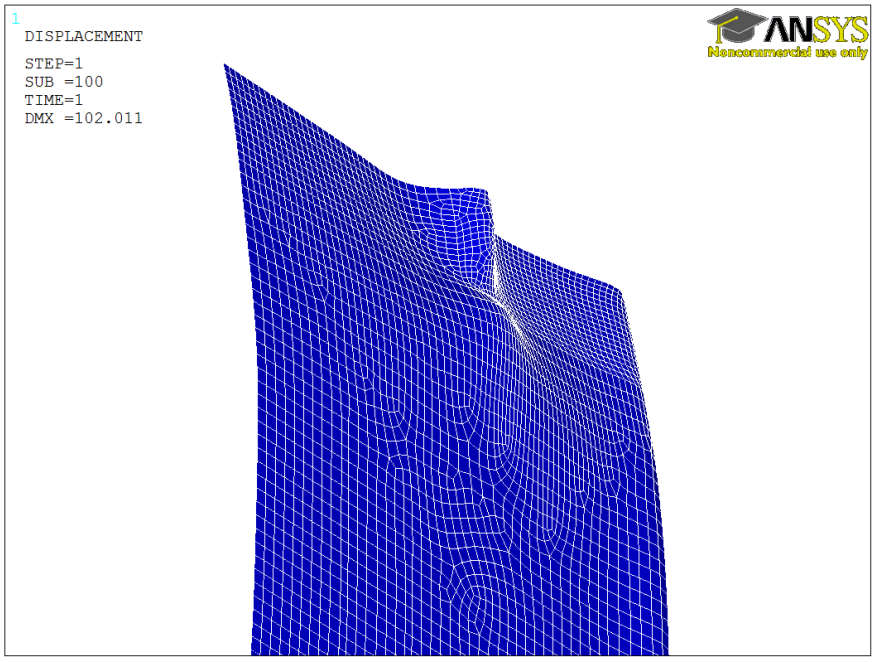

Fig. 3.15 Deformation Profile of Tank with LTA

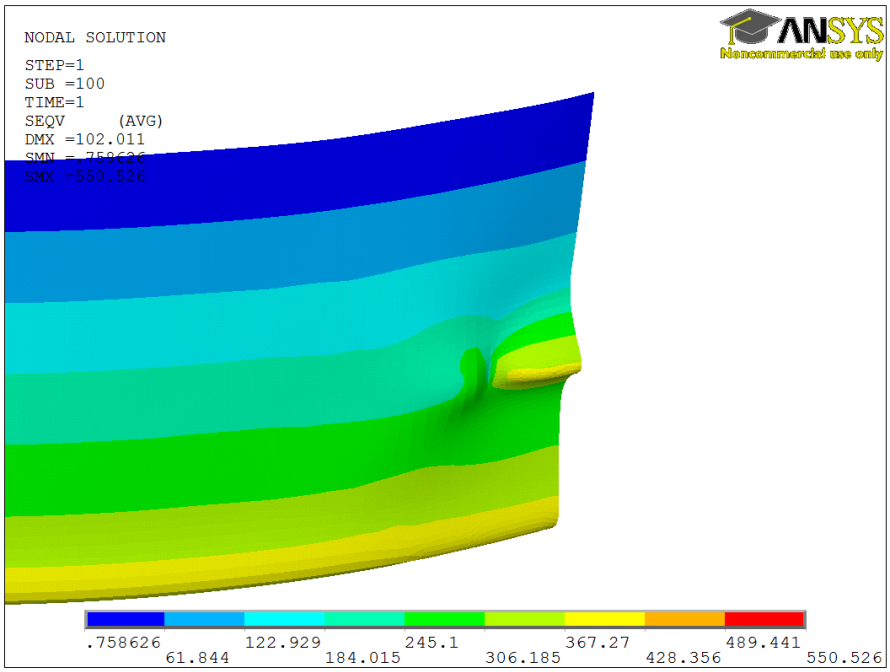

Fig. 3.16 von Mises Stress Profile of Tank with LTA

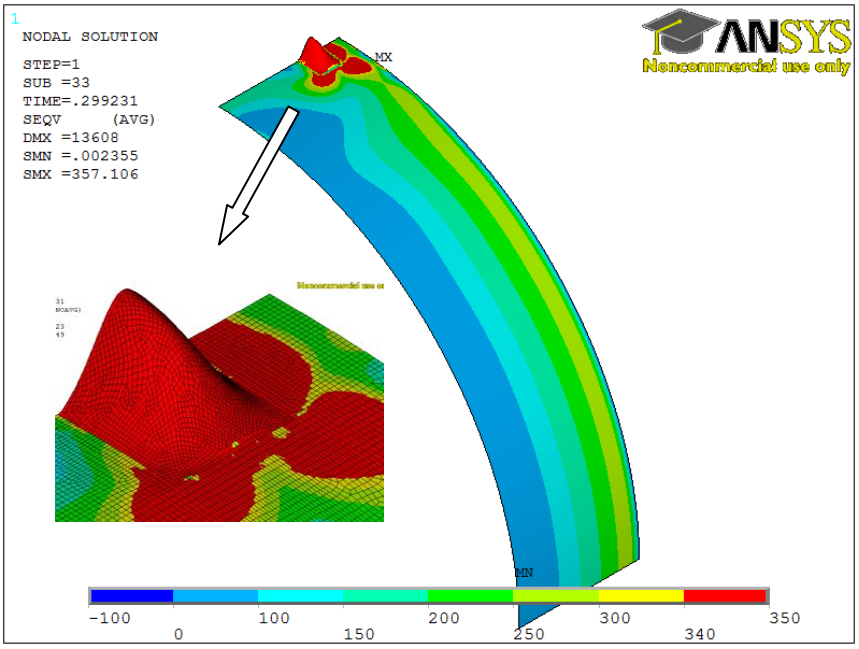

Fig. 3.17 LTA of Tank at Failure

3.5 DIMENSIONS OF TANKS USED IN THE ANALYSIS

The following details describe some of the different cases of tanks used in the present study. The dimensions of the tanks (Figures 3.18-3.20) are chosen such that they represent lower, middle and upper end of the design range for typical ASTs.

Case 1

Geometric Data:

Diameter	:	60,000 mm
Height	:	12,000 mm
Thickness of shell wall	:	18 mm
Thickness of Bottom plate	:	6 mm
Projection of Bottom plate	:	50 mm (Beyond shell)

Material Data:

Young's Modulus	:	200,000 MPa
Yield Strength	:	345 MPa
Product Design Stress	:	194 MPa
Hydro Static Test Stress	:	208 MPa
Density of liquid (water)	:	9.81 kN/m^3
Density of steel	:	77.1 kN/m^3
Poisson's ratio of steel	:	0.3

The required shell thickness is determined using 1-foot method as 18 mm (as prescribed in Clause 5.6.3.2 of API 650 [2012].

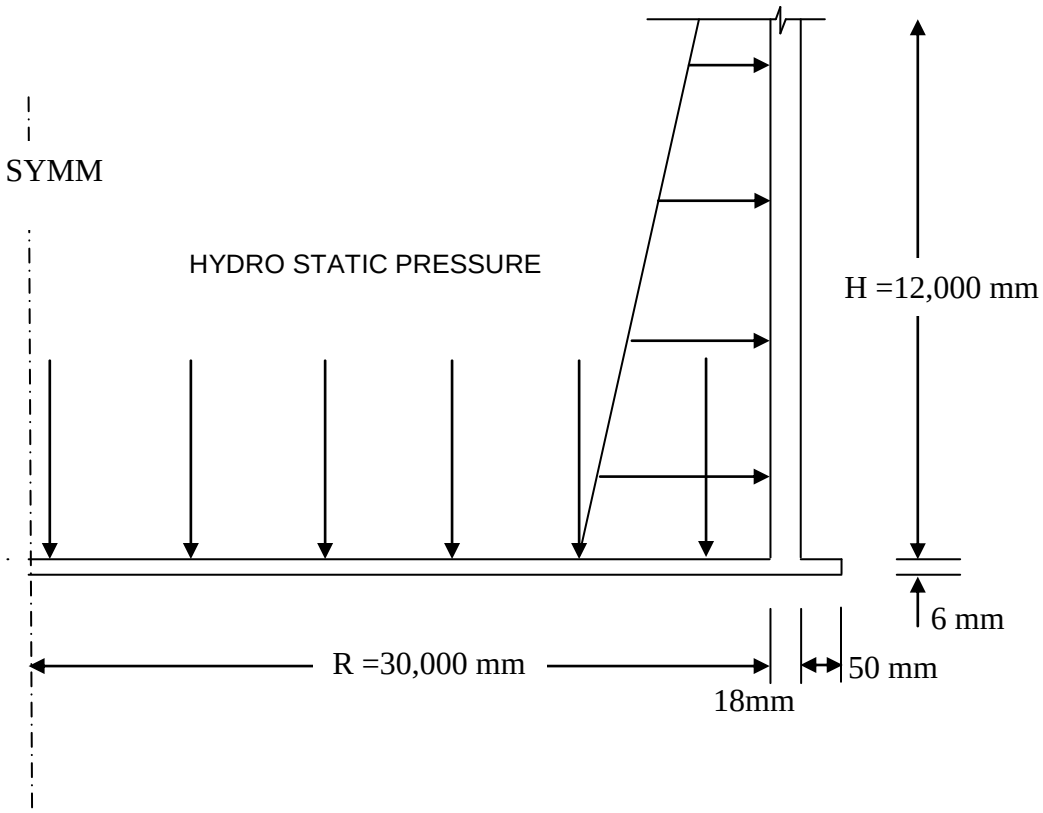

Fig. 3.18 Dimensions of Tank (Case 1)

Case 2

Geometric Data:

Diameter : 90,000 mm

Height : 16,800 mm

Required thicknesses of shell wall :

t_1	t_2	t_3	t_4	t_5	t_6	t_7
33.98 mm	31.33 mm	22.82 mm	18.46 mm	13.46 mm	10 mm	10 mm

The suffixes of "t" represent the successive shell courses from bottom.

Thickness of Annular plate : 14 mm

Width of Annular plate : 735 mm

Thickness of Bottom plate : 6 mm

Projection of Annular plate : 50 mm (Beyond shell)

Material Data : Similar to Case 1

The thicknesses of the tank wall obtained above are the values at the end of design run as described in Clause 5.6.4 of API 650 (variable design point method). It is not rounded off nor is the corrosion allowance added to it.

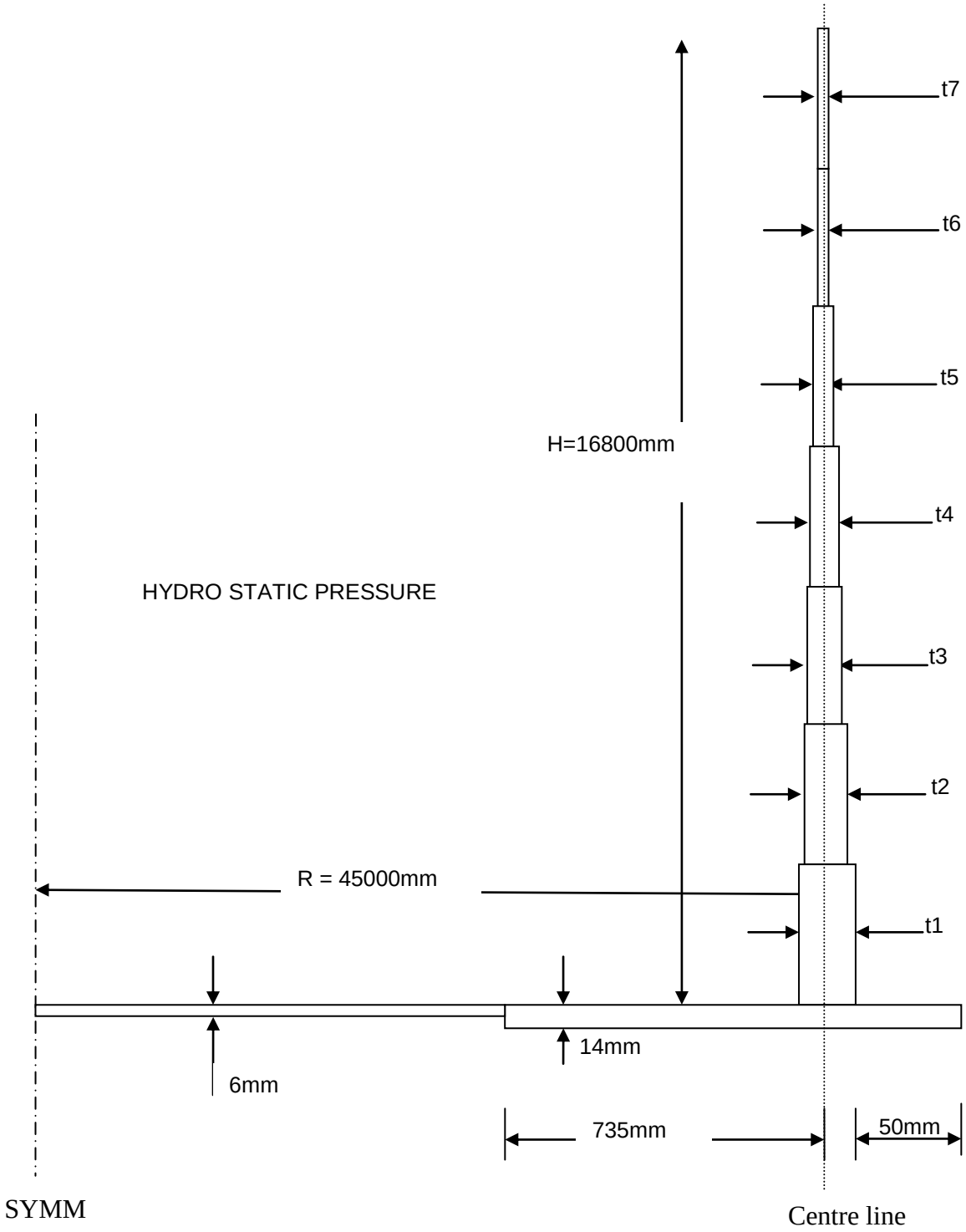

Fig. 3.19 Dimensions of Tank (Case 2)

Case 3

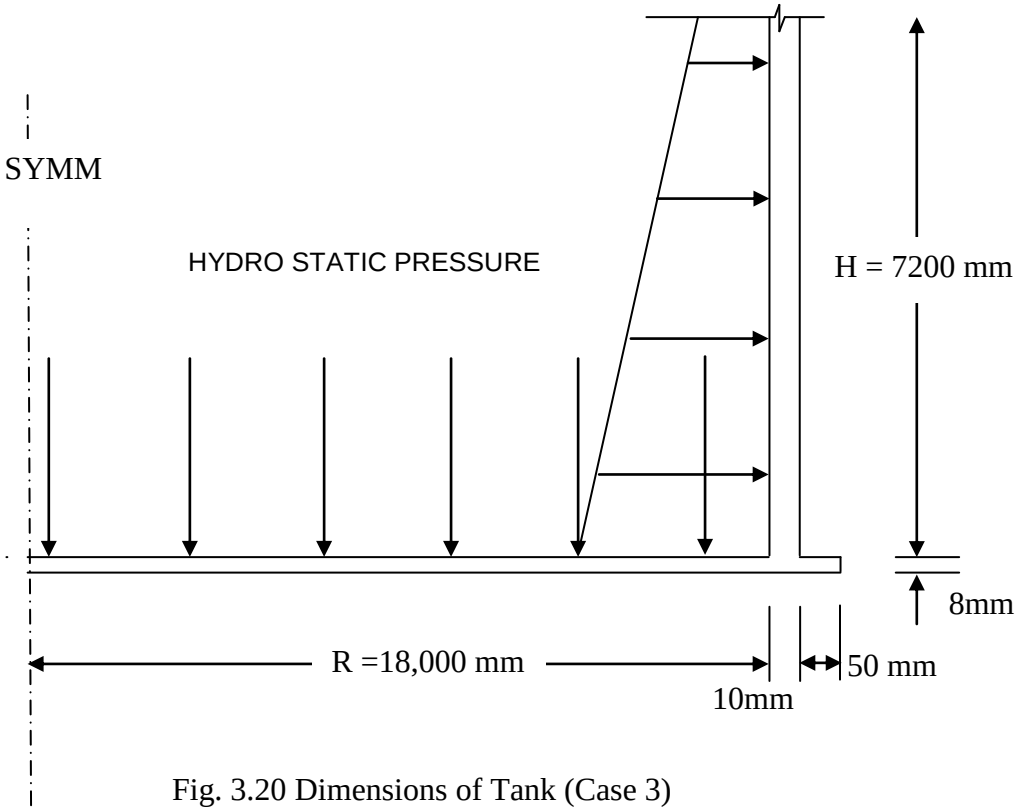

Fig. 3.20 Dimensions of Tank (Case 3)

Diameter	:	36,000 mm
Height	:	7200 mm
Thickness of shell wall	:	10 mm
Thickness of Bottom plate	:	8 mm
Projection of Bottom plate	:	50 mm beyond shell (also with variable projection lengths as explained in Chapter4)
Young's Modulus	:	200,000 MPa
Density of liquid (water)	:	9.81 kN/m^3
Density of Steel	:	77.1 kN/m^3
Steel Poisson's ratio	:	0.3

This tank is designed using the “Appendix A Optional Design Basis for small tanks” with an allowable stress of 145 MPa and joint efficiency factor 0.85.

3.6 SUMMARY

In the present Chapter, the finite element modeling of tanks is discussed. The details regarding elements used and the problems encountered during the analysis are given. A review of contact elements and the contact algorithms applicable to the present problem is provided. The details of finite element analysis and the interpretation of the results are given in the following Chapters. Typical tank dimensions, material and loading data used in the present research are included.

The FE model of the tank is initially checked with shell equations with fixed boundary conditions at the bottom. Later the friction interaction at bottom is introduced and the restraint friction deformation is compared with mathematical model developed in this thesis. In order to establish the validity of using axisymmetric model, comparisons were also made with half symmetry models. In order to achieve convergence, different types of contact algorithms and their modelling parameters were tried before finalising the model. For study of locally thinned areas the limits loads of damaged tanks from FEA and their corresponding RSF values were checked against the empirical RSF procedures prescribed by API 579 standard. The measures taken to optimise the mesh by zoning the cross-section are also presented. It is also ensured that local changes in the model for the sake of numerical stability do not affect the global behaviour of the tank.

CHAPTER 4

ISSUES WITH BOTTOM PLATE PROJECTION AT SHELL-TO-BOTTOM JOINT

This Chapter describes the importance of shell to bottom joint in tanks and studies the effect of bottom plate projection length at this joint. The beam model used by Denham, et al., [1968] to analyze the bottom plate is introduced and the FEM results to validate this model are presented. The effect of increasing the bottom plate projection length is studied both theoretically and numerically. The beam model is modified to determine the length of bottom plate projection needed for maximum effect. Nonlinear failure behavior of the tank, specifically near the bottom is studied using FEA. The formation of plastic hinges in the bottom plate on the inside and outside of this joint is discussed in detail.

4.0 SHELL-TO-BOTTOM JOINT

The cylindrical shell of the tank is designed for hoop stress while the bottom plate for the most part is a membrane without any structural function other than to act as a barrier between liquid and foundation. However, the shell to bottom joint is a critical location in many failure modes of the tank since the bending stresses in the bottom plate

are close to yield in most practical cases. The radial growth of the shell at the bottom is restricted because of the bottom plate. This induces discontinuity stresses near this joint. Even though the tank is basically designed for hoop stress, the bottom portion of the shell (approximately till a height of $(D\ t_s)^{0.5}$, where, D is the diameter and t_s is the thickness of the shell) is influenced by the bending stresses and the free radial expansion of the tank wall is realized only after this height [Long and Garner, 2004].

When the tank is filled with the liquid, the shell tends to rotate as shown in Fig. 4.1. The welded joint is constructed as a rigid joint (fillet weld on both sides with the requirements as specified in Cl.5.1.5.7 of API 650, 2010). Hence the bottom plate rotates to the same amount as the shell at the joint. This rotation could cause the bottom plate to lift off the foundation over a distance L as shown in Fig. 4.1, until the liquid pressure acting on the plate is sufficient enough to balance the uplift. The internal moment (M_o) causing the rotation in the plate is balanced by that in the shell. The magnitude of this moment depends upon the parameters R, H, t_s, t_b and the specific gravity of the liquid (G). In addition to these factors, the type of foundation directly beneath the tank shell and the temperature of the stored liquid influence the magnitude of this moment. The plate separation (uplift) from the foundation is especially significant for concrete ring walls and slabs. Because of this, the present Chapter assumes that the tank wall is resting on a foundation of high rigidity. Knowing the value of the bottom moment will help to determine the stresses in the shell and bottom plate.

The stresses in the shell to bottom zone are also influenced to some extent by the type of weld used (double fillet/full penetration). In the case of double fillet weld

(Fig.4.1), the stresses in the bottom plate will be high near the toe of the weld, whereas in full penetration weld the stresses will be high at the face of the shell. It is assumed that the latter case is slightly conservative because of the small increase in the lever arm. Hence it is adopted for the current work.

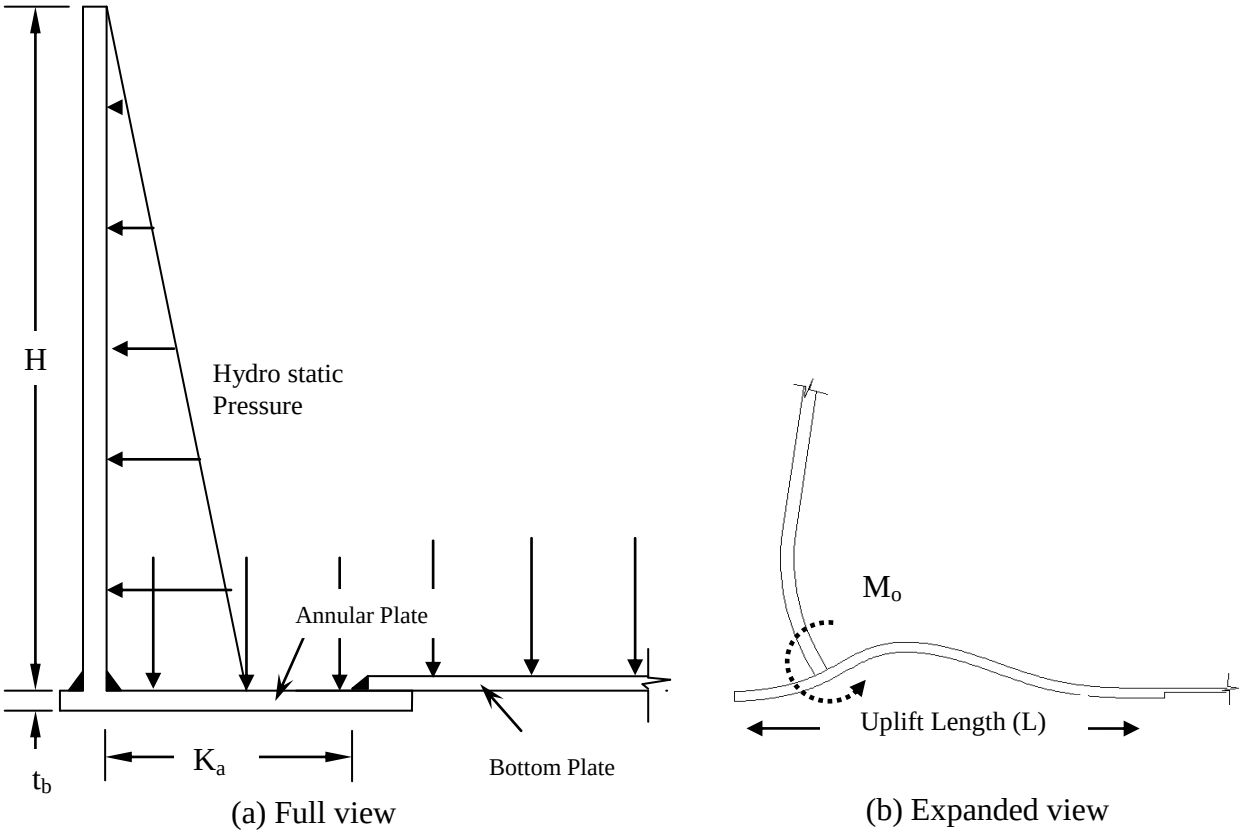

Fig. 4.1 Shell to Bottom Joint in the Tank

4.1 ANNULAR PLATE

As the bottom plate is subjected to very high bending stresses near the shell joint, in practice, the bottom plate close to the joint is made slightly thicker than the rest of the

plate and is sometimes called as annular plate (Fig.4.1). API 650 recommends the annular plate only if the local stresses near this joint will be substantial, otherwise the same bottom plate which is used elsewhere will be extended below the shell wall. Similarly, the width of the annular plate (K_a) as shown in Fig. 4.1, should be chosen such that it would be sufficient to assure that all bending stresses by the moment have damped out. This is based on the consideration that it is desirable to avoid bending in the conventional lap welded tank bottom construction [Karcher 1978 a, 1978 b, 1981a].

Various aspects of storage tank analysis and design with regard to tank wall and bottom plate had been studied by Zick and McGrath [1968], Denham et al.[1968a, b], Karcher [1978, 1981a, b], Jones and Seshadri [1989], Wu and Liu [1996, 2000], etc. Among them, Wu and Liu [1996, 2000] and Denham, et al. [1968a, b] proposed models to predict the stresses in the annular plate near the shell to bottom joint.

API 650 recommends the following formula for the minimum width of annular plate:

$$K_a = 215\ t_b/(G\ H)^{0.5} \qquad (4.1)$$

The minimum width formula recommended by API can be established by assuming that the annular plate behaves like a cantilever beam subjected to vertical hydrostatic pressure and determining the length required to form a plastic hinge at the shell-to-bottom joint [Jawad and Farr 1984].

$$M = w\ (K_a)^2/2\ \ ;\ S_Y = 4M/t_b^2 \qquad (4.2)$$

where, M is the moment at the shell to bottom joint (by assuming the annular plate as a cantilever beam), w is the liquid pressure acting above the annular plate, S_Y is the yield strength, t_b is the bottom plate thickness and G is the specific gravity. Rearranging Eq.4.2

$$K_a = \left(\frac{S_Y t_b^2}{\gamma G H} \right)^{0.5} \tag{4.3}$$

In Eq. 4.3 'γ' represents the specific weight of water. From Eq. 4.3, by using a suitable S_Y and a factor of safety, Eq. 4.1 can be arrived at. For example if S_Y = 345 MPa, the constant coefficient from Eq. 4.3 will be 187.5 compared to 215 from Eq.4.1. Since the coefficient of '215' is given in Eq.4.1 without any parameter for the yield strength, the factor of safety will change with respect to the S_Y value of the plate used. Plates with higher yield strengths will have lower factor of safety and vice–versa. It is unclear if this done deliberately by API 650. However, it will be good to change this practice and make the margin of safety uniform for all plate materials.

Apart from the recommendation for thickness and width, API 650 specifies that the annular plate must extend at least 50 mm from the shell surface or 13mm beyond the toe of fillet weld whichever is greater. This minimum projection seems to have been advised for providing a proper fillet weld on the outer side of the shell. API is silent about providing extra projection length beyond this requirement and its effects on shell or bottom plate stresses. The effects of providing higher projection length on the stresses in this zone, or the theory to determine the maximum projection length are not well known to many practitioners. In this Chapter the effect of increased projection length is studied both theoretically and numerically.

4.2 PLASTIC HINGES

Even though the bottom plate is subjected to bending to a distance L (uplift length), this length is small compared to the radius of the tank. Hence, except for this length, the bottom plates are simple membranes (without any bending stresses) used to hold the tank liquid, fully supported by the subgrade underneath. The design procedure implicitly allows the bottom plate to yield completely to form a plastic hinge near the shell to bottom joint. The formation of plastic hinge here will not disturb the functions of the tank or render it unsafe. A typical joint can have plastic hinge on the inside, outside or both sides of the shell as shown in Fig. 4.2. This again depends on the thickness ratio between the shell and bottom plate and the type of foundation beneath the shell, i.e., earthen foundation without ring wall, or earthen foundation with crushed stone/concrete ring wall, or concrete slab foundation.

API 650 lists the minimum thickness of annular plate based on the hoop stress at the lowest layer of shell (Table 4.1). Using FEA, it can be shown that the minimum recommended dimensions are such that the bottom plate stresses are at or close to yield near the joint when the tank is filled fully. It should be noted that API recommends only the minimum required thickness. The designer has no restriction on adopting a thickness higher than the prescribed minimum. In such a situation, the stresses in the annular plate could be fully elastic.

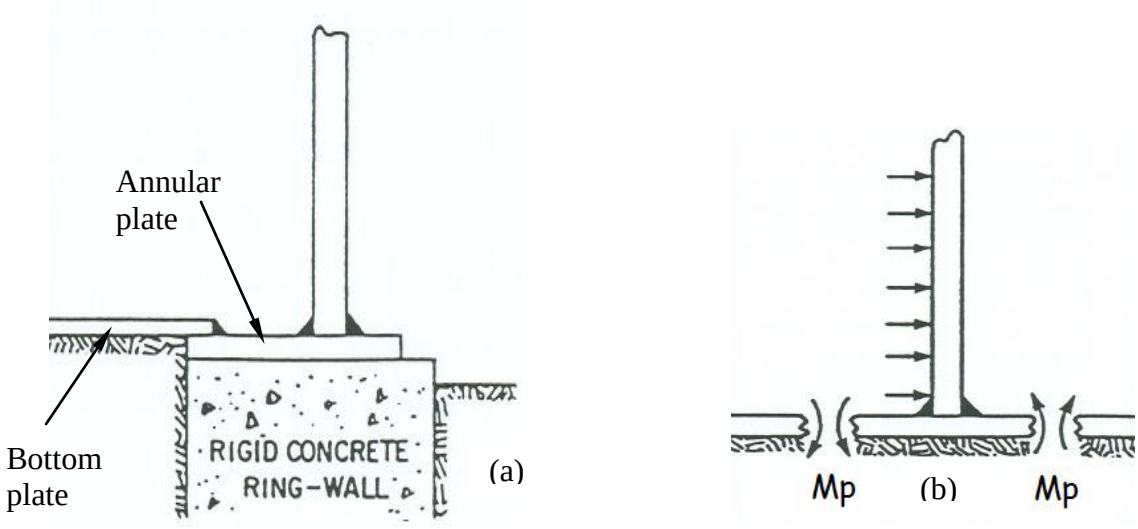

Fig. 4.2 (a) Annular Plate on Concrete ring wall (b) Plastic Hinges at the Shell to Bottom Joint [Jones and Seshadri, 1989]

Table 4.1 Annular Plate Thickness in millimetres [API 650, Cl.5.5.3]

Plate Thickness of First Shell Course t_s, mm (mm)	Stress in First Shell Course (MPa)			
	$\sigma \leq 190$	$\sigma \leq 210$	$\sigma \leq 220$	$\sigma \leq 250$
$t_s \leq 19$	6	6	7	9
$19 < t \leq 25$	6	7	10	11
$25 < t \leq 32$	6	9	12	14
$32 < t \leq 40$	8	11	14	17
$40 < t \leq 45$	9	13	16	19

When the tank is filled to a height less than the design height or the specific gravity of the liquid used is less than the design specific gravity of the liquid and in other similar situations, the stresses in the bottom plate could be completely elastic.

Proper understanding of hinge formation in this area is necessary for the design and analysis of tanks, as the moments at this joint essentially form the boundary condition for the shell analysis. Also, the shell stresses close to the bottom are important since most of the fixtures, nozzles, openings, etc., are located in the lower portion of the shell close to the bottom. In order to understand the stress distribution in shell and the bottom plate, the following issues have to be studied.

1. The internal moment at the joint for operating loads, if the plastic hinge has not formed
2. The load at which the hinge will be formed completely
3. If the plastic hinge is formed, then the number of hinges - one/two, if one hinge – then is it inside or outside or if two hinges, do they form simultaneously
4. If one hinge is formed either inside or outside, then the moment from the other side of the shell
5. Will the shell remain completely elastic till the plastic hinges are formed completely?

4.3 TEMPERATURE EFFECTS

In many situations, storage tanks are required to hold liquids like asphalt, residuum, high pour point hydrocarbons, etc., at higher temperature than the ambient and such tanks are called as Elevated Temperature tanks. The temperature loading gives rise to thermal stresses in the tank, especially near the shell to bottom joint. For tanks

operating at elevated temperatures (200°F to 500°F), in addition to the factors considered for ambient temperature tanks, the stresses in the shell to bottom zone depend upon the radial expansion of the tank bottom and the frictional forces acting in between the bottom plate and the subgrade. In addition to the induced thermal stresses in the tank, the cyclic loading due to continual filling and emptying of the tank is reported to cause low cycle fatigue in the shell to bottom joint. Karcher [1978a, b] proposed a theoretical model to determine the stresses in the bottom plate and tank wall and the safe design cycle life for elevated temperature tanks. The details of this model and further information about the elevated temperature tanks are provided in Chapter 5 and 6.

4.4 ANALYTICAL MODEL AS PROPOSED BY DENHAM ET AL.

In order to analyze the bottom plate, Denham, et al., [1968a] proposed a beam model as shown in Fig. 4.3 that is compatible with the shell rotation at the shell to bottom junction. They assumed a projection length as a fixed value of 3" while the uplift length inside the tank is a variable that changes depending on the applied forces and stiffness of the shell and plate. This elastic method was also compared with field measured data. The strain gage data confirmed that the annular plate would reach yield close to shell and hence a high stress low cycle fatigue situation can be expected at this joint. The field data from the remaining portion of the annular plate showed considerable variation from the theoretical results. The authors ascertained that the probable cause could be the annular plates being uplifted from the foundation for a distance exceeding uplift length L before water filling. There wasn't any comparison with numerical models like FEM reported in

the article. In the current work, the model as proposed by Denham, et al., is verified with FE model and is further extended.

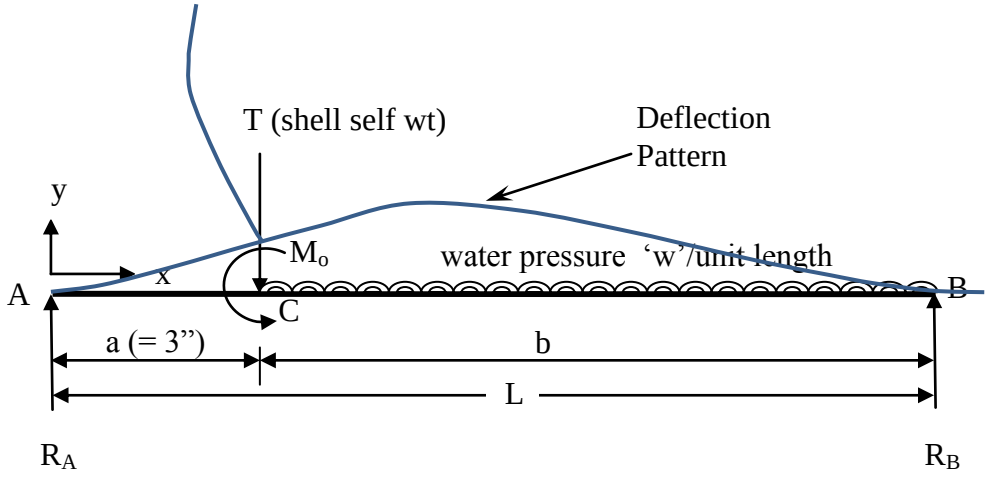

Fig. 4.3 Denham's Model of Shell to Bottom Joint

Denham used the shell theory for the tank wall and beam theory for the annular plate with the following assumptions:

1. The annular plate lifts clear off the foundation for some distance L
2. Support points A & B do not yield (no settlement)
3. The deflection and moment are zero at the outer support (A)
4. The deflection, moment and also the slope are zero at the inside support (B)
5. The slope of the shell and the slope of the annular plate, at the shell to bottom joint (C) are same, i.e., slope compatibility is assumed at the joint
6. There is no radial deformation of the shell at the bottom

The procedure is to first consider a beam of unit width with hydrostatic load and self-weight of shell wall acting on it as shown in Fig. 4.3. Because of the rigid joint at the shell to bottom junction, an internal moment M_o from the tank wall will be applied. Its value depends on the uplift length, weight of liquid and other parameters of geometry. Hence, as a first step an arbitrary value for the uplift length L is assumed and the moment and slope at the shell to bottom joint location are determined. For an assumed uplift length L, the beam model is a determinate problem, hence the moment and slope can be found using equilibrium conditions.

The slope of the shell bottom for this assumed moment (Fig.4.4) must be compatible with the slope that was calculated from the beam model at this location. The assumed uplift length is suitably changed to satisfy this condition. This will be a trial and error procedure and was solved graphically by Denham, et al. [1968a]. The equations for shell and annular plate are as given below:

Shell equations:

$$y_s = \frac{\gamma(H - x_s)R^2}{Et_s} - \frac{e^{-\beta x_s}}{E}[c_1 \cos(\beta x_s) + c_2 \sin(\beta x_s)] \tag{4.4}$$

where, $\beta = \sqrt[4]{\frac{3(1-\mu^2)}{R^2 t_s^{\,2}}}$ (4.5)

$$\frac{dy_s}{dx_s} = \frac{-\gamma R^2}{Et_s} - \beta\frac{e^{-\beta x_s}}{E}[(c_2 - c_1)\cos(\beta x_s) + (c_2 + c_1)\sin(\beta x_s)] \tag{4.6}$$

where, y_s is the radial deflection of shell wall and x_s is the height of the location in the shell wall from bottom, t_s is the thickness of the shell and γ is the specific weight of the liquid infill.

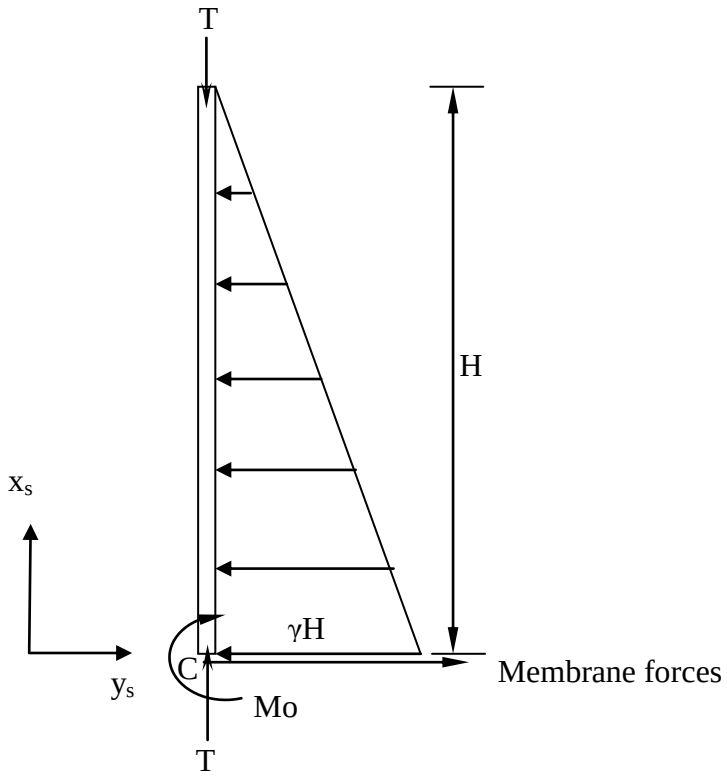

Fig. 4.4 Freebody Diagram of Shell

Annular plate equations:

Case (i): when x ≥ a

$$EI\frac{d^2y}{dx^2} = R_B(L-x) - \frac{w(L-x)^2}{2} \tag{4.7}$$

$$EI\frac{dy}{dx} = \frac{R_B(L-x)^2}{2} - \frac{w(L-x)^3}{6} \tag{4.8}$$

$$EIy = \frac{R_B(L-x)^3}{6} - \frac{w(L-x)^4}{24} \tag{4.9}$$

The integrations constants in Eq.4.8 and 4.9 are eliminated using the boundary conditions of zero slope and deflection at x = L

It should be noted that the parameter 'y' in the equations above is the vertical deflection of the tank bottom plate, whereas 'y_s' denotes the radial deformation of the tank shell. Similarly 'x' is the horizontal distance from the outer edge of the bottom/annular plate to a point under consideration in the bottom plate and 'x_s' is the vertical distance of any point in the shell wall from bottom.

Case (ii): when $x \leq a$

$$EI\frac{d^2y}{dx^2} = R_B(L-x) - \frac{w(L-x)^2}{2} - T(a-x) + \frac{w(a-x)^2}{2} + M_o \tag{4.10}$$

$$EI\frac{dy}{dx} = \frac{R_B(L-x)^2}{2} - \frac{w(L-x)^3}{6} - \frac{T(a-x)^2}{2} + \frac{w(a-x)^3}{6} + M_o(x) - M_o(a) \tag{4.11}$$

$$EIy = \frac{R_B(L-x)^3}{6} - \frac{w(L-x)^4}{24} - \frac{T(a-x)^3}{6} + \frac{w(a-x)^4}{24} + M_o(\frac{x^2}{2}) - M_o(ax) + M_o(\frac{a^2}{2}) \tag{4.12}$$

The integration constants in Eq.4.11 and 4.12 are eliminated using compatibility conditions of slope and deflection at x = 'a' from Eq.4.8 & 4.11 and from Eq.4.9 & 4.12.

Taking a moment of all forces about point A,

$$R_B = \frac{w}{2L}(L^2 - a^2) + \frac{Ta}{L} - \frac{M_o}{L} \tag{4.13}$$

Similarly using the boundary condition of zero deflection at the outer edge of the bottom plate (x=0, y =0), in Eq.4.12,

$$R_B = \frac{wL}{4} + \frac{Ta^3}{L^3} - \frac{w}{4}\frac{a^4}{L^3} - 3\frac{a^2 M_o}{L^3} \tag{4.14}$$

Subsequently the Moment M_o can be found explicitly using Eq. 4.13 & 4.14.

$$M_0 = \frac{L^2 - a^2}{L^2 - 3a^2}\left[\frac{w}{4}\left(L^2 - a^2\right) + T\left(a\right)\right] \tag{4.15}$$

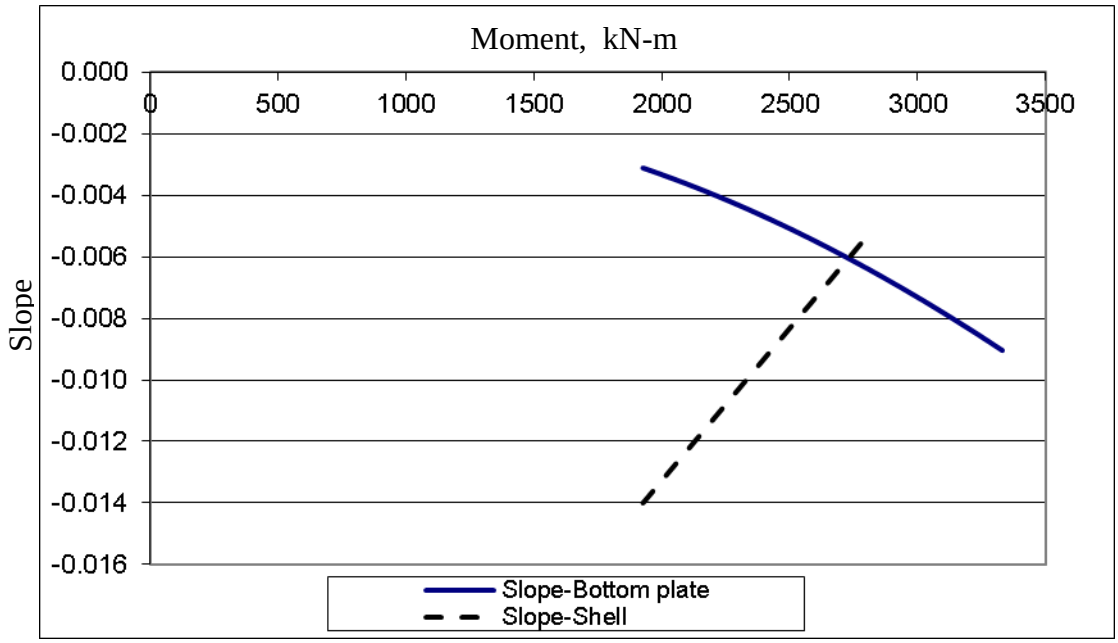

Fig. 4.5 Moment vs. Slope Graph to Find Uplift Length

Finally, the iterative procedure can include a typical graph as shown in Fig.4.5. The solid line indicates the slope values at the shell to bottom joint calculated for different values of M_o from annular plate slope equation (Eq.4.8). Similarly the dashed line is the slope from shell equation (Eq.4.6). For slope compatibility, a particular

moment value should produce same slope in both the annular plate and the shell wall. This is determined graphically by Denham as shown in Fig.4.5. Though the slope to moment relation is nonlinear, the graph seems to be fairely linear. This could be because only a small portion of the lines near the intersection is plotted.

Denham, et al., [1968a], compared the theoretical results with actual strain measurements from an instrumented tank. The theoretical calculations indicated that stresses in the annular plate would reach yield close to the shell. This was confirmed from the field data. However for locations away from the shell to bottom joint, the field data showed considerable variation. The probable reason stated is that, the annular plate would have been uplifted from the foundation for a distance exceeding the uplift length L prior to water filling.

4.5 VERIFICATION OF DENHAM'S MODEL USING FEA

As mentioned above, Denham, et al. [1968a], in their paper, compared the theoretical model with field data and found that the annular plate stresses are not predicted satisfactorily for location away from the shell joint. Hence, in the present work, a finite element model is used for verification of the theoretical model.

The dimensions of the tank are as per Case 3 Model as described in Section 3.5. A detailed description of the Finite element modeling is also provided in Chapter 3. The FEA was carried out using an axisymmetric model with plane elements (8 node PLANE183 elements with u-p capabilities) and material nonlinearity. The bottom support is modeled with contact elements resting on a rigid surface capable of

sliding/sticking/separation. The loading is the pressure due to fully filled tank. The accuracy of modeling the tank using this type of finite element mesh was examined by comparing the results for a fixed bottom tank with those obtained from using Timoshenko and Woinowsky-Kreiger [1959]. For the example tank (H= 16.8m, t_s = 30mm, R = 45m), maximum deflections differed by less than 0.05%. Similarly maximum bending stress in the shell differed by less than 0.3%. The yield strength of the material is taken as 345 MPa. The meshes are appropriately sized at different parts of the tank. The outer tip of the bottom plate and the area near the shell to bottom joint is very finely meshed to account for the local stress concentration and formation of plastic hinges, respectively. Based on the importance of the location and convergence issues, several trials were performed before the mesh sizes were finalised.

Fig. 4.6 and 4.7 compare the theoretical and numerical results for the bending stress and the uplift in the bottom plate. The friction coefficient between the bottom plate and the subgrade is assumed as 0.2. This value is used only for demonstration purpose; the actual friction coefficient varies depending on the site conditions. The value of friction coefficient does not play a significant role for the current problem since the tank shell expansion at the bottom due to hydrostatic loading is negligible due to the presence of membrane action of the bottom plate (due to high axial stiffness). The friction coefficient will be of much greater significance if temperature expansion is fully or partly curtailed due to frictional forces at the bottom. This issue is studied in detail in the next Chapter.

From the stress plots, it is shown that theoretical model and FEA results are in reasonable agreement. The small difference in the peak stress locations can be ascertained mainly because of the fact that, in the theoretical model the shell is idealized as a single concentrated point and hence it causes two different stresses (the positive maximum and the negative maximum) at the same 'x' location, whereas in the FE model the tank wall has thickness and hence the positive and negative peaks are not in the same 'x' location. Although the beam model is simple looking, the results of FEA show that it is reasonably good in predicting the stresses.

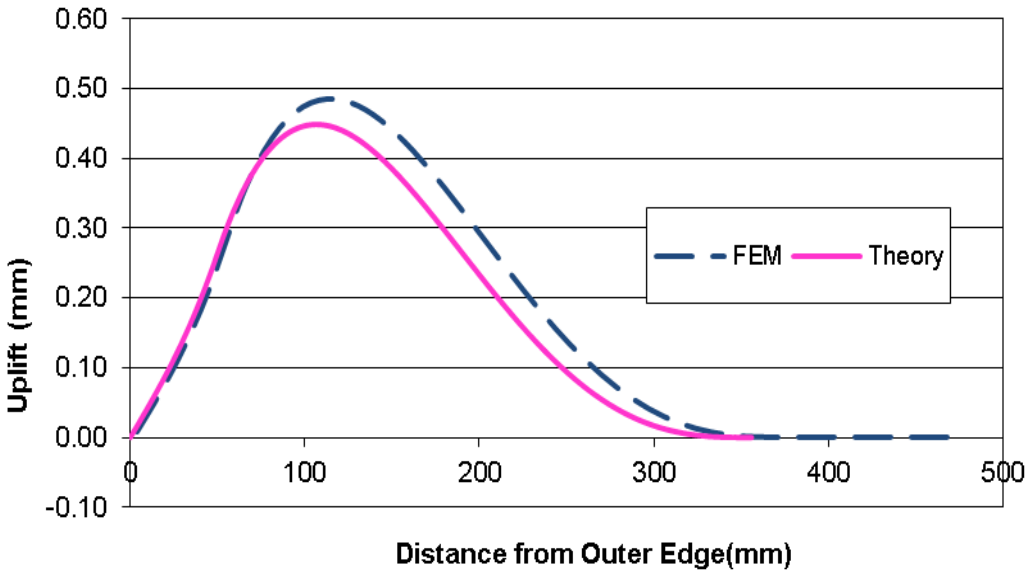

Fig. 4.6 Uplift in the Bottom Plate

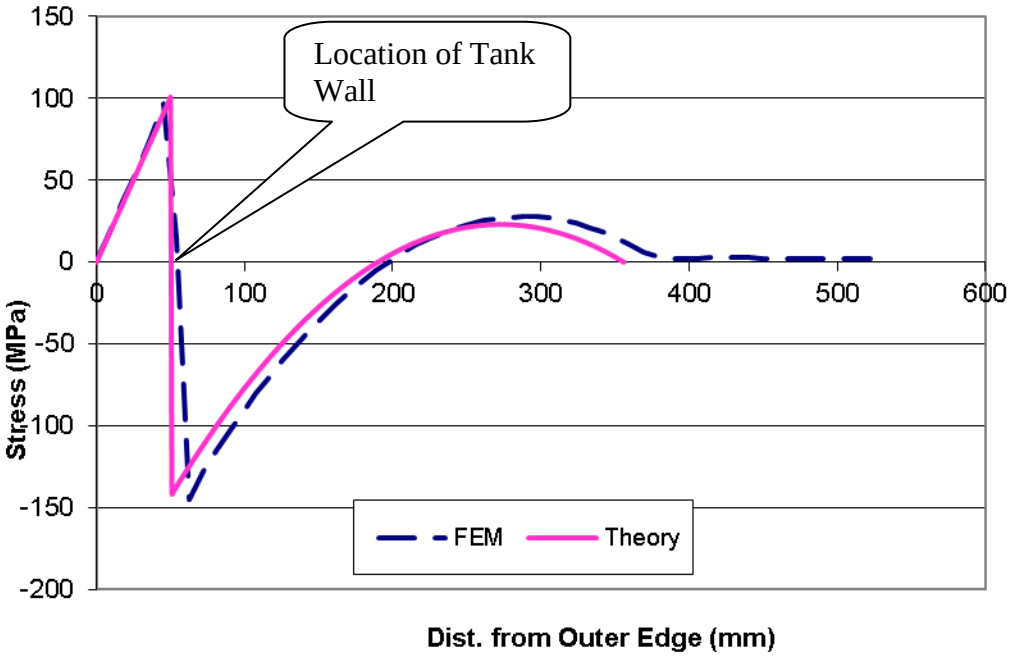

Fig. 4.7 Bending Stress on the Bottom Side of Bottom Plate with 50mm Projection Length

4.6 EFFECT OF PROJECTION OF ANNULAR PLATE BEYOND SHELL

From the theoretical model, it can be observed that, the projected length of the plate 'a' influences the peak bending stresses occurring on either side of the shell to bottom joint. Figures 4.6 and 4.7 are for a fixed length of 3" projection as used by Denham, et al. [1968a]. On further analysis it was found that, increasing the projected length till a particular value, increases the bending stress on the outside face and hence moves the maximum bending stress location from the inner side of the joint to the outer side of the joint. Any further increase in the projection length will not alter the location nor the value of the bending stresses. Figure 4.8 shows the bending stress from FEA for

the same tank described previously, but with 100 mm projection beyond the shell. Unlike the previous plot (Fig. 4.7), it can be seen here that the maximum stress lies on the outer side of the bottom joint.

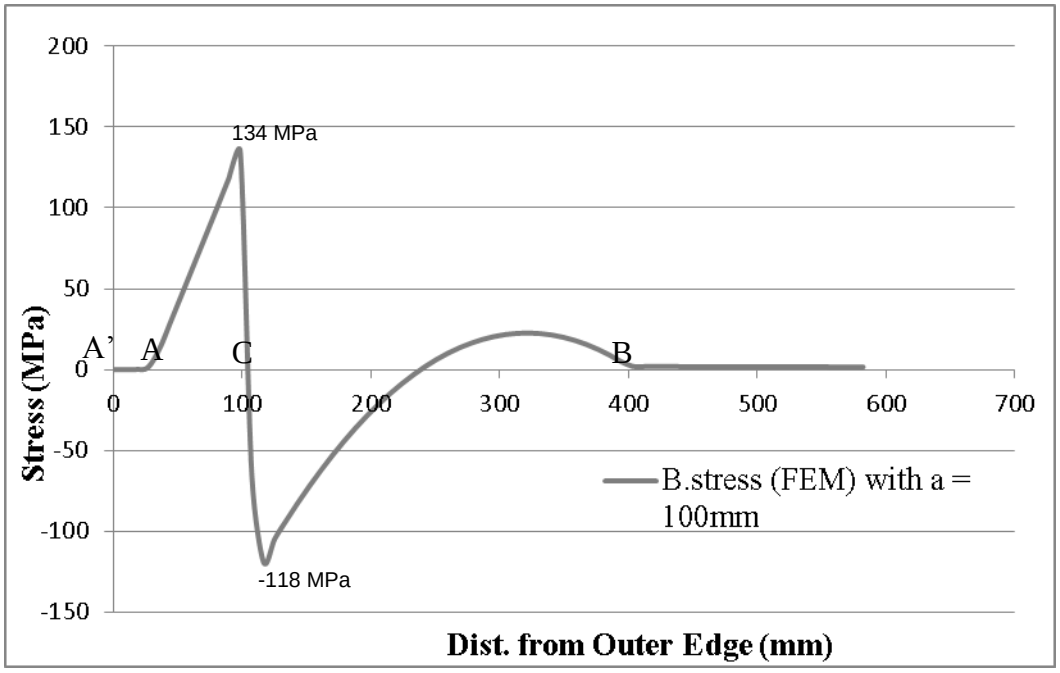

Fig. 4.8 Bending Stress in the Bottom Side of Bottom Plate for 100mm Projection Length

In Fig. 4.8, Point A' is the outer end of the plate and C is the junction where shell joins the plate. It can be observed that the bending stress becomes zero in the portion A'A where the uplift is zero. Similarly the portion of the bottom plate after point B lies on the foundation and is not subjected to bending or uplift. Hence, it can be concluded that the length of projection on the outer side, beyond a certain distance (AC in this case) will not be of practical use and hence can be curtailed. It is of interest to determine the length AC and CB as a function of tank geometry and material property.

From the FEM results it was found that the length of AC was approximately 71 mm for the example tank. Using this, the theoretical stresses are calculated. The following graph (Fig. 4.9) shows the FEA and theoretical stresses for 71mm projection.

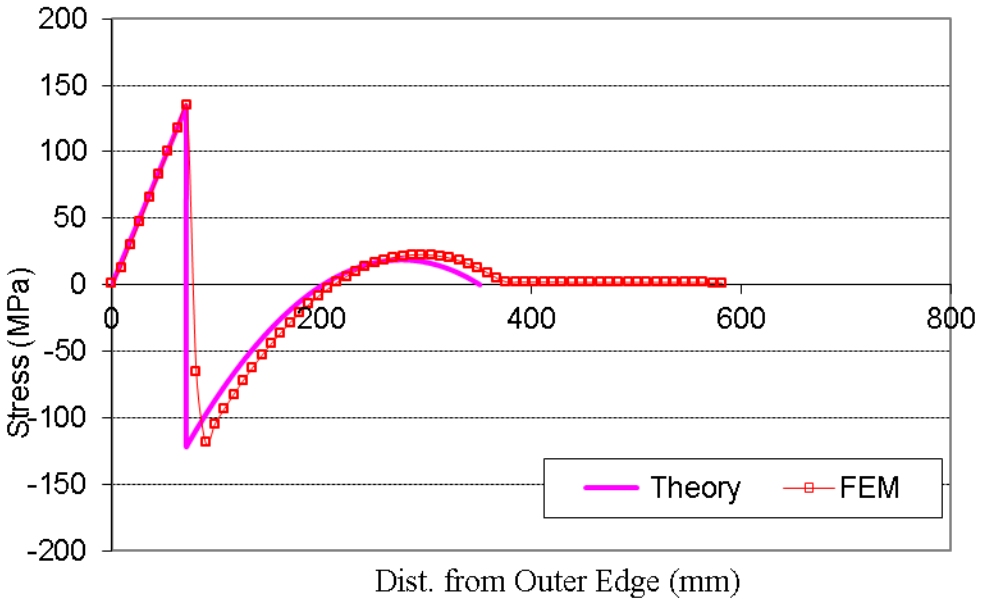

Fig. 4.9 Bending Stress in Bottom Plate for 71mm Projection

As expected, it can be seen from the plot above that the theoretical stresses match reasonably with the FEA results. The following graph (Fig. 4.10) shows the theoretical stresses for the same tank with 50mm and 71mm projection.

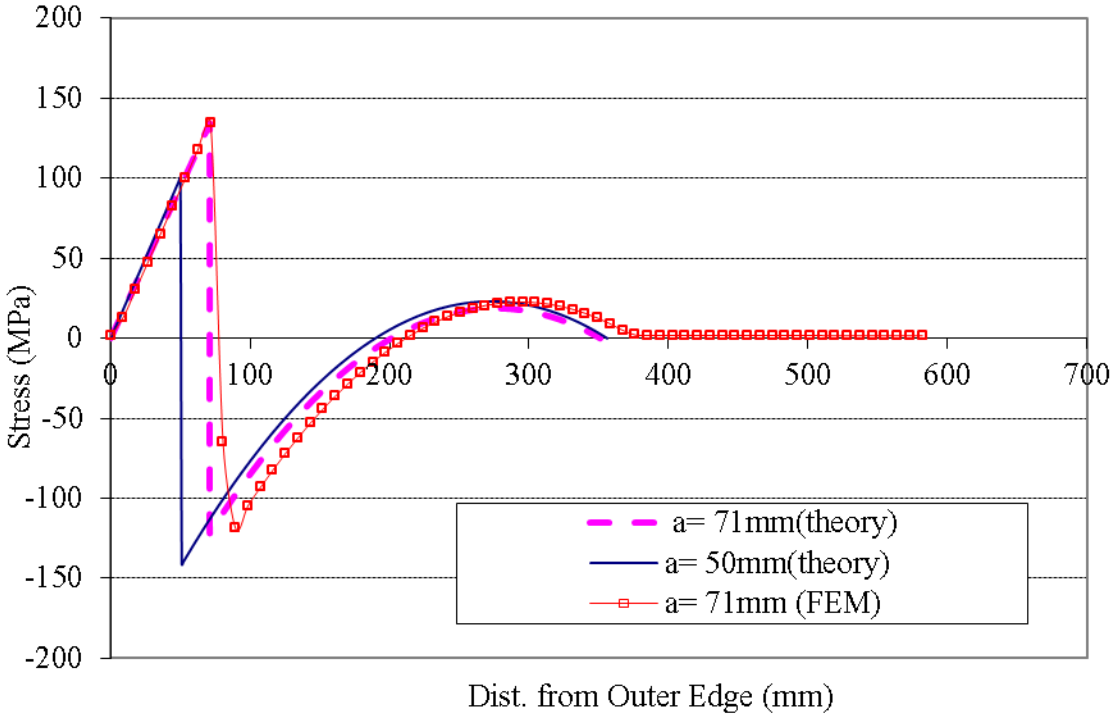

Fig. 4.10 Bending Stress in Bottom Plate for 50mm and 71mm Projection

It can be seen that because of the increased projection from 50mm to 71mm, the maximum stress location which was occurring at the inner face (for 50mm) of the shell to bottom joint has moved to the outer face (for 71mm). Hence within the elastic limit, providing longer projection helps in moving the maximum stress location to outside the tank shell.

4.7 DETERMINATION OF FULL PROJECTION LENGTH

It is easy to see that for a sufficiently wide outer plate (dimension "a" in Fig. 4.11), the slope of the plate on the outer edge will be zero, just as the case at the end

of dimension “b”. Consider this to be “full” projection width, since a larger value of “a” has no additional impact.

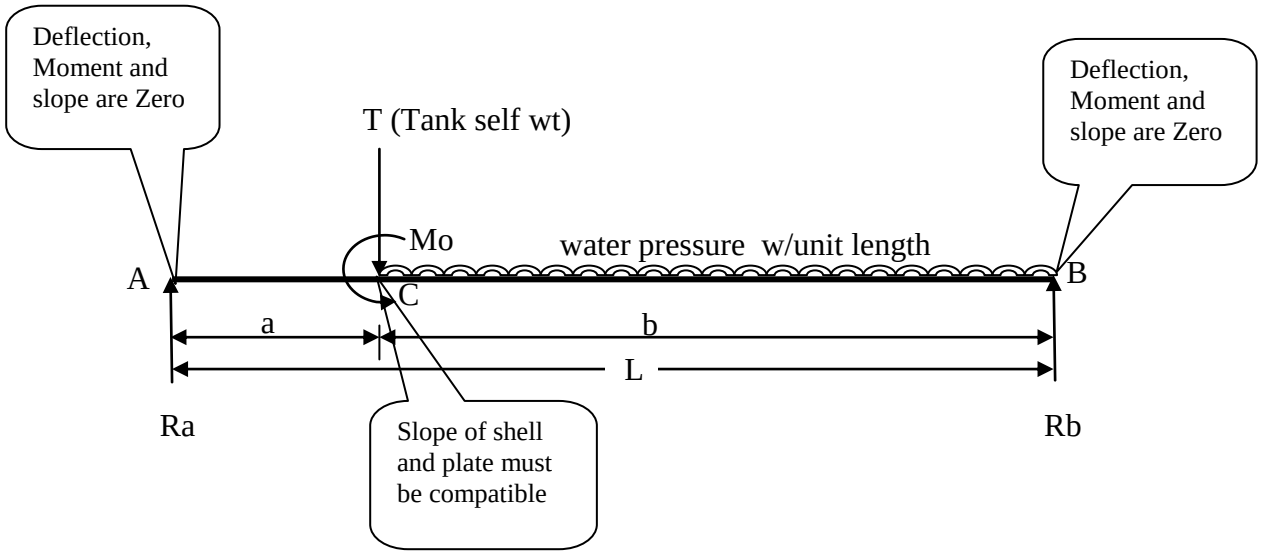

Fig. 4.11 Beam Model of Shell to Bottom Joint for “Full” Projection

It should be noted that even though the slopes are zero at supports A and B, it does not imply that there are fixed end moments at A and B. Proceeding as before and setting $\theta_A = 0$,

$$\theta_A = \frac{1}{24DL}[4M_o(2L^2 - 6aL + 3a^2) - 4Tb(\frac{L^2 - b^2}{6DL}) - wb^2(2L^2 - b^2)] = 0 \qquad (4.16)$$

$$M_o = \left[\frac{4Tb(L^2 - b^2) + wb^2(2L^2 - b^2)}{4(2L^2 - 6aL + 3a^2)}\right] \qquad (4.17)$$

Similarly for $\theta_B = 0$,

$$\theta_B = \frac{1}{24DL}[4M_o(3a^2 - L^2) + 4Ta(L^2 - a^2) + w(L^2 - a^2)] = 0 \qquad (4.18)$$

This gives,

$$M_o = -\left[\frac{4Ta(L^2 - a^2) + w(L^2 - a^2)^2}{4(3a^2 - L^2)}\right] \tag{4.19}$$

As before,

$$\theta_c(shell) = \frac{\gamma R^2}{Et_s}(\beta H - 1) - \frac{M_o}{2D_s\beta} \tag{4.20}$$

$$\theta_c(plate) = \frac{M_o}{3DL}[3a^2 + L^2 - 3aL] - \frac{Tb(L^2 - b^2)}{6DL} + \frac{Tba^2)}{2DL} - \frac{wb^2}{24DL}[2L^2 - b^2 - 6a^2] \tag{4.21}$$

$$M_o = \frac{1}{\left[\frac{3a^2 + L^2 - 3aL}{3DL} + \frac{1}{2Ds\beta}\right]}\left[\frac{\gamma R^2}{Et_s}(\beta H - 1)\right] + \frac{Tb(L^2 - b^2 - 3a^2)}{6DL} + \frac{wb^2}{24DL}[2L^2 - b^2 - 6a^2] \tag{4.22}$$

Equating the Moment (M_o) expressions (4.17) & (4.19) and equations (4.19) & (4.22) results in a nonlinear equation of 6th degree which is not explicitly solvable. The value of M_o, 'a', and 'b' should satisfy equations 4.17, 4.19 & 4.22.

4.7.1 Ratio of Lengths "b" and "a"

Let λ = b/a and assuming T is negligible compared to the liquid weight acting at the tank bottom, from Eq.4.17,

$$M_o = -\frac{wa^2}{4}\frac{(2\lambda + \lambda^2)^2}{(2 - 2\lambda - \lambda^2)} \tag{4.23}$$

Similarly from Eq.4.19,

$$M_o = \frac{wa^2}{4}\frac{\lambda^2(2+4\lambda+\lambda^2)}{(2\lambda^2-2\lambda-1)} \tag{4.24}$$

Equating the Eq. 4.23 and 4.24 and simplifying

$$\lambda = \frac{1+\sqrt{33}}{2} = 3.372 \tag{4.25}$$

If the shell self-weight T is assumed negligible and the relation b = λa is used, then a simple relation between the unknowns M_o and a can be obtained. The effect of self-weight on the bending stresses is discussed later in section 4.11.

Using the relation $\lambda = \frac{1+\sqrt{33}}{2}$ in Eq. 4.16 gives:

$$\frac{M_o}{2L}(a^2+L^2) - \frac{R_a L^2}{6} + \frac{w(L-a)^4}{24L} - M_o a = 0 \tag{4.26}$$

Slope at B is zero gives:

$$\frac{M_o}{2L}(a^2+L^2) + \frac{R_a L^2}{3} - \frac{w(L-a)^3}{6} - M_o L + \frac{w(L-a)^4}{24L} = 0 \tag{4.27}$$

Simplifying the above equations,

$$Mo = 5.091(wa^2) \tag{4.28}$$

Note that the above equation needs to be used in conjunction with the value of "a" obtained by solving equations 4.17, 4.19 and 4.22.

4.8 RELATIONSHIP BETWEEN MOMENTS M_o AND M_{fx} FOR FULL PROJECTION LENGTH

It has been observed that the moment created in the shell bottom for fixed boundary condition (M_{fx}) will have some relation to the moment (M_o) from the previous section. From shell theory, the fixed end moment M_{fx} at the bottom of shell is expressed as [Timoshenko and Woinowsky-Krieger, 1959]:

$$M_{fx} = \frac{\gamma R H t_s}{\sqrt{12(1-\nu^2)}}\left(1-\frac{1}{\beta H}\right) \tag{4.29}$$

Let $\psi = Mo / M_{fx}$

Using Eq. 4.22 and 4.29 and assuming $\nu = 0.3$, the following relationship between moment ratio (ψ)and thickness ratio (t_s/t_a) can be obtained

$$\frac{\psi^3\left[1-\frac{1}{\beta H}\right]}{35.97}\left(\frac{t_s}{t_a}\right)^6 - \frac{\psi^2}{0.83} + 2.2\psi - 1 = 0 \tag{4.30}$$

This is a cubic equation in terms of the M_o/M_{fx} ratio, which can be solved for a given ratio of t_s/t_a and the value of βH.

Table 4.2 presents a range of tank dimensions obtained from the standard design procedure as per API 650 [2012]. The table includes elastic analysis results for M_o and M_{fx} for each tank. It must be pointed out that these M_o values are for 'full projection length' of bottom plate outside the tank wall (not the standard minimum of 50 mm projection length).

Table 4.2 Design Details for Several Typical Tank Sizes

Group	All. Design Stress, MPa	Radius R, mm	Height H, mm	Shell Thickness t_s, mm	Ann.Plate thickness t_a, mm	Moment M_o, N-mm	Moment M_{fx}, N-mm	M_{fx}/M_o	t_s/t_a
I	159	30000	12000	22	6	4675	22273	4.76	3.67
		37500	12000	27	6	4994	33716	6.75	4.50
		40000	12000	28	6	5165	37161	7.20	4.67
		57500	12000	38	8	9561	70379	7.36	4.75
		27500	14400	24	6	4874	26976	5.53	4.00
		37500	14400	32	6	5251	48262	9.19	5.33
		45000	14400	38	8	9153	67936	7.42	4.75
		25000	16800	26	6	4897	31207	6.37	4.33
		32500	16800	33	8	8737	50924	5.83	4.13
		38500	16800	39	9	11151	70635	6.33	4.33
		25000	19200	30	6	5010	41248	8.23	5.00
		31250	19200	37	8	8832	63032	7.14	4.63
II	208	37500	12000	21	7	7661	26440	3.45	3.00
		52500	12000	29	12	19796	49898	2.52	2.42
		60000	12000	31	12	21941	60402	2.75	2.58

Group	All. Design Stress, MPa	Radius R, mm	Height H, mm	Shell Thickness t_s, mm	Ann.Plate thickness t_a, mm	Moment M_o, N-mm	Moment M_{fx}, N-mm	M_{fx}/M_o	t_s/t_a
III	236	32500	14400	22	7	7840	29169	3.72	3.14
		50000	14400	32	12	22026	63723	2.89	2.67
		60000	14400	37	14	30642	87262	2.85	2.64
		30000	16800	24	7	8057	34498	4.28	3.43
		45000	16800	34	14	28202	71935	2.55	2.43
		60000	16800	44	16	40341	121759	3.02	2.75
		32500	19200	29	12	20280	51607	2.54	2.42
		42500	19200	38	16	35204	87312	2.48	2.38
		50500	19200	44	16	39276	119000	3.03	2.75
		32500	14400	20	10	13174	26576	2.02	2.00
		50500	14400	30	14	27810	60457	2.17	2.14
		60000	14400	33	18	42757	78207	1.83	1.83
		30000	16800	21	11	15759	30265	1.92	1.91
		42500	16800	29	14	27821	58309	2.10	2.07
		60000	16800	39	22	61209	108436	1.77	1.77
		30000	19200	24	11	17717	39628	2.24	2.18

Group	All. Design Stress, MPa	Radius R, mm	Height H, mm	Shell Thickness t_s, mm	Ann.Plate thickness t_a, mm	Moment M_o, N-mm	Moment M_{fx}, N-mm	M_{fx}/M_o	t_s/t_a
IV	145	45000	19200	35	17	40936	85207	2.08	2.06
		55000	19200	42	19	54683	123557	2.26	2.21
		3000	14400	5	5	511	637	1.25	1.00
		1500	9600	5	5	170	212	1.25	1.00
		7500	19200	9	6	2458	3807	1.55	1.50
		13500	14400	12	6	3344	6775	2.03	2.00
		33000	4800	10	6	2557	4265	1.67	1.67
		12000	16800	12	6	3480	7056	2.03	2.00

Notes for Table 4.2

* Tank dimensions are based on Tables 3.1, K1, K2, K3 of API 650 [2012]
* The thickness values are rounded to next higher mm
* In determining the annular plate thickness, for the few cases where the hydrostatic stress values were beyond the limits in Table 3.1 of API 650 [2012], the thickness were suitably assumed
* The last row of the table is not taken from API 650. The appropriate design values are added for completeness of design range

4.8.1 Influence of the Term (1-1/βH)

In Eq.4.30, the only variable other than thickness ratio and moment ratio is the term (1-1/βH). This term is a function of H and R (since the shell thickness t_s, present in the shell parameter β is also a function of R). Table 4.3 shows the variation of (1-1/βH) for the minimum and maximum values of R and H specified in API 650 tank data:

Table 4.3 Variation of (1-1/βH) with Radius and Height

R	H	(1-1/βH)
1500	4800	0.9965
60000	16800	0.9225
1500	16800	0.9981
60000	4800	0.8584

It can be seen that only the case where the radius is extremely large and height is relatively very small has the (1-1/βH) value less than the 0.91-0.99 range. For practical applications this is a rare situation.

To study the influence of (1-1/βH) on M_{fx}/M_o ratio (for full projection length), an example tank with the following geometry is considered. The geometry is chosen such that it has a high moment ratio (assuming the higher moment ratio will be influenced more by the (1-1/βH) variation). Let R = 37500 mm, H = 14400 mm, t_s = 32mm, t_b = 6mm. Table 4.4 gives M_{fx}/M_o values for three different assumed values of (1-1/βH) for this tank using Eq.4.30.

Table 4.4 Variation of M_{fx}/M_o with (1-1/βH) Value

(1-1/βH)	M_{fx}/M_o
0.999	9.362
0.900	9.068
0.858	8.936

The variation of (1-1/βH) produces a variation of 4.6% between the extreme M_{fx}/M_o values. For the dimensions given, the actual (1-1/βH) = 0.9408 and M_{fx}/M_o = 9.1912. The deviation of the extreme value from the actual M_{fx}/M_o is only 1.86%.

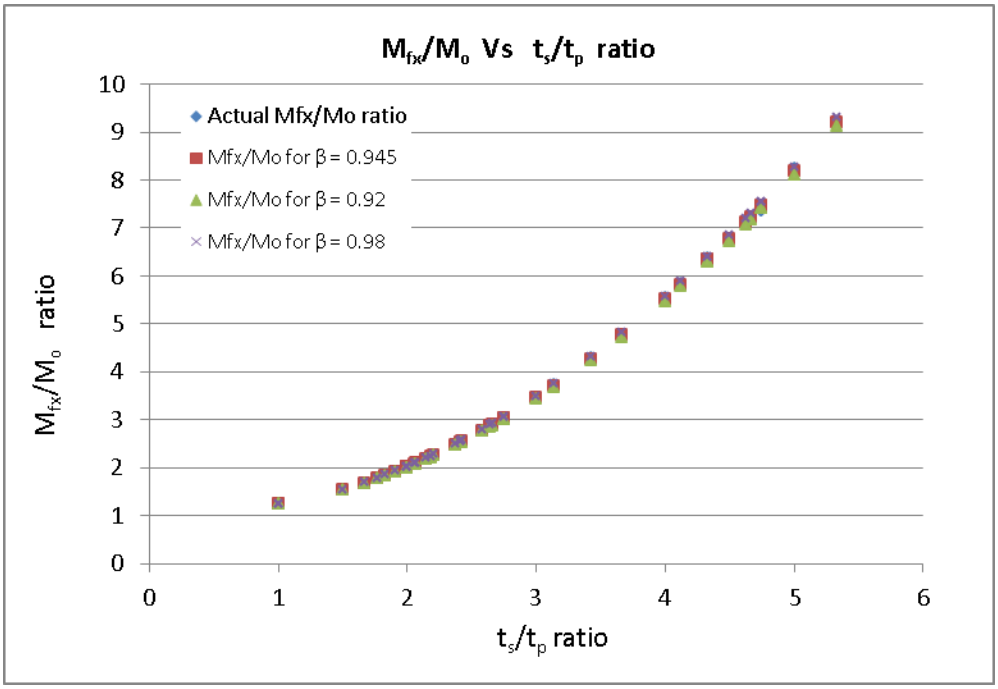

Fig. 4.12 M_{fx}/M_o vs. t_s/t_p for Different Values of (1-1/βH)

Extending the analysis to the entire design data as given in Table 4.2, the above graph (Fig.4.12) is plotted. Figure 4.12 shows the plots of M_{fx}/M_o ratio for a constant value of (1-1/βH) as 0.92, 0.945, and 0.98. It can be seen that, all these three cases coincide very closely with the actual M_{fx}/M_o values.

Assuming an average value of 0.945 for the (1-1/βH) term, Eq.4.30 can be expressed as

$$\psi^3\left(\frac{t_s}{t_a}\right)^6 - 45.86\psi^2 + 83.74\psi - 38.06 = 0 \qquad (4.31)$$

Equation 4.31 can be used to find the value of the elastic moment that will be induced in the shell to bottom joint. This moment could form the boundary condition to find the stresses in the shell and bottom plate provided that plastic hinge formation does not limit the bottom moment. It should be noted that the compression due to wall weight is not included in this analysis but can be done if needed.

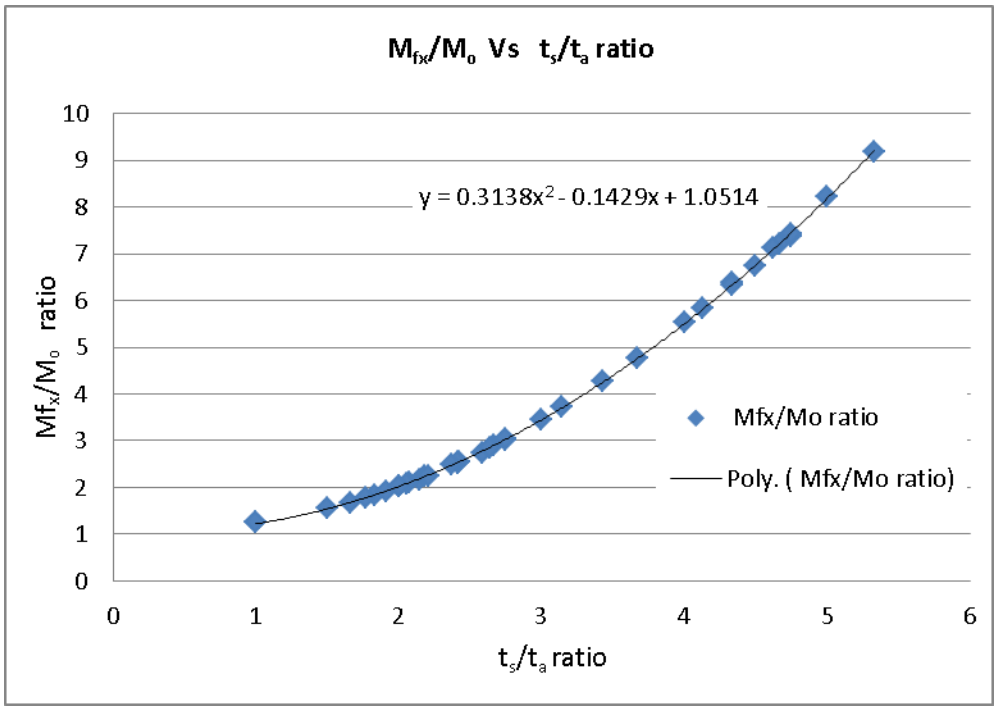

Fig. 4.13 Bottom Moment for Thickness Ratio

The values from Table 4.2 are plotted again in Fig. 4.13. Although Eqs. 4.31 and 4.32 are cubic, the figure shows that M_{fx}/M_o and t_s/t_a have a simple quadratic relationship. It can be obtained from curve fitting the graph in Fig. 4.13 as follows:

$$\psi = 0.3138\left(\frac{t_s}{t_a}\right)^2 - 0.1429\left(\frac{t_s}{t_a}\right) + 1.0514 \qquad (4.31a)$$

It is to be noted that even though this relationship is deduced from design data (Table 4.2) using minimum required thickness for the annular plate, it works for other cases when the annular plate thickness used is greater than the minimum required.

4.9 VERIFICATION OF THEORETICAL RESULTS WITH FEA

A typical tank Model, (Case 1 as described in Chapter 3) is used for study. Figure 4.14 shows the bending stress in the bottom plate due to hydrostatic loading. Due to higher allowable stresses and larger tank size, the maximum stress values for this example are higher than those for the previous example considered.

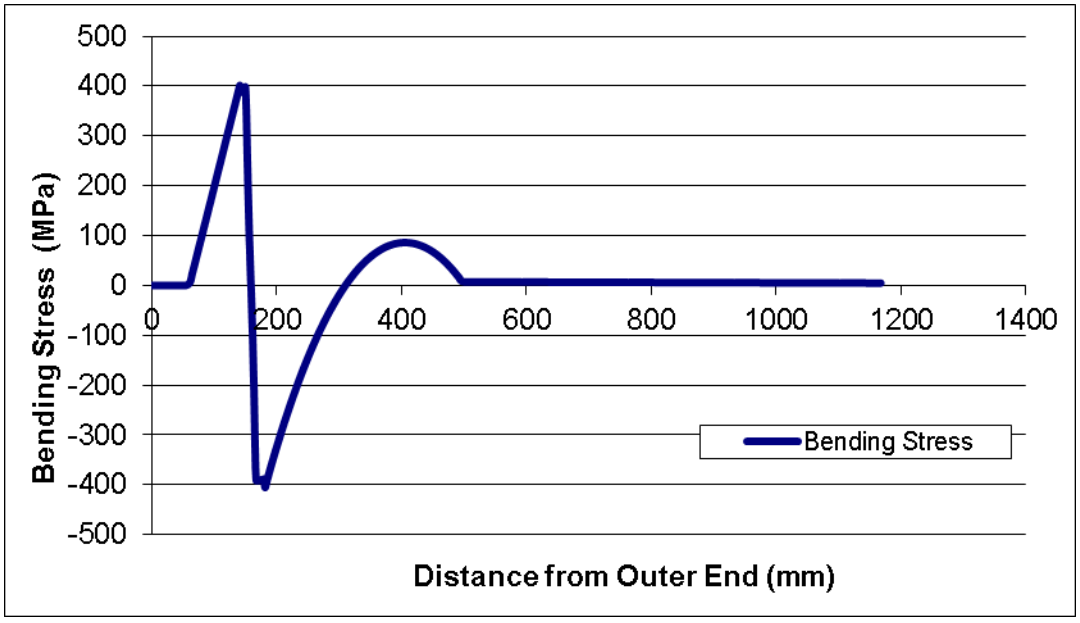

Fig. 4.14 Bending Stresses in Bottom Plate from FEA

The values of dimensions “a” and “b” (as per Fig.4.11) from FEA and theory are compared as given below:

Table 4.5 Comparison of Theoretical and FEA Results for Uplift Lengths ‘a’ and ‘b’

	FEA	Theory
a, mm	96	94
b, mm	332	317

The values are in good agreement with each other. The minor difference can be due to the fact that in theoretical model the tank wall is idealized as a single concentrated point, whereas in FE Model (PLANE element Model), thickness of tank wall is considered. In the calculations above, the self-weight has been ignored both in FEA and theoretical calculations. If the self-weight of the tank is included, the proposed theoretical approach with increased projection gives a slightly lower value for the parameters, ‘a’ and ‘b’ and a slightly higher value for the moment at the shell to bottom junction.

In practical applications, the shell wall for this height will have different course thicknesses along the height (Fig.3.19). The multiple thicknesses have two effects, viz., reduction in self-weight and reduction in stiffness along the height. From the theoretical analysis it is found that reduction in self-weight alone will increase the value of ‘a’ & ‘b’ parameters and reduce the internal moment, while reduction in stiffness will increase the value of ‘a’ and ‘b’ parameters and also increase the internal moment. Hence, ignoring the self-weight will have conservative effect in majority of the cases.

In order to support the above statement, the influence of considering or ignoring the self-weight and assuming uniform wall thickness (even in case of tanks with multiple wall thicknesses) on the parameters ‘a’ & ‘b’ and the stresses on the inner and outer side

of the shell to bottom joint is studied in detail. In the theoretical model, the self-weight of the tank wall is considered as a concentrated force acting at the shell to bottom joint. It is easy to find the actual self-weight for a multiple layered or single layered tank and apply it as force at the joint. But for stiffness considerations, a uniform thick wall is assumed (for tanks with single/multiple wall thicknesses). The question arises, whether it is acceptable to use the bottom layer thickness for the entire tank wall height for stiffness purposes. The argument in support of using it is that the height of the bottom course is generally 2400mm (except for rare cases where it is 1800mm) and this height, even though less than $3.46\sqrt{Dt_s}$ (i.e. $4.89\ \sqrt{Rt_s}$) the change in thickness above it will not influence the stiffness at the bottom joint significantly.

Table 4.6 presents data obtained from the CASE 2 model (tank with multiple courses) as described in Chapter 3. The actual data obtained from the ANSYS is compared with different scenarios in the theoretical model.

Table 4.6 Effect of Self-Weight on Parameters 'a' and 'b'

S.No	a, mm	b, mm	Stress at shell to bottom joint, MPa		Self-weight	Wall thickness used for Stiffness Calculations
			Outer Side	Inner Side		
1	185	635	325	-318	Included -VT	DATA obtained from FEM
2	132	591	386	-298	Included - UT	Uniform thickness
3	183	618	300	-320	Excluded	Uniform thickness
4	149	601	355	-306	Included -VT	Uniform thickness
5	151	609	363	-314	Included -VT	uniform thickness is reduced by 10%
6	152	613	368	-318	Included -VT	uniform thickness is reduced by 25%

Notes:

- VT: Variable Thickness, - the self-weight is calculated for the tank with multiple layers
- UT: Uniform Thickness - the self-weight is calculated for the tank assuming that the entire height of tank wall has same thickness as that of the bottom layer
- "uniform thickness" in the stiffness calculations indicate that the thickness of the entire wall is assumed same as bottom layer thickness

From examining the data in Table 4.6, it can be seen that, for finding the required projection length of the bottom plate and the corresponding stress values on either side of the joint, excluding the self-weight and assuming the bottom layer thickness for the entire wall for stiffness is appropriate. This assumption will give a slightly lower value of bending stress on the outer side of joint. Since it is a location outside the tank, and yielding and plastic hinge are allowed in this zone, this can be ignored. Similar to the case with ambient temperature tanks, providing extra projection length in elevated temperature tanks reduces the plate stress on the inner side of the shell to bottom joint and increases the stresses on the outer side. Apart from the joint, the stresses are also generally reduced in the inner portion of the bottom plate as shown in Fig. 4.15.

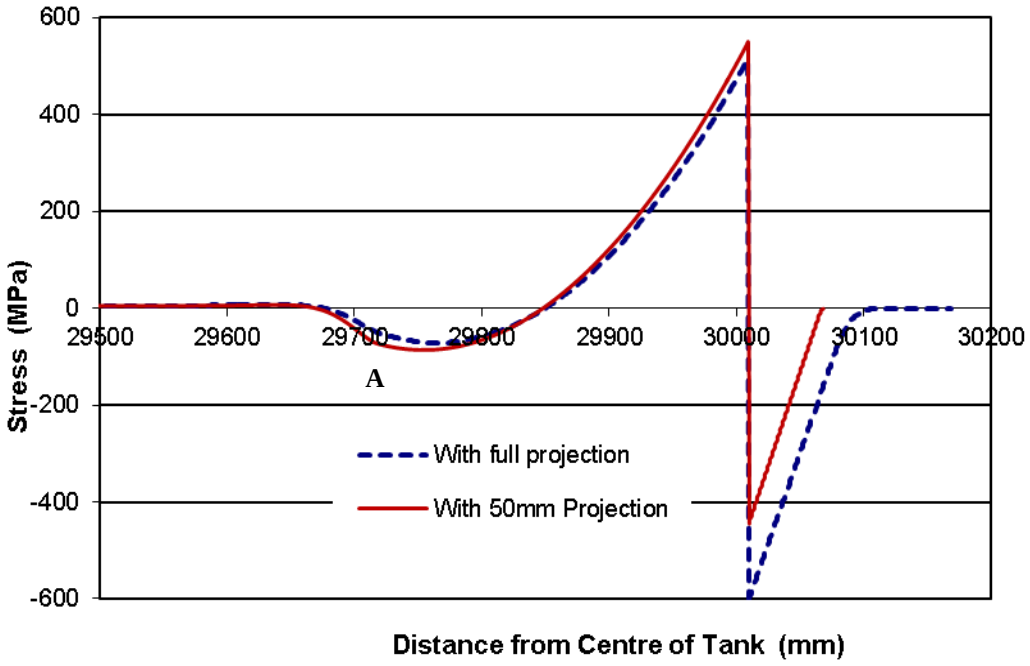

Fig. 4.15 Bending Stress in the Bottom Plate of Elevated Temperature Tank

The figure refers to a tank with 30m radius, 12m height, 18mm shell thickness and 6mm bottom plate subjected to a uniform temperature rise of 347°F (175°C). Axisymmetric shell elements are used to model the tank wall and bottom plate with contact elements for bottom plate - subgrade interaction.

4.10 EFFECT OF SELF-WEIGHT ON STRESSES (COMPARISON USING FEA)

This section discusses the effect of self-weight on the stresses in the tank wall and bottom plate. A tank with multiple wall thicknesses (CASE 2 - described in Chapter 3) is considered. It is a fairly big tank in the upper end of the design range. Two FE models with and without the self-weight effect are used for the study

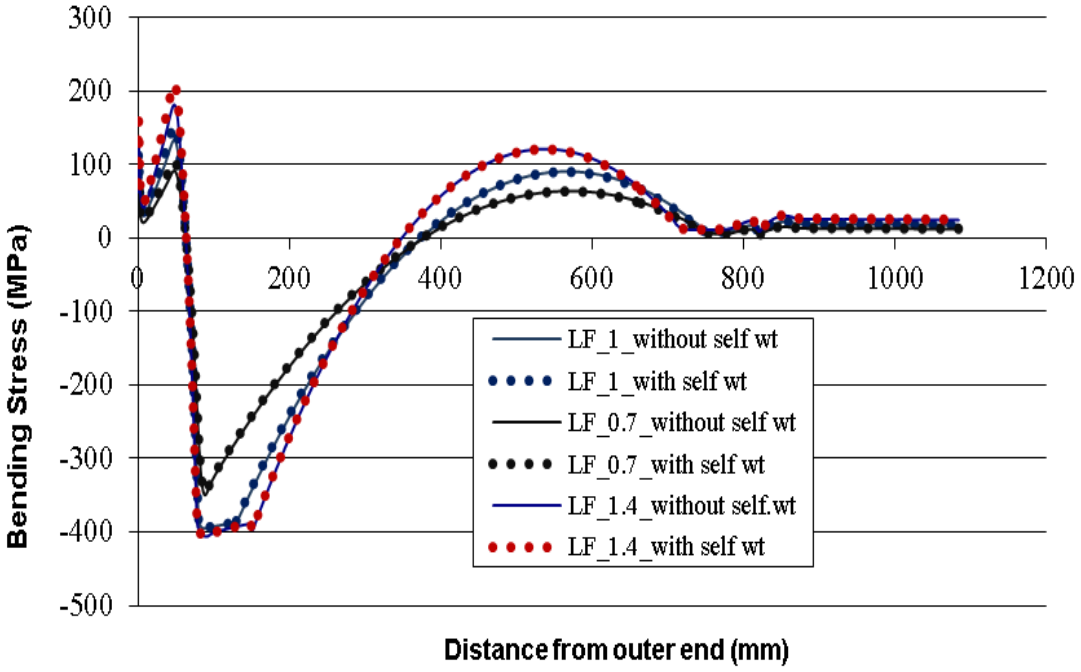

Fig. 4.16 Bending Stress in Bottom Plate (Bottom Side) – With and Without Self-weight

. Figures 4.16 and 4.17 show the bending stress in the bottom plate for three different load factors (0.7, 1, and 1.4). "LF" indicates Load Factor; a value of 1 indicates that the tank is filled fully with a liquid of specific gravity 1. Fig 4.17 is the same as Fig.4.16 but zoomed and expanded near the shell-to-bottom joint.

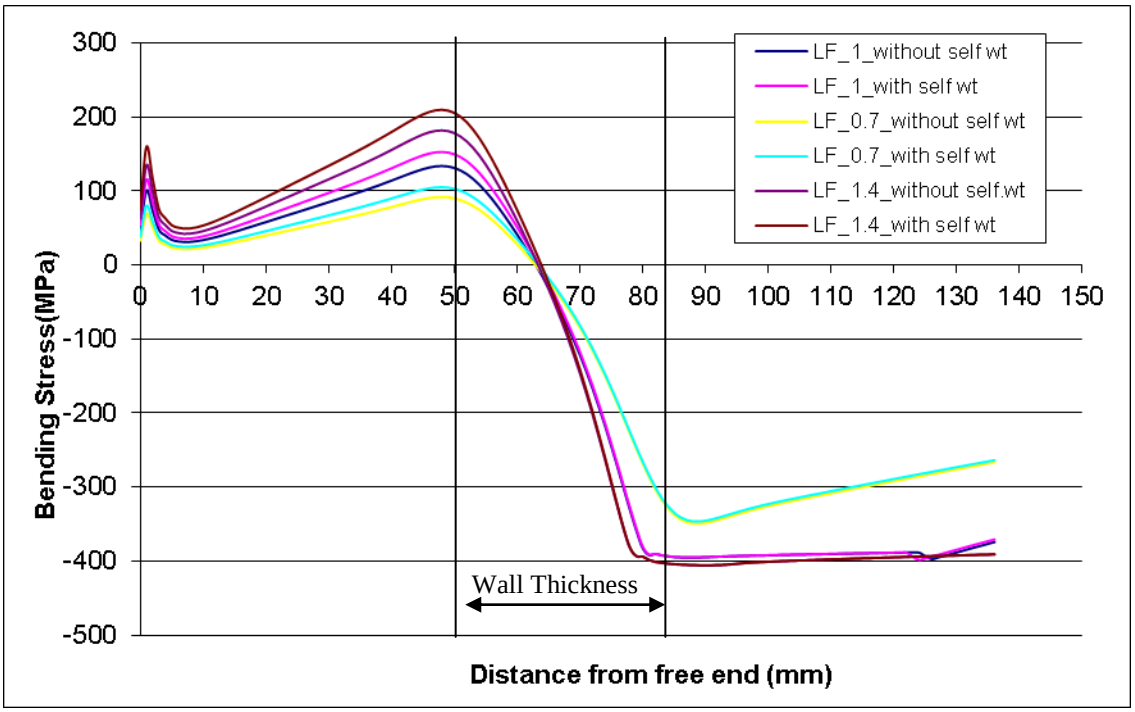

Fig. 4.17 Bending Stress in Bottom Plate – With and Without Self wt. – Expanded View Near Tank Wall

From the plots above it can be seen that the self-weight affects the bending stress of the bottom plate only in a small portion on the outer side of the shell to bottom joint. Inner side, the stresses are not significantly affected by the self-weight. For the LF=1 case, the maximum difference occurs close to the joint (3mm from the shell on the outer side). The stresses increase from 133 MPa to 152 MPa with the inclusion of self-weight effect (14.3% increase). For small tanks or for lower loads, it can be expected that the percentage change will be much less. However, it should be noted that this zone is outside the tank and yielding is permissible in this region. Hence ignoring the self-weight may not have adverse effects.

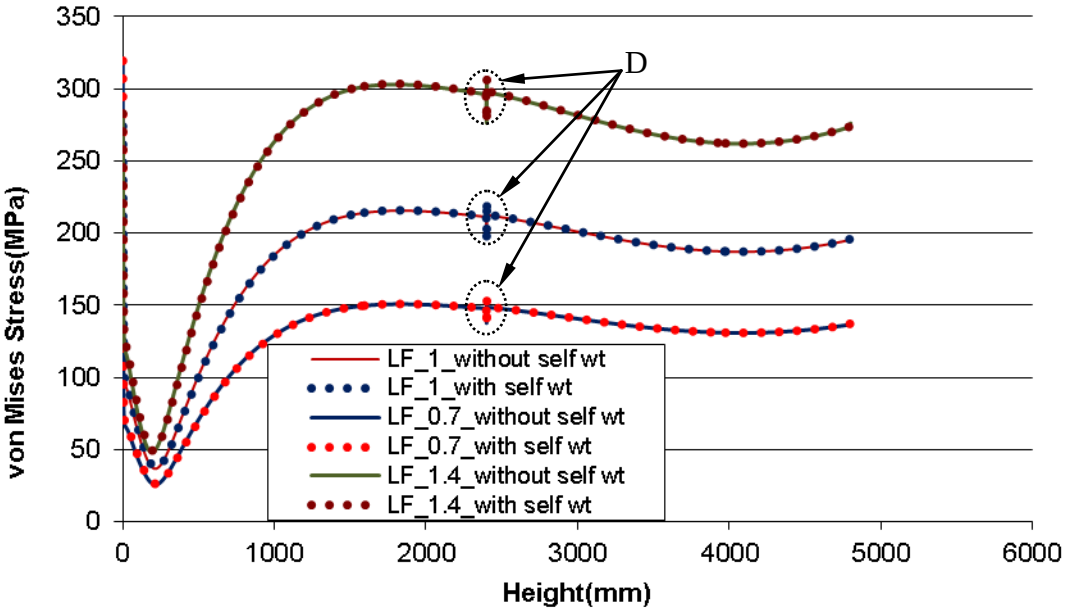

Fig. 4.18 von Mises Stress in Shell Wall – With and Without Self-weight Consideration

Figure 4.18 shows the stresses in the tank wall. As expected, shell stresses are not significantly affected by the self-weight. The maximum difference in stress for load case LF=1 is only 3 MPa higher with self-weight. The zones marked as 'D' in the stress plot for each load case are due to discontinuity resulting from change in tank wall thickness.

In case of openings at tank bottom, it can be qualitatively said that there will not be uplift of the bottom plate directly below the opening and hence the projection length determined using the proposed analysis will be conservative. However, the uplift length may be larger near the edges of opening because of the extra moments transmitted from the shell. This may cause the strains in the bottom plate to slightly increase on the inner side. The nozzle loads may increase or decrease the corresponding bottom plate stresses slightly based on the direction of the nozzle load.

4.11 CLOSURE

The shell to bottom joint is an important high stress location in the tank where the material is close to yield or in plastic range. This joint is a critical failure zone for tank failure. Hence proper evaluation of stresses in this zone is very important. Denham's beam model (where the projection length is assumed to be fixed as 3") is reviewed and validated using FEA. The model is extended to any arbitrary projection length. Using this theoretical approach and FEA, the effect of bottom plate projection beyond the shell wall has been studied for tanks on rigid ring wall foundations. It is found that the length of projection changes the stresses in the shell as well as the bottom plate near the shell to bottom joint. Increasing the length is beneficial. The stresses will not alter if the length is increased beyond a certain limit, which is being termed as 'full projection length'. An extension to Denham's model is proposed to determine this 'full projection length'. The theoretical results are validated using FEA. The effect of assuming a uniform thickness for a variable thickness tank wall for the sake of determining the 'full projection length' is studied and found to be acceptable. Similarly the results of including or excluding the self-weight of the tanks are compared. The self-weight of tank does not increase the stresses in the tank wall or the bottom plate on the inner side of the shell to bottom joint, whereas it may increase the stresses marginally on the outer side of the joint.

An expression for the tank wall bottom moment has been presented for ambient temperature tanks. Using the expression the designer can readily find the moment at the shell to bottom joint and hence the stresses in that zone. This equation is based on a fully elastic model and may be used to find the stresses near the shell to bottom joint.

CHAPTER 5

INCORPORATION OF FRICTION COEFFICIENT IN ELEVATED TEMPERATURE TANK DESIGN

Storage tanks operating at elevated temperatures (200°F to 500°F) need to consider stresses due to thermal expansions and restraints to the expansion in addition to the design requirements for ambient temperature tanks. Appendix M of API Standard 650 provides additional requirements and guidelines for the design of tanks operating at elevated temperatures. These are based on Karcher's method [Karcher, 1978a, b] which gives a simplified procedure for determining the stresses in the tank wall and bottom plate. During temperature cycle, the tank will expand radially at the bottom. This expansion is partially or fully restrained by friction between the tank bottom and foundation components. A factor named 'C' is used for defining the ratio of actual expansion to free expansion of the tank. Such partial expansion causes significant thermal stresses. API uses these stresses to estimate the low cycle fatigue life of the tanks. At present, a range of 'C' values (0.25–1.0) is allowed by API without clear guidelines for selecting a suitable value. If no other choice is available, API 650 specifies that 'C' be taken as 0.85. API 650 does not provide any guidelines to determine the 'C' factor. The present study is aimed at systematic estimation of the 'C' factor by relating it to the friction coefficient. This Chapter evaluates the current procedure and suggests an

alternate method by incorporating the friction coefficient directly in the stress equations, instead of the ‘C’ factor.

5.0 BACKGROUND

In many industries, storage tanks are needed to hold liquids like asphalt, residuum, high pour point hydrocarbons, etc., at higher temperature than the ambient. This gives rise to thermal stresses in the tank, especially near the shell-to-bottom joint. The magnitude of thermal stress occurring in the tank wall and the bottom plate is influenced by the amount of radial restraint, which in turn depends upon factors like liquid pressure, friction between the bottom plate and the foundation, piping connections and differential settlement. In addition, from low cycle fatigue point of view, the cyclic loading due to continual filling and draw down is reported [Long and Garner, 2004] to be more severe for elevated temperature tanks compared to that for ambient temperature tanks.

The general basis of the tank wall design for tanks operating at ambient temperature (any temperature less than 200°F or 93°C) is to limit the hoop stress to the allowable limits using either the 1-Foot Method or the more accurate Variable-Design-Point Method. American Petroleum Institute Standard, API 650 [2012] adopted these design procedures which were originally proposed by Zick and McGrath [1986]. In the case of elevated temperature tanks, API 650 provides guidelines in Appendix M “Additional Requirements for Tanks Operating at Elevated Temperatures.” This gives requirements for operation of large storage tanks at temperatures up to 500 °F (260 °C). It

is recommended that, for designing the tank wall, the same procedure as that of ambient temperature tanks shall be used with modified allowable stress limits based on strength reduction factors for the design temperature. This Appendix provides design considerations for limiting the loadings and strains resulting from thermal effects, such as differential thermal expansion, tank bottom plate buckling and thermal cycling.

A typical complete thermal cycle for an elevated temperature tank can be described as follows [Jones and Seshadri, 1989]:

- Gasoil is pumped in to the storage tank and then heated to a specified temperature
- The Gasoil is heated slowly to allow any excess water to be removed by drainage or blow off. This step will also allow gradual thermal expansion of the tank and shell
- The tank is filled with a high pour point hydrocarbon. When there is a demand for stored fluid, the tank is drawn down to a specified level and the procedure is repeated as needed.

For tanks with maximum design temperature greater than 93°C (200°F), particular consideration should be given to the following thermal effects [API 650]:

- Temperature differences between the tank bottom and the lower portion of the shell. Such thermal differences may result from factors such as the method and sequence of filling and heating or cooling, the degree of internal circulation, and heat losses to the foundation and from the shell to the atmosphere. With such

temperature differences, it may be necessary to provide for increased piping flexibility, an improved bottom-to-shell joint, and a thicker annular ring or bottom sketch plates to compensate for increased rotation of the bottom-to-shell joint.

- The ability of the bottom to expand thermally, which may be limited by the method of filling and heating. With such a condition, it may be necessary to provide improved bottom welding in addition to the details suggested above.
- Temperature differences or gradients between members, such as the shell and the roof or stairways, the shell and stiffeners, the roof or shell and the roof supports, and locations with insulation discontinuities.
- Whether or not the contents are allowed to solidify and are later reheated to a liquid, including the effect on columns, beams, and rafters. The possible build-up of solids on these components and the potential for plugging of the vent system should also be considered.
- The number and magnitude of temperature cycles the tank is expected to undergo during its design life.

The shell-to-bottom joint is a critical location vulnerable in many modes of failure. Denham, et al. [1968a, b], Wu and Liu [2000] and Sathyanarayanan and Adluri [2011] have proposed methods to determine the stresses in the bottom plate near this joint for ambient temperature tanks. As mentioned above, this joint is subjected to low cycle fatigue due to cyclic loading of the stored liquid (fill–draw down cycle) or the fluctuation in the temperature of the stored liquid or both. Karcher [1978a, 1978 b, 1981a, 1981b] carried out a ground breaking and very useful study on elevated temperature tanks. He

provided stress equations based on an assumed plastic hinge boundary condition at the shell-to-bottom joint. Based on these, he proposed a simplified procedure to find the fatigue design life of the tank considering the maximum stress developed at the shell-to-bottom joint and a relevant stress concentration factor. API 650 has adopted Karcher's procedure for determining the design cyclic life of the tank.

5.1 CURRENT PRACTICE

The current practice assumes uniform temperature increase in the tank, i.e., without any temperature gradient across the thickness of the shell wall. This is a reasonable assumption since the shell wall thickness is relatively thin and carbon steel is a conductive material. At steady state, the difference in temperature should not be significant. In addition to these, the temperature difference (if any) between the bottom region of the shell and the bottom plate that might be caused by heat loss is ignored. The stresses are determined using shell theory for tank wall while beam-on-elastic foundation theory is used for the bottom plate. It is assumed that complete plastic hinges are formed in the bottom plate near the shell-to-bottom joint [Karcher 1978 a, 1978b, 1981a, 1981b], while the shell stresses are assumed to be elastic. Essentially the equations as given by Timoshenko and Woinowsky-Kreiger [1959] for cylindrical tanks with clamped end conditions are suitably modified to have the plastic moment at the bottom as the boundary condition. The hydrostatic stresses caused by liquid infill are combined with the stresses that may be induced due to heating of the filled liquid. Two plastic hinges are

assumed at the bottom plate for a rigid foundation (such as concrete ring wall or pile cap) while one hinge is used for flexible subgrade below the tank wall.

5.1.1 Stresses in Shell (Tank Wall)

Based on the shell theory [Timoshenko and Woinowsky-Kreiger, 1959], the following equations were given by Karcher [1981a, b] with an assumption of a single plastic hinge at the shell bottom (applicable for the earthen foundation case),

The radial deflection of the tank wall (y_s) is given by

$$y_s = -\frac{\gamma R^2}{Et_s}\left\{H - x_s + \frac{\alpha \Delta T E t_s}{\gamma R} - e^{-\beta x_s}\left[\left(H + \frac{C\alpha \Delta T E t_s}{\gamma R}\right)\cos\beta x_s + \frac{2\beta^2 M_o}{\gamma}\sin\beta x_s\right]\right\} \quad (5.1)$$

where, α is the coefficient of thermal expansion, ΔT is the uniform temperature rise, C is the reduction factor for ΔT to account for the friction restraint, M_o is the moment at the shell to bottom joint and 'x_s' is the height of a point along the tank wall at which the deflection is calculated.

The bending moment, hoop force and shear force of the tank wall at a distance 'x_s' from the tank bottom are given by

$$M_{x_s} = -\frac{\gamma}{2\beta^2} e^{-\beta x_s}\left[\left(H + \frac{C\alpha \Delta T E t_s}{\gamma R}\right)\sin\beta x_s - \frac{2\beta^2 M_o}{\gamma}\cos\beta x_s\right] \quad (5.2)$$

$$N_\theta = \gamma R\left\{H - x_s - e^{-\beta x_s}\left[\left(H + \frac{C\alpha \Delta T E t_s}{\gamma R}\right)\cos\beta x_s + \frac{2\beta^2 M_o}{\gamma}\sin\beta x_s\right]\right\} \quad (5.3)$$

$$Q_{x_s} = -\frac{\gamma}{2\beta} e^{-\beta x_s}\left\{\left(H + \frac{C\alpha \Delta T E t_s}{\gamma R}\right)(\cos\beta x_s - \sin\beta x_s) + \frac{2\beta^2 M_o}{\gamma}(\sin\beta x_s + \cos\beta x_s)\right\} \quad (5.4)$$

If ΔT in the equations above is assumed to be zero, then these equations reduce to those for a cylindrical shell loaded by hydrostatic pressure as given by Timoshenko and Woinowsky-Kreiger [1959]. These equations can be used to find maximum stress intensities in the shell and hence fatigue evaluation can be carried out, if required, for the loading cycles that are expected during the design life of the tank.

All the above equations were developed based on the assumption that the boundary condition at the shell to bottom joint is represented by a moment M_o and zero radial deflection. Both of these assumptions (with M_o replaced by a single plastic hinge) were first used by Zick and McGrath [1968] for finding the stresses in the shell wall for an ambient temperature tank. The basis of these assumptions is given in their report to the API. The validity of the first assumption will be discussed in Chapter 6. Regarding the second assumption, Karcher [1978a, 1978 b] explains that even though the assumption of zero deflection seems to be open to question, in actual practice, an elevated temperature tank is usually filled initially to a level of several meters with only partially heated or cold product. Then internal heaters and mixers are used to increase and maintain product temperature. This start up procedure (with a smaller liquid head being heated to full temperature) results in the tank bottom expanding more freely than the case where the full liquid head is heated from ambient temperature. This results in lower frictional resistance between tank bottom and the foundation. Preliminary observations on several tanks indicate that the annular plate expands radially by about one half of the calculated value of $\alpha R \Delta T$. Therefore assuming that the annular plate expansion is between zero and

half of $\alpha R\Delta T$ is a reasonable approximation with the former being more conservative [Karcher, 1981a].

Karcher accounted for the partial radial expansion of bottom plate by employing a reduction factor ('C') in the equations above. A 'C' value of 1 assumes a fully restrained bottom to shell junction (0% radial expansion) and a value of zero assumes free (100%) radial expansion. The bottom will have free expansion (equal to $R\alpha\Delta T$) if there is essentially no friction. But in reality, there are friction forces under the tank bottom/annular plate (including backing plates, etc.) and hence the plate expands partially ($0.25 \leq C \leq 1.0$). The magnitude of friction forces also depends on the liquid head in the tank available at the time of heating.

5.1.2 Stresses in Annular Plate

The shell-to-bottom joint location is a region of high strains and plastic hinges are assumed to form in the bottom plate near this location. The stress created here can be classified as secondary bending stress and hence should be limited to twice the yield strength of the annular plate material to assure shakedown to an elastic action. The pseudo bending stress representing the strain range that occurs in the tank annular plate at the shell-to-bottom joint is obtained by the following procedure [Karcher, 1978a]:

- From Eq. 5.1, assuming a fully plastic annular plate moment at the shell bottom (i.e., $M_o = M_p$), the slope at the bottom of the tank wall is determined as

$$\theta_S = \left.\frac{dy_s}{dx_s}\right|_{x_s=0} = \frac{\gamma R^2}{Et_s}\left\{1 - \beta H - \frac{\beta C\alpha\Delta T E t_s}{\gamma R} + \frac{\beta^3 S_Y t_b^2}{2\gamma}\right\} \qquad (5.5)$$

- In order to find the strain range in the annular plate at the shell-to-bottom junction, it is assumed that annular plate reacts like a beam-on-elastic foundation. Following Hetenyi [1971], the moment in the plate is $M = K\theta/4\Omega^3$, where, $\Omega = \sqrt[4]{\frac{3K}{Et_b^3}}$ and K is the modulus of the subgrade.

- The value of slope as obtained from Eq. 5.5 is used in $M = K\theta/4\Omega^3$ resulting in

$$S_b = \pm \frac{0.658\gamma R^2}{t_s} \sqrt[4]{\frac{Kt_b}{E}} \left\{ 1 - \beta H - \frac{\beta C \alpha \Delta T E t_s}{\gamma R} + \frac{\beta^3 S_Y t_b^2}{2\gamma} \right\} \tag{5.6}$$

where, S_b is the pseudo bending stress representing the strain range at the bottom plate

Equation 5.6 is valid only if the following condition is true.

$$\left(\gamma\beta H + \frac{\beta C \alpha \Delta T E t_s}{R} - \gamma \right) > \frac{\beta^3 S_Y t_b^2}{2} \tag{5.7}$$

This condition ensures that the tank is loaded thermally or hydrostatically such that a single plastic hinge forms in the bottom plate near the shell-to-bottom joint. The safe design cycle life, N, is given by,

$$N = \left(\frac{9700}{K_c S} \right)^{2.44} \tag{5.8}$$

where, S is the alternating stress range in MPa (=S_b/2), K_c is the stress concentration factor. This procedure to ensure the safe cyclic life of tank can be avoided if a significant head of heated liquid (close to design temperature) is maintained in the tank between cycles. A significant liquid head can be defined as being equal to or greater than $0.4(Dt_s)^{0.5}$ ft, where, diameter D is in feet and t_s is in inches [API 650].

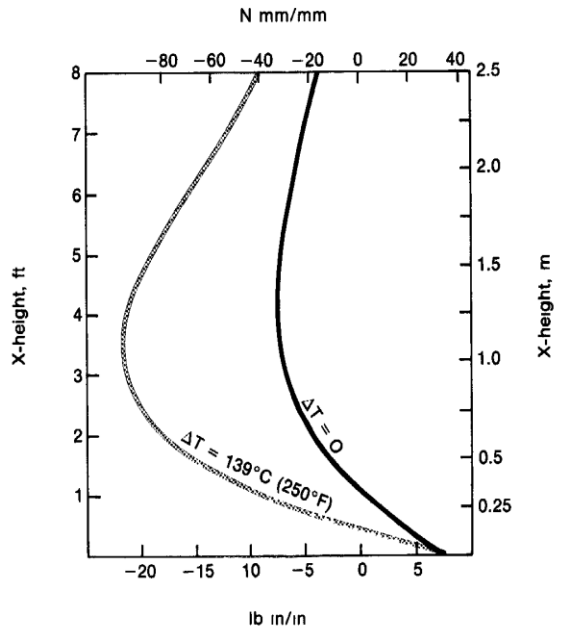

Fig. 5.1 Meridional Moment in the tank [Karcher, 1978a]

Figures 5.1 and 5.2 demonstrate the effect of temperature rise on moments and equivalent stresses (strain range) in the tank wall and the bottom plate. The results show that these stresses can be significant on the lower shell courses and annular plate regions close to shell bottom. Equations 5.5 – 5.8 depends on the C factor and hence using a proper C value becomes important.

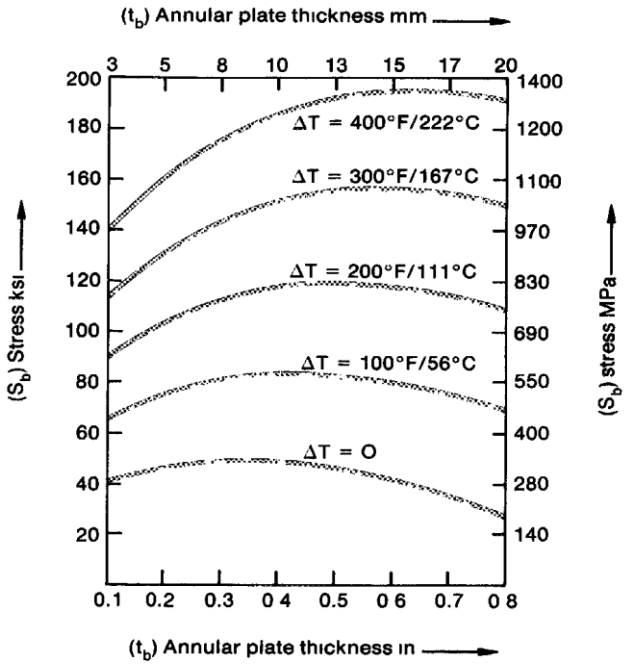

Fig. 5.2 Annular Plate Bending Stress Caused by Hydrostatic and Thermal Loads [Karcher, 1978a]

Equations 5.1-5.4 are valid for ambient and elevated temperature tanks. The basic assumptions involved in these equations regarding radial growth characteristics and the bottom moment of the tank wall have significant influence on the stresses in the tank wall. Regarding the radial deformation, as mentioned earlier, it is obvious that bottom plate can expand anywhere between zero to full radial growth ($R\alpha\Delta T$). No guidelines for selecting the actual value (within the allowable range) are available either from API or other sources. Although the current practice has not been publicly reported to have resulted in field failures and hence can be construed to be safe, use of a set value of C for all situations is not appropriate as discussed later in the Chapter. An equivalent but considerably less problematic approach using friction coefficient is discussed below.

5.2 INCORPORATION OF FRICTION COEFFICIENT IN DESIGN EXPRESSIONS

If the tank foundation does not restrain the expansion due to temperature (at least partially), then the thermal stresses will be minimal. However the foundation generally offers significant frictional resistance that restrict the free radial expansion of elevated temperature tanks which in turn induces additional thermal stresses in the tank wall. The following model obtains the partial radial expansion by first finding the effective contraction due to the friction forces and subtracting it from the free thermal expansion. The treatment is similar to that of a disc subjected to centrifugal forces. Considering the equilibrium of an infinitesimal element in the bottom plate of the tank as shown in Fig. 5.3 (a).

$$\left(\sigma_{rr}+d\sigma_{rr}\right)\left(r+dr\right)d\theta\, t_p-\sigma_{rr}\,(r\,d\theta)\,t_p-2\,\sigma_{\theta\theta}\left(\frac{d\theta}{2}\right)dr\,t_p=r\,d\theta\,dr\,\mu\gamma H \tag{5.9}$$

where, σ_{rr} and $\sigma_{\theta\theta}$ are the stress components in the radial and circumferential directions, μ is the coefficient of friction between the bottom plate and the foundation as appropriate to the given conditions. It is generally assumed that the tank bottom is resting on well compacted dry sand/gravel. The equation assumes that the friction forces are predominantly in the membrane direction of the bottom plate [Sathyanarayanan and Adluri, 2013c].

Neglecting higher order terms in Eq.5.9,

$$\frac{d\sigma_{rr}}{dr}+\frac{1}{r}\left(\sigma_{rr}-\sigma_{\theta\theta}\right)=-\frac{\mu\gamma H}{t_p} \tag{5.10}$$

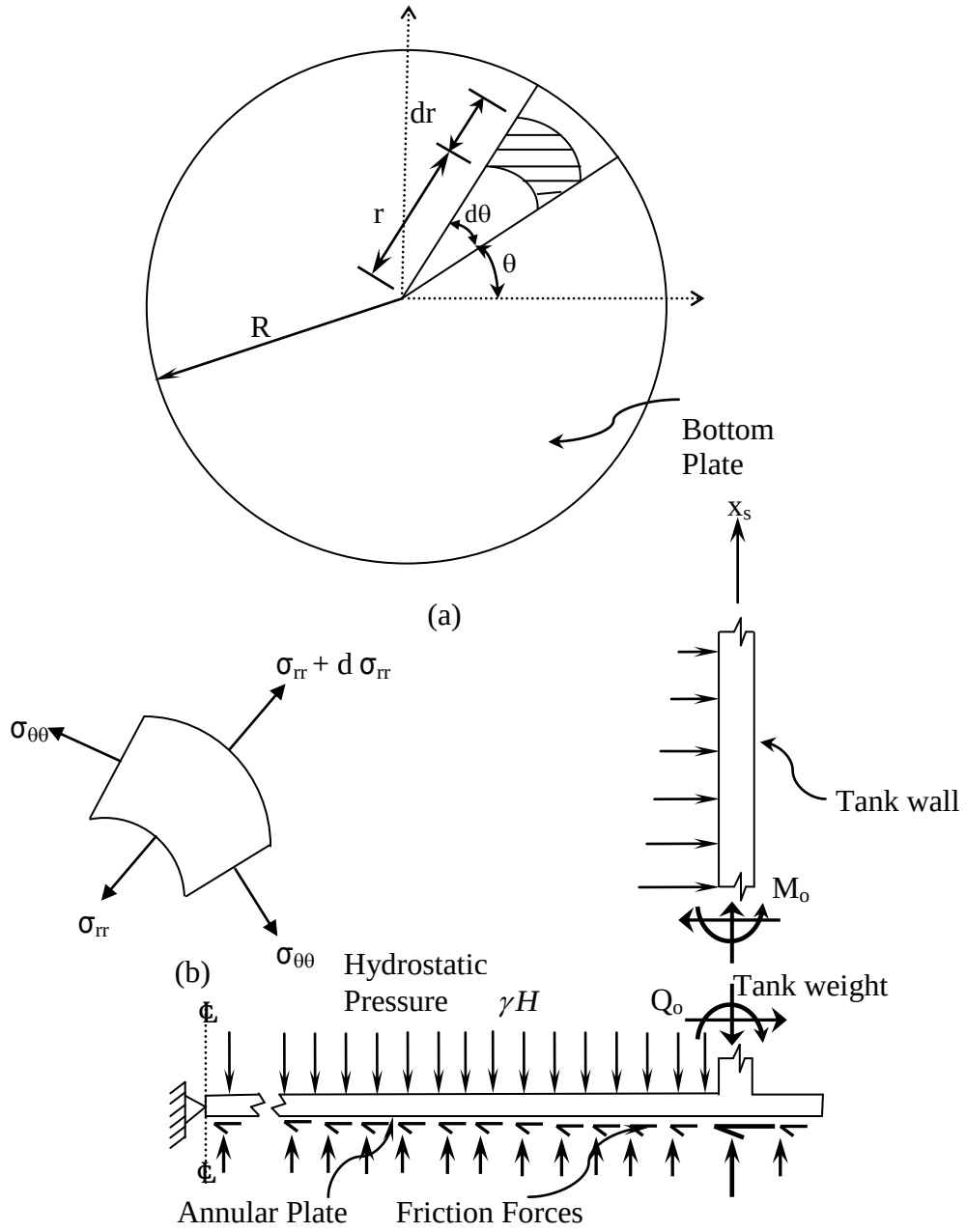

Fig. 5.3 Friction Forces Below Bottom Plate

For axisymmetric plates the stress displacement relationships are given by [Boresi and Schmidt, 1993]

$$\sigma_{rr} = \frac{E}{1-\nu^2}\left(\frac{du}{dr} + \nu\frac{u}{r}\right) \tag{5.11}$$

$$\sigma_{\theta\theta} = \frac{E}{1-\nu^2}\left(\nu\frac{du}{dr} + \frac{u}{r}\right) \tag{5.12}$$

where, *u* is the radial displacement at any point in the bottom plate due to friction forces. The negative sign in Eq. 5.10 indicates the contraction of the plate.

Substituting (5.11) and (5.12) in (5.10)

$$\frac{E}{1-\nu^2}\left(\frac{d^2u}{dr^2} + \frac{1}{r}\frac{du}{dr} - \frac{u}{r^2}\right) = -\frac{\mu\,\gamma\,H}{t_p} \tag{5.13}$$

Solving Eq.5.13,

$$u = \frac{-\left(1-\nu^2\right)}{E}\frac{\mu\gamma H}{t_p}\frac{r^2}{3} + C_1 r + \frac{C_2}{r}$$

where, C_1 and C_2 are constants of integration. Using appropriate boundary conditions for the given loading,

$$u = \frac{\left(1-\nu\right)}{3E}\frac{\mu\,\gamma\,H}{t_p}r^2 \tag{5.14}$$

It must be pointed out that in addition to the above, there will be other effects due to shear at the bottom, self-weight of bottom plate and tank wall stiffness (in relation to that of the bottom plate). These can be shown [Adluri, 2012] to have only a small influence. Other effects such as those due to local loss of contact with the foundation, local bending of bottom plate due to bulging (or buckling), bottom plate lap welds, weld

reinforcements, backing strips, horizontal soil pressure due to uneven bottom surface of the plate, etc., have also been omitted in the present treatment. Although the bottom plate is treated with a single thickness here, multiple thickness plate along with other effects omitted above can be incorporated. In a recent report, Adluri [2012] extended the treatment given in the present chapter and discussed these issues at length along with the effects of non-uniform friction below the bottom due to soil shearing under parts of the bottom plate. The treatment in the present thesis is a general approach that can be used with a single equivalent value for μ for the entire bottom plate.

Hence for any tank subjected to uniform temperature increase ΔT, the partial radial expansion of the tank bottom after filling the liquid to a height H and heating it to the required temperature, will be given by

$$\delta = R\alpha\Delta T - \frac{(1-\nu)}{3E}\frac{\mu\,\gamma\,H\,R^2}{t_p} \tag{5.15}$$

Note that H indicates the actual liquid height and not the constructed height of the tank wall. The 'C' factor as used currently can be interpreted to represent the ratio between the restraint deformation due to friction forces and the free expansion of the bottom plate. Hence,

$$C = \frac{(1-\nu)}{3E}\frac{\mu\,\gamma\,H\,R}{t_p\,\alpha\,\Delta T} \tag{5.16}$$

The ‘C’ value will be 1.0 when the restraint deformation as calculated is equal to or more than the free thermal expansion. The C-factor will be zero if the restraint deformation is zero.

5.2.1 Incorporation of Friction Coefficient in Shell Equations

The governing equation for circular cylindrical shell (Fig.5.4) loaded symmetrically with respect to its axis [Timoshenko and Woinowsky-Kreiger, 1959] is as follows

$$\frac{d^4 y_s}{dx_s^4} + 4\beta^4 y_s = \frac{w}{D_s} \tag{5.17}$$

where, y_s is the radial deflection, w is the liquid pressure acting inside the cylinder, β and D_s are shell parameters, where $D_s = \frac{Et_s^3}{12\left(1-\nu^2\right)}$

The general solution for the above equation is

$$y_s = e^{\beta x_s}\left(c_1 \cos\beta x_s + c_2 \sin\beta x_s\right) + e^{-\beta x}\left(c_3 \cos\beta x_s + c_4 \sin\beta x_s\right) + f\left(x_s\right) \tag{5.18}$$

For circular tanks with uniform wall thickness, Eq. 5.17 is modified as

$$\frac{d^4 y_s}{dx_s^4} + 4\beta^4 y_s = \frac{\gamma\left(H - x_s\right)}{D_s} \tag{5.19}$$

A particular solution of Eq.5.19 is

$$y_s = \frac{\gamma\left(H - x_s\right)R^2}{Et_s} \tag{5.20}$$

The complete solution of Eq. 5.19 is

$$y_s = e^{\beta x_s}\left(c_1 \cos\beta x_s + c_2 \sin\beta x_s\right) + e^{-\beta x_s}\left(c_3 \cos\beta x_s + c_4 \sin\beta x_s\right) - \frac{\gamma\left(H - x_s\right)R^2}{Et_s} \tag{5.21}$$

Considering the shell as infinitely long; $c_1 = c_2 = 0$

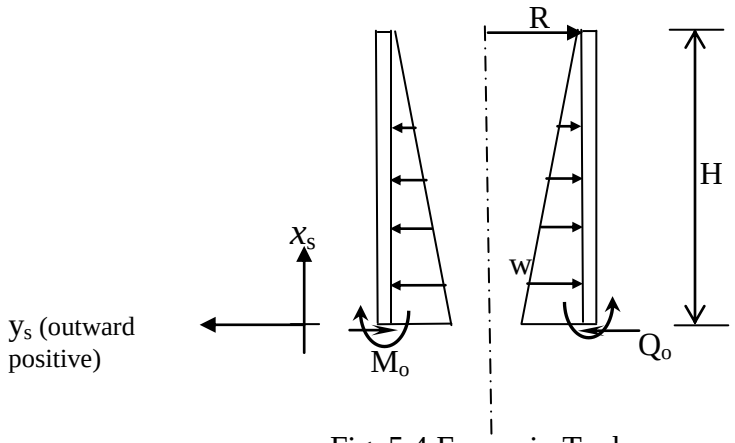

Fig. 5.4 Forces in Tank

Using the boundary condition that there is no radial expansion at the bottom of the tank (for hydraulic loading only) and the moment at the tank bottom is M_o, Eq. 5.22 is obtained. The moment (M_o) at the tank bottom can be a maximum of one/two times the plastic moment capacity of the bottom plate. It is denoted by M_b.

In case of earthen foundation, with a single plastic hinge on the inside $M_b = \frac{S_y t_p^2}{4}$ and in case of concrete ring wall foundation, with a plastic hinge on either side of shell $M_b = \frac{S_y t_p^2}{2}$. This gives,

$$y_s = e^{-\beta x_s}\left(\frac{\gamma H R^2}{E t_s}\cos\beta x_s + \frac{M_b}{2D_s\beta^2}\sin\beta x_s\right) - \frac{\gamma\left(H - x_s\right)R^2}{E t_s} \qquad (5.22)$$

$$\frac{dy_s}{dx_s} = \beta e^{-\beta x_s}\left(\frac{M_b}{2D_s\beta^2}\left(\cos\beta x_s - \sin\beta x_s\right) - \frac{\gamma HR^2}{Et_s}\left(\cos\beta x_s + \sin\beta x_s\right)\right) + \frac{\gamma R^2}{Et_s} \qquad (5.23)$$

$$\frac{d^2y_s}{dx_s^{\,2}} = 2\beta^2 e^{-\beta x_s}\left(\frac{\gamma HR^2}{Et_s}\sin\beta x_s - \frac{M_b}{2D_s\beta^2}\cos\beta x_s\right) \qquad \ldots\ldots\ldots \qquad (5.24)$$

5.2.2 Thermal Stresses in Cylinders

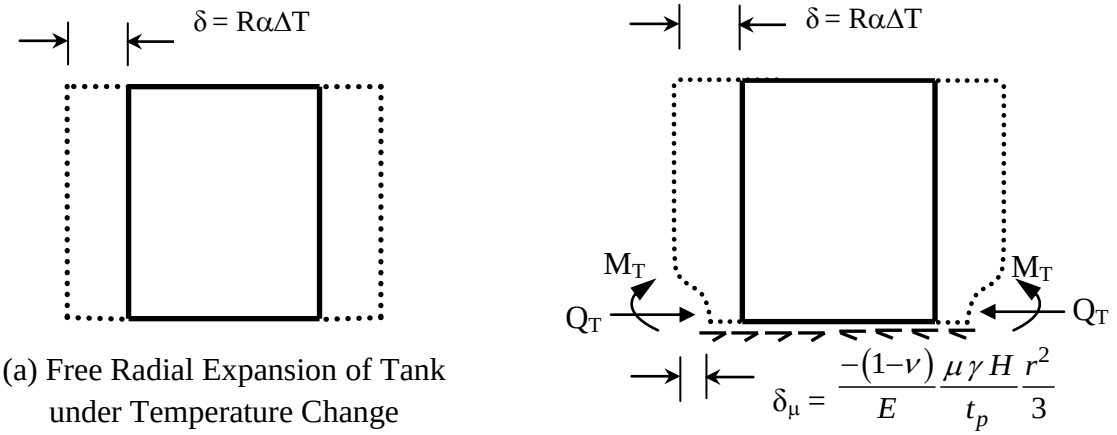

(a) Free Radial Expansion of Tank under Temperature Change

(b) Thermal Expansion of Tank with Frictional Forces

Fig. 5.5 Schematic Expansion of Tank

In Fig. 5.5, δ is the free expansion of cylinder for a uniform temperature increase of ΔT. If friction is present, δμ is the expansion at the bottom of the cylinder (and the bottom plate) for a uniform temperature increase. From Eq.5.17 & 5.18 and considering the shell as infinitely long with only temperature loading, Eq.5.25 can be obtained. The term $f(x_s)$ representing the particular solution in Eq.5.18 becomes zero since there is no pressure loading for pure temperature loading (which can be added to the separate solution obtained for hydrostatic loading).

$$y_s = e^{-\beta x_s}\left(c_3 \cos \beta x_s + c_4 \sin \beta x_s\right) \tag{5.25}$$

$$\frac{dy_s}{dx_s} = \beta e^{-\beta x_s}\left[c_4\left(\cos \beta x_s - \sin \beta x_s\right) - c_3\left(\cos \beta x_s + \sin \beta x_s\right)\right] \tag{5.26}$$

$$\frac{d^2 y_s}{dx_s^{\,2}} = 2\beta^2 e^{-\beta x_s}\left(c_3 \sin \beta x_s - c_4 \cos \beta x_s\right) \tag{5.27}$$

$$\frac{d^3 y_s}{dx_s^{\,3}} = 2\beta^3 e^{-\beta x_s}\left(c_3 \cos \beta x_s - c_3 \sin \beta x_s\right) + \left(c_4 \sin \beta x_s + c_4 \cos \beta x_s\right) \tag{5.28}$$

Let M_T and Q_T be the moment and shear force induced at the bottom due to thermal loading,

$$\left(M_{x_s}\right)_{x_s=0} = -D_s\left(\frac{d^2 y_s}{dx_s^{\,2}}\right) = M_T \tag{5.29}$$

$$\left(Q_{x_s}\right)_{x_s=0} = \left(\frac{dM_{x_s}}{dx_s}\right)_{x=0} = -D_s\left(\frac{d^3 y_s}{dx_s^{\,3}}\right)_{x_s=0} \tag{5.30}$$

From Eq. 5.29 and Eq. 5.27

$$c_4 = \frac{M_T}{2D_s\beta^2} \tag{5.31}$$

From Eq. 5.30 and Eq. 5.28

$$c_3 = -\frac{1}{2D_s\beta^3}\left(Q_t + \beta M_T\right) \tag{5.32}$$

Substituting the constants,

$$y_s = \frac{-e^{-\beta x_s}}{2D_s\beta^3}\left(Q_T + \beta M_T\right)\cos\beta x_s + \frac{e^{-\beta x_s}M_T}{2D_s\beta^2}\sin\beta x_s \tag{5.33}$$

$$\frac{dy_s}{dx_s} = \frac{e^{-\beta x_s}}{2D_s\beta}\left[M_T\left(\cos\beta x_s - \sin\beta x_s\right) - \left(\frac{Q_T + \beta M_T}{\beta}\right)\left(\cos\beta x_s + \sin\beta x_s\right)\right] \tag{5.34}$$

Considering the boundary condition as shown in Fig. 5.5 (b),

$$\left(y_s\right)_{x_s=0} = -\frac{(1-\nu)}{3t_pE}R^2\mu\gamma H \tag{5.35}$$

Equating Eq. 5.33 and Eq. 5.35 at $x_s = 0$

$$\frac{-1}{2D\beta^3}\left(Q_T + \beta M_T\right) = \frac{(1-\nu)}{3t_pE}R^2\mu\gamma H \tag{5.36}$$

Using Eq. 5.36 in Eq. 5.33

$$y_s = e^{-\beta x_s}\left(\frac{(1-\nu)}{3t_pE}R^2\mu\gamma H\right)\cos\beta x_s + \frac{e^{-\beta x_s}M_T}{2D_s\beta^2}\sin\beta x_s \tag{5.37}$$

$$\frac{dy_s}{dx_s} = e^{-\beta x_s}\beta\left[\frac{M_T}{2D_s\beta^2}\left(\cos\beta x_s - \sin\beta x_s\right) - \left(\frac{(1-\nu)}{3t_pE}R^2\mu\gamma H\right)\left(\cos\beta x_s + \sin\beta x_s\right)\right] \tag{5.38}$$

$$\frac{d^2y_s}{dx_s^2} = 2e^{-\beta x_s}\beta^2\left[\left(\frac{(1-\nu)}{3t_pE}R^2\mu\gamma H\right)\sin\beta x_s - \frac{M_T}{2D_s\beta^2}\cos\beta x_s\right] \tag{5.39}$$

Using the principle of superposition, displacement (w), moment (M_x) and shear (Q_x) due to the liquid infill and the temperature rise is given by

$$y_s = e^{-\beta x_s}\left[\left(\frac{1}{t_s} + \frac{(1-\nu)}{3t_p}\mu\right)\frac{R^2\gamma H}{E}\cos\beta x_s + \frac{\left(M_T + M_b\right)}{2D_s\beta^2}\sin\beta x_s\right] - \frac{\gamma\left(H - x_s\right)R^2}{Et_s} \tag{5.40}$$

$$\frac{dy_s}{dx_s} = \beta e^{-\beta x_s}\left[\begin{array}{l}\dfrac{(M_T + M_b)}{2D_s\beta^2}(\cos\beta x_s - \sin\beta x_s) \\ -\left(\dfrac{1}{t_s} + \dfrac{(1-\nu)}{3t_p}\mu\right)\dfrac{R^2\gamma H}{E}(\cos\beta x_s + \sin\beta x_s)\end{array}\right] + \frac{\gamma R^2}{E t_s} \quad \text{..(5.41)}$$

$$M_{x_s} = -D_s\frac{d^2y_s}{dx_s^2} = 2\beta^2 D_s e^{-\beta x_s}\left[\begin{array}{l}\dfrac{(M_T + M_b)}{2D_s\beta^2}\cos\beta x_s \\ -\left(\dfrac{1}{t_s} + \dfrac{(1-\nu)}{3t_p}\mu\right)\dfrac{R^2\gamma H}{E}\sin\beta x_s\end{array}\right] \quad (5.42)$$

$$Q_{x_s} = -D_s\frac{d^3y_s}{dx_s^3} = 2\beta^3 D_s e^{-\beta x_s}\left[\begin{array}{l}\left(\dfrac{1}{t_s} + \dfrac{(1-\nu)}{3t_p}\mu\right)\dfrac{R^2\gamma H}{E}(\cos\beta x_s - \sin\beta x_s) \\ +\dfrac{(M_T + M_b)}{2D_s\beta^2}(\sin\beta x_s + \cos\beta x_s)\end{array}\right] \quad (5.43)$$

$$N_\theta = \frac{e^{-\beta x_s} E t_s}{R}\left[\begin{array}{l}\left(\dfrac{1}{t_s} + \dfrac{(1-\nu)}{3t_p}\mu\right)\dfrac{R^2\gamma H}{E}\cos\beta x_s \\ +\dfrac{(M_T + M_b)}{2D_s\beta^2}\sin\beta x_s\end{array}\right] - \gamma(H - x_s)R \quad (5.44)$$

where, M_T and M_b represent the moment induced at the bottom due to thermal and hydrostatic loadings. The sum of these moments cannot exceed $2M_p$ for rigid foundations and M_p for flexible foundations. These equations (Eq. 5.40- 5.44) are similar to Eq. 5.1 - 5.4, where, C is replaced with the expression from Eq. 5.16. Equations 5.40 – 5.44 are valid only if 'δ' from Eq.5.15 is greater than zero i.e. the thermal expansion of bottom plate is not less than the restraint offered by the frictional forces at the tank bottom. If this is not so, it implies that the bottom of the tank does not expand at all because of high

amount of frictional resistance. For this case, replace the term $(1-\nu)\mu/3t_p$ with $E\alpha\Delta T/R\gamma H$ in the eq. 5.40-5.44.

With respect to stresses in the tank wall, Karcher's equations will yield the same results as those of the proposed model provided an exact C-factor is used. The value of 'C' has a significant influence on tank wall stresses. Predicting this factor during the design stage or even during operation without any field measurements is a difficult task. Hence using standard friction coefficients between known materials and determining the stresses using Eq. 5.40 - 5.44 will be an appropriate choice.

5.3 RESULTS AND DISCUSSION

Finite element analyzes were carried out using ANSYS to explore the effect of friction and validate the theory above. The foundation is assumed to be a concrete ring wall with highly compacted infill. Axisymmetric SHELL elements were used for modeling the tank wall and bottom plate. Both elastic and elastic-perfectly plastic material models were used as described in Chapter3.

The example tank (CASE 1) from Chapter3 with $\Delta T = 347°F$ (175°C) and $\mu = 0.3$ is considered for the study. Figure 5.6 shows theoretical deflection in tank wall with a double hinge condition for bottom plate as specified by Zick and McGrath [1968] and Karcher [1978 a,b,1981 a,b]. The shell stresses from nonlinear FEA (which does not rely on the double hinge assumption) match well with theoretical stresses. This implicitly

confirms the formation of two plastic hinges in the bottom plate near shell bottom in the FE model. The bending and hoop stresses for this analysis are shown in Figs.5.7 and 5.8. It is to be noted that eventhough the bottom plate can reach plastic stage, the shell stresses are designed to be within elastic limits for operational loads.

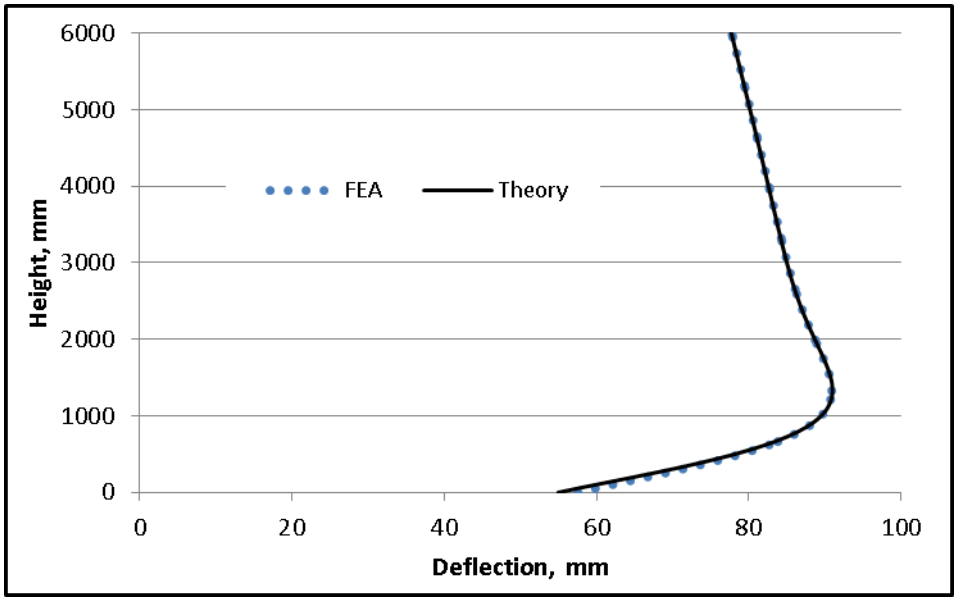

Fig. 5.6 Deflection in the Tank Wall Including the Effect of Friction (μ=0.3)

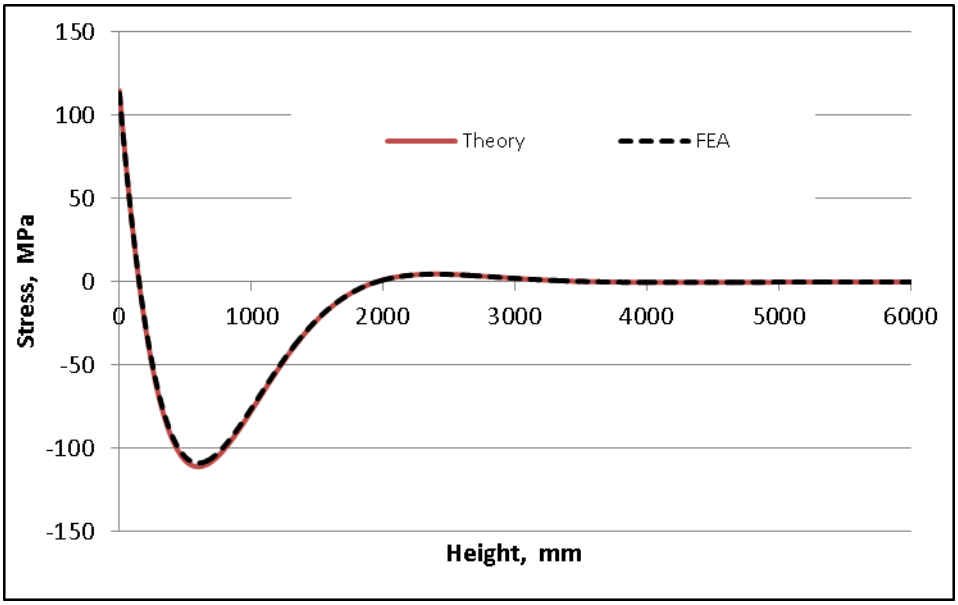

Fig. 5.7 Bending Stress (S_x) in Tank Wall Including Friction Effects (μ=0.3)

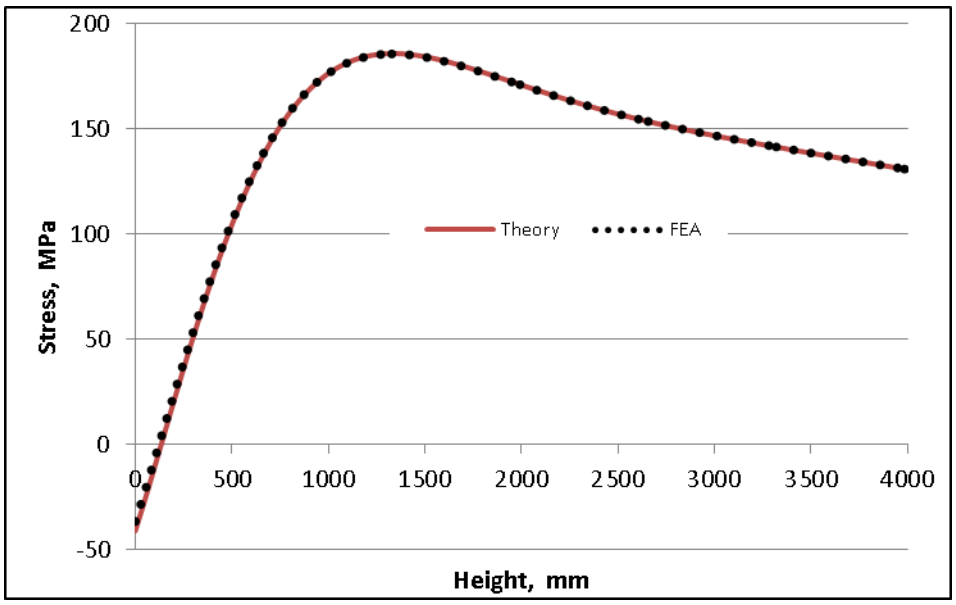

Fig. 5.8 Hoop Stress in Tank Wall Including Friction Effects (μ=0.3)

The same tank with $\mu = 0.5$ is analyzed using elastic-plastic FE model. Figure 5.9 compares the FEA results and the theoretical values. The theoretical radial displacement (horizontal movement) at the outer edge of the annular plate (Eq. 5.15) is 52.7 mm. The corresponding radial displacement as obtained from FEA (including friction effects) is 53.4 mm. If there were no friction forces, the expansion would be $R\alpha\Delta T$=63mm (with $\alpha=12x10^{6}$). For this example the value of C can be calculated as 0.15 (=[63-53.4]/63). It can be seen that this value is far smaller than the value of 0.85 recommended by API 650.

Even though, the analysis indicates that two plastic hinges form at the bottom plate for this case, a complete double hinge may not always form at the bottom for general tanks. For the tank considered, two full hinges will not form if either the friction coefficient or the temperature is less than the values used above. Hence using two plastic hinges as boundary condition for lower temperature tanks or those with smaller friction coefficient will underestimate the maximum stresses in the tank wall.

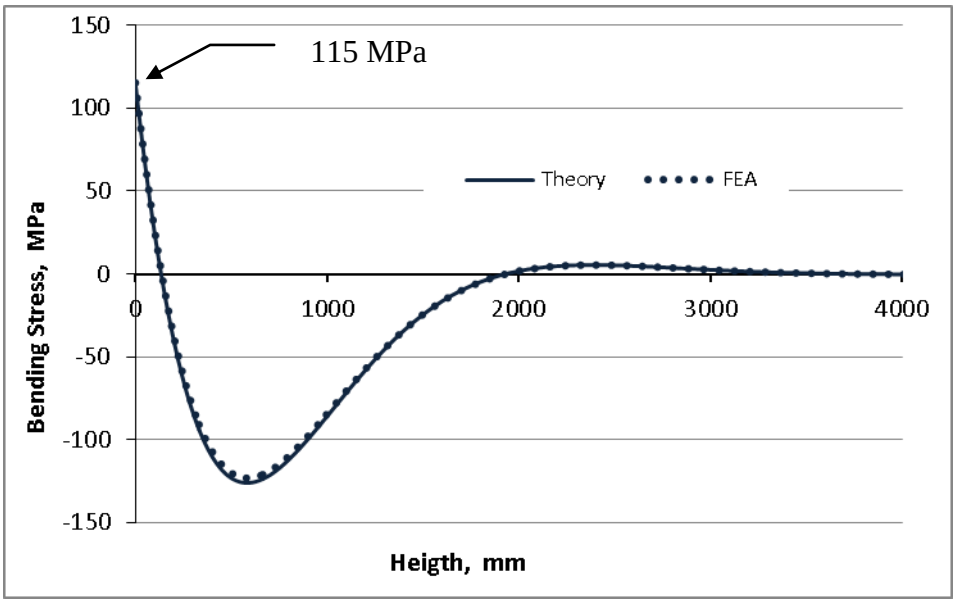

Fig. 5.9 Bending Stress in the Tank Wall Including Friction Effects – (Elastic-Plastic FEA)

Hoop and Bending stress values are obtained for a tank with the same dimensions as before but with different values of μ and C. The comparisons are shown in Fig. 5.10 and 5.11. From the figures it can be seen that the bending stress in tank wall for even a friction coefficient as high as 1.0 is considerably less than the stress obtained using a C value of 0.5. Hoop stress in the tank wall also shows a similar trend. Hence for the example tank dimensions, using a C-factor of more than 0.5 is excessively conservative.

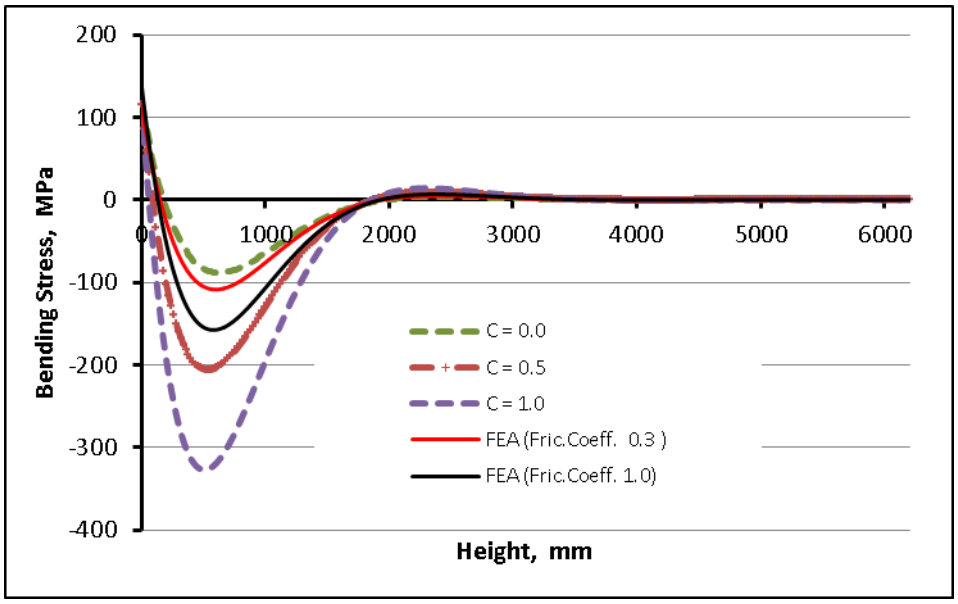

Fig. 5.10 Tank Wall Bending Stress for Various Values of 'C' and μ

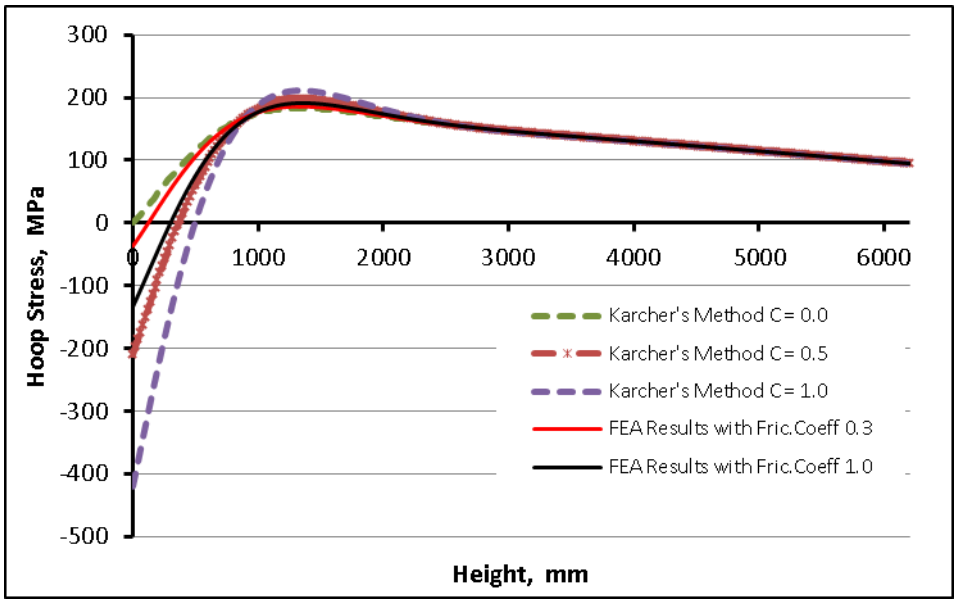

Fig. 5.11 Tank Wall Hoop Stress for Various Values of 'C' and μ

For a value of μ in the range 0.3~0.5 the difference will be even more pronounced. Figure 5.12 shows the variation of shell stresses as temperature increases with friction being constant (for a friction coefficient of $\mu = 0.7$).

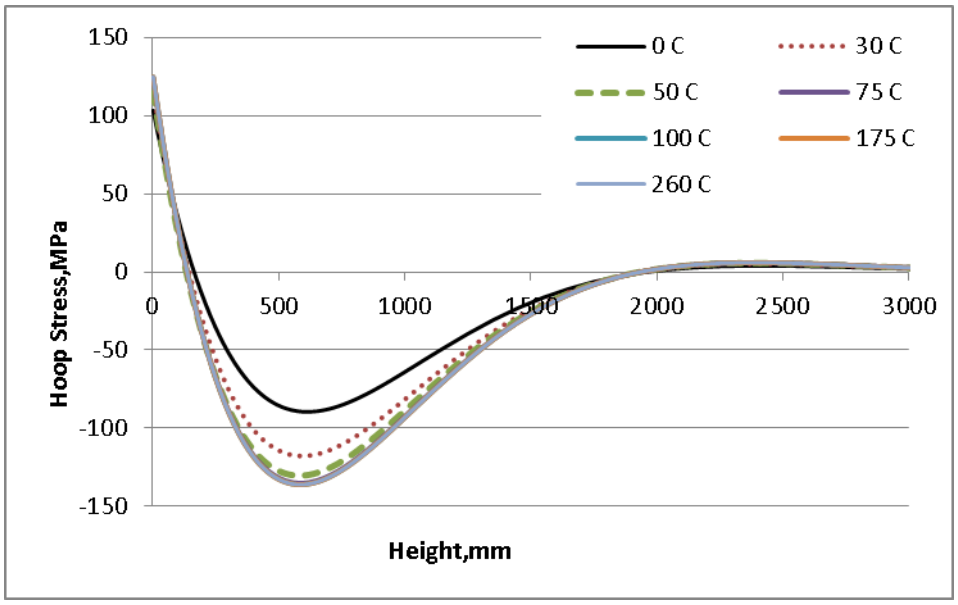

Fig. 5.12 Tank Wall Bending Stress at Different Temperatures for μ = 0.7

For a given tank, the bending stress caused by friction will be maximum when $u = R\alpha\Delta T$ or C =1. Hence from Eq. 5.14, for a particular friction coefficient

$$\Delta T_L = \frac{(1-\nu)}{3E\alpha}\frac{\mu\,\gamma\,H\,R}{t_p} \tag{5.45}$$

where, ΔT_L is the limiting temperature beyond which increase in temperature will not increase the stresses. Conversely, the limiting friction coefficient can also be obtained as below.

$$\mu_L = \frac{3E\alpha}{(1-\nu)} \frac{\Delta T\, t_p}{\gamma H\, R} \tag{5.46}$$

where, μ_L is the friction coefficient that will cause maximum stresses for a particular temperature. If a friction coefficient value is chosen higher than μ_L, there will be no further increase in the stresses. In other words, this is the 'μ' at which the C becomes 1. For any μ greater than this value, C continues to be 1 as it represents zero expansion condition.

For the example tank used earlier, ΔT_L is 40°C, it can be seen from Fig. 5.12 that the stresses (from FEA) in the tank wall do not increase when the temperature is increased beyond this limit. Basically, if the restraint deformation due to friction is equal to or greater than the free radial expansion due to temperature, the stresses in the tank wall will reach a maximum and further increase in temperature does not have any impact.

For the same tank as above but with a friction coefficient of 0.7, the C-factor changes with temperature as shown in Fig. 5.13. The plot indicates that C value is 1.0 till the temperature is 40°C, which is the temperature limit ΔT_L for this tank. The stresses in the tank bottom increase till the temperature reaches the limit ΔT_L and remain constant after this limit. Hence after ΔT_L, the C value reduces inversely with temperature such that the state of stress at ΔT_L is maintained throughout. It should be noted that though C value reduces, the product of ΔT and C will remain constant. This is a unique value for each tank and is directly proportional to the friction coefficient. The pattern for C-factor as shown in Fig. 5.13 holds good for any typical tank. The tank dimensions will only alter

the value of ΔT_L limit. This observation implies that the present recommendation of C=0.85 [API 650] for any tank may or may not be conservative (although no failures are reported to the best of the author's knowledge in general literature). If the temperature is relatively low and the friction coefficient of the tank is high, then its C value could sometimes be in the region A-B of Fig. 5.13 (before ΔT_L limit) and hence C = 1. For this case, using C < 1 is unconservative. On the other hand, stresses predicted using C = 0.85 for temperatures at the end of region B-C will be very highly conservative.

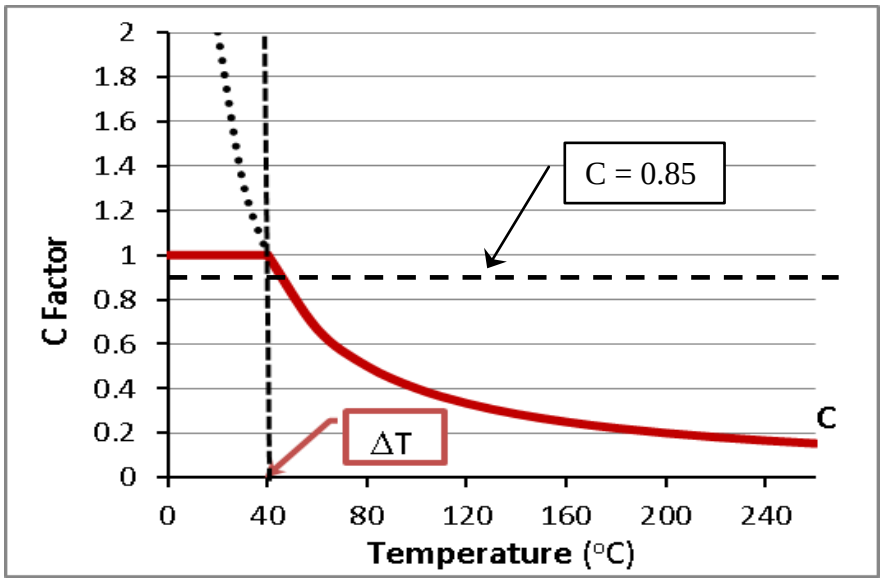

Fig. 5.13 Temperature Influence on C-Factor

Using a flat value for the C-factor (be it 0.5 or 0.85) gives inconsistent results. At present there are no clear guidelines on choosing a value of C other than 0.85. The margin of safety varies with operating temperature and could result in slightly unconservative estimates temperature ranges less than ΔT_L and grossly conservative predictions at higher temperatures. This is further illustrated in Table 5.1 which shows

the implied coefficient of friction for fixed values of C equal to 0.5 and 0.85 for typical elevated temperature tanks.

Table 5.1 Implied Coefficient of Friction for Fixed Values of C-Factor

	H m	D m	t_b mm	ΔT °C	Implied μ
C = 0.5	11	16	6	93	3.32
	11	16	6	260	9.29
	11	90	7	93	0.69
	11	90	7	260	1.93
	19.2	16	8	93	2.54
	19.2	16	8	260	7.10
	19.2	61	8	93	0.67
	19.2	61	8	260	1.86
C = 0.85	11	16	6	90	5.47
	11	16	6	250	15.19
	11	90	7	90	1.13
	11	90	7	250	3.15
	19.2	16	8	90	4.18
	19.2	16	8	250	11.60
	19.2	61	9	90	1.23
	19.2	90	11	90	1.02
	19.2	61	9	250	3.42

The implied coefficient of friction in Table 5.1 is calculated using Eq. 5.16. As can be seen, except for very large tanks at relatively low temperatures, the implied values of μ are unacceptable if the C-factor is fixed as 0.5. It is reported that C = 0.5 was based on anecdotal observations on some tanks [Karcher, 1978a]. No Data regarding those tanks is available. It is possible that they were very large tanks at temperatures in the 200 - 250°F range. For these tanks, a C-factor of 0.5 may sometimes be acceptable. However,

as can be seen from the table, for other ranges of H, R and ΔT, the implied values of μ (for C = 0.5) are too high. API 650 recommends a value of C = 0.85 in case other information is not available. This is generally assumed to be a conservative recommendation. However for most tanks, the implied values of μ for this value of C are even larger than those for C=0.5. Acceptable vales of μ are implied only for large diameter tanks with low temperatures. Therefore, instead of using a seemingly conservative value for the C-factor, it may be preferable to use a conservative estimate for the friction coefficient μ. The actual value depends upon the type of subgrade and can be obtained from established literature or other means. Adluri [2012] provided extensive discussion on this issue.

It should also be understood that friction resistance depends on liquid heights, foundation and bottom plate/annular plate characteristics. The value of the friction coefficient is not likely to alter significantly within the temperature range being considered (unlike the change in yield strength based on temperature change as given in Table M-1 of API 650). Because of this, thermal effects do not necessarily increase linearly with temperature. The extraordinary values for implied μ in Table 5.1 can be understood by examining Eq. 5.15. Free thermal expansion is proportional to R and ΔT whereas the restraining displacement due to friction is proportional to R^2 and H (and does not depend significantly on ΔT).

For smaller tanks in the Table, the friction resistance is not sufficient to provide appreciable restraint against thermal expansion. As liquid height increases, friction

resistance proportionately increases while free thermal expansion ($R\alpha\Delta T$) stays the same. When the radius increases, this effect is compounded. Hence as the tank size increases in radius and height, the total friction force builds up and the restraining displacement starts to approach the free thermal expansion. The opposite happens with increasing temperature. These points can be further illustrated through Table 5.2 which lists the implied C-factor for a fixed value of $\mu = 0.85$. For smaller tanks, the implied C-factor is quite small. Only for large tanks with relatively low temperature increase, the implied C-factor approaches the values currently being used. At the outer edge of the range of parameters, the implied C-factor can become slightly unconservative if a lower C value is chosen for design. Hence, it is more rational to choose a conservative estimate for the coefficient of friction than for the C-factor.

Table 5.2 Implied C-Factor for Fixed Values of Coefficient of Friction

	H m	D m	t_b mm	ΔT °C	Implied C-factor
$\mu = 0.85$	11	16	6	90	0.13
	11	16	6	250	0.05
	11	90	7	90	0.64
	11	90	7	250	0.23
	19.2	16	8	90	0.17
	19.2	16	8	250	0.06
	19.2	61	9	90	0.59
	19.2	90	11	90	0.71
	19.2	61	9	250	0.21

5.3.1 Influence of Friction on Fatigue Life

In the current practice, the alternating stress required for fatigue life estimation of tank (number of fill/draw cycles the tank can safely withstand) is determined by Eq. 5.6. In this equation, the friction forces are indirectly represented by the C-factor. For the tank example considered earlier, Fig. 5.14 shows the influence of C-factor on the fatigue life of the tank (for ΔT = 175°C). The fatigue life reduces drastically if the C-factor is increased.

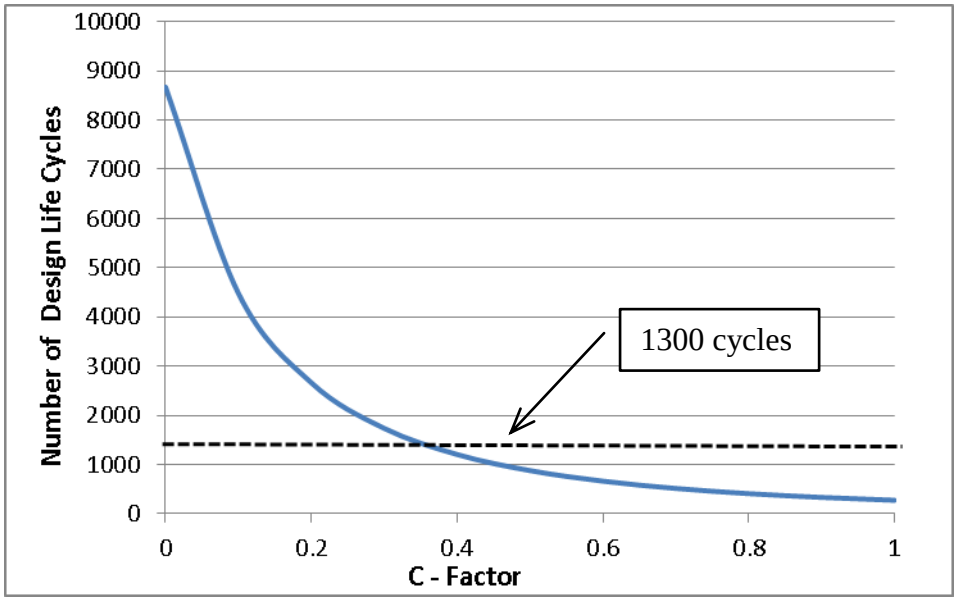

Fig. 5.14 Influence of C-Factor on Fatigue Life

As per API 650, the tank has to safely withstand at least 1300 fill/draw cycles. If C is assumed to be 0.85 (and K=2) as recommended by the API, the tank fails by a significant margin (N=369). If the same tank is considered with a (most likely conservative) friction coefficient estimate, say, 0.85, the number of design life cycles (N) that the tank can

withstand becomes 1896 (which is well above the required limit). This is a case where the API recommendation is overly conservative. If the tank is larger and is operating at temperatures below 100 ^{o}C, using a smaller C value could sometimes be slightly unconservative.

5.3.2 Influence of Filling Procedure

API 650 recognises (in Clause M.4.2) that the tank filling procedure influences the amount of radial expansion and hence the stresses and fatigue life. Generally if the tank is initially filled to a low height (at least $0.3(Dt)^{0.5}$, where, D is in ft and t is in inches, [API 650] and heated to the required temperature as a first step, the tank will radially expand almost to its full expansion and hence the thermal shell stresses induced will not be very significant. However it must be noted that it may be difficult to guarantee that this will always be followed when the tank is likely to be in operation for many decades. On the other hand if the tank is heated with a significant liquid head, it induces thermal stresses due to the friction forces. These stresses have been explored throughout the paper. In order to verify the API recommendation of preheating the tank with low liquid head, a finite element analysis was carried out. Using Eq. 5.15 for the example tank used in finite element analysis, the radial expansion is 62 mm for a 2 m liquid head heated to 175°C. FEA results give 62.2 mm confirming the theoretical prediction. The corresponding free expansion ($R\alpha\Delta T$) is 63 mm (with $\alpha=12x10^{6}$). The results show that with very low liquid head, the radial expansion of the bottom is almost the same as that of free radial expansion. The stresses for this analysis are very close to those of the same

tank at ambient temperature thus indicating that the thermal stresses can be neglected if the above procedure for liquid filling and heating is used.

5.4 CONCLUSIONS

This present study examines the influence of bottom plate friction forces on the stresses in the wall of elevated temperature tanks. Karcher's equations used for finding the stresses in the tank wall are verified using a finite element model with contact elements. The equations use a value called as C-factor to include the effect of partial expansion due to temperature change. It is observed that the equations give correct results if the exact C-factor is used. Since the C-factor is highly sensitive in influencing the tank wall stresses, the designer needs expertise and judgement in deciding on the factor during the design stage. The current practice does not have clear guidelines for selecting a C value. In the absence of such guidelines, a set value (like 0.85) for the C-factor is being used irrespective of the tank dimensions and temperature change. The present study shows that this approach is grossly conservative for most of the range of design parameters (H, R & ΔT). On the other hand, for very large tanks at relatively low temperature changes, this could become slightly unconservative. This study shows that the C-factor is directly related to the friction coefficient (μ) and tank parameters. Appropriate equations for stresses and by extension, fatigue life are presented. It is shown that for a given tank with a particular friction coefficient, there is a limiting temperature (ΔT_L) beyond which any further increase in temperature will not increase the tank wall

stresses. Similarly for a given temperature increase in a tank, the stresses will not increase further even if the friction coefficient is higher than a particular value (μ_L). Several related issues are discussed. The results are verified using finite element analysis incorporating friction forces through contact elements between foundation and tank bottom plate. The study shows that it is much more rational to use a conservative estimate for the coefficient of friction than for the C-factor.

CHAPTER 6

FATIGUE ANALYSIS OF SHELL TO BOTTOM JOINT OF TANKS

Shell to bottom joint of hydrocarbon storage tanks is a critical failure location which needs careful evaluation especially in the case of elevated temperature tanks. The fill/draw down cycle of the stored liquid causes low cycle fatigue near this joint and hence a fatigue evaluation is recommended as explained in previous Chapters. The peak alternating stress at this location, used to enter the fatigue curves is currently determined using a pseudo elastic stress that represents strain range due to inelastic deformations. For this, API 650 employs beam-on-elastic foundation theory. This theory is being used for tanks resting fully on earthen foundation as well as those on concrete ring wall. This Chapter studies the validity of using this theory for tanks with concrete ring wall foundation which are much more rigid compared to earthen foundations. Some of the difficulties in the current practice are highlighted. An alternative to the current model is proposed to determine the peak stress at the shell to bottom joint of tanks resting on concrete ring wall. The results are validated using finite element analysis.

6.0 INTRODUCTION

The shell (tank wall) to bottom joint of storage tank is subjected to low cycle fatigue due to fill/draw down cycle and the temperature fluctuation of the stored liquid. The storage tank standards API 650 and 653 consider this aspect in detail and provide guidelines for determining the safe cyclic life of the tank based on the fatigue analysis of this joint.

For the elevated temperature tanks, API 650 provides guidelines to determine the appropriate thicknesses of structural members and determine the design cycle life of the tank (based on the fatigue evaluation of the shell to bottom joint). As per API 650, it is expected that the tank withstands at least 1300 load cycles in its lifetime. In Appendix M of API 650, the peak alternating stress to be used for fatigue analysis of this joint is determined using the original work by Karcher [1978, 1981 a, b]. He proposed a set of design equations to determine the tank wall stress and the fatigue life of elevated temperature tanks as given in Chapter 5. Jones and Seshadri [1989] studied the validity of Karcher's model using elastic finite element analysis of the shell with an assumed hinge condition at the bottom.

In the current practice, the bottom plate is analyzed using beam-on-elastic foundation theory. The resulting equations were derived basically for tanks on earthen foundation by Karcher [1981a]. The same are applied to concrete ring wall foundations except that two plastic hinges are assumed in the bottom plate (or annular plate) instead of one plastic hinge in the case of earthen foundation. However, it must be noted that the

bottom plate resting on concrete wall loses contact in the immediate vicinity of the inside face of the tank wall. This was recognized by the previous research works [Denham, 1968; Wu, 2000; Sathyanarayanan and Adluri, 2011] as well as the seminal work by Zick and McGrath [1968]. The uplift, although small, is sufficient to cause clear separation of bottom plate from the top of the concrete ring wall on the inside. Hence the stresses in this region are not directly governed by beam-on-elastic foundation model.

6.1 FATIGUE AT SHELL TO BOTTOM JOINT

Figure 6.1 shows the rotation of shell to bottom joint of a tank resting on a rigid base. As explained in Chapter 4, this rotation causes the bottom plate to lift off the ground over a small distance (say, uplift length L). Beyond this, the downward liquid pressure acting on the plate is sufficient to make the plate fully rest on the foundation.

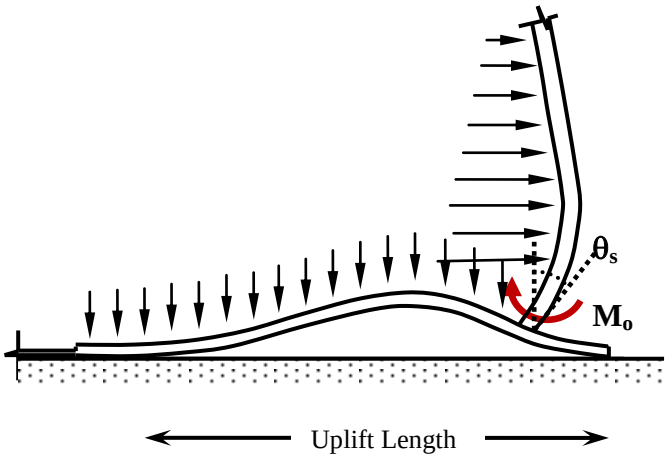

Fig. 6.1 Shell to Bottom Joint in the Tank on a Rigid Base

The internal moment that forces the rotation is caused by the hydrostatic pressure on the wall and is balanced by the moments (on either side of the wall) in the bottom plate. Because of this bottom moment, the bottom plate on the inner and outer side of the shell is subjected to high bending stresses in the radial direction. The thickness ratios of the shell and bottom plates are such that in most of the tanks the bottom plates undergo substantial yielding near this joint. The fatigue strength of this joint has to be evaluated in order to determine the number of load cycles the tank can safely withstand.

6.2 DESIGN FOR FATIGUE

For short projection lengths (such as the minimum prescribed value of 50mm), the bending moment in the bottom plate on the inside will be larger than that on the outside. The inside portion of the shell to bottom joint needs to be evaluated for fatigue. Since the material yields due to high stress in the bottom plate, strain range analysis (pseudo stress) is used for fatigue evaluation. The rotation of the shell as shown in Fig.6.1 induces the bending strain. The magnitude depends upon the tank parameters R, H, t_s, t_b and the specific gravity of the stored liquid (G). In addition to these factors, the type of foundation directly beneath the tank shell and the type of weld used (double fillet/full penetration) will influence the fatigue evaluation.

The design cycle evaluation procedure of the elevated temperature tank as described by the API 650 assumes uniform temperature increase in the tank, i.e., without any temperature gradient across the thickness of the shell wall. This is a reasonable assumption since the shell wall thickness is quite small. At steady state, the difference in

temperature between inner and outer surfaces of the wall may not be significant. The same is adopted in this study. The current procedure [API 650] is outlined briefly below:

Using the Eq.5.6 from Chapter 5 and substituting the following coefficients [Karcher 1981a] used by API 650, the peak alternating stress (S) can be obtained as:

γ = G x 9.81 x10^{-6} N/mm^3; E = 190986 MPa; K = 0.2715 N/mm^2/mm; α = 11.7 x 10^{-6}/°C;

$\beta = \dfrac{1.285}{\sqrt{500 D t_s}}$;

$$S = \frac{S_b}{2} = \frac{0.028\, D^2 t_b^{0.25}}{t_s}\left[\frac{58HG}{(Dt_s)^{0.5}} + \frac{26.2C\Delta T t_s^{0.5}}{D^{1.5}} - \frac{4.8BS_Y t_b^2}{(Dt_s)^{1.5}} - G\right] \tag{6.1}$$

where, S is one-half of the maximum stress range (S_b) that occurs in the annular plate at the shell to bottom junction, in MPa. The dimensions of D & H are in metres whereas the dimensions of t_s and t_b are in mm.

Similarly using the above coefficients in the Eq.5.7, the following (Eq. 6.2) inequality condition can be obtained. Equation 6.1 is valid only if this condition is true.

$$\left[\frac{58HG}{(Dt_s)^{0.5}} + \frac{26.2C\Delta T t_s^{0.5}}{D^{1.5}} - G\right] > \left[\frac{4.8BS_Y t_b^2}{(Dt_s)^{1.5}}\right] \tag{6.2}$$

As stated earlier, this condition is prescribed to ensure that the tank is loaded such that boundary conditions (plastic hinge) assumed for developing these equations are valid.

The stress created at the shell to bottom joint can be classified as secondary bending stress (as per ASME section VIII DIV 2) and hence should be limited to twice the yield strength of the annular plate material to assure shakedown to an elastic action. The shell theory used in this method basically assumes that the influence of the radial expansion of bottom plate due to the hydrostatic load is negligible.

6.3 ISSUES IN EXISTING PROCEDURE

6.3.1 Necessity of the Condition in Eq.6.2

Karcher [1978,b] has mentioned that the current practice is applicable only when Eq.6.2 is valid. This can be interpreted that Eq.6.2 is specified as a necessary condition for the assumed plastic hinges to form. Satisfying Eq.6.2 ensures that the stress determined from Eq.6.1 is not negative. Essentially it determines whether the slope of the shell at the bottom, after the application of load, is inward or outward. Although API 650 does not say so, satisfying Eq.6.2 is not a sufficient condition to confirm the formation of two complete hinges at the bottom [Sathyanarayanan and Adluri, 2012a, 2013a]

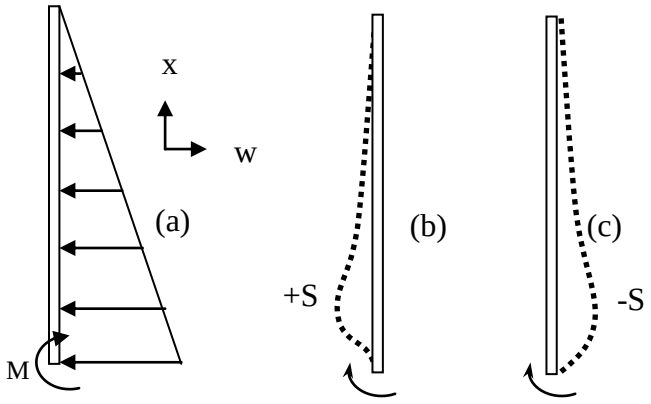

Fig. 6.2 Free Body Diagram of Shell

The sign of stress S is determined by the sign of the term $\left[\frac{58HG}{(Dt_s)^{0.5}}+\frac{26.2C\Delta Tt_s^{0.5}}{D^{1.5}}-\frac{4.8BS_Yt_b^2}{(Dt_s)^{1.5}}-G\right]$ in Eq. 6.1. Figure 6.2 (a) represents free body diagram of the tank wall. Fig. 6.2 (b) represents positive value for the stress S from Eq.6.1 while Fig. 6.2 (c) represents negative value for the stress. The condition from Eq.6.2 can be rearranged in non-dimensional terms as

$$\beta H+\beta H\left(\frac{H}{R}\right)\left(\frac{S_Y}{\gamma H}\right)\left(\frac{E}{S_Y}\right)\left(\frac{C\alpha\Delta T}{\frac{H}{t_s}}\right)-1-\frac{1}{2}\left(\frac{(\beta H)^3}{\frac{H}{t_s}}\right)\left(\frac{S_Y}{\gamma H}\right)\left(\frac{t_b}{t_s}\right)^2>0 \qquad (6.3)$$

where, $\beta H=\sqrt{\left(\frac{H}{R}\right)\left(\frac{H}{t_s}\right)}\left(3\left(1-\nu^2\right)\right)^{0.25}$ and $\frac{H}{t_s}=\left(\frac{S_d}{\gamma H}\right)\left(\frac{H}{R}\right)$

The validity of this condition for various situations can be easily examined. The following ranges of parameters are considered:

$$0.3\le\left(\frac{t_b}{t_s}\right)\le 0.8,\quad 550\le\left(\frac{E}{S_Y}\right)\le 800,\quad 0.3\le\left(\frac{H}{R}\right)\le 6,$$
$$1300\le\frac{S_Y}{\gamma H}\le 7300,\quad 0.25\le C\le 1,$$
$$\alpha=12\times10^{-6}/{}^\circ C,\quad 93\,{}^\circ C\le\Delta T\le 260\,{}^\circ C$$

A simple calculation shows that the condition is satisfied for practical ranges of variables. The only exception seems to be tanks where the design thickness of tank wall comes to be less than what the minimum thickness rule prescribes. For all other tanks, this rule need not be checked.

6.3.2 Use of Beam-on-elastic Foundation Theory

The existing procedure assumes that beam-on-elastic foundation theory is valid for the immediate vicinity of tank wall bottom. In the current practice, the same procedure is used for tanks on earthen foundation and concrete ring wall foundation except that in the former case, a single plastic hinge is used and in later case two plastic hinges are used as the shell bottom moment. It is clearly applicable to tanks on earthen foundation with appropriate conditions. However, it is not suitable for concrete ring wall foundation as explained below:

If the shell to bottom joint is supported on a rigid concrete ring wall, the internal moment (M_o) lifts the bottom plate slightly thereby loosing contact with the foundation (Fig. 6.3). This uplift is present even after accounting for the effect of liquid (hydrostatic) head, self-weight of plate and compression from the wall (including roofing weight, wind girder, etc.).

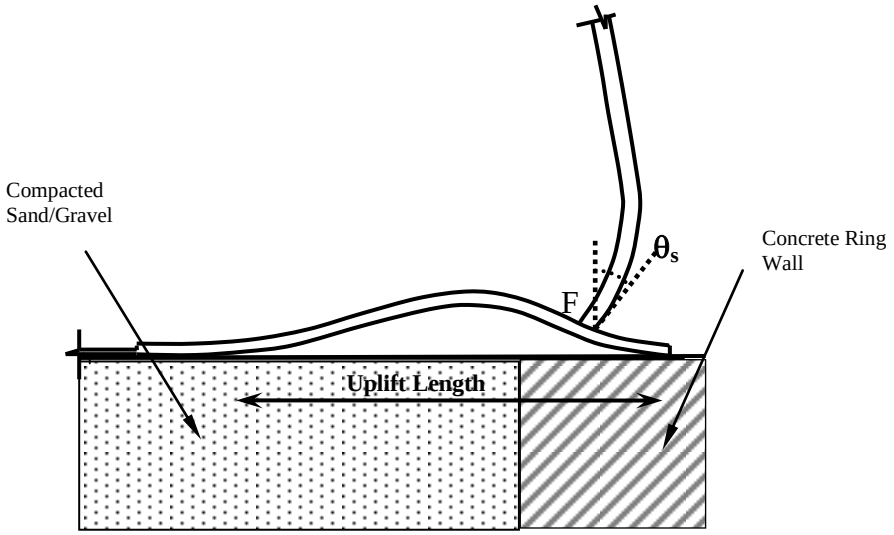

Fig. 6.3 Uplift at Shell to Bottom Joint of a Tank on Concrete Ring Wall

The uplift length has been studied variously by Denham,et al [1968], Sathyanarayanan and Adluri [2011], among others [Long and Garner, 2004]. Typical uplift lengths range from 150 – 400mm. Annular Plates (Cl.5.5.2 of API 650) has lengths typically larger than this. In addition to theory, a detailed finite element analysis of a tank (as described in Chapter3 – Case1 with 8 mm bottom plate), along with roof load has been carried out. Fig. 6.4 shows the uplift and von Mises stress profiles at the shell to bottom joint from the nonlinear FEA. The figure is captured at the end of a time step analysis performed with factored loads to see formation of plastic hinges.

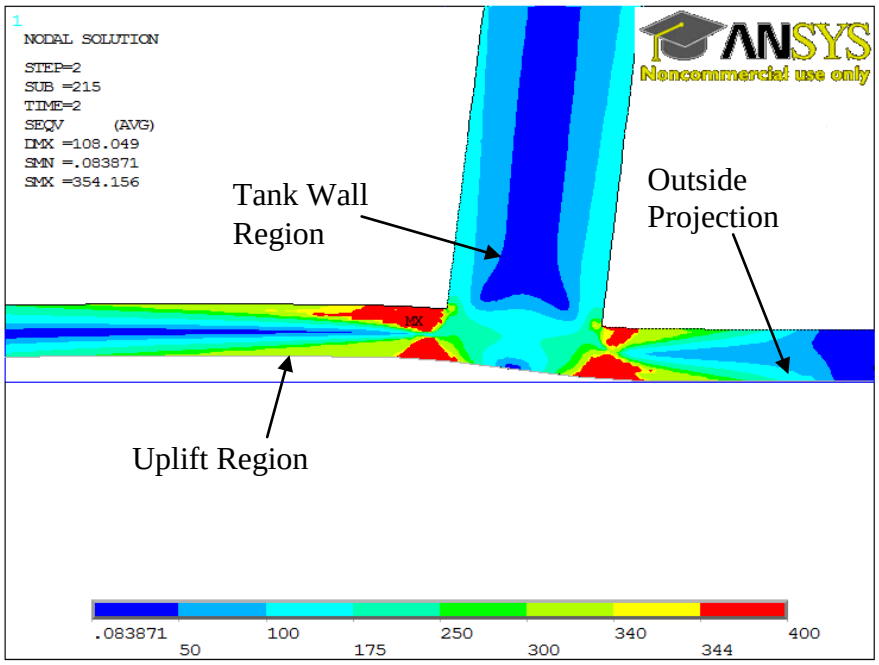

Fig. 6.4 Uplift of Bottom Plate from FE Model with 2D Axisymmetric Elements

The region (Point F in Fig.6.3) in which the peak alternating stress is determined for fatigue calculation is not in direct contact with the earthen subgrade. Hence the beam-on-elastic foundation theory as used in the present method is not directly applicable. The direction of the internal moment M_o is such that it uplifts the bottom plate at point 'F' since the moment cannot push the projection part in to the concrete ring wall. Because of this, the deflection of the plate is not significantly influenced by the foundation modulus. Only if there is a significant uneven settlement, the foundation modulus might have some influence on tanks resting on concrete ring wall. This is not the objective of the present investigation. Since the uplift zone is supported only at the ends, a regular beam model is more appropriate than beam-on-elastic foundation model.

6.4 PROPOSED CHANGES IN THE DETERMINATION OF PEAK ALTERNATING STRESS

The safe cyclic life (number of safe load cycles) is determined from the strain range of the bottom plate at point 'F'. The stress (S_b) in the existing procedure is only a pseudo stress used to quantify the strain range. The rotation of the shell to bottom joint during the cyclic loading determines the strain range at 'F', which in turn controls the fatigue life of the joint. The calculation of this rotation depends on the loading, geometry of the tank and the double plastic hinge assumption used in the model. It should be noted that, for a given geometry and loading, a single plastic hinge in bottom plate will cause more rotation and hence shorter fatigue life estimation than the assumption of double plastic hinge. However, the current practice is to use two plastic hinges (one on the inside and another on the outside) for the estimation of peak alternating stress. This is retained

in the current study and follows the recommendation by Karcher [1981a, b] and Zick and McGrath [1968]. The bottom plate near the shell can be idealized as a beam shown in Fig. 6.5. Using beam theory and shell theory, the uplift length (L) and the moment (M_{bp}) in the bottom plate near the shell can be determined as follows:

$$M_{bp} = \frac{qL^2}{4} \tag{6.4}$$

$$L = \sqrt[3]{\frac{24EI_P\theta_s}{q}} \tag{6.5}$$

The basic idea of the procedure is that the strain in the bottom plate is governed by the rotation of the shell bottom, and the maximum rotation of shell bottom occurs at the limiting condition of a double plastic hinge of the bottom plate. Following on the same lines as the current practice except for the equations above, the peak alternating pseudo-elastic stress is given by

$$S_b = \pm\frac{3}{2}\left(\frac{2}{1-\nu^2}\right)^{2/3}\gamma H\left[\frac{R^2}{Ht_s}\left\{\beta H + \frac{\beta E t_s}{\gamma R}C\alpha\Delta T - \frac{\beta^3 S_Y t_b^2}{\gamma} - 1\right\}\right]^{2/3} \tag{6.6}$$

This equation generally gives higher stress than that predicted by Eq.6.1 because this equation does not have the benefit offered by the elastic subgrade.

The safe design cycle life, N, is then given by [API 650],

$$N = \left(\frac{9700}{K_c S} \right)^{2.44} \tag{6.7}$$

where, S is the alternating stress range ($S_b/2$), K_c is the stress concentration factor which can be conservatively taken as 4.0 for lap welded bottom plates/ butt-welded annular plate (examined as per API 650 Specification). In case of butt welded annular plate with 100% surface examination and blend grinding, K_c = 2.0 [Karcher, 1981b].

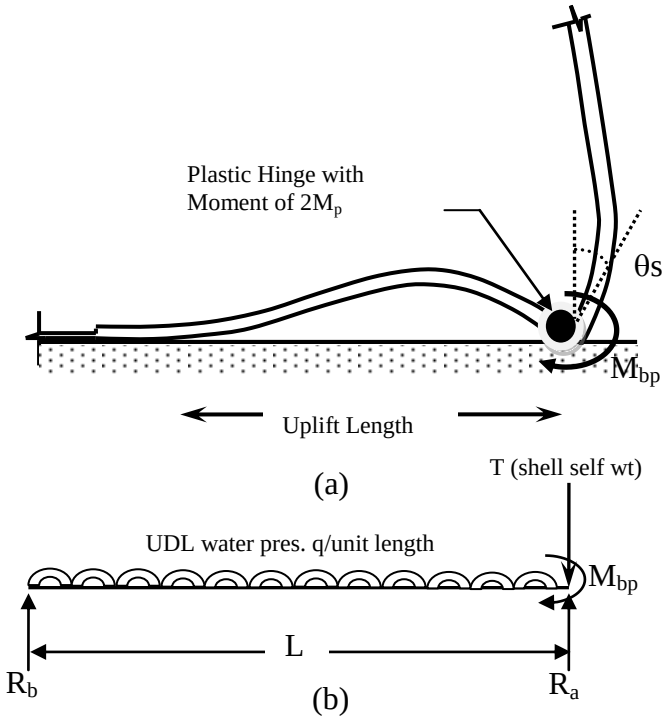

Fig. 6.5 Idealized Beam Model

6.5 RESULTS AND DISCUSSION

As shown in Fig. 6.3, finite element analyzes were carried out assuming the foundation to be a concrete ring wall with highly compacted infill. In addition, axisymmetric SHELL elements were also used for modeling the tank wall and bottom plate. Both elastic and elastic-perfectly-plastic material models were examined. The advantage of using plane elements is that, the elasto-plastic stress/strain profiles and the formation of plastic hinges can be explicitly viewed, whereas in shell models which are line elements, the through the thickness stress profile cannot be seen. Unless otherwise mentioned, the example tank – Case 1 as given in Chapter 3 with 6mm bottom plate and a friction coefficient of 0.8 is used for all the finite element analysis.

For the same tank operating at an elevated temperature of 175°C (ΔT), Fig.6.6 shows the uplift deformation of the bottom plate and Fig.6.7 shows deformation pattern at the shell to bottom joint as shown by FE shell model. It is the expanded view of deformation profile at the shell to bottom joint.

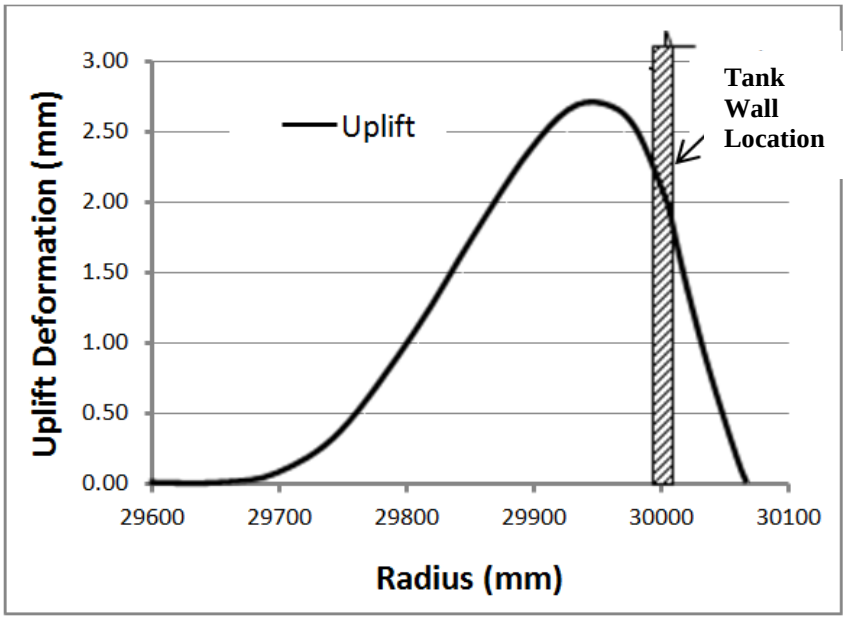

Fig. 6.6 Uplift Deformation of Bottom Plate

Figure 6.8 shows the radial direction stress (S_x) of the bottom plate at the joint. It must be noted that stress (S_x) can exceed yield as long as the equivalent von Mises stress is within the yield limit. The bending stress (S_x in the radial direction) and von Mises stress in the bottom plate near the shell are plotted in Fig.6.9 for two complete loading cycles. As can be seen, even though the yield strength of the material is 345 MPa, S_x reached 400 MPa indicating the effect of multi-axial stress field. The combined effect of all the stresses at that point represented by von Mises equivalent stress is within the yield limit. The tank is gradually loaded to full height, unloaded gradually and the cycle is repeated one more time.

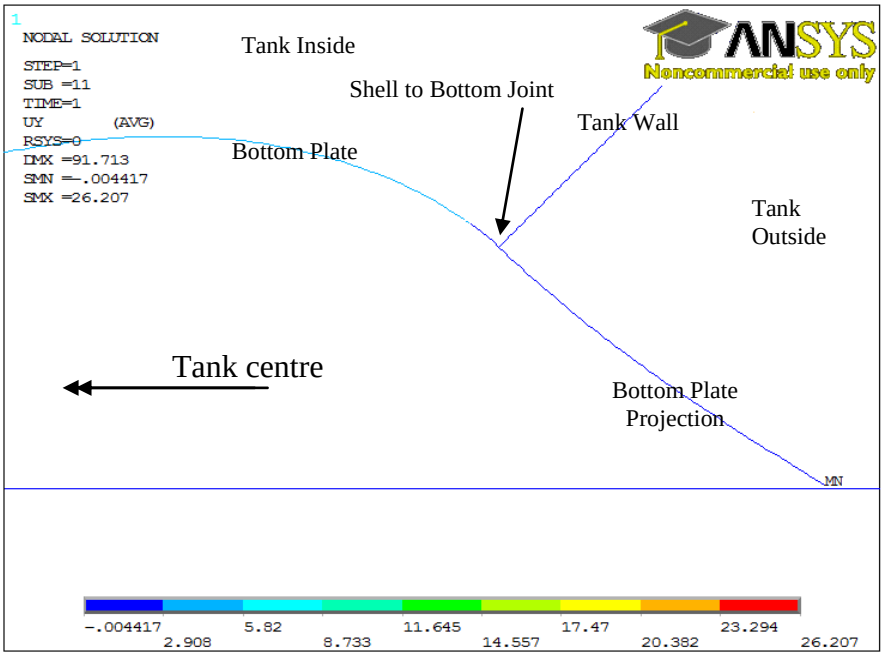

Fig. 6.7 Uplift Deformation from FE Model with Shell Elements

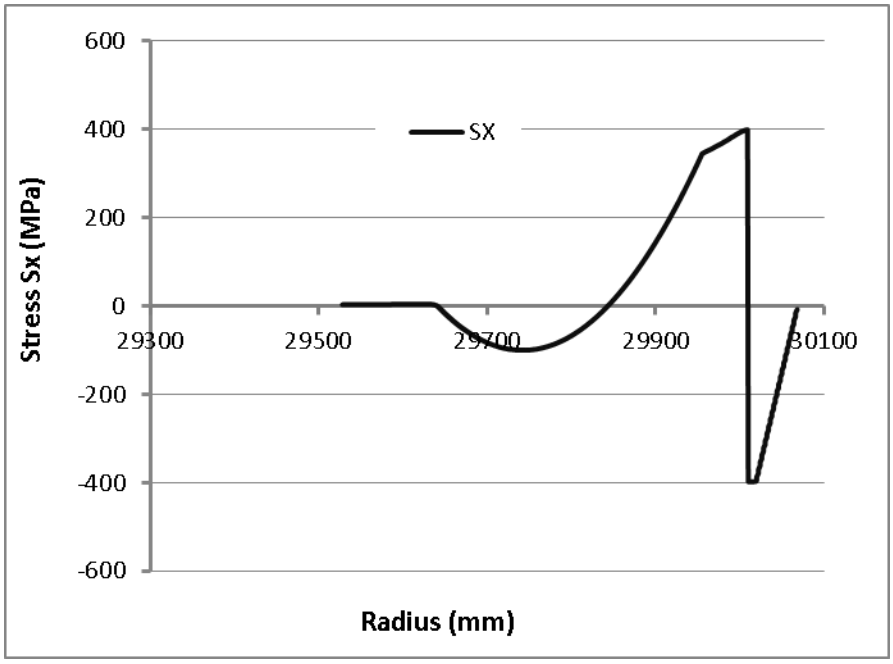

Fig. 6.8 Stress Sx in Bottom Plate near Shell Joint

Each loading or unloading is considered to be one load cycle stage. Therefore, stage 4 ends when the tank is fully loaded and unloaded twice. As can be seen, the first stage of full loading ends with the bottom plate (on the inside) yielding. At the end of stage 2, the tank is unloaded where the bottom plate shows residual stresses. The next cycle (shown by stages 3 & 4) is fully elastic indicating shake down behavior. The radial direction stress S_X varies from -219 to 398 MPa and hence the range from FEA is 617 MPa, whereas the predicted stress range using API (Eq.6.1) is 419 MPa. For the same tank Eq.6.6 gives a stress range of 612 MPa. The partial radial expansion from FEA is 47 mm (against the free expansion of 63 mm with $\alpha=12x10^{6}$) and hence the C factor is computed as 0.25. The von Mises stress values show the yield limit of 345 MPa at load stage 1 and the formation of residual stress at stage 2. Fig.6.10 shows the stress S_x in the bottom plate near the outer face of shell to bottom joint.

Similarly for the same tank, but with 8mm bottom plate the bending stress (S_x) and von Mises Stress (on the inside) are plotted in Fig.6.11. The stress S_x varies from -75 to 398 MPa. Hence the range of S_x from FEA is 473 MPa. The stress range predicted using current API (Eq.6.1) is 305 MPa. The stress range obtained by the proposed equation (Eq.6.6) is 470 MPa

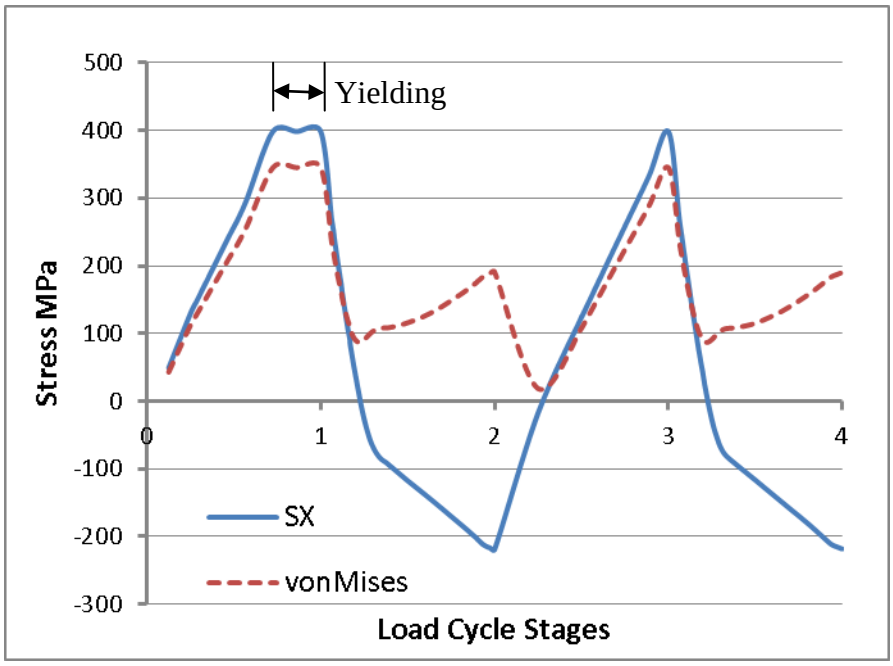

Fig. 6.9 Bending and von Mises Stress in 6mm Thick Bottom Plate (On the Inside)

The partial radial expansion of bottom plate due to temperature from the FEA results is 51 mm against the free expansion of 63 mm (with $\alpha=12x10^{6}$) and hence the C factor can be computed as 0.19 which is used with both API and beam equations. The idea that the strain and hence the stress range of the bottom plate is controlled by the shell rotation is appropriate for concrete ring wall foundations as well as earthen foundations. However, since the bottom plate uplifts near the joint for the concrete ring wall, the beam-on-elastic foundation theory could be under predicting the stresses. As can be seen from the results, the beam model used in the current research predicts stress results quite close to FEA results.

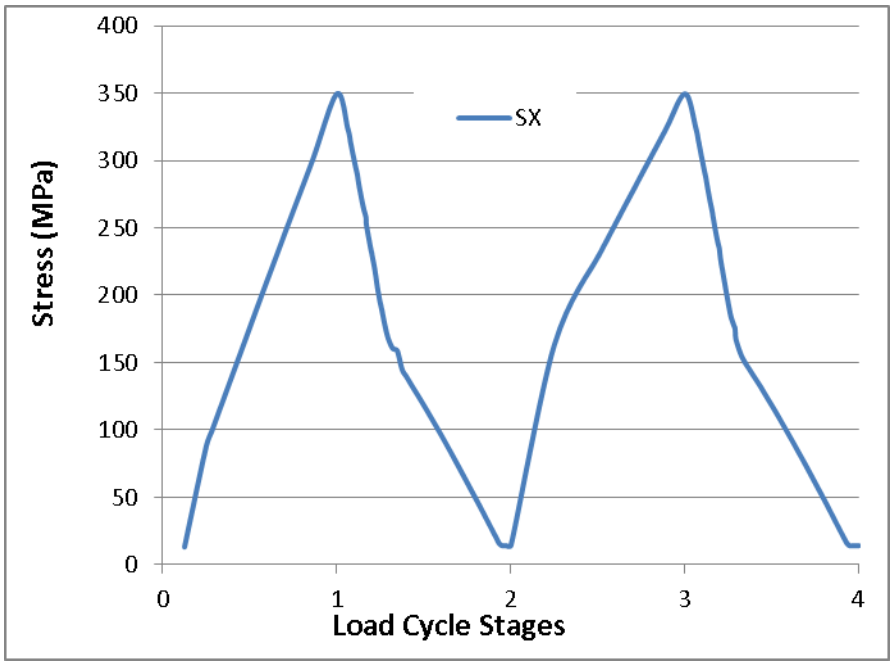

Fig. 6.10 Bending Stress in 6mm Bottom Plate (on the Outside)

It is to be noted that the stress range computed in FEA is indicative of the elastic strain range during all the shakedown load cycles after the first cycle. These results indicate that the model used in the present work is more appropriate for concrete ring walls than that of the current API 650. However, the proposed model predicts higher stresses than those given by API 650 and hence a smaller fatigue life cycle estimate. It must be pointed out that, the API procedure, originally developed by Karcher has been in practice for about 30 years. To the best of our knowledge, no major failures due to fatigue have been reported in public domain. This is likely because no failures actually occurred or because failures were not recognised to be due to this issue or due to the embedded margin of safety.

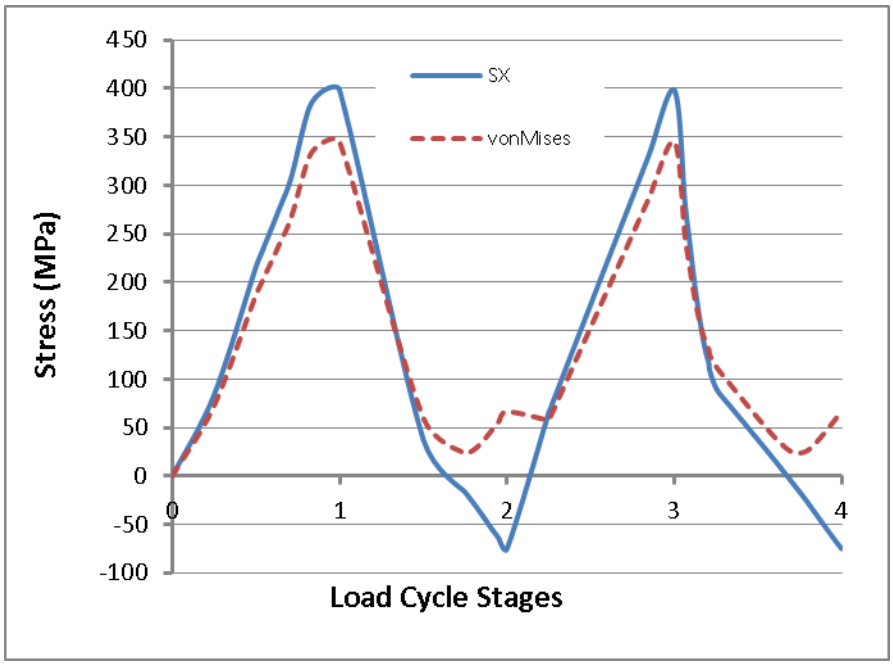

Fig. 6.11 Bending and von Mises Stress in 8 mm Thick Bottom Plate

The current procedure although not reported (publicly) to be problematic in the field is not very rational in comparison to the model presented here. On the other hand, the model presented here seems to reduce the life cycle estimates from current levels. In view of this, the current procedures as well as the model developed in this thesis must be looked at thoroughly by relevant API committees to arrive at a rational, safe and economical procedure.

6.6 INFLUENCE OF PLASTIC HINGES

Apart from the influence of the foundation, the other important factor that contributes to the fatigue design is the assumption of single/double hinge boundary

condition at the shell bottom. Figure 6.12 shows the locations where high bending moments are induced due to the liquid infill.

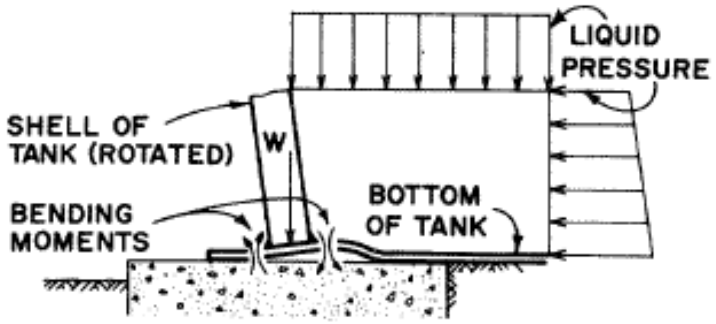

(a) In Concrete Ring Wall

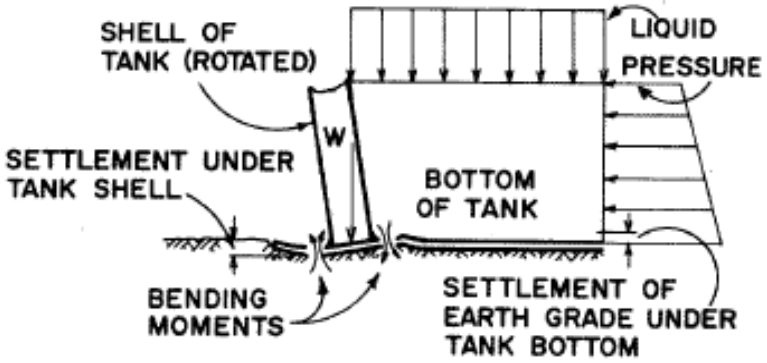

(b) In Earthen Foundation

Fig. 6.12 Bending of Bottom Plate in Shell to Bottom Joint [Zick and McGrath, 1968]

Zick and McGrath [1968] suggested that "where the resisting moment of the tank bottom is to be evaluated, a reasonable approach would be to use the full yielding moment in the bottom plate on one side (inner side) for an earth foundation and to use two moments (one on each side) for concrete ring wall foundation." The influence of the

assumed bottom moment on tank wall bending stress is shown in Fig.6.13 for the example tank from earlier. For a concrete ring wall foundation, two plastic hinges assumption is used. But in actual field conditions, two complete hinges may or may not form at the bottom because the loading and geometry do not necessarily allow it to happen. The smaller the bottom moment, greater is the rotation of the shell due to hydrostatic load. All other factors being same, the maximum bending stress is less if the bottom moment is more and vice – versa. Hence, if an assumed bottom moment is used, it is more conservative to assume smaller than the "exact" moment as opposed to a larger than "exact" moment. This issue also needs to be looked at more thoroughly by relevant API committees.

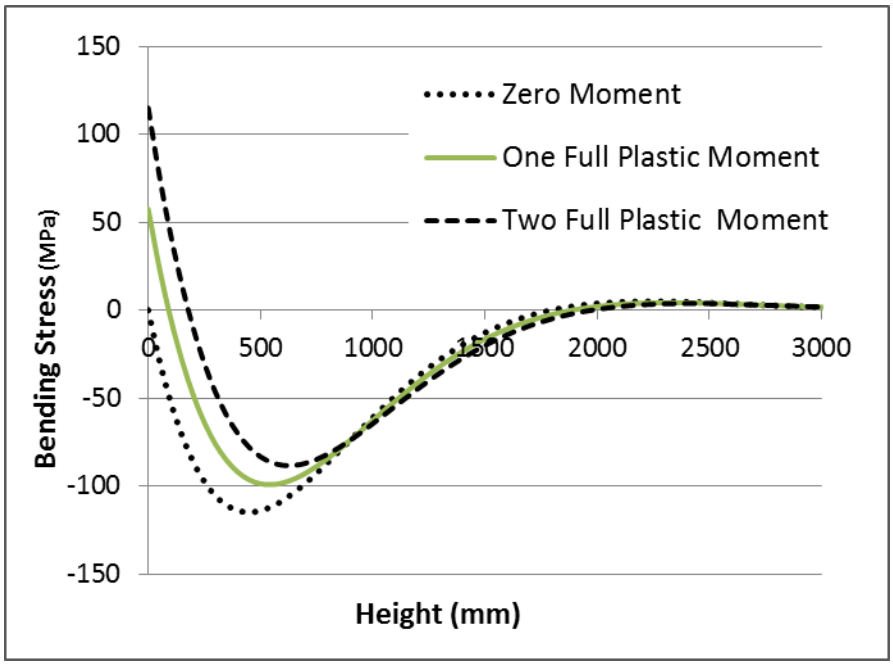

Fig. 6.13 Influence of Bottom Moment on Tank Wall Bending Stresses

6.7 CONCLUSION

The Chapter traces the development of the current API 650 procedure for life cycle evaluation of elevated temperature steel storage tanks subjected to low cycle fatigue. The current procedure uses beam-on-elastic foundation model for tanks resting on earthen foundations as well as those using concrete ring walls. In the vicinity of the ring wall, the inside portion of the bottom/annular plate looses contact with the foundation due to the outward rotation of the tank wall at the bottom. Hence, the theory of beam-on-elastic foundation is not applicable to tanks with concrete ring wall supports below the wall plate joint. Modifications have been carried out in this study to arrive at an alternative estimate for pseudo elastic peak alternating stress (strain range) for fatigue calculations. Detailed finite element analysis using non linear models and friction-contact elements were carried out. The results show that the alternative model is quite close to FEA results where as the current procedures under predict the stress. The current procedure is clearly less rational than that developed in this thesis. However, the current procedure is long standing without major problems. In light of this, it is recommended that API committees take a close look at this issue in order to arrive at a rational and yet acceptably safe decision on the matter. Related issues regarding the inequality condition and the assumption of two full plastic hinges at the bottom are also discussed.

CHAPTER 7

LOCALLY THINNED AREAS

Various types of damages can occur to tanks due to environmental and in-service factors. The issues dealt in the previous chapters, like the effect of bottom plate friction and low cycle fatigue at shell to bottom joint were structural integrity considerations during operation of the tank. Similarly degradation due to wall thinning is an important and most prevalent structural integrity issue that occurs due to either corrosion or erosion or both together.

Local thin area (LTA) is type of wall thinning degradation wherein the metal loss is constrained to patches of local zones in the tank wall. LTAs unattended can cause local failure by leakage or rupture if the remaining wall thickness is not sufficient to withstand the liquid pressure [Antaki, 2005]. Also, depending on the geometry and location, it can also lead to buckling and related issues. As mentioned in Chapter 2, replacing a slightly damaged tank is not a cost effective option compared to safely operating the tank and extending its life. This Chapter deals with Fitness for Service (FFS) assessments for LTAs in tanks. A level 2 procedure is proposed for the purpose of estimating remaining strength factor (RSF). The use of m_α-tangent multiplier method with modified reference volume assessment procedures for determining the RSF is explored.

7.0 CURRENT PRACTICE

Structural integrity assessment is of considerable importance in many industrial sectors. Fitness for service assessments are periodically performed for in service tanks to ensure their structural integrity and safety. A number of FFS procedures are available in practice, e.g., API 579-1/ASME FFS-1(2012), R5 (2003) and R6 (2001), **S**tructural **INT**egrity Assessment **P**rocedures for European Industry (SINTAP, 1999), etc. Among these, the API 579-1/ASME FFS-1 procedure is widely used in the industry. As explained in Chapter 2, the fitness for service assessments are quantified using remaining strength factor (Clause 2.4.2.2 of API 579-1/ASME FFS-1),

$$\text{RSF} = \frac{\text{Limit or Plastic Collapse Load of Damaged Component}}{\text{Limit or Plastic Collapse Load of Undamaged Component}}$$

The following is a brief description of the Level 1 procedure given by API to determine the RSF of pressure vessels/tanks/pipes with Locally Thinned Areas (LTAs). It forms the basis for all other advanced procedures used for complex loading or damage conditions. Based on the Critical Thickness Profile (CTP), the remaining thickness ratio (R_t) and the shell parameter (λ) are computed as

$$R_t = \frac{t_{mm} - FCA}{t_{\min}} \tag{7.1}$$

$$\lambda = \frac{1.285s}{\sqrt{Dt_{\min}}} \tag{7.2}$$

where, t_{mm} is minimum measured remaining wall thickness, FCA is future corrosion allowance, and t_{min} is minimum required wall thickness determined in accordance with

the original construction code. Similarly ‘s’ is the length of the flaw in the axial direction of the tank and ‘D’ is the diameter of the tank. Then the RSF and stress at failure of LTA are computed as

$$\sigma_{fail} = \frac{\sigma_y \ RSF}{0.9} \tag{7.3}$$

$$RSF = \frac{R_t}{1-(1-R_t)M^{-1}} \tag{7.4}$$

where M, is the Folias factor equal to $\sqrt{1+0.48\lambda^2}$.

The remaining strength factor (RSF) given above is based on a Dugdale plastic-zone-size model, “Folias” factor and an empirically established flaw depth to wall thickness relationship [Janelle, 2005]. Folias factor is a stress magnification factor due to bulging caused by an axial crack in a pressurised cylinder [Folias, 1969]. An empirical flaw-depth-to-pipe-thickness relationship is used to modify the Folias factor to account for part-through wall effects based on “effective” cross sectional area. This method assumes that the flaw fails when the stress in the flaw reaches the flow stress σ_{flow}. The flow stress is assumed to be equal to $\sigma_y/0.9$ (= $1.111\sigma_y$) similar to that of ASME B31G. The procedure also assumes that the region of metal loss is not influenced by any structural discontinuity, welded joints, change in geometry, etc. To ensure this, API 579-1/ASME FFS-1 specifies that $L_{msd} \geq 1.8\sqrt{Dt_{\min}}$ where, L_{msd} is the shortest distance between the edge of corrosion area and the discontinuity. Additionally the remaining thickness should be such that, t_{mm} - FCA ≥ 2.5mm and $R_t \geq 0.20$. The former condition

is to ensure safety against leakage and mechanical damage while the latter can possibly be due to the absence of validation results for very deep flaws greater than 80% of design thickness.

The Folias factor or bulging factor is basically a factor that relates stress near the cracked portion of a flat plate to that of cylindrical plate. The factor is derived from the following governing differential equations where the pressure is assumed to be uniform.

$$\nabla^2 F + \frac{Et}{R}\frac{\partial^2 \omega}{\partial x^2} = 0 \tag{7.5}$$

$$\nabla^2 \omega + \frac{1}{RD}\frac{\partial^2 F}{\partial x^2} = \frac{q_o}{D_s} \tag{7.6}$$

where ∇^4 is the biharmonic operator, $\omega(x,y)$ is the displacement function, $F(x,y)$ is the stress function, E the young's modulus, t the thickness of the vessel, D_s the flexural rigidity, R the radius and q_o the internal pressure.

In the equations above, it can be noted that the pressure q_o is assumed to be a constant (uniform internal pressure). This is obviously the case for most pipes and pressure vessels. However in the current practice, the same Folias factor is used for determining the RSF of tanks with hydrostatic pressure as well. The product of the RSF and the existing pressure or wall thickness will give the rerated pressure or wall thickness. In case of tanks, since the pressure is varying along the height (axial dimension), the minimum acceptable thickness and the Maximum Fill Height (MFL) are

calculated at one foot above the bottom end of LTA (Clause A.6.1 of API 579-1/ASME FFS-1).

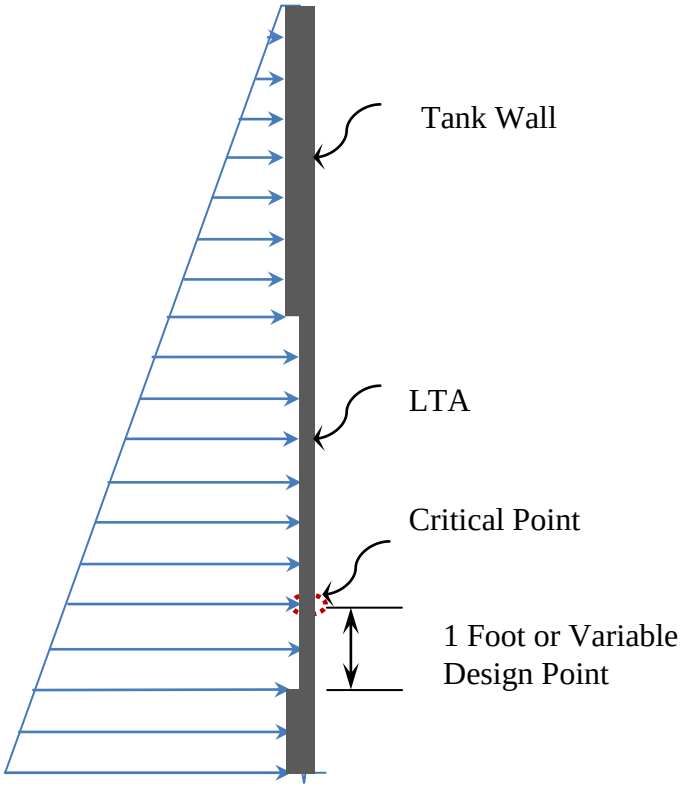

Fig. 7.1 Critical Point in LTA for a Tank

The concept of considering the pressure one foot above the junction of two different thicknesses in the tank wall (see Fig.7.1), also known as 'one foot method', is a long standing practice used in design of tanks. The one foot is an approximate location where the tank stresses are assumed to be maximum in any particular shell course of the tank wall or LTA in consideration. In lieu of the one foot rule, a more precise location of maximum stress point can be calculated using the variable design point method given by Clause 5.6.4 of API 650 [2012]. If the height of the flaw is small, the pressure can be simply considered at the bottom of the flaw (Clause 4.3.3 of API 653), which will give a

conservative estimate. A detailed procedure for calculating the minimum thickness and the actual length of flaw (to be used for determining RSF) are discussed in API 653. To summarize the current procedure, RSF for tank is determined in exactly the same manner as that for cylindrical vessel with uniform pressure. Although the tank has hydrostatic pressure, no special discussion seems to have taken place about applying the uniform pressure procedure for tanks except that while rerating the tank, the pressure to be used is taken at one foot above the bottom.

7.1 CONCEPT OF DECAY LENGTH AND REFERENCE VOLUME

The concept of "Decay Length" is widely used in pressure vessel theory. It is a known fact that the effect of a localized force (such as that due to discontinuities) dissipates as the distance from the point of application of the force increases. The decay length of cylinders is the distance required for the effect of a force/moment applied on the shell to dissipate (decay) to a negligible amount. It is a characteristic length based on the geometry of the shell and the nature of force and is independent of the magnitude of the force [Tantichattanont, 2009]. Generally larger decay lengths have larger volume for energy dissipation and hence indicate higher load carrying capacity. For cylindrical shells the decay length in the axial direction (x_l) is shown by many sources [ex. Gill, S.S., 1970] as,

$$x_l = 2.5\sqrt{Rt} \tag{7.7}$$

where, 't' is the nominal thickness of the cylinder

Tantichattanont, et al., [2009] have discussed this in detail and showed the circumferential decay length of cylindrical shell to be

$$x_c = 6.3\sqrt{Rt} \tag{7.8}$$

The above expressions are obtained using shell theory applied to axisymmetric cylindrical shell subjected to line loads along circumferential or longitudinal directions, respectively. They are generally applicable for thin shells with R/t ratios in the range of 20 to 100.

When the tank fails by plastic collapse due to an LTA or any other localized damage in the tank wall, it is well known that only a portion of the tank wall participates in the plastic action and the remaining regions (Dead Volume) that do not participate in the plastic action may remain unaffected. The "kinematically active" portion of the component or structure that participates in plastic action due to the presence of the damage is termed as "Reference Volume" by Seshadri and coworkers [Adibi-Asl, et al., 2011]. The total volume of the component is the sum of this reference volume and the "dead volume" (Fig.7.2). The accuracy of the limit loads predicted by m_α-tangent method depends primarily upon the accuracy of the reference volume assumed.

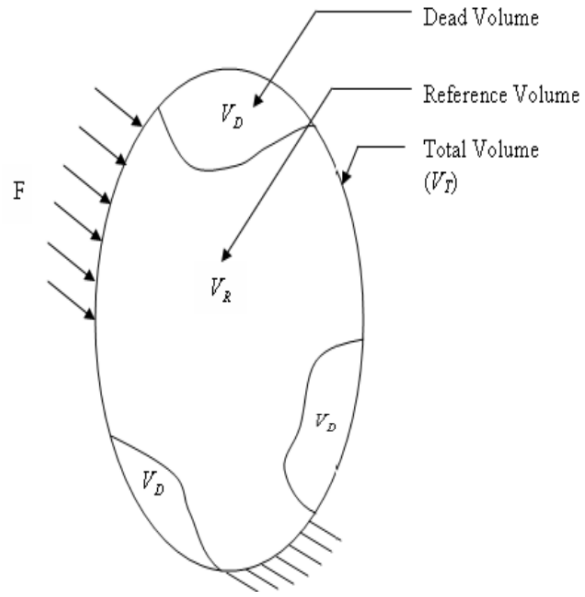

Fig. 7.2 Reference Volume and 'Dead Volume'

7.2 CIRCUMFERENTIAL DECAY LENGTH FOR TANKS

As mentioned earlier, using the expression ($2.5\sqrt{Rt}$) for decay length in axial direction of cylinders is a well-established practice. It is shown theoretically and verified numerically [Tantichattanont, et al., 2009] that the decay length in circumferential direction is larger than that in the axial direction at $6.3\sqrt{Rt}$. The reason for this seems to be the change in curvature from axial to circumferential direction. However in case of tanks, because of very large radius compared to pipes and pressure vessels, the curvature in circumferential direction is substantially smaller (R/t for tanks can be substantially larger than 1000 as opposed to R/t of around 50 to 100 for typical pressure vessels). Hence, the circumferential decay lengths could be smaller than $6.3\sqrt{Rt}$. In order to

study this, the example tank as specified in Chapter 3 (Sec.3.5 Case1) is analyzed using FEA for varying sizes of LTA.

The finite element modeling was carried out using eight noded shell elements (SHELL 281 of ANSYS). The element has six degrees of freedom at each node and is suitable for analysing thin to moderately-thick shell structures. An elastic-perfectly plastic material model is used and the nonlinear analysis is carried out as per the guidelines given in Clause B1.2.4.2 of API 579-1/ASME FFS-1 [2012] standard. The plastic collapse load is taken as the load corresponding to 1% plastic strain at the middle fiber of any location in the LTA. This approach is consistent with the work reported by earlier researchers on FFS assessment [Seshadri, et al., 2004, Tantichattamont and Adluri, 2008]. The analysis is carried out using up to 7 integration points across each layer. Multiple layers are used across the thickness. For example, an 8mm bottom plate has 8 layers (with 3 integration points across each layer) and an 18mm shell wall has 3 layers (with 7 integration points across each layer). Since the yielding occurs in the bottom plate and it is the zone of interest in this research work, the bottom plate is modeled with more layers than the shell plate. This approach is adopted to optimize the computational effort and data handling in FEA. A macro is developed in ANSYS to incorporate decay lengths in the post processing analyses and extract stress values from different layers of the shell element if needed.

The following stress plots (Fig.7.3 & 7.4) obtained from the analysis show the hoop stress values at the centre of LTA as the ordinate and the height or width of LTA as

the abscissa. The notation LTAW 100% represents LTA width equal to $6.3\sqrt{Rt}$ and LTAH 100% represents height equal to $2.5\sqrt{Rt}$. Various lines in the plots refer to hoop stress at the centre of LTAs of different sizes. For example, in Fig.7.3, the series LTAW 60% shows the hoop stress for different heights of LTA with the LTA width being constant at 60% of $6.3\sqrt{Rt}$. From this figure, it can be observed that the hoop stress increases as height of LTA increases, but the width of LTA doesn't seem to influence the hoop stress beyond 40% of $6.3\sqrt{Rt}$, which is approximately $2.5\sqrt{Rt}$. All the series from 40% -100% LTAW show the same pattern.

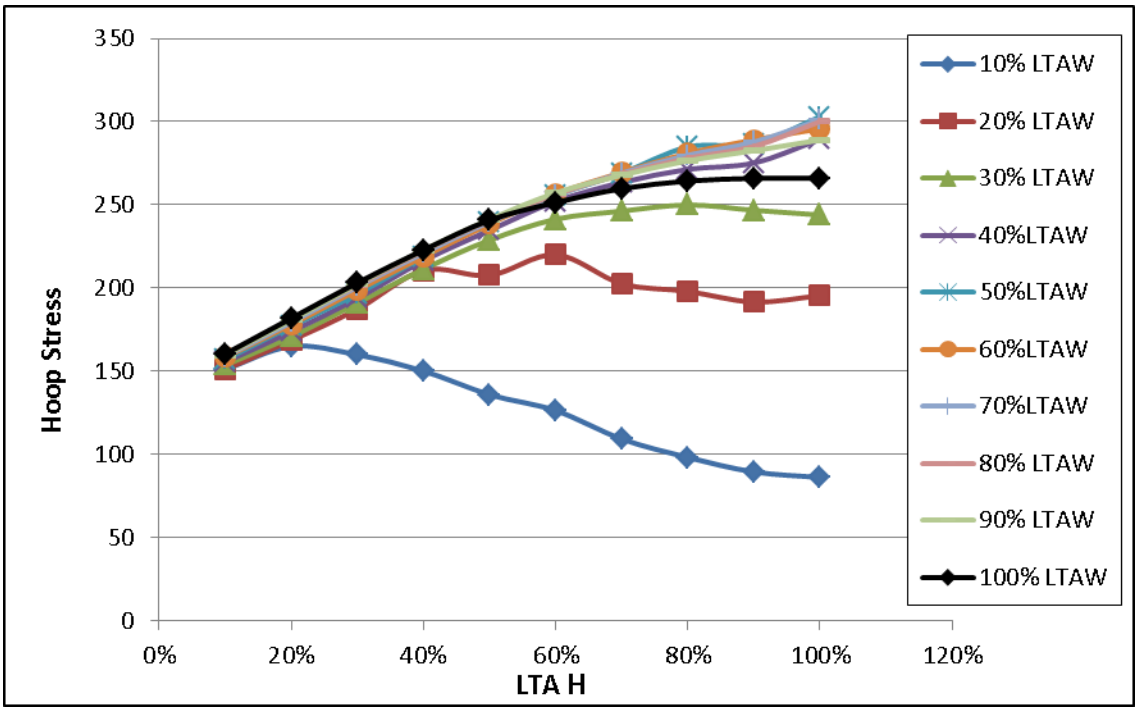

Fig. 7.3 Hoop Stress Variation with Height of LTA

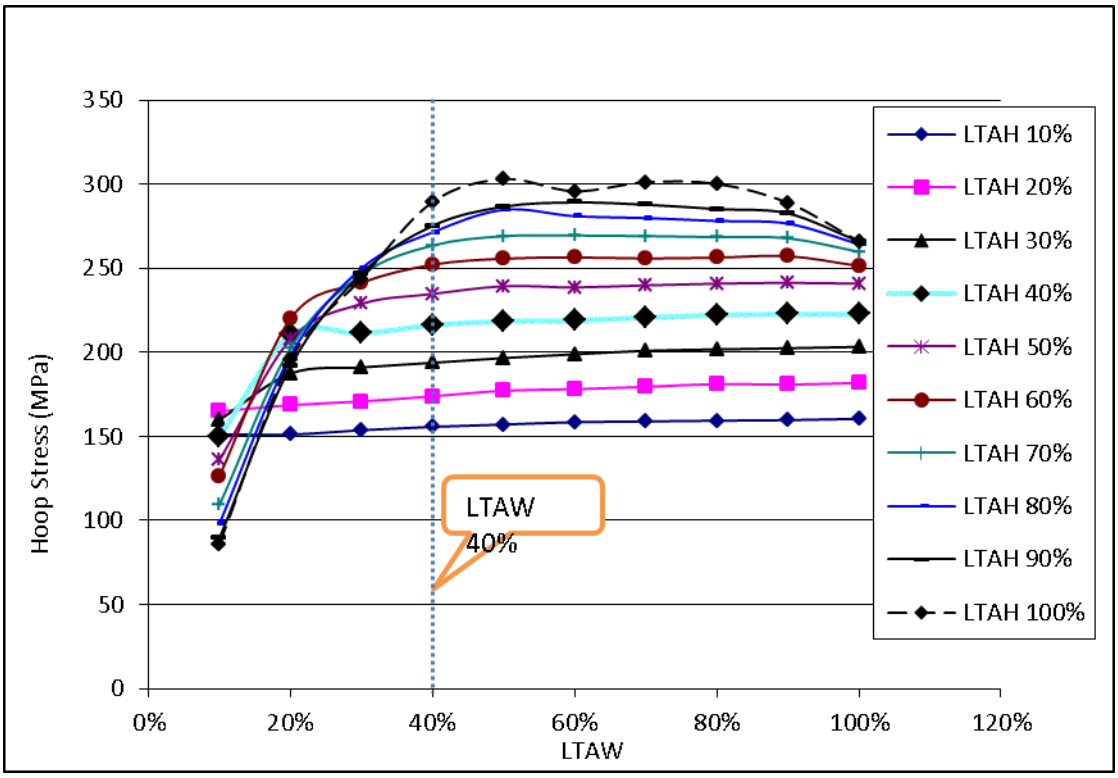

Fig. 7.4 Hoop Stress Variation with Width of LTA

Similar observation can be made from Fig.7.4., i.e., no significant change in the hoop stress when the width is larger than 40% of $6.3\sqrt{Rt}$. Hence, in the present study, for the RSF calculations in tanks, a decay length of $2.5\sqrt{Rt}$ ($\approx$ 40% of $6.3\sqrt{Rt}$) is used in the circumferential direction as well as the axial direction. This leads to the recommendation that $2.5\sqrt{Rt}$ be used instead of $6.3\sqrt{Rt}$ as circumferential decay length for tanks and other vessels that have very large R/t ratio. More shells can be analyzed to establish the limits of this recommendation for various R/t ratios.

7.3 DETERMINATION OF RSF USING m_α-TANGENT METHOD

As mentioned earlier, the remaining strength factor (RSF) is used as a basis for the evaluation of locally thinned areas in storage tanks. Detailed discussion about RSF and the methods for determining it are already presented in Chapter 2. For tankage, the RSF acceptance criterion is [API 579-1/ASME FFS-1, 2012]:

$$MFH_r = MFH\ (RSF/RSF_a) \quad \text{for} \quad RSF < RSF_a \tag{7.9}$$

$$MFH_r = MFH \quad \text{for} \quad RSF \geq RSF_a \tag{7.10}$$

where,

MFH_r = Reduced permissible maximum fill height of the damaged tank

MFH = Maximum fill height of the undamaged tank

RSF = Remaining Strength Factor of the damaged tank

RSF_a = Allowable Remaining Strength Factor

If the calculated RSF is higher than the allowable RSF_a, the tank is safe for full operation. The recommended value for the allowable Remaining Strength Factor is 0.90 for tanks in process services [API 579-1/ASME FFS-1, 2012]. This value can be reduced based upon the type of loading (e.g., normal operating loads, occasional loads or short-time upset conditions) and/or the consequence of failure.

The RSF of a structure/component can be determined in different ways as already mentioned in Chapter 2. The material/geometry/loading conditions of a given problem can be too complicated to have a closed form solution to determine the RSF. Similarly, performing 'nonlinear' FEA in those situations can also become impractical. For these

cases, performing a FFS assessment using linear FEA and simplified limit load procedures is very useful. Using the simplified methods, the RSF can be estimated to a reasonable accuracy in a shorter time and with much lesser effort.

The m_α-tangent multiplier method is a robust simplified limit load procedure, that can be used for FFS assessments utilizing linear analyzes instead of full scale nonlinear FEA. The linear analyzes can be done either using shell theory, FEA or any other linear methods. The only requirement is that the method needs a statically admissible stress field for the tank being analyzed. Hossain and Seshadri [2009] have used this method for fitness for service assessments of pipes/pressure vessels with corrosion damages and thermal hotspots. Recently Ahmad, et al., [2010] have made a preliminary study to use this procedure for hydrocarbon tanks.

7.3.1 RSF using Analytical Approach

Seshadri, et al., [2005] have shown the use of Mura's "integral mean of yield criterion" for determining limit loads of components and hence the RSF of damaged components.

For incipient plastic flow condition, the integral mean of yield criterion is expressed as

$$\int_{V_R} \mu^0 \left[f(\bar{s}_{ij}^0) + \left(\varphi^0\right)^2 \right] dV = 0 \tag{7.11}$$

where, $\bar{s}_{ij}^0$ is the statically admissible deviatoric stress for impending plastic flow, μ^0 is flow parameter, φ^0 is a point function which takes in a value of zero if $\bar{s}_{ij}^0$ is at yield and

remains positive below yield, and V_R is the reference volume. The yield criterion can be expressed as

$$f(\bar{s}_{ij}^{0}) = \left[\left(m_d^o \sigma_e \right)^2 - \sigma_y^2 \right] = 0 \tag{7.12}$$

where, m_d^o is the appropriate statically admissible upper bound multiplier for the damaged component, σ_e is the equivalent stress and σ_y is the yield stress of the material. For components containing LTAs, the integral mean of yield criterion can be expressed as [Seshadri, 2005]

$$[(m_d^0 \sigma_{eU})^2 - \sigma_y^2]\ V_U + [(m_d^0 \sigma_{eD})^2 - \sigma_y^2]\ V_D = 0 \tag{7.13}$$

where, suffix U(or u) refers to the uncorroded region of the reference volume and suffix D(or d) refers to the corroded (damaged) region, σ_{eU} is the equivalent stress in the original shell and σ_{eD} is the equivalent stress in the corroded area of the shell.

Rearranging Eq. 7.13,

$$m_d^0 = \sqrt{\frac{\sigma_y^2 V_R}{\sigma_{eU}^2 V_U + \sigma_{eD}^2 V_D}} \tag{7.14}$$

Based on the above multiplier, the following three approaches are used to determine the RSF of damaged tanks.

7.3.1.1 RSF Based on Upper Bound Multiplier

The remaining strength factor RSF_U is based on the integral mean of yield criterion, along with the von Mises failure criterion. The upper bound RSF_U is obtained using m_d^0 as

$$RSF_U = \frac{m_d^0}{m_u^0} \tag{7.15}$$

where, $m_u^0 = \sigma_y / \sigma_{eU}$ is the upper bound multiplier for the undamaged tank, and m_d^0 (Eq. 7.14) is obtained from the integral mean of yield criterion. Since RSF_U is the ratio of an upper bound multiplier of a damaged tank to that of an undamaged tank, the RSF will be an upper bound estimate.

7.3.1.2 RSF Based on the m_α-Tangent Multiplier

The second *RSF* is obtained by using the m_α-tangent multiplier (m_α^T), proposed by Seshadri and Hossain [2009]. The m_α-tangent multiplier based on Eq. 2.28, can be used to calculate the RSF as

$$\mathrm{RSF}^{\mathrm{T}} = \frac{\mathrm{m}_\alpha^{\mathrm{T}} \text{ of damaged component}}{\mathrm{m}_\alpha^{\mathrm{T}} \text{ of undamaged component}} \tag{7.16}$$

while using Eq. 2.28 in order to evaluate RSF^T, the classical lower bound multiplier can be obtained as $m_L = m_{Ld} (= \sigma_y / \sigma_{eD})$ and the upper bound multiplier m^0 as equal to m_d^0 as defined in Eq. 7.14.

For $m_\alpha{}^T$ calculations, the stress distribution is obtained within the reference volume of a damaged tank either using shell theory or from a linear elastic analysis as mentioned earlier. The m_α-tangent multiplier is determined (Eq.2.28) for the reference volume with and without damage, i.e., for the undamaged case the same reference volume as that of the damaged case is used but with the undamaged thickness. The value of m_L is calculated from the maximum stress value in the reference volume and m^0 is determined using a macro incorporating Eq.7.14 in the postprocessor of ANSYS. Using these multipliers, the $m_\alpha{}^T$ value and RSF can be determined. The same procedure is repeated for different sizes of LTA.

7.3.1.3 RSF Based on Classical Lower Bound Multiplier

The third remaining strength factor RSF_L is based on the classical lower bound limit load multiplier m_L and is given by,

$$RSF_L = \frac{m_{Ld}}{m_u^0} \tag{7.17}$$

where, the classical lower bound multiplier $m_L = m_{Ld}(=\sigma_y/\sigma_{eD})$ for corrosion damage. This RSF gives very conservative estimation of RSF.

7.3.2 RSF Based on Non Linear Finite Element Analysis (NLFEA)

The RSF can be determined more accurately using Nonlinear FEA. In this thesis, a Level 3 FFS evaluation is performed using full scale elastic-plastic FEA (EPFEA) for comparison purposes. The RSF is calculated as the ratio of the limit pressure (pressure corresponding to 1% membrane plastic strain in the LTA) of damaged tank to the

corresponding limit pressure of the tank without loss of thickness. The limit pressure of the tank without LTA is calculated at the same damage location as used in the tank with LTA. Although the location of maximum plastic strain in the LTA is slightly below the centre of LTA, it can be approximated to be at the centre for most cases

7.4 REFERENCE VOLUME FOR LTA IN TANKS

The reference volume is computed using the shell decay length and damage geometry. At present, the m_α-tangent method considers the reference volume as the full volume of LTA plus a portion of the undamaged tank bound by the appropriate decay lengths on all sides of LTA [Seshadri, et al., 2009; Hossain, et al., 2010; Ahmad, et al., 2010]. Figures 7.5 & 7.6 show the damaged zone and the corresponding reference volume used by Ahmad, et al., [2010]. The actual LTA profile is generally irregular both in shape and thickness. However, the existing level 2 practice [API 579, 2012] is to use representative uniform rectangles with averaged thicknesses across several strips to evaluate the irregular flaw. The treatment in the present study is a demonstration for one such rectangular stip. This can be extended in a manner similar to that in the current API practice. This is in line with earlier work by Tantichattnont, et al. [2008] and others.

For a damaged area of width '*2a'* in circumferential direction and length '*2b'* in the axial/longitudinal direction (Fig.7.5), the volume of damaged zone (V_D) is given by

$$V_D = 4abt_{mm} \tag{7.18}$$

where, t_{mm} is the minimum measured remaining wall thickness of the tank in the corroded area. The adjacent undamaged zone (V_U) bounded by the decay lengths and assumed to be a part of reference volume is given by

$$V_U = 4t_c((x_c+a)(x_l+b)-ab) \quad (7.19)$$

where, t_c is the corroded thickness of the tank wall away from the region of LTA, x_l and x_c are the decay lengths in the axial and circumferential direction (Fig.7.6). The reference volume (V_R) is therefore the sum of damaged and undamaged volumes.

$$V_R = V_D + V_U \quad (7.20)$$

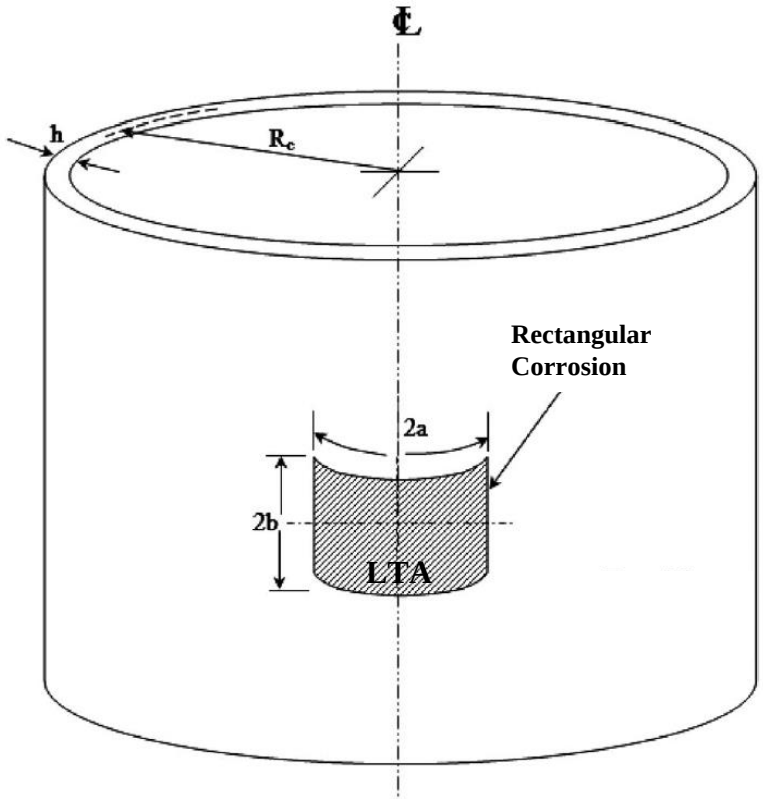

Fig. 7.5 Tank with Locally Thinned Area [Ahmad, et al., 2010]

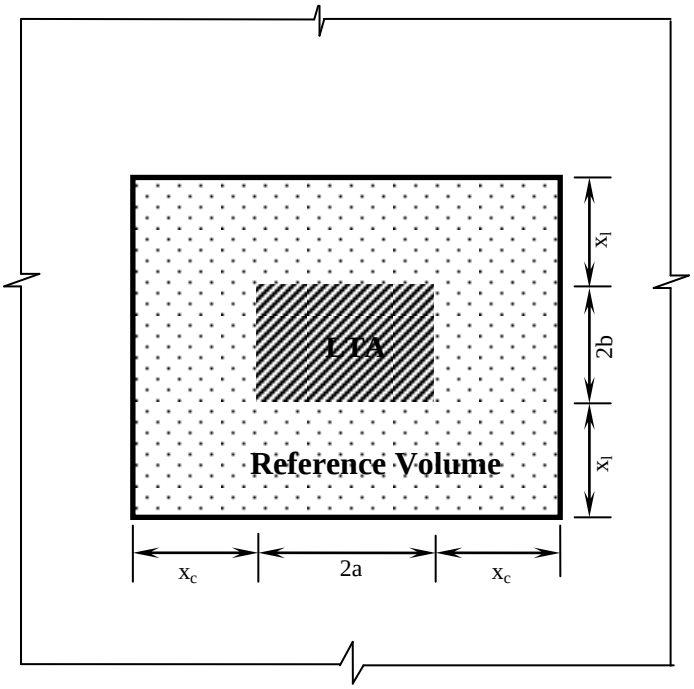

Fig. 7.6 Tank with LTA and Reference Volume as used by Ahmad et al. [2010]

As mentioned earlier in Chapter.2, the m_α multiplier is a function of m^o and m_L where, m^o depends upon reference volume. The accuracy of the multipliers depend on the choice of reference volume. Using the reference volume adopted by Ahmad, et al., [2010], RSF for various heights of damage zone sizes are computed using the analytical approach. These are shown in Fig.7.7. The method is quite conservative for small damage sizes. However, the results show that the approach is significantly unconservative for larger damage sizes. Even more importantly, the approach does not taper down to the bottom limit that the RSF must converge to as the damage becomes large.

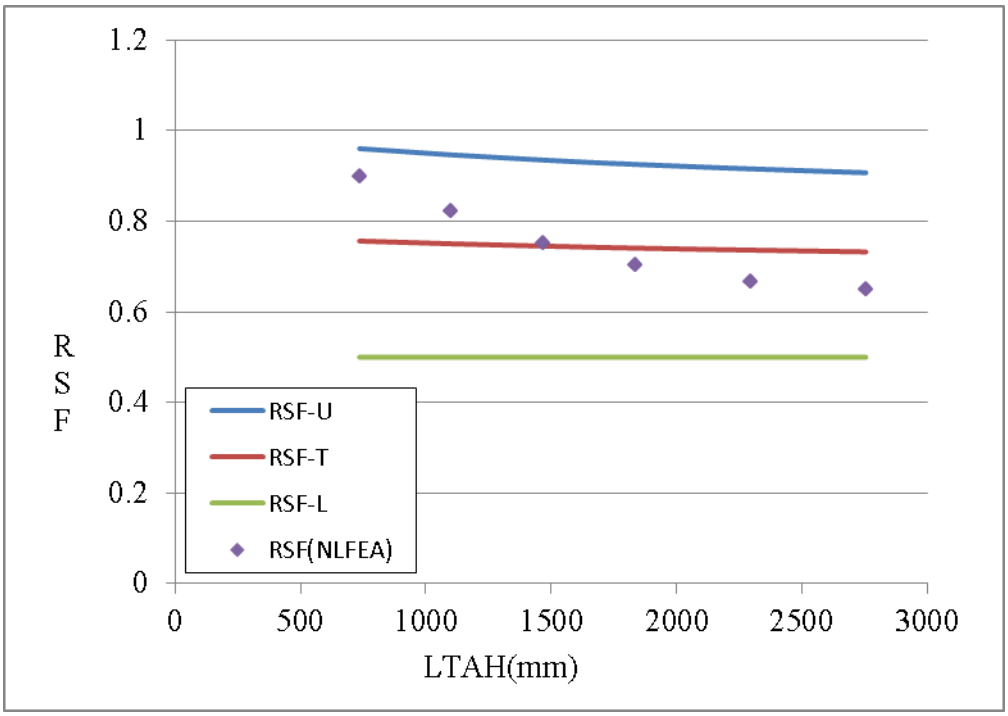

Fig. 7.7 RSF using Analytical Approach –Ahmad, et al. [2010]

In the above procedure, the centre of the LTA also forms the centroid of the reference volume, i.e., the reference volume is symmetric in both directions with respect to the centroidal axes of LTA. The effect of pressure being non-uniform (Hydrostatic) on the reference volume is not included. Also, the decay lengths used in the procedure are based on elastic theory. However, it must be noted that the reference volume based on elastic theory may not exactly be the same as the volume participating in plastic collapse.

7.5 MODIFIED REFERENCE VOLUME APPROACH

Ahmad's reference volume taken as LTA plus decay length on the outside is reasonable from the point of view that it must be equal to the kinematically active volume. However, as outlined above, this approach seems to give inconsistent results that

are most likely unacceptable for larger damages. One of the reasons for this could be the choice of reference volume. A brief explanation is given below. For a simple cylinder, subject to hydrostatic loading, the limit pressure of the tank is given by

$$p_{Limit} = \frac{\sigma_y t}{R} \tag{7.21}$$

$$m^0 = \sqrt{\frac{\sigma_y^2 V_R}{\int_{VR} \sigma_{eq}^2 dv}} \tag{7.22}$$

$$m_L = \frac{\sigma_y}{\sigma_{\max}} \tag{7.23}$$

Since the pressure is varying with respect to height,

$$\int_{V_R} \sigma_{eq}^2 dv = \int_{h_1}^{h_2} \sigma_{eq}^2 t dh \tag{7.24}$$

Since the tank wall is subjected only to hoop stress

$$\int_{h_1}^{h_2} \sigma_{eq}^2 t dh = \int_{h_1}^{h_2} \left[\frac{\gamma h R}{t}\right]^2 t dh = \left[\frac{(\gamma R)^2}{t}\right] \int_{h_1}^{h_2} h^2 dh \tag{7.25}$$

$$m^0 = \left[\frac{\gamma R^2 h^3}{3t}\right]_{h_1}^{h_2} \tag{7.26}$$

Using the tank geometry as given in Chapter2 CASE 2 (H = 12000mm; R = 30000mm; t = 18mm) and employing the m_α-tangent method (Eq.7.22 - 7.26), Fig. 7.8 shows the effect of changing reference volume. The actual limit load multiplier for the

hydrostatic loading case is 2.29. This is the same as that of the uniform pressure case since the limit load depends on the highest pressure at the bottom. The true reference volume for this case is a point at the bottom of the tank wall. Hence, for tanks with hydrostatic loading, considering a larger volume or the entire volume as reference volume deviates the m_α-tangent values away from the actual limit load values. However, in case of uniform pressure components such as pipes, even assuming a slightly larger volume as reference volume has less impact on the m_α-tangent values.

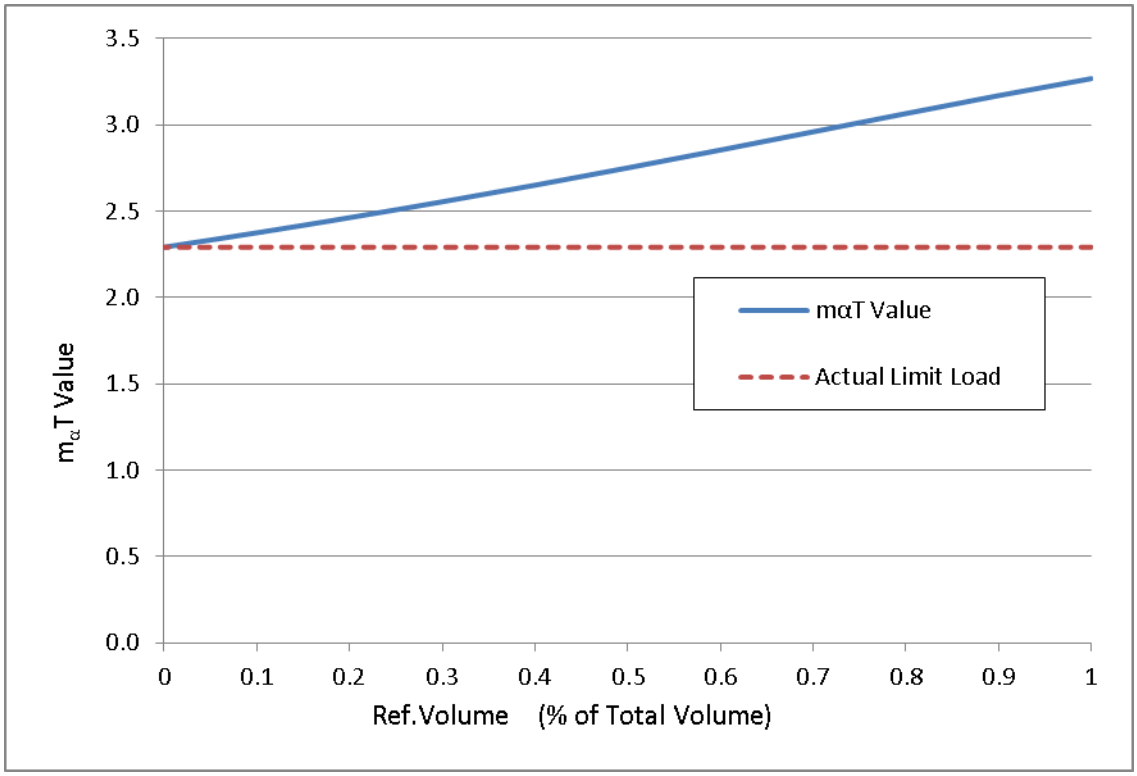

Fig. 7.8 m_α-Tangent Value for Tank with Hydrostatic Pressure

A more detailed study of a tank (with hydrostatic pressure) whose bottom is fixed has been carried out with ANSYS [2011]. Some of the results are shown in Fig.7.9. The deviation from the full scale nonlinear analysis is very pronounced for small reference

lengths (less than $2.5\sqrt{Rt}$ from maximum stress location). The error is quite small at $2.5\sqrt{Rt}$ beyond which the error increases again. Therefore, a good choice for reference volume estimate plays a major role in the computation of limit load

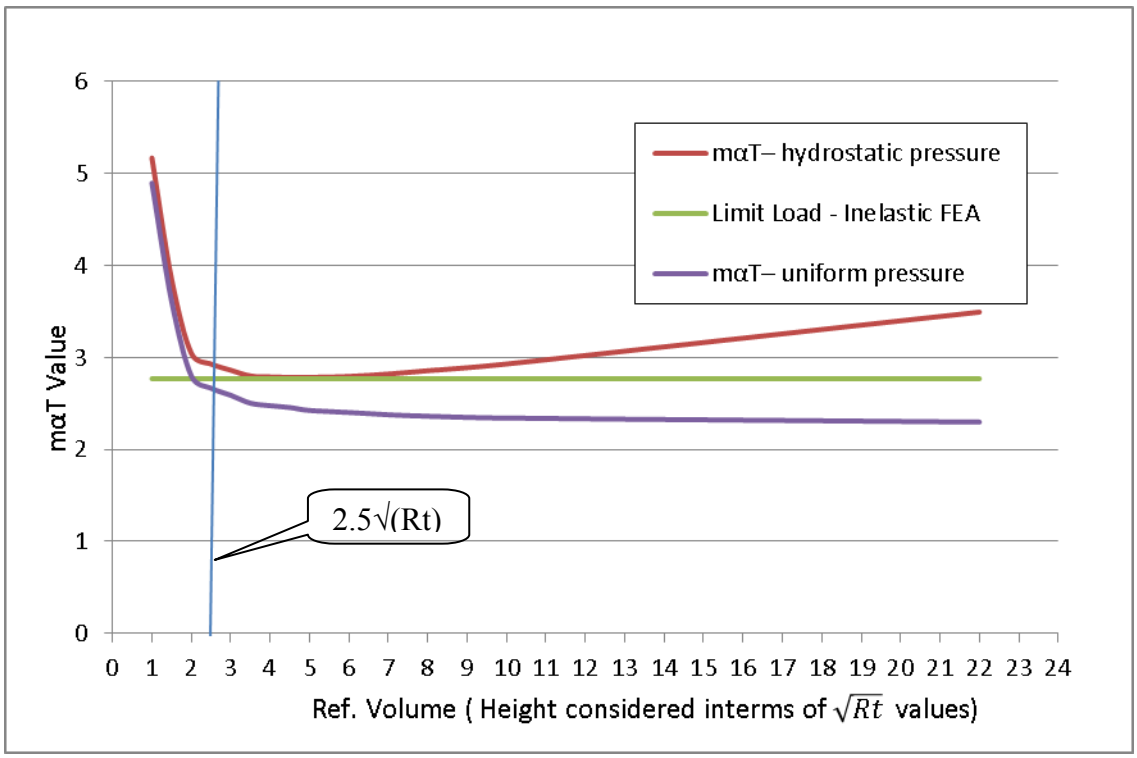

Fig.7.9 m_α-Tangent Value for Tank with Hydrostatic and Uniform Pressure

From the concepts of decay length, it is obvious that the influence of discontinuity moments at the bottom of the tank wall becomes insignificant beyond a height of $2.5\sqrt{Rt}$. Hence considering the volume till this height, as reference volume gives results close to nonlinear FEA. Beyond this limit, the values diverge (increases) because the stress in the tank wall decreases with height. In case the bottom hydrostatic pressure is applied as a uniform pressure throughout the height, the m_α-tangent value doesn't change

significantly. Hence for tanks with hydrostatic pressure, considering larger volumes as reference volume is unconservative.

Earlier Researchers (Seshadri [2005], Tantichattonont [2007]) had considered the damaged volume and the undamaged volume enclosed by decay lengths outside the damage as the reference volume. For tanks with hydrostatic pressure, this approach assumes a relatively large volume to be part of the reference volume and hence the m_α-tangent multiplier value was higher than that from non-linear FEA.

In light of the above, in this current study the use of a modified reference volume estimate has been explored. This assumes that the most active volume is covered by the zone obtained by overlapping decay lengths from either side of the discontinuity. There may be some adjacent volume that is also kinematically active to some extent. However, it is neglected for the purpose of simplicity. This is shown in Fig. 7.10. If the flaw is large and the decay lengths from the discontinuity do not overlap, the most active volume is the in-between zone of the highly stressed portion of LTA. It can be shown theoretically that this is guaranteed to taper down the RSF to its lower limit (t_{mm}/t_c) for large flaws. Hence this zone is considered as reference volume although this idea is not fully in line with the original thinking behind the reference volume concept. It must be noted that for small damage, the decay lengths from the edges will spill over on the other edge of LTA. The reference volume will then include an appropriate undamaged zone as well.

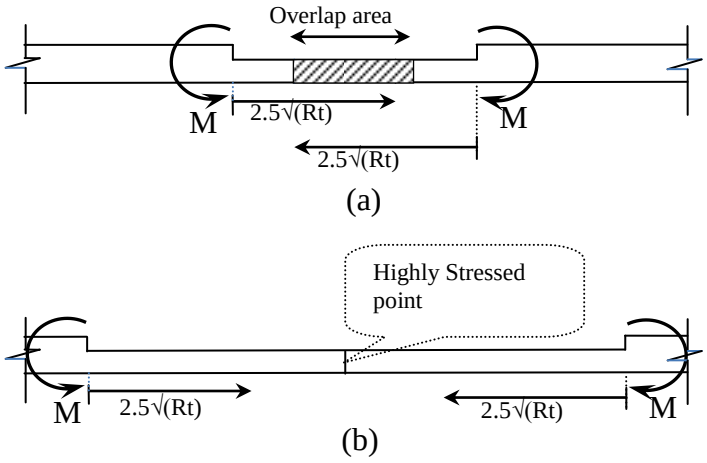

Fig.7.10 Reference Zone for LTA

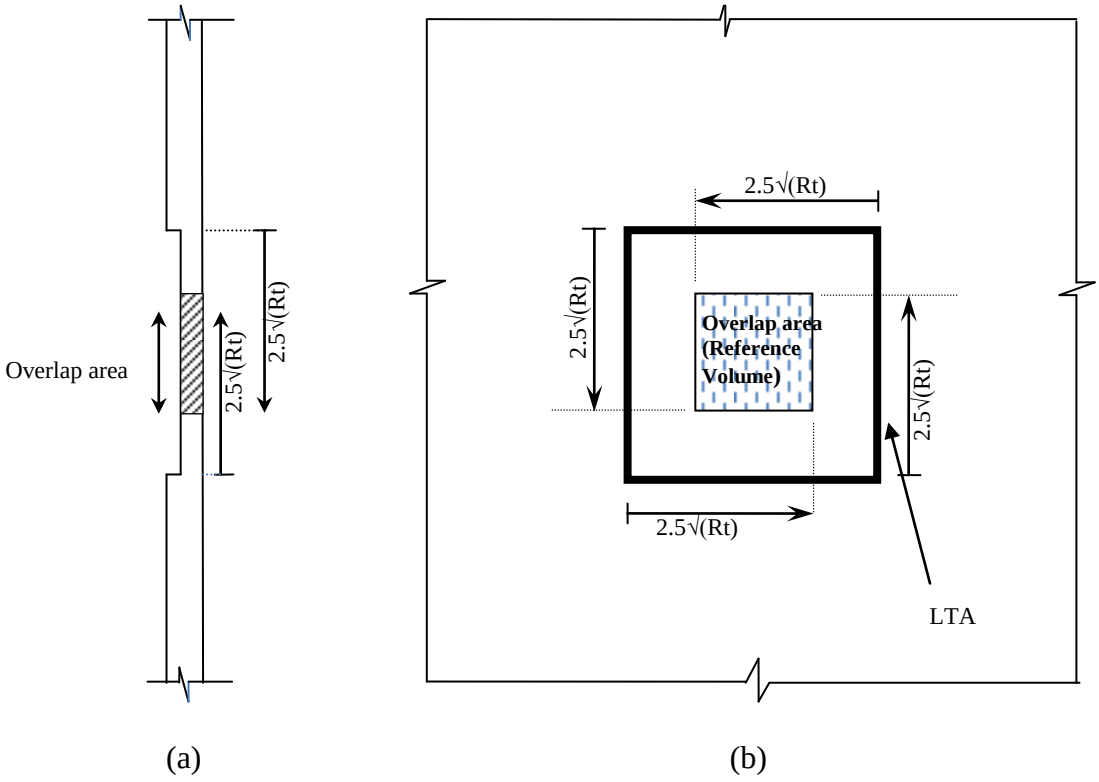

Fig.7.11 Modified Reference Volume (Decay Lengths Smaller than Flaw)

Figure 7.11 shows the overlap area obtained by considering the decay lengths in both longitudinal and circumferential direction for flaw sizes that are larger than decay

lengths. In case the decay lengths are larger than the size of the flaw and spill beyond the flaw (Fig.7.12), the entire volume of the flaw is included in the reference volume.

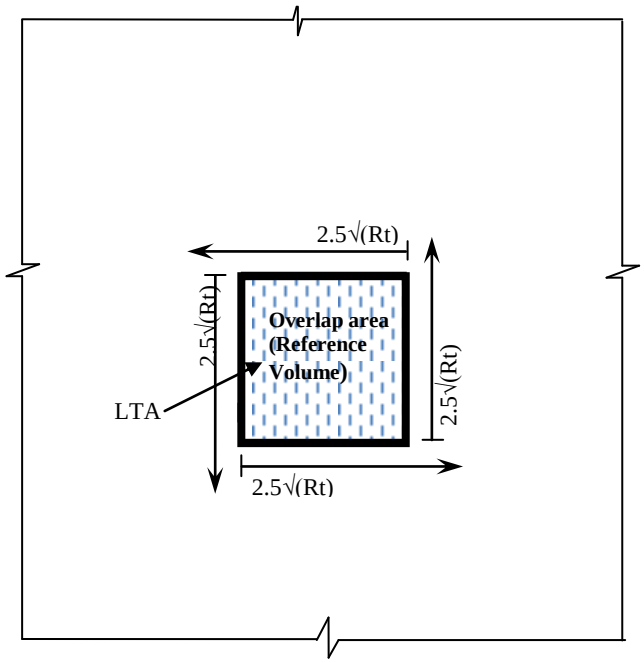

Fig.7.12 Modified Reference Volume (Decay Lengths Larger than Flaw)

It must be noted that the failure of the tank with LTA damage happens only in the region of reduced thickness, except for situations where the flaw is small and located away from the bottom. In those exceptional situations, the damage does not affect the limit capacity of the tank and the bending zone above the tank bottom will become critical even if there is a minor damage elsewhere, as in the case of any undamaged tank.

7.6 ILLUSTRATIVE EXAMPLE

The example tank as given in Sect.3.5 CASE1 with the following specifications is used for illustration. The tank is analyzed for hydrostatic pressure due to water at ambient temperature.

Geometric Data:

Diameter	:	60,000 mm
Height	:	12,000 mm
Thickness of shell wall	:	18 mm
Thickness of Bottom plate	:	6 mm
Projection of Bottom plate	:	50 mm (Beyond shell)

Material Data:

Young's Modulus	:	200,000 MPa
Yield Strength	:	345 MPa
Product Design Stress	:	194 MPa
Specific weight of liquid (water)	:	9.81 kN/m^3
Density of Steel	:	77.1 kN/m^3
Poisson's ratio	:	0.3

The required shell thickness (t_d) is determined using 1-foot method as prescribed in 5.6.3.2 of API 650

$$t_d = \frac{4.9D(H-0.3)G}{S_d} = 17.75\text{mm, say t} = 18\text{mm}$$

where S_d is the allowable product design stress (Table 5.2 of API 650) and G is the specific gravity of the liquid.

Axial decay length: $X_l = 2.5\sqrt{Rt} = 1837\text{mm}$

Circumferential decay length: $X_C = 6.3\sqrt{Rt} = 4630\text{mm}$ (as per the existing guidelines)

$X_C = 2.5\sqrt{Rt}$ = 1837mm as per decay length proposed

LTA Dimensions:

For this illustrative calculation the longitudinal dimension (LTAH) of the LTA is taken as 1.25 times $2.5\sqrt{Rt}$ (i.e., 2b =2296mm) and the circumferential dimension (LTAW) is taken as $6.3\sqrt{Rt}$ (i.e., 2a = 4630 mm). The corroded thickness (t_{mm}) is assumed to be 9mm (50% corrosion).

Calculation of Reference Volume – Current Procedure [Ahmad, et al., 2010]:

- Volume of LTA (V_D) = $4abt_{mm}$ = 95.67 x 10^6 mm^3
- Uncorroded Volume (V_U) = $[(2X_C+2a)(2X_L+2b)-4ab]t_c$ = 13.96 x 10^8 mm^3
- Reference Volume (V_R) = (V_U +V_D) = 14.92 x 10^8 mm^3

Evaluation of Hydrostatic Equivalent Pressure and Corresponding Stresses:

In order to account for the pressure varying hydrostatically over the reference volume zone, Ahmad, et al. [2010], used the equivalent pressure which be determined by centroidal calculations of pressure area as shown in Fig.7.13.

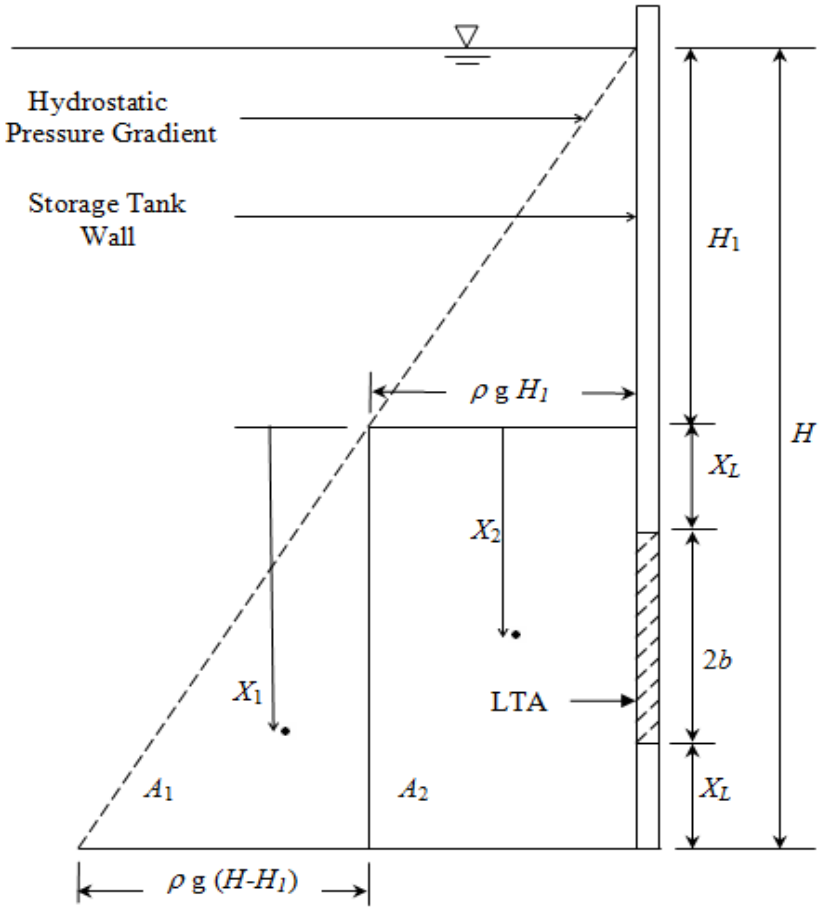

Fig.7.13 Evaluation of Hydrostatic Equivalent Pressure

Triangular Area of LTA A_1 = [(½) {γ (H-H_1)} ($2X_L$ +2b)] = 174.832 N/mm

Rectangular Area of LTA A_2 =[(γ H_1) ($2X_L$ +2b)] = 353.15 N/ mm

Equivalent distance $\overline{X}_G = \dfrac{\left(A_1 x_1 + A_2 x_2\right)}{A_1 + A_2}$ = 9344mm

Hydrostatic equivalent pressure on LTA:

$\boldsymbol{p}_{avg} = \bar{X}_G \rho g = 91.66$ kPa

Hoop stress in corroded region:

$\sigma_{tc} = (p_{avg} R_c)/t_{mm} = 305.56$ MPa

where, R_c is the outer radius of the corroded thickness.

Hoop stress in uncorroded region:

$\sigma_t = (p_{avg} R)/t_c = 152.8$ MPa

Only hoop stress is considered here as the tank is subjected to only hydrostatic pressure, without any blanket pressure. Tank blanketing, or padding, refers to applying a cover of gas (usually nitrogen) over the surface of a stored liquid to prevent it from vaporizing into the atmosphere. It can maintain the atmosphere above a flammable or combustible liquid to reduce ignition potential. It can make up the volume caused by cooling of the tank contents, preventing vacuum and the ingress of atmospheric air. Hence in this situation the equivalent stress is the same as hoop stress.

Therefore, $\sigma_{eu} = 152.8$ MPa ; $\sigma_{ec} = 305.6$ MPa

Evaluation of Multipliers:

Upper bound multiplier for the undamaged tank: $m_U^0 = \frac{\sigma_y}{\sigma_{eu}} = 2.258$

Lower bound multiplier for the damaged tank: $m_{Ld} = \frac{\sigma_y}{\sigma_{ec}} = 1.129$

Upper bound multiplier for damaged tank: $m_d^0 = \sqrt{\dfrac{\sigma_y^2 V_R}{\sigma_{eU}^2 V_U + \sigma_{eC}^2 V_D}} = 2.068$

The m_α-tangent multiplier for damaged tank using Eq. 2.28 is

$$m_\alpha^T = \frac{m^0}{1 + 0.2929(\zeta - 1)} = 1.663; \quad \text{where, } \zeta = \frac{m_d^0}{m_{Ld}}$$

7.7 RSF USING ANALYTICAL APPROACH

Three different RSFs are evaluated here using the aforementioned limit load multipliers.

Using Eq. 7.15, $RSF_U = \dfrac{m_d^0}{m_u^0} = 0.916$

Using Eq. 7.16, $RSF^T = \dfrac{m_\alpha^T}{m_u^0} = 0.736$

Using Eq. 7.17, $RSF_L = \dfrac{m_{Ld}}{m_u^0} = 0.5$

All of the above RSF values are determined without using FEA.

7.8 RESULTS AND DISCUSSION

The RSF values from different approaches are compared with those from nonlinear FEA results. The results are for different damage heights as indicated in the tables. For all damages, the width is kept as 4630 mm ($6.3\sqrt{Rt}$). As mentioned earlier, the stress values required as input for $m_\alpha{}^T$ calculations can be determined theoretically

(using shell theory or any other acceptable method) or from a linear elastic FEA (LEFEA). The approach using LEFEA is more precise since the variation of stress in the damage zone and the surrounding reference volume is taken in to account, whereas in a simplified analytical approach the maximum stress is assumed for the entire damage zone or the surrounding reference volume.

7.8.1 Results from m_α-Tangent Method Using LEFEA

In all the following tables, RSF1 indicates remaining strength factor determined using $m_\alpha{}^T$ method with proposed reference volume aproach and LEFEA using $2.5\sqrt{Rt}$ as circumferential decay length. RSF2 is similar to RSF1 but the circumferential decay length is taken as $6.3\sqrt{Rt}$. RSF3 results are from LEFEA with the full volume taken as reference volume in accordance wih Ahmad, et al. [2010].

Table 7.1 RSF Values from Nonlinear FEA and m_α-Tangent Method Using $x_c = 2.5\sqrt{Rt}$

LTAH (mm)	$m_\alpha{}^T$ Method ($x_c = 2.5\sqrt{RT}$)			RSF (NLFEA)
	$m_\alpha{}^T$ Damaged Tank	$m_\alpha{}^T$ Undamaged Tank	RSF1	
735	1.584	2.152	0.736	0.899
1102	1.54	2.22	0.694	0.824
1470	1.55	2.282	0.679	0.752
1837	1.59	2.346	0.678	0.703
2296	1.328	2.408	0.551	0.666
2756	1.255	2.459	0.51	0.649

In Tables 7.1-7.5, the '$m_\alpha{}^T$ Damaged (or Undamaged) tank' column shows the limit load multiplier for the damaged (or undamaged) tank. Table 7.1 compares the RSF

value from nonlinear FEA and RSF1. The RSF1 values are conservative compared to the nonlinear FEA results but follow the same trend.

Table 7.2 compares the RSF values (from m_α^T method) calculated using two different circumferential decay lengths of $2.5\sqrt{Rt}$ (RSF1) and $6.3\sqrt{Rt}$ (RSF2). The RSF values from both the cases are similar except for the RSF value corresponding to a damage height of 1837mm. The LTA height of 1837mm is at the transition zone ($=2.5\sqrt{Rt}$) for the decay length and a further adjustment in the proposed reference volume may smooth this transition. The results show that the RSF results from the m_α^T method do not change significantly if the circumferential decay length is increased from $2.5\sqrt{Rt}$ to $6.3\sqrt{Rt}$. Based on this observation and from the results given in Section 7.3, it can be said that the decay length for large tanks can be taken as $2.5\sqrt{Rt}$ instead of $6.3\sqrt{Rt}$. This is based on the current flaw sizes only. However, it is reasonable to assume that this holds for smaller flaw sizes as well.

Table 7.2 Comparison of RSF Values from m_α-Tangent Method ($x_{c=}6.3\sqrt{Rt}$ & $2.5\sqrt{Rt}$)

LTAH (mm)	m_α -Tangent Method ($\boldsymbol{x_c}=6.3\sqrt{Rt}$)			RSF1 ($\boldsymbol{x_c}=2.5\sqrt{Rt}$)
	Damaged Tank	Undamaged Tank	RSF2	
735	1.561	2.152	0.726	0.736
1102	1.540	2.220	0.694	0.694
1470	1.550	2.282	0.679	0.679
1837	1.652	1.997	0.827	0.678
2296	1.328	2.408	0.551	0.551
2756	1.255	2.459	0.510	0.510

Table 7.3 gives the RSF3 values (using entire volume as reference volume as used by Ahmed, et al. [2010]) in comparison with elastic plastic FEA results. The results show that RSF3 approach overpredicts the RSF significantly. The current results show that it is necessary to use an appropriate reference volume even if LEFEA is used to determine the stress field for m_α-tangent method.

Table 7.3 RSF Values from m_α-Tangent Method Considering Entire Volume as Reference Volume [Ahmad, et al., 2010]

LTAH (mm)	m_α-Tangent considering entire volume			RSF (NLFEA)
	$m_\alpha{}^T$ Damaged Tank	$m_\alpha{}^T$ Undamaged Tank	RSF3	
735	2.197	2.223	0.988	0.899
1102	2.183	2.443	0.894	0.824
1470	2.101	2.495	0.842	0.752
1837	2.084	2.449	0.851	0.703
2296	2.090	2.424	0.862	0.666
2756	2.102	2.408	0.873	0.649

7.8.2 Results from m_α-Tangent Method Using Analytical Approach

The RSF values obtained from the analytical approach without using FEA [Ahmad, et al., 2010] are given in Table 7.4. The RSF-U and RSF-L values represent RSF based on upper bound and lower bound multipliers whereas RSF-T is based on $m_\alpha{}^T$ multiplier. The results show a very broad range within which the actual RSF value will be located.

Table 7.4 RSF from m_α-Tangent Method using Analytical Approach

LTAH (mm)	RSF - U	RSF - T	RSF-L	RSF (NLFEA)
735	0.961	0.757	0.5	0.899
1102	0.947	0.750	0.5	0.824
1470	0.935	0.745	0.5	0.752
1837	0.926	0.741	0.5	0.703
2296	0.916	0.736	0.5	0.666
2756	0.907	0.733	0.5	0.649

7.8.3 Influence of Hydrostatic vs. Uniform Pressure Loading on RSF from m_α-Tangent Method

The m_α family of methods were initially applied to pressure vessels with uniform pressure by Tantichattanonot and others where it works reasonably well. A brief study is carried out in this thesis to understand if there are any significant differences in RSF obtained from tank loaded with hydrostatic pressure and uniform pressure. The same tank geometry and LTA dimensions as used previously in this Chapter are considered. RSF1 values (from m_α-tangent method using LEFEA) of the tank for the two types of loading are compared in Fig. 7.14 and Table 7.5. The uniform pressure for an LTA is taken as equivalent to the hydrostatic pressure at the centre of the flaw. As can be seen there is very little difference in RSF between these two cases.

The results suggest that eventhough there is a stress gradient in the LTA due to hydrostatic pressure, the average stress in the LTA (i.e., the stress at the centre of LTA) is the prime factor that governs the RSF obtained using m_α-tangent method. Hence taking

the maximum stress at the centre of LTA (even though in reality it is slightly lower than the centre) for m_α-tangent analytical method may be a reasonable assumption.

Table 7.5 Comparison of RSF Values for Hydrostaic Pressure and Uniform Pressure Loading

LTAH (mm)	Uniform Pressure Loading			RSF1 (Hydrostatic Pressure)
	m_α^T Damaged Tank	m_α^T Undamaged Tank	RSF (Uniform Pressure)	
735	2.124	1.553	0.731	0.736
1102	2.172	1.491	0.687	0.694
1470	2.214	1.482	0.669	0.679
1837	2.256	1.500	0.665	0.678
2296	2.334	1.265	0.542	0.551
2756	2.334	1.220	0.523	0.510

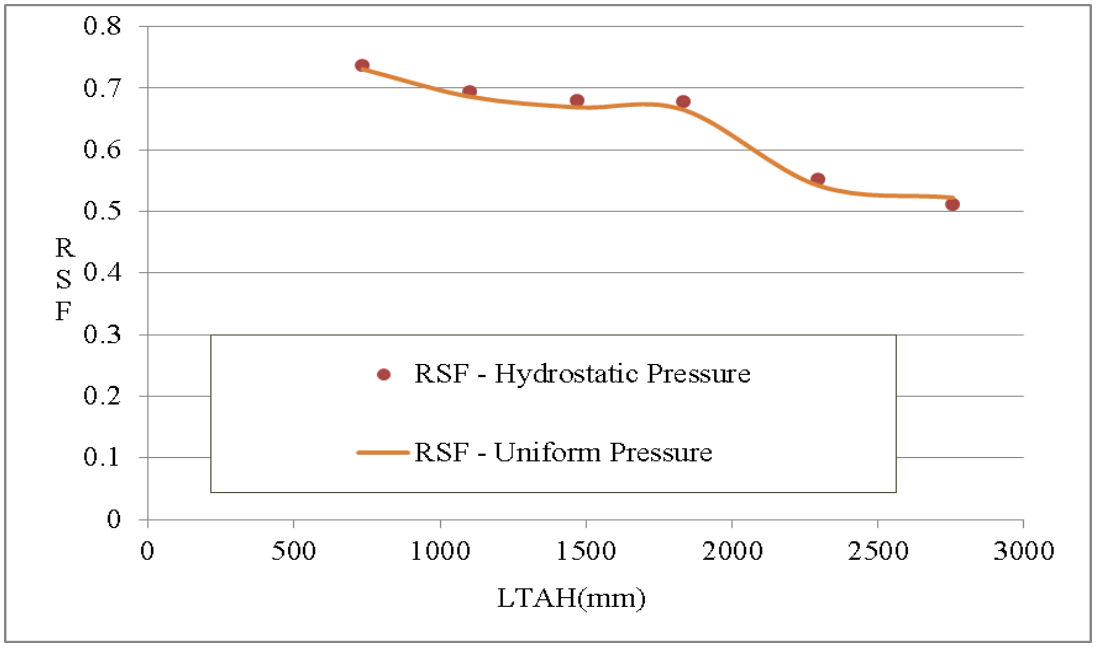

Fig.7.14 RSF Values for Hydrostatic and Uniform Pressure Loadings

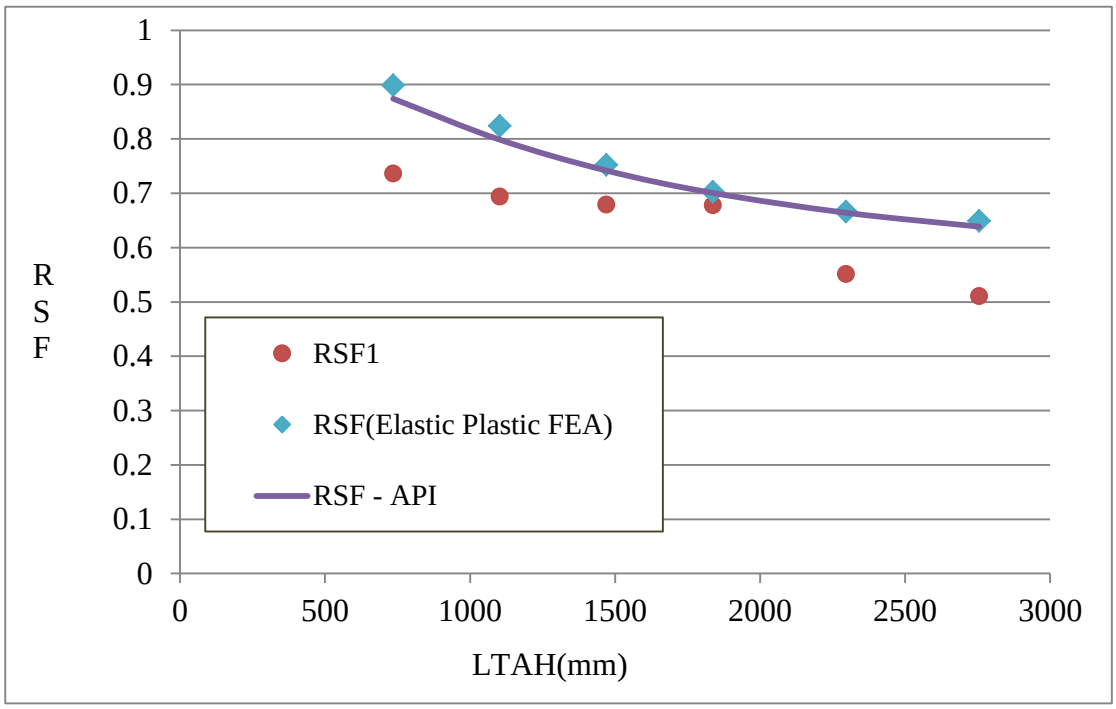

Fig.7.15 RSF Using Proposed Reference Volume Approach

Figure 7.15 compares the RSF calculated using nonlinear FEA, m_α-tangent method (RSF1) and API 579-1/ASME FFS-1 procedure. It must be pointed out that ASME FFS-1 is based on curvefitting adjustments to Folias formula using a massive number of nonlinear finite element analyses for certain types of flaw geometries in pipe like structures. The flaw geometry that is used in the current study falls into this category. Although no special studies have been conducted for tanks in this regard, the results for pipe like structures have been extended to tank structures by API 579-1 and API 650. It seems to be a reasonable thing to do in light of the results shown in Table 7.5. This explains the very close agreement between API 579 values and nonlinear FEA carried out in the current thesis. Such closeness may or may not be present for all

geometries. On the basis of assuming nonlinear FEA values to be accurate, the RSF1 values are conservative However, the method is still quite general in its scope and is applicable for a wide variety of situations and structures.

One of the aims of the present work is to test its applicability for FFS assessment of LTAs in tanks. An important issue in applying m_α-tangent method is the selection of a good reference volume. The choice employed in the present work seems to be quite promising in the sense that the results are significantly improved from the previous study using the m_α-tangent method. However, there is also scope for improvement in order to bring the results close to those from NLFEA. This clearly has the potential to provide an alternative approach to current FFS methods as well as extend the general applicability of m_α-tangent method.

Figure 7.16 summarizes the full set of RSF results from before. The RSF3 values obtained by taking the entire volume as reference volume [Ahmad, et al., 2010] are, as expected, higher than NLFEA values and do not follow the common trend seen in other methods. Again the RSF1 values from the proposed method relate favourably with nonlinear FEA. It can be observed that, even though determining the exact reference volume for the tank is a difficult task, incorporating the proposed approach for reference volume will improve the results compared to the previous approach. However, some modification to the reference volume is needed to avoid the transition spike seen when the decay length overlaps transition from one pattern to another. This could be the subject of further study [Sathyanarayanan and Adluri, 2013b].

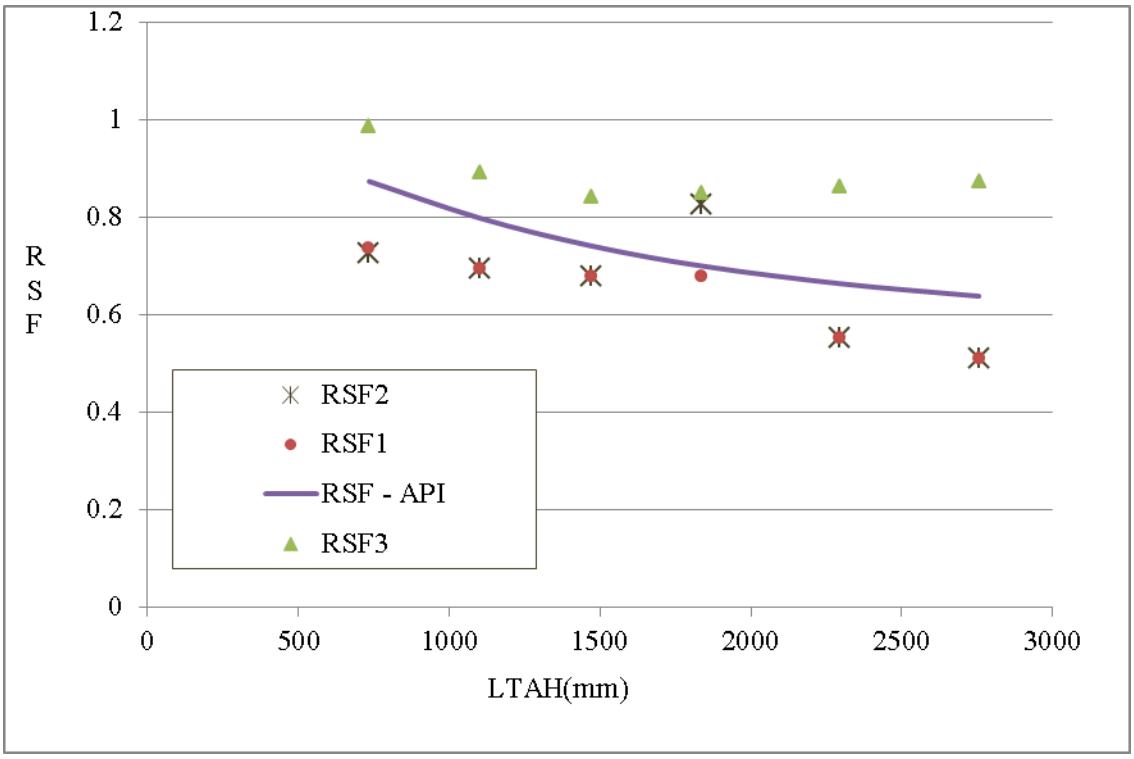

Fig.7.16 RSF Using Three Different Approaches for Reference Volume

7.9 SUMMARY

Locally thinned areas in tank wall are analyzed to determine the remaining strength factor. The `m_α-tangent method based on 'integral mean of yield' and variational priciples to determine limit loads has been shown to be very useful for a range of applications by earlier researchers. The current work adapts this method for RSF estimates of partially damaged above ground storage tanks and presents preliminary results. The tanks typically have very large R/t ratio (1000 or more) compared to regular pipes and other cylindrical pressure vessels with much lower R/t ratios (50 to 100). In view of this, the applicability of using $6.3\sqrt{Rt}$ as circumferential decay length is

examined. Based on FEA results of tank models, it is observed that the stress levels do not change significantly beyond a value of $2.5\sqrt{Rt}$ and hence this value is recommended as circumferential decay length as well as longitudinal decay length for practical tank sizes. A modified procedure for reference volume estimate is examined. The RSF results from m_α-tangent method using this modified reference volume are conservative and compare reasonably well with API 579-1/ASME FFS-1 and full scale nonlinear results. The modified reference volume seems to be considerably better than that used before. The present work shows the applicability of m_α-tangent method for FFS assessments of LTAs in tanks. The proposed method can be refined further to improve the performance near transition zones (of decay length overlaps), and can be extended to include interaction of two or more flaws.

CHAPTER 8

CONCLUSIONS AND RECOMMENDATIONS

8.0 SUMMARY

Large steel storage tanks with flat bottoms placed above ground are part of several industries. Design and construction of these tanks involves significant engineering expertise and cost. This thesis examines several issues regarding the design and evaluation of such tanks with respect to the widely used design standard API 650.

The shell to bottom joint is a critical failure zone in the tanks. The hydrostatic pressure from the liquid infill (combined with temperature loading in some cases) induces internal moment at this joint. The high magnitude of this moment results in yielding of the bottom plate near shell wall in most of the tanks. The fill-draw cycle, especially in case of tanks operating in elevated temperatures causes low cycle fatigue in this region which subsequently decides the overall life of the tank. Even though the problem of plastic yielding and fatigue at this joint are recognized by earlier researchers and the current design standards, very few works have been directed to study this problem.

Denham, et al., proposed a beam model with a fixed bottom plate projection length beyond shell wall to analyze the stresses in this zone. In this thesis, Denham's model is reviewed and validated using FEA. It is extended to include arbitrary projection lengths. The effect of increasing projection length beyond the shell wall has been studied

for tanks on ring wall foundations.It is found that the projection length influences the stresses in the shell as well as the bottom plate near the shell to bottom joint. Increasing the length is beneficial to a certain extent beyond which the stresses will not be altered. This maximum projection length is termed as 'full projection length' and an extension to Denham's model is proposed to determine this length.

The influence of bottom plate friction forces on the stresses in the wall of elevated temperature tanks is studied. The current API 650 procedure based on Karcher's work employs a factor called C to represent the bottom plate restraint due to friction forces. Karcher's equations used for finding the stresses in elevated temperature tank wall are verified using a detailed finite element model with contact elements. It is observed that the equations give correct results if the exact C-factor is used. Since the current practice does not have clear guidelines for selecting a C value, a set value (like 0.85) is being used irrespective of the tank dimensions and temperature change. The present study shows that this approach is grossly conservative for most of the range of design parameters (H, R & ΔT) and could become slightly unconservative for very large tanks at relatively low temperature changes. It is shown that the C-factor is directly related to the friction coefficient (μ) and tank parameters. Using plate theory the frictional restraint to bottom plate expansion is formulated as function of μ. Appropriate equations for stresses and by extension, fatigue life are presented incorporating μ instead of C.

The bending stress in the shell increases with increasing friction forces. It is found that for any tank geometry with a defined operating temperature, there is a limiting

friction coefficient (μ_L) that will cause maximum stresses in shell. A friction coefficient value greater than μ_L will not increase the stresses any further. On the other hand, increase in operating temperature also increases stresses in shell. Similar to limiting friction coefficient, there exists a limiting temperature (ΔT_L) beyond which increase in temperature will not induce additional stresses. Expressions were formulated to obtain μ_L and (ΔT_L).

As mentioned earlier, the low cycle fatigue at the shell to bottom joint caused by the fill/draw down cycle of the stored liquid determines the cyclic life of the tank. The peak alternating stress at this location, used to enter the fatigue curves is currently determined using a pseudo elastic stress that represents strain range due to inelastic deformations. The API 650 procedure for life cycle evaluation of elevated temperature steel storage tanks subjected to low cycle fatigue is reviewed. The current procedure uses beam-on-elastic foundation model to determine the peak alternating stress. In the current study, it is observed that this model is not appropriate for tanks resting on concrete ring walls and hence an alternate approach is recommended based on beam model (instead of beam on elastic foundation model). The results are validated using finite element analysis.

Apart from the damage issues at the shell to bottom joint, corrosion damage in the tank wall as a locally thin area (LTA) is a widespread problem. In this thesis, a modified reference volume procedure for a Level 2 fitness for service assessment method using m_α-tangent method is proposed for tanks containing LTA. The current method for reference

volume determination is modified to improve the accuracy of results. The volume inside the flaw overlapped by the decay lengths from the edges of the flaw appears to give better estimates. The circumferential decay length for tanks with very large R/t ratio is examined and new recommendations are made.

8.1 CONCLUSIONS

The main conclusions from present research are as follows:

1. Increasing the projection length of annular plate outside the tank up to a certain limit termed as ‘full projection length’ is beneficial to the shell stresses. A model is proposed to determine this ‘full projection length’. Relevant equations are presented. Since most of the large tanks are constructed with multiple wall thicknesses, the effect of assuming a uniform thickness for a variable thickness tank wall for the sake of determining the ‘full projection length’ is studied and found to be acceptable.
2. The results of including or excluding the self-weight of the tanks in the procedure to determine the ‘full projection length’ are compared and found that including the self-weight does not increase the stresses in the tank wall or on the inner side of bottom plate significantly, whereas it may increase the stresses marginally on the outer side of the bottom plate.
3. Based on the slope compatibility at shell to bottom joint, the following new equation is proposed to determine the elastic moment (M_o) at the bottom when the bottom plate has ‘full projection length’ outside the shell.

$$\left(\frac{M_o}{M_{fx}}\right)^3\left(\frac{t_s}{t_a}\right)^6 - 45.86\psi^2 + 83.74\psi - 38.06 = 0$$

4. In the current design procedure for elevated temperature tanks, the friction has not been considered. This is sometimes quite confusing and leads the designer to arbitrarily choose a C-factor value. The C-factor from the present practice can be replaced using the following

$$C = \frac{(1-\nu)}{3E}\frac{\mu\ \gamma H\ R}{t_p\ \alpha\ \Delta T}$$

Appropriate equations for stresses and by extension, fatigue life are also presented.

5. The current practice for shell to bottom joint rotation uses beam-on-elastic foundation theory. It is shown that this is not valid for concrete ring walls. Appropriate modifications have been proposed to estimate the peak alternating stress (strain range) for fatigue design as below

$$S_b = \pm\frac{3}{2}\left(\frac{2}{1-\nu^2}\right)^{2/3}\gamma H\left[\frac{R^2}{Ht_s}\left\{\beta H + \frac{\beta E t_s}{\gamma R}C\alpha\Delta T - \frac{\beta^3 S_Y t_b^2}{\gamma} - 1\right\}\right]^{2/3}$$

Detailed finite element analysis using nonlinear models and friction-contact elements show that the alternative model is quite close to FEA results whereas the current procedures under predict the fatigue stress significantly. The current API procedure is clearly less rational than that developed in the present study. The study recommends that the relevant API committee take a close look at this practice.

6. The inequality condition in the fatigue design procedure of API 650 is examined and found that though it is a necessary condition, it is not a sufficient condition to ensure the formation of plastic hinges. It is also found that this inequality is satisfied automatically for most of the design range and hence becomes superficial unless the shell or plate thicknesses are more than the values necessary from stress point of view.
7. Circumferential decay length for large tanks is studied using FEA and a value of $2.5\sqrt{Rt}$ is recommended instead of $6.3\sqrt{Rt}$ for reference volume calculations of tanks. This reduction is likely the result of very large R/t ratios for tanks.
8. In order to improve the accuracy of fitness for service estimates using the versatile m_α-tangent method, a modified reference volume scheme for determination of remaining strength factor is examined. The RSF determined using this modified reference volume follows elastic-plastic FEA results much better compared to the results of previous studies. The reference volume estimate can be refined to improve the performance further.

8.1.1 Guidelines for Designers

The following table gives guidelines for tank designers based on some of the main results of this thesis work.

Existing Procedure	Proposed Procedure
C =0.25 to 1; C=0.85 if no value is given by purchases	Obtain C from the following expression by substituting the standard friction coefficient values $C=\frac{(1-\nu)}{3E}\frac{\mu\,\gamma H R}{t_p\,\alpha\,\Delta T}$
The peak alternating stress range is found using $S_b=\pm\frac{0.658\gamma R^2}{t_s}\sqrt[4]{\frac{Kt_b}{E}}\left(1-\beta H-\frac{\beta C\alpha\Delta T E t_s}{\gamma R}+\frac{\beta^3 S_Y t_b^2}{2\gamma}\right)$	Using the proposed beam model the peak alternating stress is given by $S_b=\pm\frac{3}{2}\left(\frac{2}{1-\nu^2}\right)^{2/3}\gamma H\left[\frac{R^2}{Ht_s}\left\{\beta H+\frac{\beta E t_s}{\gamma R}C\alpha\Delta T-\frac{\beta^3 S_Y t_b^2}{\gamma}-1\right\}\right]^{2/3}$
The peak alternating stress equation as given above can be used only if the following is true $\left[\frac{58HG}{(Dt_s)^{0.5}}+\frac{26.2C\Delta T t_s^{0.5}}{D^{1.5}}-G\right]>\left[\frac{4.8BS_Y t_b^2}{(Dt_s)^{1.5}}\right]$	The condition is superfluous and need not be checked
Projection length of Annular plate beyond shell shall be minimum 50 mm.	The projection shall be "full projection length (a)" given by the following expressions $a=\sqrt{\frac{M_o}{5.09w}}$ where $M_o=\left(0.3138\left(\frac{t_s}{t_p}\right)^2-0.1429\left(\frac{t_s}{t_p}\right)+1.0514\right)\frac{\gamma RHt_s}{\sqrt{12(1-\nu^2)}}\left(1-\frac{1}{\beta H}\right)$

8.1.2 Recommendations for Future Study

1. In this thesis, an elastic beam model with plastic hinge boundary condition is used to determine the peak alternating stress for fatigue life evaluation. This model can be improved to elastic-plastic beam model to account for partial plastic hinge conditions at the shell to bottom joint
2. A field test using instrumented strain gages on an elevated temperature tank can be performed to confirm the stresses in the tank shell due to bottom plate friction. This will show the influence of fill/draw cycle on the friction stresses. The influence of lap joints, backing strips and other constructional joints underneath the bottom plate on the shell stresses can be studied.
3. In this work, the foundation underneath the bottom plate is assumed to have very high stiffness. The analysis can be extended to a flexible foundation and the influence of the foundation deformations on the frictional stresses can be studied.
4. The influence of R/t ratio on the decay length of vessels with larger R/t ratio can be studied theoretically. Since the decay lengths are used in FFS procedures to assess plastic collapse, the decay length values obtained from the elastic theory can also be compared using elastic-plastic analysis.
5. The LTA is assumed to be rectangular with uniform thickness loss. Complex shapes and varying thickness profiles can be studied. The proposed modifications to the reference volume can be extended to include interaction effects from multiple flaws.

6. The author has attempted to evaluate and improve specific design issues currently adopted by the widely used American Petroleum Institute standard – API 650. The relevant loadings to address these issues have been used. The issues addressed are specific to the dead, live and thermal loadings only. The tank can obviously be subjected to other loading types. The standard addresses them in an entirely different manner and hence they are not examined in this thesis. They could be part of further study.

PUBLICATIONS AND PRESENTATIONS FROM THE PH.D. PROGRAM

1. Sathyanarayanan, S. and Adluri, Seshu M. R., 2013, "Fatigue Stress Evaluation at Shell to Bottom Joint in Elevated Temperature Steel Tanks on Concrete Ringwalls," *ASME Journal of Pressure Vessel Technology, (Provisionally Accepted).*
2. Sathyanarayanan, S. and Adluri, Seshu M. R., 2013, "Improvements in Adapting m_α–Tangent Method for Fitness for Service Evaluation of Local Thin Areas in Storage Tanks,*"Proc. of ASME 2013 Pressure Vessels & Piping Division Conference (PVP2013),* Paris, France.
3. Sathyanarayanan, S. and Adluri, Seshu M. R., 2013, "Incorporation of Friction Coefficient in the Design Equations of Elevated Temperature Tanks,*" ASME Journal of Pressure Vessel Technology,* **135(2),** March 2013.
4. Sathyanarayanan, S. and Adluri, Seshu M. R., 2012, "Modified Fatigue Stress at Shell-To-Bottom Joint of Steel Tanks on Ring Walls,*" Proc. of ASME 2012 Pressure Vessels & Piping Division Conference (PVP2012),* Toronto, Canada.
5. Sathyanarayanan, S. and Adluri, Seshu M. R., 2012, "Locally Thin Areas in Above Ground Steel Storage Tanks," Presented at the Aldrich Conference, St. John's, Canada.
6. Sathyanarayanan, S., Adluri, Seshu M. R., 2011, "Effect of Annular Plate Projection Length on the Stresses in the Above Ground Steel Storage Tanks on Rigid Ring Wall Foundations," *Proceedings of the ASME 2011 Pressure Vessels & Piping Division Conference (PVP2011),* Baltimore, Maryland, USA.

REFERENCES

Adibi-Asl, R. and Seshadri, R., 2011, "Thermal Hot Spot and Corrosion Damage in Conical Pressure Components," *ASME Journal Pressure Vessel Technology*, **133**.

Adluri, Seshu M. R., 2012, "Effects of Friction on the Bottom Plate of Large Elevated Temperature Steel Tanks," *Research Report, Faculty of Engineering and Applied Science, Memorial University of Newfoundland, Canada.*

Ahmad, F., Hossain, M. M., and Seshadri, R., 2010, "Fitness for Service Assessment of Hydrocarbon Storage Tanks," *ASME Journal Pressure Vessel Technology*, **132(2)**.

American Petroleum Institute Standard, 2012, *Welded Tanks for Oil Storage –API 650,* Eleventh Ed.

American Petroleum Institute Standard, 2012, *Fitness-For-Service API 579-1/ASME FFS-1*, Second Ed.

American Petroleum Institute Standard, 2009, *Tank Inspection, Repair, Alteration, and Reconstruction API 653*, Fourth Ed.

American Society of Mechanical Engineers (ASME), 2002, *ASME Boiler and Pressure Vessel Code, Section III and VIII*, New York.

Andreani, J. L., Osage, D. A., Parikh, P. D., Horwege, J. A., 1995, "An Evaluation of Procedures for Determining the Fitness-for-Service of Settled Aboveground Storage

Tanks," Proceedings of the ASME Pressure Vessel and Piping Conference-ASME PVP 1995 , **315**, pp.45-66.

ANSYS, 2009, University Research Version 11.0, SASIP Inc.

Ansys Contact Technology Guide, 2009, Release 11.0, SASIP Inc.

Antaki, G., 2005, *Fitness-for-Service and Integrity of Piping, Vessels, and Tanks, ASME CODE SIMPLIFIED*, McGraw-Hill Inc., New York.

Batte,A. D., Fu, B., Kirkwood, M.G., and Vu, D., 1997, "Advanced Methods for Integrity Assessment of Corroded Pipelines," *Pipes and Pipelines International*, **42 (1)**.

Boresi, A. P., and Schmidt, R. J., 1993, *Advanced Mechanics of Materials*, Fifth Ed., John Wiley & Sons, Inc., New York.

Digrado, B. D., and Thorp, G. A., 2004, *The Aboveground Steel Storage Tank Handbook*, John Wiley & Sons, Inc., New Jersey.

Burgreen, D., 1975, *Design Methods for Power Plant Structures*, First Edition, C. P. Press, Jamaica, New York.

Calladine, C. R., 2000, *Plasticity for Engineers: Theory and Application*, Horwood Publishing, Chichester, England.

Chen, H. F., and Shu, D. W., 2000, "The Effects of the Distance Between Two Defects on the Load Carrying Capacity of a Pressure Vessel," *ASME Journal of Pressure Vessel Technology*, **122**, pp.198-203.

Chen, Z. P., Duan, Y. Y., Shen, J. M., and Jiang, J. L., 2007, "A Simplified Method for Calculating the Stress of a Large Storage Tank Wall," *Proceedings of the Institution of Mechanical Engineers, PART E: Journal of Process Mechanical Engineering*, **221(3)**, pp.119-127.

Chopra, O. K., Shack, W. J., 2003, "Review of the Margins for ASME Code Fatigue Design Curve - Effects of Surface Roughness and Material Variability," Report for U.S. Nuclear Regulatory Commission, Washington, D.C.,USA (Available online http://www.nrc.gov/reading-rm/doc-collections/nuregs/contract/cr6815/cr6815.pdf - excerpted on 19-Dec-2013)

Comfort, L., Abrams, J., Camillus, J., and Ricci, E., 1989, "From Crisis to Community: the Pittsburgh Oil Spill," Industrial Crisis Quarterly, **3(1)**, pp.17-39.

Cornell, J. R., and Baker, M. A., 2002, "Catastrophic Tank Failures: Highlights of Past Failures along with Proactive Tank Designs," *Proceedings of the US EPA Fourth Biennial Freshwater Spills Symposium (FSS 2002)*, Ohio, USA.

Denham, J. B., Russell, J., and Wills, C. M. R., 1968a, "How to Design a 600 000-BBL. Tank," Hydrocarbon Processing, **47(5)**, pp.137-142.

Denham, J. B., Russel, J., and Wills, C. M. R., 1968b, "Comparison of Predicted and Measured Stresses in a Large Storage Tank," *Proceedings of Division of Refining – API*, pp.1034-1074.

European Committee for Standardization, 2004, *EN 14015 - Specification for the design and manufacture of site built, vertical, cylindrical, flat-bottomed, above ground, welded, steel tanks for the storage of liquids at ambient temperature and above.*

Folias, E. S., 1969, "On the Effect of Initial Curvature on Cracked Flat Sheets," *International Journal of Fracture Mechanics*, **5(4)**, pp. 327-346.

Folias, E. S., 1999, "Failure Correlation between Cylindrical Pressurized Vessels and Flat Plates," *International Journal of Pressure Vessels and Piping*, **76**, pp.803–811.

Fu, B., and Kirkwood, M. G., 1995, "Determination of Failure Pressure of Corroded Pipelines using the Non-Linear Finite Element Method", *Proc. of 2nd International Pipeline Technology Conference*, Ostend, Belgium.

Gill, S. S., 1970, *The Stress Analysis of Pressure Vessels and Pressure Vessel Components*, Pergamon Publishing, London, UK.

Hetenyi, M., 1971, *Beams on Elastic Foundation*, University of Michigan Press, Ann Arbor, MI, USA.

Indermohan, H., and Seshadri, R., 2004, "Fitness-for-service Methodology based on Variational Principles in Plasticity," *ASME Pressure Vessels Piping Div Publ PVP 2004*, **473**, pp. 83-91.

Janelle, J., Osage, D. A., and Burkhart, S. J., 2005, *An Overview and Validation of the Fitness-For-Service Assessment Procedures for Local Thin Areas in API 579*, Welding Research Council (WRC) Bulletin, **505**.

Janelle, J. L., and Osage, D. A., 2007, "Validation and Development of Fitness for Service Procedures for Local Thin Areas in API RP579," *Proceedings of 2007 ASME Pressure Vessel and Piping Division Conference*, **6**, pp.809-824.

Jawad, M. H., and Farr, J. R., 1984, *Structural Analysis and Design of Process Equipment,* John Wiley & Sons

Jones, R., and Seshadri, R., 1989, "Analysis and Design of High Temperature Storage Tanks," *Design and Analysis of Pressure Vessels and Components – 1989 (PVP)*, **175**, pp. 45-52.

Kanninen, M. F., Pagalthivarthi, K. V., and Popelar, C. H., 1991 "A Theoretical Analysis for the Residual Strength of Corroded Gas and Oil Transmission Pipelines," *Proceedings of the Symposium on Corrosion forms and Control for Infrastructure, California, USA.*

Kanninen, M. F., Roy, S., Couque, H. R. A., Grigory, S. C., and Smith, M. Q., 1994, "Generalized Guidelines for Determining the Residual Strength of Corroded Oil and Gas

Pipelines," *Proceedings of The Energy Transportation, Transfer and Storage Conference*, pp. 391-40.

Karcher, G. G., 1978a, "Thermal Stresses in Tanks Operating at Elevated Temperatures," *Proceedings - API Division of Refining*, American Petroleum Institute, New York, **57**, pp. 515-521.

Karcher, G. G., 1978b, "New Design Calculations for High Temperature Storage Tanks," *Hydrocarbon Processing*, October 1978, pp.137-140.

Karcher, G. G., 1981a, "Simplified Stress Equations for Elevated Storage Tanks," *Hydrocarbon Processing*, July 1981, pp. 515-521.

Karcher, G. G., 1981b, "Stresses at the Shell-To-Bottom Junction of Elevated Temperature Tanks," *Proceedings - API Division of Refining*, American Petroleum Institute, New York, **60**, pp. 154-159.

Kiefner, J. F., Maxey, W. A., Eiber, R. J., and Duffy, A. R., 1973, "Failure Stress Levels of Flaws in Pressurized Cylinders," *Progress in Flaw Growth and Fracture Toughness, ASTM STP 536*, American Society for Testing and Materials, pp. 461-481.

Kiefner, J. F. and Vieth, P.H., 1989, *A Modified Criterion for Evaluating the Remaining Strength of Corroded Pipe (with RSTRENG),* American Gas Association, Catalog No. **L51609**, PR3-805.

Kiefner, J. F., 1990, "The Remaining Strength of Corroded Pipe," *API Pipeline Conference*, American Petroleum Institute.

Kim, J., An, D., Lee, S., and Lee, B., 2009, "A failure analysis of fillet joint cracking in an oil storage tank," *Journal of Loss Prevention in the Process Industries*, **22**, pp. 845-849.

Konusu, S., Kano, M., Mukaimachi, N., and Kanamaru, S., 2010, "Validity of Assesment Procedure in p-M method for Multiple Volumetric Flaws," *ASME Journal of Pressure Vessel Technology*, **132**, 021402 1-10.

Long, B., and Garner, B., 2004, *Guide to Storage tanks and equipments*, Professional Engineering Publishing.

Osage, D. A., Janelle, J., and Henry, P. A., 2000, "Fitness-for-Service Local Metal Loss Assesment Rules in API 579," *Proceedings of ASME Pressure Vessel and Piping conference 2000 – Service Experience and Fitness-for-Service in Power and Petroleum Processing*, **411**, pp. 143-176.

Osage, D. A., Krishnaswamy, P., Stephens, D. R., Scott, P., Mohan, R., Janelle, J., and Wilkowski, G. M., 2001, *Technologies For The Evaluation Of Non-Crack-Like Flaws In Pressurized Components - Erosion/Corrosion, Pitting, Blisters, Shell Out-Of-Roundness, Weld Misalignment, Bulges And Dents*, Welding Research Council (WRC) Bulletin, **465**.

Peng,J., Zhou, C., Xue, J., Dai, Q., and He, X., 2011,"Safety Assessment of Pipes with Multiple Local Wall Thinning Defects Under Pressure and Bending Moment," *Journal of Nuclear Engineering and Design*, **241**, pp.2578-2765.

Sathyanarayanan, S. and Adluri, Seshu M. R., 2013a, "Fatigue Stress Evaluation at Shell to Bottom Joint in Elevated Temperature Steel Tanks on Concrete Ringwalls," *ASME Journal of Pressure Vessel Technology, (Provisionally Accepted).*

Sathyanarayanan, S. and Adluri, Seshu M. R., 2013b, "Improvements in Adapting m_α– Tangent Method for Fitness for Service Evaluation of Local Thin Areas in Storage Tanks,*"Proc. of ASME 2013 Pressure Vessels & Piping Division Conference(PVP2013),* Paris, France.

Sathyanarayanan, S. and Adluri, Seshu M. R., 2013c, "Incorporation of Friction Coefficient in the Design Equations of Elevated Temperature Tanks,*" ASME Journal of Pressure Vessel Technology,* **135(2),** March 2013.

Sathyanarayanan, S. and Adluri, Seshu M. R., 2012a, "Modified Fatigue Stress at Shell-To-Bottom Joint of Steel Tanks on Ring Walls,*" Proc. of ASME 2012 Pressure Vessels & Piping Division Conference (PVP2012),* Toronto, Canada.

Sathyanarayanan, S. and Adluri, Seshu M. R., 2011, "Effect of Annular Plate Projection Length on the Stresses in the Above Ground Steel Storage Tanks on Rigid Ring Wall Foundations," *Proceedings of the ASME 2011 Pressure Vessels & Piping Division Conference(PVP2011),* Baltimore, Maryland, USA.

Seshadri, R., 2004, "Integrity Assessment of Pressure Components with Local Hot Spots," *Proc. of ASME 2004 Pressure Vessels Piping Division Conference*, **480**, pp. 177-185.

Seshadri, R., 2005, "Integrity Assessment of Pressure Components with Local Hot Spots," *ASME Journal of Pressure Vessel Technology*, **127**, pp.137-142.

Seshadri, R. and Hossain, M. M., 2008, "Simplified Limit Load Determination Using the m_α-Tangent Method," *Proc. of* 2008 *ASME Pressure Vessels and Piping Division Conference*, Paper No. PVP2008-61171, July, Chicago, USA.

Sims, J. R., Hantz, B. F., and Kuehn, K. E., 1992, "A Basis for the Fitness for Service Evaluation of Thin Areas in Pressure Vessels and Storage Tanks," *Proc. of ASME 1992 Pressure Vessels and Piping Division Conference*, **233**, pp. 51-58.

Tantichattanont, P., 2006, "Fitness-for-Service Assessment for Thermal Hot Spots and Corrosion in Pressure Vessels", *Ph.D. Thesis*, Memorial University of Newfoundland, Canada.

Tantichattanont, P., Adluri, Seshu M. R., and Seshadri, R., 2006a, "Integrity Assesment of Spherical Components with Local Corrosion and Hot spots," *Proc. of ASME 2006 Pressure Vessels and Piping/ICPVT-11 Conference*, **3**, pp.653-662.

Tantichattanont, P., Adluri, Seshu M. R., and Seshadri, R., 2007a, "Fitness for Service Evaluation of Thermal Hotspots and Corrosion Damage in Cylindrical Pressure Components," *Proc. of ASME 2007 Pressure Vessel and Piping Conference*, 2, pp. 71-82.

Tantichattanont, P., Adluri, Seshu M. R., and Seshadri, R., 2007b, "Structural Integrity Evaluation for Corrosion in Spherical Pressure Vessels," *Int. Journal of Pressure Vessels & Piping*, **84**, pp. 749–761.

Tantichattanont, P., Adluri, Seshu M. R., and Seshadri, R., 2007c, "Fitness for Service Assessment of Spherical Pressure Vessels with Hotspots," *Int. Journal of Pressure Vessels & Piping*, **84**, pp. 762-772.

Timoshenko, S., and Woinowsky-Kreiger, S., 1959, *Theory of Plates and Shells*, McGraw-Hill, New York, Second Edition.

Wang, Y. H., Tham, L. G., and Cheung, Y. K., 2005, "Beams and Plates on Elastic Foundation: a Review," *Journal of Progress in Structural Engineering and Materials*, **7**, pp. 174-182.

Wiki, 2013, "Fatigue (material)," excerpted from online Wikipedia, the free encyclopedia on 18- Dec-2013 at: http://en.wikipedia.org/wiki/Fatigue_(material)

Wu, T. Y., and Liu, G. R., 2000, "Comparison of Design Methods for a Tank-Bottom Annular Plate and Concrete Ring Wall," *Int. Journal of Pressure Vessels and Piping*, **77**, pp. 511-517.

Wu, T. Y., 1996, "More Accurate Method Devised for Tank-Bottom Annular Plate Design," *Oil and Gas Journal*, **94(21)**, pp. 81-83.

Zick, L. P. and McGrath, R. V., 1968, “Design of Large Diameter Cylindrical Shells”, *Proceedings - API Division of Refining*, American Petroleum Institute, New York, **48**, pp. 1114-1140.

BIBLIOGRAPHY

The following have been consulted during the research although they have not been directly referred to in the thesis.

Ahari, M.N., Eshghi, S., and Ashtiany, M.G., 2009, "The Tapered Beam Model for Bottom Plate Uplift Analysis of Unanchored Cylindrical Steel Storage Tanks," *Journal of Engineering Structures*, **31**, 623-632.

American Petroleum Institute Standard,2004, *Design and Construction of Large, Welded, Low-Pressure Storage Tanks, API – 620,* Tenth Ed.

Anderson, T. L., and Osage, D. A., 2000, "API 579: a Comprehensive Fitness-for-Service Guide," *International Journal of Pressure Vessels and Piping,* **77**, pp. 953-963.

Baltay, P., and Gjelsvik, A., 1990, "Coefficient of Friction for Steel on Concrete at High Normal Stress," *Journal of Materials in Civil Engineering-ASCE,* **Vol.2 (1),** pp. 46-49.

Berardi, R., and Lancellotta, R., ,2002, "Yielding from Field Behavior and its Influence on Oil Tank Settlements", *ASCE Journal of Geotechnical and Geo environmental Engineering*, **128 (5),** pp. 404-415.

Brownell, L. E., and Young, E. H., 1959, *Process Equipment Design*, John Wiley & Sons Inc.

Carucci, V. A., and Delahunt, J. F., 2002, "Corrosion Considerations for Aboveground Atmospheric Storage Tanks," *Proc. of NACE CORROSION/2002*, Denver, USA, Paper No. 02487.

Chen, Z. P., Sun, B., Yu, C. L., and Zeng, M., 2009, "Finite Element Analysis of Liquid Storage Tank Foundations using Settlement Difference as Boundary Condition," *Proc. of the Institution of Mechanical Engineers, PART E: Journal of Process Mechanical Engineering*, **223(4)**, pp. 225-231.

Cinquini, C., Lamblin, D. O., and Guerlement, G., 1984, "Limit Analysis of Circular Cylindrical Shells under Hydrostatic Pressure," *Journal of Structural Mechanics*, **12**, pp. 263-278.

Daviea, M., Nolana, P. F., and Hoban, T. W. S., 1994, "Case Histories of Incidents in Heated Bitumen Storage Tanks," *Journal of Loss Prevention in Process Industries*, **7(3)**, pp. 212-221.

Gorochov, Y., Muschanov, V., Kulik, A., and Tsyplukhin, A., 2005, "Vertical Cylindrical Tank with Angular Geometrical Imperfection", *Journal of Civil Engineering and Management- Lithuania Academy*, **11(3)**, pp. 175-18.

Greiner, R., and Ofner, R., 2003, "Large Cylindrical Flat-Bottom Storage Tanks – Design Calculations for Seismic Effects," *Proc. of the Conference on Design, Inspection, Maintenance and Operation of Cylindrical Steel Tanks and Pipelines*, Prague.

Hamdan, M. N., 2002, "A Simplified Analysis of Edge Settlement of a Large Aboveground Liquid Storage tank," *Proc. of the 6th Saudi Engineering Conference*, KFUPM, Dhahran, **3**, pp. 19-35.

Hamdan, M. N., Abuzeid, O., and Al-Salaymeh, A., 2007, "Assesment of an Edge type Settlement of Above Ground Storage tanks using a Simple Beam model," *Journal of Applied Mathematical Modeling,* **31**, pp. 2461-2474.

James, R. W., and Raba, G. W., 1991, "Behavior of Welded Steel Water-Storage Tank," *ASCE - Journal of Structural Engineering*, **117**, pp. 61-79.

Jaske, C. E., 2001, "Process Equipment Fitness-for-Service Assesments Using API RP 579," *Proc. of the Process and Power Plant Reliability Conference.*

Jonaidi, M., and Ansourian, P., 1998, "Harmonic Settlement Effects on Uniform and Tapered Tank Shells*," Journal of Thin Walled Structures*, **31**, pp. 237-255.

Jones, R. D, 1991, "Stress Analysis of High Temperature Storage tanks," *Master's Thesis,* University of Regina, Regina, Saskatchewan, Canada.

Mackerle, J., 2004, "Finite Elements in the Analysis of Pressure Vessel and Piping, an Addendum: A bibliography (2001-2004)," *International Journal of Pressure Vessel and Piping*, **82**, pp. 571-592.

Malhotra, P. K., and Veletsos, A. S., 1994, "Uplifting Analysis of Base Plates in Cylindrical Tanks," *Journal of Structural Engineering*, **120 (12),** pp**.** 3489-3505.

Malhotra, P. K., 1995, "Base Uplifting Analysis of Flexibly Supported Liquid-Storage Tanks," *Journal of Earthquake Engineering and Structural Dynamics*, **24 (12),** pp. 1591-1607.

Marr, W. A., Ramos, J. A., and Lambe, T. W., 1982, "Criteria for Settlement of Tanks," *ASCE Journal of Geotechnical Engineering Division*, **108**, pp. 1017-1039.

May, I. L., 2007, "Structural Integrity and Petrochemical Industry," *Proc. of 9th International Conference on Engineering Structural Integrity Assesment – ESIA9*, Beijing.

McGrath, R. V., 1963, "Stability of API Standard 650 Tank Shells," *API Division of Refining Report*, **43(3)**, pp. 458-469.

Melerski, E. S., 1992, "An Efficient Computer Analysis of Cylindrical Liquid Storage Tanks under conditions of Axial Symmetry," Journal of Computer and Structures, **45(2)**, pp. 281-295.

Myers, P. E, 1997, *Aboveground Storage Tanks*, McGraw-Hill Inc.

Peek, R., and Jennings, P. C., 1988, "Simplified Analysis of Unanchored Tanks," *Journal of Earthquake Engineering and Structural Dynamics*, **16(7),** pp. 1073-1085.

Rabbat, B. G., and Russet, H. G., 1985, "Friction Coefficient of Steel on Concrete or Grout," *Journal of Structural Engineering – ASCE*, **111(3)**, pp. 505-515.

Rasiulis, K., Sapalas, A., Vadluga, R., and Samofalov, M., 2006, "Stress/strain State Investigations for Extreme Points of Thin Wall Cylindrical Tanks," *Journal of Constructional Steel Research*, **62**, pp. 1232-1237.

Slagis, G. C., 2006, "ASME Section III Design by Analysis Criteria Concepts and Stress Limits," *ASME Journal of Pressure Vessel Technology*, **128**, pp. 25-32.

Sun, X., Liu, Y., Wang, J., and Cen, Z., 2008, "Stress and Deflection Analyzes of Floating Roofs Based on Load-Modifying Method," *International Journal of Pressure Vessels and Piping*, **85**, pp. 728-738.

Tin-Loi, F., and Pulmano, V. A., 1991, "Limit Loads of Cylindrical Shells under Hydrostatic Pressure," *Journal of Structural Engineering*, **117(3)**, pp. 643-656.

Trebuna, F., Simcak, F., and Bocko, J., 2009, "Failure Analysis of Storage Tank," *Journal of Engineering Failure Analysis*, **16**, pp. 26-38.

Wozniak, R. S., and Mitchell, W. W., 1978, "Basis of Seismic Design Provisions for Welded Steel Oil Storage Tanks," *API Division of Refining Report – Advances in Storage Tank Design.*

Yoshida, S., 2002, "Behavior of Localised Bottom Bulge in Above Ground Oil Storage Tanks under Liquid Pressure," *ASME Journal of Pressure Vessel Technology*, **124 (1)**, pp. 59-65.

APPENDIX A

This Appendix gives the ANSYS APDL Macro for performing nonlinear analysis of the example tank given in Chapter 3-CASE 1. The load is hydrostatic pressure due to water with material properties specified in Ch.3. Shell elements are used to model the tank wall and bottom plate. Friction interaction between the tank bottom and the foundation is taken in to account using friction elements. The information given after exclamatory mark (!) is for understanding of the user and is not part of the APDL.

```
/PREP7          ! Enter the Preprocessor module
ET,1,SHELL208       ! Element Type selected (Type 1)- Axisymmetric shell element
KEYOPT,1,8,2                ! This kepoint enables storing top,mid and bottom surface
results for all layers
sect,1,shell,,    ! Sectional Properties (Geometry) - Type 1
secdata, 6,1,0.0,7       ! Each layer is 6mm with seven integration points
secdata, 6,1,0.0,7       ! totally three layers, each with 6mm thickness
secdata, 6,1,0.0,7
secoffset,TOP           ! the centre line is at the top of thickness
seccontrol,,,, , , ,
sect,2,shell,,    ! Sectional Properties - Type 2
secdata, 1,1,0.0,3       ! 8 layers, each 1mm thick with 3 integration points
secdata, 1,1,0.0,3
secdata, 1,1,0.0,3
secdata, 1,1,0.0,3
secdata, 1,1,0.0,3
secdata, 1,1,0.0,3
secdata, 1,1,0.0,3
secdata, 1,1,0.0,3
secoffset,TOP
```

```
seccontrol,,,, , , ,
MPTEMP,,,,,,,,          ! Material Property Table
MPTEMP,1,0
MPDATA,EX,1,,2e5  ! Youngs' Modulus
MPDATA,PRXY,1,,0.3        ! Poisson's Ratio
MP,DENS,1,7.86e-6  ! Density
MP,ALPX,1,12E-6     ! Coefficient of Linear Expansion
MP,KXX,1,60.5         ! Thermal film coefficient - used for thermal analysis
*SET,PM,0              ! PM is the tag used for Plastic modulus; here the value is zero indication perfectly plastic model
*SET,YS,345           !Define Yield strength
TB,BKIN,1,,1                !Bilinear Kinematic material model (see the option in Ansys at Material properties)
TBDATA,,YS,PM              !since  Plastic modulus has no value it indicates elastic-perfectly plastic  material model
K,1,200,1000           ! Keypoints defining the axisymmetric geometry
K,2,29200,1000
k,3,30009,1000
k,4,30068,1000
k,5,30009,2000
K,6,30009,13000
k,7,200,999.5          ! Keypoints defining the base
k,8,31768,999.5
LSTR,      1,      2  ! constructing straight lines from keypoints
LSTR,      2,      3
LSTR,      3,      4
LSTR,      3,      5
LSTR,      5,      6
LSTR,      7,      8
LESIZE,1,50            ! Assigning element size for lines
LESIZE,2,1
LESIZE,3,1
```

```
LESIZE,4,0.5
LESIZE,5,100
LSEL, , , ,1              !Selecting Line 1
LATT,1, ,1, , , ,2        !Assigning attributes to Line 1 for meshing here sectional properties - Type 2 is assigned
LSEL, , , ,2
LATT,1, ,1, , , ,2
LSEL, , , ,3
LATT,1, ,1, , , ,2
LSEL, , , ,4
LATT,1, ,1, , , ,1
LSEL, , , ,5
LATT,1, ,1, , , ,1
allsel
LMESH, 1                  ! Meshing Line 1
LMESH, 2
LMESH, 3
LMESH, 4
LMESH, 5
!--------CONTACT MODELING----------
! creating a entity " source"
NSEL,R,LOC,X,0,32000      ! Selecting the nodes at the bottom of tank that will be in contact
NSEL,R,LOC,Y,1000,1000.5
CM,source,NODE            ! Creating an entity "source" from the selected nodes
Nsel,all
! /COM, CONTACT PAIR CREATION - START
CM,_NODECM,NODE
CM,_ELEMCM,ELEM
CM,_KPCM,KP
CM,_LINECM,LINE
```

```
CM,_AREACM,AREA
CM,_VOLUCM,VOLU
! /GSAV,cwz,gsav,,temp
MP,MU,1,0.85 !GIVE THE VALUE OF FRICTION HERE MU=0.2  (from greiner paper)
MAT,1
MP,EMIS,1,7.88860905221e-031
R,3
REAL,3
ET,2,169
ET,3,171
R,3,,,1,-.02,0, ! SPECIFY FKN HERE and the tolerance
RMORE,,,1.0E20,0.0,1.0,
RMORE,0.0,0,1.0,,1.0,0.5
RMORE,0,1.0,1.0,0.0,,1.0
KEYOPT,3,3,0
KEYOPT,3,4,0
KEYOPT,3,5,1
KEYOPT,3,6,2
KEYOPT,3,7,0
KEYOPT,3,8,0
KEYOPT,3,9,0
KEYOPT,3,10,2
KEYOPT,3,11,0
KEYOPT,3,12,0
KEYOPT,3,2,0          ! contact algorithm 0 -  augmented lagran(default),1-penalty,4-pure
lagrangian
KEYOPT,2,2,0
KEYOPT,2,3,0
! Generate the target surface
LSEL,S,,,6      ! specify the target line here
CM,_TARGET,LINE
```

```
TYPE,2
LATT,-1,3,2,-1
TYPE,2
LMESH,ALL
! Generate the contact surface
NSEL,S,,,SOURCE    ! selecting the entity "source"
CM,_CONTACT,NODE
TYPE,3
ESLN,S,0
ESURF
*SET,_REALID,3
ALLSEL
ESEL,ALL
ESEL,S,TYPE,,2
ESEL,A,TYPE,,3
ESEL,R,REAL,,3
LSEL,S,REAL,,3
! The normals of the contact and the target surface has to meet in order to make the contact.
! Else the normals of contact or target or both has to be reversed based on the situation
!-----------reverse contact elements normals----------------
CM,_CWZ_EL,ELEM
CM,_CWZ_ND,NODE
CM,_CWZ_KP,KP
CM,_CWZ_LN,LINE
CM,_CWZ_AR,AREA
CM,_CWZ_VL,VOLU
ESEL,NONE
ESEL,A,REAL,,3
ESEL,R,ENAME,,171,177
NSLE
*GET,_z1,ELEM,,NUM,MAX
```

```
KSLN,S
LSLK,S,1
ASLL,S,1
*CREATE,cwzplot,mac
/COM,
/COM,PLOT CONTACT PAIR(S)
~eui,'::apdl::noprint 1'
~eui,'::apdl::nooutput 1'
/PNUM,REAL,1
/NUM,1
/PSYMB,ESYS,1
EPLOT
/PSYMB,ESYS,0
/NUM,0
/PNUM,TYPE,0
/PNUM,REAL,0
/mrep,cwzplot
~eui,'::apdl::nooutput 0'
~eui,'::apdl::noprint 0'
*END
cwzplot
*SET,_REALID,3
FLST,5,4168,2,ORDE,2
FITEM,5,16170
FITEM,5,-20337
CM,_ELMCM,ELEM
ESEL,S, , ,all
ESURF,,REVERSE
! /REPLOT
CMSEL,S,_ELMCM
CMDELE,_ELMCM
```

```
CMSEL,S,_CWZ_EL
CMDEL,_CWZ_EL
CMSEL,S,_CWZ_ND
CMDEL,_CWZ_ND
CMSEL,S,_CWZ_KP
CMDEL,_CWZ_KP
CMSEL,S,_CWZ_LN
CMDEL,_CWZ_LN
CMSEL,S,_CWZ_AR
CMDEL,_CWZ_AR
CMSEL,S,_CWZ_VL
CMDEL,_CWZ_VL
! /MREP,EPLOT
!-----------------end of reversing----------------
! /REPLOT
ESEL,ALL
ESEL,S,TYPE,,2
ESEL,A,TYPE,,3
ESEL,R,REAL,,3
LSEL,S,REAL,,3
ESEL,ALL
ESEL,S,TYPE,,2
ESEL,A,TYPE,,3
ESEL,R,REAL,,3
LSEL,S,REAL,,3
CMSEL,A,_NODECM
CMDEL,_NODECM
CMSEL,A,_ELEMCM
CMDEL,_ELEMCM
CMSEL,S,_KPCM
CMDEL,_KPCM
```

```
CMSEL,S,_LINECM
CMDEL,_LINECM
CMSEL,S,_AREACM
CMDEL,_AREACM
CMSEL,S,_VOLUCM
CMDEL,_VOLUCM
CMDEL,_TARGET
CMDEL,_CONTACT
! /COM, CONTACT PAIR CREATION - END
FINISH


/SOL                ! Entering solution phase to adjust contacts
ANTYPE,0            ! Static analysis
ALLSEL
SOLCONTROL, ON, ON, !Specifies to use optimized nonlinear solution defualts and some enhaced internal solution algorithms
                    ! The time step is adjusted automatically based on the non linearity due to contact element
CNCHECK,ADJUST      ! Adjust the initial status of the contact pair
NEQIT,46            ! Specifies the maximum no. of equilibrium for the nonlinear analysis ( Default is 15-25)
FINISH
/SOL                ! Entering solution phase to solve the problem
ANTYPE,0   ! Static analysis
ALLSEL
SOLCONTROL, ON, ON,
NEQIT,96
NROPT,UNSYM
ACEL,,9.81  ! Set the constant for accelaration due to gravity i.e to include self-weight of the model
RESCONTROL,DEFINE,ALL,-2,2  ! Restart control
TREF,273                    ! Reference base temperature for thermal strain calculations
```

```
DK,1,UX, , ,                ! DOF of Node 1 constrained in x dirn.
*SET,LF,1                   ! Set LF as 1 i.e the load factor(LF) that is used to multiply the loads
                            ! LF is set to 1 for analysis with hydrostatic pressure and set to 5 (or any suitable value for limit load analysis
!LOAD STEP 1
R,3,,,10,-.3,0,
SFL,1,PRES,0.11772*LF       ! Apply pressure on line 1
SFL,2,PRES,0.11772*LF
SFL,4,PRES,0.11772*LF,0.10791*LF
SFL,5,PRES,0.10791*LF,0
BFL,4,TEMP,523              ! Apply temperature to line 4
BFL,1,TEMP,523
BFL,2,TEMP,523
BFL,3,TEMP,523
BFL,5,TEMP,523
OUTRES,ALL,ALL
/OUTPUT,OUT,DAT,,APPEND  !APPENDS THE TEXT OUTPUT TO THE EXISTING OUTPUT FILE
SOLVE           ! Solve the routine
SAVE            ! save the database with results

!LOAD STEP 2
BFL,4,TEMP,0            ! In the second load step the temp is brought down to zero , hence apply zero temp
BFL,1,TEMP,0            ! at same locations
BFL,2,TEMP,0
BFL,3,TEMP,0
BFL,5,TEMP,0
OUTRES,ALL,ALL  ! write all the solution data for all substeps in the database
/OUTPUT,OUT,DAT,,APPEND  !Appends the text output to the existing output file
SOLVE
SAVE
```

APPENDIX B

This Appendix gives the ANSYS APDL Macro for performing nonlinear analysis of the example tank given in Chapter 3-CASE 2 i.e. the tank with multiple wall thicknesses. The load is hydrostatic pressure due to water with material properties specified in Ch.3. Plane elements are used to model the tank wall and bottom plate. Friction interaction between the tank bottom and the foundation is taken in to account using friction elements. The information given after exclamatory mark (!) is for understanding of the user and is not part of the APDL.

```
/PREP7  ! Enter the Preprocessor Module
ET,1,PLANE183  ! Define Element Type
KEYOPT,1,3,1  ! axisymmetric option
KEYOPT,1,1,0  ! indicates quad & not triangle element type
KEYOPT,1,6,1  ! Mixed U-P Formulation –Refer ANSYS help for more details
*SET,LF,2.0   !  Set a value of 2.0 to variable LF i.e here LF is meant for Load Factor
MP,EX,1,2e5  !Material Property – Youngs Modulus
MP,PRXY,1,.3 !Poissons ratio
MP,DENS,1,7.86e-6 ! Density
*SET,PM,1000          ! PM is the variable used for Plastic Modulus and in this example it is given a value of 1000 MPa
*SET,YS,345  !Define Yield strength (YS) as 345 MPa
TB,BKIN,1,,,1  !Bilinear(see the option in ANSYS at Material properties)
TBDATA,,YS,PM  !Here if Plastic modulus has no value it means elastic perfectly plastic material model
! Providing key points for shell wall construction
k, 1 , 45016.99 , 0
```

k, 2 , 45000 , 0
k, 3 , 45000 , 2400
k, 4 , 45001.325 , 2400
k, 5 , 45001.325 , 4800
k, 6 , 45005.58000 , 4800
k, 7 , 45005.58 , 7200
k, 8 , 45007.76 , 7200
k, 9 , 45007.76 , 9600
k, 10 , 45010.26 , 9600
k, 11 , 45010.26 , 12000
k, 12 , 45011.99 , 12000
k, 13 , 45011.99 , 14400
k, 14 , 45011.99 , 16800
k, 15 , 45016.99 , 16800
k, 16 , 45021.99 , 16800
k, 17 , 45021.99 , 14400
k, 18 , 45021.99 , 12000
k, 19 , 45023.72 , 12000
k, 20 , 45023.72 , 9600
k, 21 , 45026.22 , 9600
k, 22 , 45026.22 , 7200
k, 23 , 45028.4 , 7200
k, 24 , 45028.4 , 4800
k, 25 , 45032.655 , 4800
k, 26 , 45032.655 , 2400
k, 27 , 45033.98 , 2400
k, 28 , 45033.98 , 0
!ANNULAR PLATE KEY POINTS
K, 29 , 45083.98 , 0
K, 30 , 45083.98 , -14
K, 31 , 40000 , -14

K, 32 , 40000 , -8

K, 33 , 44265 , -8

K, 34 , 44265 , 0

! EXTRA KEY POINTS TO DIVIDE AREAS TO OPTIMISE MESH

K, 35 , 43000 , -8

K, 36 , 43000 , -14

K, 37 , 45005.58 , 5000

K, 38 , 45028.4 , 5000

! CREATING LINES FOR SHELL CONSTRUCTION USING KEY POINTS

l, 2 , 3

l, 3 , 4

l, 4 , 5

l, 5 , 6

l, 6 , 7

l, 7 , 8

l, 8 , 9

l, 9 , 10

l, 10 , 11

l, 11 , 12

l, 12 , 13

l, 13 , 14

l, 14 , 15

l, 15 , 16

l, 16 , 17

l, 17 , 18

l, 18 , 19

l, 19 , 20

l, 20 , 21

l, 21 , 22

l, 22 , 23

l, 23 , 24

```
l, 24 , 25
l, 25 , 26
l, 26 , 27
l, 27 , 28
! CREATING BOTTOM & ANNULAR PLATE
l , 28 , 29
l , 29 , 30
l , 30 , 36
l , 31 , 32
l , 32 , 35
l , 33 , 34
l , 34 , 2
!EXTRA LINES
L,2,28
L,6,24
L,35,36
L,36,31
L,35,33
LPLOT
! CREATING AREAS FROM CONSTRUCTED LINES
AL,30,31,36,37  ! area 1
AL,27,28,29,36,38,32,33,34 !area 2
AL,1,2,3,4,35,23,24,25,26,34 !area3
lsel,s,line,,5,22,1        ! Selecting lines for creating area
lsel,a,line,,35
AL,all  !area 4
AESIZE,1,2              ! Sizing the area for element formulation
AESIZE,2,1
AESIZE,3,2
AESIZE,4,6
MSHAPE,0,2D         ! Instructing to form 2D  Trapeziodal Element
```

```
MSHKEY,2
AMESH,ALL   ! Mesh the areas to create Elements
!Creating Contact pair
K, 39 , 40000 , -14.1 ! Creating key points for constructing bottom rigid support
K, 40 , 45084.98 , -14.1
L,39,40 ! Creating Line 4 as bottom rigid support
! creating a entity " source"
NSEL,R,LOC,X,40000,45083.98  ! Node Selection
NSEL,R,LOC,Y,-14
CM,source,NODE  ! Creating a module with Selected Nodes
Nsel,all
! /COM, CONTACT PAIR CREATION - START
CM,_NODECM,NODE
CM,_ELEMCM,ELEM
CM,_KPCM,KP
CM,_LINECM,LINE
CM,_AREACM,AREA
CM,_VOLUCM,VOLU
! /GSAV,cwz,gsav,,temp
MP,MU,1,0.2  !The Friction Coefficient is given here are 0.2
MAT,1
MP,EMIS,1,7.88860905221e-031
R,3
REAL,3
ET,2,169 ! Specifying Contact Elements
ET,3,172
R,3,,,10,-.09,0, ! Specify FKN here and the tolerance
RMORE,,,1.0E20,0.0,1.0,
RMORE,0.0,0,1.0,,1.0,0.5
RMORE,0,1.0,1.0,0.0,,1.0
KEYOPT,3,3,0
```

```
KEYOPT,3,4,0
KEYOPT,3,5,1
KEYOPT,3,6,2
KEYOPT,3,7,0
KEYOPT,3,8,0
KEYOPT,3,9,0
KEYOPT,3,10,2
KEYOPT,3,11,0
KEYOPT,3,12,0
KEYOPT,3,2,0   ! contact algorithm 0 -  augmented lagran(default),1-penalty,4-pure lagrangian
KEYOPT,2,2,0
KEYOPT,2,3,0
! Generate the target surface
LSEL,S,,,39   ! SPECIFY THE TARGET LINE HERE
CM,_TARGET,LINE
TYPE,2
LATT,-1,3,2,-1  ! Providing Line Attributes
TYPE,2
LMESH,ALL   ! Meshing the Line for Contact element- Target Elements
! Generate the contact surface
NSEL,S,,,SOURCE
CM,_CONTACT,NODE
TYPE,3
ESLN,S,0
ESURF
*SET,_REALID,3
ALLSEL
ESEL,ALL
ESEL,S,TYPE,,2
ESEL,A,TYPE,,3
```

```
ESEL,R,REAL,,3
LSEL,S,REAL,,3
! /PSYMB,ESYS,1
! /PNUM,TYPE,1
! /NUM,1
! EPLOT
! Reverse target normals – since the normals of Source and Target contact elements should meet
CM,_Y,LINE
LSEL,S,,,39  ! SPECIFY THE TARGET LINE HERE
CM,_YEL,ELEM
CM,_YND,NODE
NSLL,S,1
ESLN,S,1
ESEL,R,REAL,,_REALID
ESURF,,REVERSE  ! Reversing the surface of elements i.e the normals
CMSEL,S,_Y
CMSEL,S,_YEL
CMSEL,S,_YND
CMDELE,_Y
CMDELE,_YEL
CMDELE,_YND
! /REPLOT
!*
ESEL,ALL
ESEL,S,TYPE,,2
ESEL,A,TYPE,,3
ESEL,R,REAL,,3
LSEL,S,REAL,,3
! /PSYMB,ESYS,1
! /PNUM,TYPE,1
```

```
! /NUM,1
! EPLOT
ESEL,ALL
ESEL,S,TYPE,,2
ESEL,A,TYPE,,3
ESEL,R,REAL,,3
LSEL,S,REAL,,3
CMSEL,A,_NODECM
CMDEL,_NODECM
CMSEL,A,_ELEMCM
CMDEL,_ELEMCM
CMSEL,S,_KPCM
CMDEL,_KPCM
CMSEL,S,_LINECM
CMDEL,_LINECM
CMSEL,S,_AREACM
CMDEL,_AREACM
CMSEL,S,_VOLUCM
CMDEL,_VOLUCM
! /GRES,cwz,gsav
CMDEL,_TARGET
CMDEL,_CONTACT
! /COM, CONTACT PAIR CREATION - END
! /MREP,EPLOT
FINISH
/SOLUTION
ANTYPE,0   ! Static analysis
NLGEOM,ON   ! Include Nonlinear Geometry effect during Analysis i.e include Large Strain/Rotation effect – See ANSYS help for more details
SOLCONTROL, ON, ON, ! Activate the default solution control techniques in ANSYS to achieve convergence
```

```
CNCHECK,ADJUST ! Contact check and adjust for any small gaps
NROPT,FULL  ! Emply full Newton Raphson technique to achieve convergence
neqit,35 ! Maximum no. of equilibrium equations to try for convergence is 35
ACEL,,9.81  ! Set gravity constant
DL,30,1,SYMM,   ! UX=0 FOR LINE 30 ..LINE AT THE CENTRE OF TANK
!DL,30,1,UY,   ! UY=0
LSEL,ALL   ! Re-select all lines
! PRESSURE ON SHELL WALL MULTIPLIED BY LOAD FACTOR
SFL, 1 , PRES, 0.164808000*LF , 0.141264000*LF
SFL, 3 , PRES, 0.141264000*LF , 0.117720000*LF
SFL, 5 , PRES, 0.117720000*LF , 0.094176000*LF
SFL, 7 , PRES, 0.094176000*LF , 0.070632000*LF
SFL, 9 , PRES, 0.070632000*LF , 0.047088000*LF
SFL, 11 , PRES, 0.047088000*LF , 0.023544000*LF
SFL, 12 , PRES, 0.023544000*LF , 0.000000000*LF
SFL, 2 , PRES, 0.141264000*LF
SFL, 4 , PRES, 0.117720000*LF
SFL, 6 , PRES, 0.094176000*LF
SFL, 8 , PRES, 0.070632000*LF
SFL, 10 , PRES, 0.047088000*LF
!PRESSURE ON BOTTOM AND ANNULAR PLATE
SFL, 31 , PRES, 0.164886000*LF ,
SFL, 38 , PRES, 0.164808000*LF ,
SFL, 33 , PRES, 0.164808000*LF ,
SFL, 32 , PRES, 0.164886000*LF , 0.164808000*LF
TIME,1   !Time will go to 1 at the end of loading
!AUTOTS,ON  ! This command is to instruct ANSYS for automatic time step increase. But
not used in this particular program since the solution is controlled by NSUBST command
NSUBST,5000  !Number of sub steps in total time is 5000
OUTRES,ALL,ALL  ! write all results to database
/OUTPUT,OUT,DAT  !Creates output files in the directory
```

```
SOLVE   ! solve the model
SAVE    ! save the database
FINISH ! close the solution module
```

APPENDIX C

The following is the post processing APDL routine incorporating the m_α-tangent method. The routine has to be run after solving the FE model and results are stored in database. The routine writes the m_α-tangent multiplier values in a file named "tank_mul" in the same working directory of ANSYS.

The thickness of the shell element can be divided in to any number of layers (say 5 layers in this routine) to improve the accuracy of results. Layering especially improves the results where high bending strain is expected. But layering increases the computational effort and the volume of results data. In this thesis layering was used in few situations to check the accuracy of results obtained without layers (i.e., the entire shell thickness is a single layer). The following routine can also be modified to run for shell elements without any layers by removing the LAYER commands. Even though, the following macro has worked previously, it is added here without final checking (using ANSYS), with latest version.

```
/POST1   ! Enter Postprocessing module
PLDISP,2        ! Plots the displaced structure
SHELL,MID   ! choose the Middle plane of the shell layer
*SET,YS,206.8430     !YIELD STRENGTH
ETABLE,Sig,S,EQV !SIG is user given name, S,EQV is VON Misses Equivalent stress
ETABLE,Vol,VOLU  !Element volume
!Counting total number of elements
*GET,Emax,ELEM,0,COUNT !Emax = No of total elements will be stored in Emax
!Evaluate total volume (sum of all element volume using do loop)
*SET,Vtot,0   !initial value of volume

*DO,i,1,Emax  ! Starting the Do loop with i =1 to Emax with inc. of 1
*GET,Evol,ELEM,i,ETAB,Vol ! Get the volume of Each element inside the do-loop bracket
*SET,Vtot , Vtot + Evol         ! summation of individual element volumes
*ENDDO

*SET,NLR,5   ! Enter No. of Layers here
```

```
!Evaluate the multipliers
*SET,SumRef,0  !initial value of Stress

*DO,j,1,NLR                                    ! FINDING SUMREF FOR ONE LAYER
LAYER,j
        *DO,i,1,Emax  !i=1;i<=Emax;i++
        *GET,SigEq,ELEM,i,ETAB,Sig
        *GET,EvoL,ELEM,i,ETAB,Vol
        *SET,SumRef , SumRef + ((SigEq*SigEq)*(Evol/5))  ! (SigEq*SigEq) =
(SigEq**2)
        *ENDDO
*ENDDO



*SET,SIGref , SQRT(SumRef/Vtot)   !Reference stress

*SET,m0_1 , (YS/SIGref)
*SET,m_0,m0_1
*SET,SIGmax,0  !initial value of Max.Stress

*DO,j,1,NLR
LAYER,j
ESORT,ETAB,Sig,0    !Getting max value of Sig from ETABLE
*GET,SMAX,SORT,0,MAX
*IF,SMAX,GT,SIGmax,THEN
*SET,SIGmax,SMAX
*ENDDO

*SET,m_L,(YS/SIGmaX)
*SET,JETA,(m_0/m_L)
*SET,Tan_theta,0.2929    !this is the fixed value shown in the formula of paper
```

```
*SET,m_tangent , m_0/(1+(Jeta-1)*Tan_theta)

!Open file
*CFOPEN,tank_mul   !tank_mul...file created
*CFWRITE,m0,m_0    !write m0=m_0 in the file
*CFWRITE,mL,m_L    !write m0=m_0 in the file
*CFWRITE,m_tangent,m_tangent  !Write m_tangent = m_tangent in file
*CFCLOS
FINISH
```